University of Alberta
Department of Civil Engineering

Structural Engineering Report No. 45

Ultimate Strength of Continuous Composite Beams

by

S. Hamada

and

J. Longworth

August, 1973

ULTIMATE STRENGTH OF CONTINUOUS COMPOSITE BEAMS

BY

SUMIO HAMADA

AND

JACK LONGWORTH

JUNE, 1973

Department of Civil Engineering

University of Alberta

Edmonton, Canada

ABSTRACT

Behavior of continuous composite beams is investigated theoretically and experimentally. Analyses for local flange buckling and lateral buckling in negative moment regions are proposed based on torsional buckling theory and thin-walled beam theory, respectively. Deformations, including the effects of shear and slip, are studied in the elastic and inelastic regions. Procedures based on Newmark's integration, finite difference and virtual work are employed for the evaluation of moment-curvature relationships, beam deflection due to bending and shear deformation, respectively. Three two-span continuous composite beams were tested. The test beams varied in terms of steel section size and amount of longitudinal slab reinforcement in the negative moment region. Behavioral studies are conducted for failure loads and failure modes for a series of beams in which steel section size, concrete slab thickness and amount of longitudinal slab reinforcement are varied. Analyses satisfactorily predict ultimate loads, failure modes and behavior throughout the loading range. Based on experimental and analytical results design requirements are proposed for ultimate strength design of continuous composite beams.

It is concluded that the maximum flange width-thickness ratio for the steel section should be less than $54/\sqrt{\sigma_y}$, if the amount of longitudinal reinforcement in a negative moment region is greater than the web area of the steel section. Strength of shear connectors

in a negative moment region is comparable with the strength of connectors in a positive moment region if sufficient development length of the longitudinal slab reinforcement is provided into the positive moment region.

ACKNOWLEDGEMENT

This investigation is part of a continuing project "Behavior of Composite Flecture Members" in progress in the Department of Civil Engineering at the University of Alberta under the direction of Professor J. Longworth. This project receives financial support from the National Research Council of Canada.

Assistance of members of the laboratory staff in the fabrication and testing of the beam specmens is appreciated. The authors wish to acknowledge the beneficial discussions held with M. Suko, S. Rajasekaran, B. Wood and other graduate students in the Structural Engineering Laboratory. The manuscript was typed by Mrs. L. Rogoczenski, whose cooperation is appreciated.

TABLE OF CONTENTS

Table of Contents, cont'd. Page

Table of Contents, cont'd. Page

Table of Contents, cont'd.

Table of Contents, cont'd.

LIST OF TABLES

List of Tables, cont'd.

LIST OF FIGURES

List of Figures (cont'd.)

List of Figures (cont'd.)

List of Figures (cont'd.)

List of Figures (cont'd.)

List of Figures (cont'd.)

List of Figures (cont'd.)

List of Figures (cont'd.)

LIST OF PLATES

LIST OF SYMBOLS

A	Area of cross-section
A_c	Area of concrete slab
A_f	Area of flange
A_r	Area of longitudinal reinforcement
A_s	Area of steel section
A_w	Area of web
a_x, a_y	x and y co-ordinates of shear center
A_1	Area of a part of the cross-section defined in Figure 3.6
b	Flange width
$[B]$	Matrix for finite difference equations with respect to second derivative
b_c	Concrete slab width
b_e	Effective slab width
b_n	The smaller of the widths of the flange and cover plate
b_w	The larger of the widths of the flange and cover plate
B_ω	$\int \sigma_z \omega dA$

C, C_1, C_2	Compression forces
$[C]$	Co-efficient matrix
c_x, c_y	x and y co-ordinates of a hinge location in the cross section
d	Depth of steel section
D_x	$E_x/(1 - \nu_x\nu_y)$
D_y	$E_y/(1 - \nu_x\nu_y)$
D_{xy}	$\nu_x D_x$
D_{yx}	$\nu_y D_y$
d_w	Web depth of steel beam
E	Elastic modulus for steel
$\overline{E}$	Modified elastic modulus
$[E]$	Unit matrix
E_c	Elastic modulus for concrete
e_c, e_s	Distances in y direction measured from the neutral axis
E_i	Initial tangent modulus for concrete
E_{sec}	Inelastic secant modulus for steel
E_{st}	Strain-hardening modulus for steel
E_t	Inelastic tangent modulus for steel

List of Symbols, cont'd.

E_x	Elastic modulus in x direction
E_y	Elastic modulus in y direction
$[F]$	Flexibility matrix
f_c	Compressive stress in concrete
f'_c	28-day cylinder strength of concrete
G	Elastic shear modulus
G_t	Inelastic shear modulus
h	E/E_t
I_c	Moment of inertia of compression zone of concrete with respect to the centroid of the compression zone
I_p	Moment of inertia of composite beam in positive bending
I_s	Moment of inertia of steel section with respect to the centroid of the steel section
I_x, I_y	Moments of inertia about the x and y axes
$I_{xy}, I_{y\omega}, I_{x\omega}$	Products of inertia in xy, $y\omega$ and ωx planes
I_ω	Warping constant
$I_{\omega c}$	Warping constant with respect to location C
J	St. Venant's torsional constant

List of Symbols, cont'd.

k	Spring constant
k_{11}~k_{22}	Co-efficients in flexibility matrix
k_c	Deflection co-efficient for a beam with a concentrated load
k_s	Rigidity constant for a shear connector
k_{sh}	Shear correction factor
k_w	Deflection co-efficient for a beam with a uniformly distributed load.
L	Flange buckling length
ℓ	Span length
L_s	Shear span
ℓ_a	Distance between two dial gages for rotation measurement
M, M_1,M_2,M_3	Bending moments
M_{AB}, M_{BA}	Moments at ends A and B
m_c	Moment co-efficient for a beam with a concentrated load
M_{eq}	Equivalent moment
M_{ex}	External moment
M_p	Simple plastic moment
M_k	Moment due to the force in longitudinal reinforcement

List of Symbols, cont'd.

m_t	Torsional moment per unit length
M_{tt}	Torsional moment
M_{ttr}	Torsional moment due to residual stresses
M_u	Ultimate moment
m_w	Moment co-efficient for a beam with a uniformly distributed load
M_x, M_y	Moments about the x and y axes
M_ρ	Stress resultant defined by $\int_A \sigma\{(a_x - x)^2 + (a_y - y)^2\}dA$
$M_{\rho r}$	Stress resultant M_ρ due to residual stresses
N_q	Static moment with respect to area A_1
N_z	Normal force in the z direction
P	Concentrated load
P_{cr}	Critical load
P_u	Ultimate load
P_z	Force in the z direction
Q, Q_1, Q_2	Forces acting on a shear connector
q	Distributed load

q_s, q_{s1}, q_{s2} Ratio of forces Q, Q_1, Q_2 to the ultimate shear connector strength

Q_u Ultimate strength per shear connector

q_x, q_y, qz Distributed loads in the x, y and z directions

q_x^*, q_y^* Statically indeterminate forces in the x and y directions resulting from restraint

r Radius of gyration

r_t, r_n Distances from point A to the tangential and normal lines through the point S (Figure A.1)

s Co-ordinate in the tangential direction in a cross section

s_1, s_2 Stiffness co-efficients in rotation equations

S_x, S_y, S_ω Static moments about x, y and ω axes

s_γ Spacing of shear connectors

u Displacement in the z direction

T, T_1, T_2 Tensile force

t Flange thickness
Thickness of a thin-walled beam section (Appendix A)

t_c Thickness of concrete slab

T_K, T_L, T_R Forces acting at the edges of a thin-walled section

V Shear force

v Displacement in the tangential direction

$\bar{V}$ Virtual shear force

Vol	Volume
w	Web thickness Plate deflection (Section 2.4.1)
X	Indeterminate force
x	Co-ordinate
y	Co-ordinate
y_d	Location of neutral axis
y_s	Distance between the centroids of the concrete slab and steel section
z	Co-ordinate
α	Angle Ratio of the negative moment region to the beam length (Appendix C)
β	Web restraint constant
γ	Shear strain
$\gamma_{\bar{\epsilon}}$	Ratio of strain at the slab centerline to that at the slab edge
δ	Deflection
δ_b	Bending deflection
Δ_{d1}, Δ_{d2}	Displacements measured by dial gages
Δ_i	Deformation at support i
δ_{ij}	Flexibility factor

δ_{io} Deformation at support i for statically determinate structure

$\Delta_s, \Delta_{s1}, \Delta_{s2}$ Slip deformations for a shear connector

δ_{sh} Shear deformation

ε Strain

ε_c Strain in concrete

ε'_c Strain in concrete at a stress equal to f'_c

ε_{cu} Strain in concrete at failure

ε_d Slip strain

ε_{st} Steel strain at the conset of strain hardening

ε_y Yield strain

ε_u Steel strain at ultimate stress

ζ Displacement in the z direction

η Displacement in the y direction

θ Rotation; angle of twist

θ_{AB}, θ_{BA} Rotations at ends A and B

$\theta'_{AB}, \theta'_{BA}$ Rotations at ends A and B of a simply-supported beam AB due to load

λ Segment length

λ_x, λ_y Segment length in the x and y directions

ν	Poisson's ratio
ν_x	Poisson's ratio in x direction
ν_y	Poisson's ratio in y direction
ξ	Displacement in the x direction
ρ, ρ_1, ρ_2	Ratios of stiffness in a negative moment region to that in a positive region
σ	Stress
σ_r	Residual stress
σ_z	Stress in the z direction
σ_{ry}	Yield stress of the longitudinal reinforcement
σ_u	Ultimate strength of structural steel
τ	Shear stress
ϕ	Curvature
ϕ_p	Plastic curvature
ω	Warping function

CHAPTER I

INTRODUCTION

1.1 Introductory Remarks

Presently in North America composite design is based to a large extent on elastic theory[1][2]. However elastic design is not entirely routine in the case of continuous beams, because the beam stiffness is different in positive and negative moment regions. An ultimate design approach would eliminate this complication. Design based on ultimate strength may tend to produce a reduction in steel section size and in total depth. This reduction is related to the shape factor of the composite section which may reach a value of 2.0 in a positive moment region and 1.6 in a negative moment region. These values are significantly larger than those for wide flange steel sections.

Extensive research on ultimate strength of simple span beams has resulted in the first requirements for limit design of simply-supported composite beams published in Britain in 1963 as Part I of CP 117[3]. However further research on ultimate strength of continuous composite beams is still required, especially concerning conditions in a negative moment region. Research at the University of Alberta has included investigations by Piepgrass[4], Davison[5], Lever[6] into the behavior of composite beams under negative bending.

1.2 Previous Research on Continuous Composite Beams

Research on ultimate strength of continuous composite beams has been conducted since 1960 at several universities including the University of Cambridge, Imperial College, Lehigh University, University of Canterbury (New Zealand), University of Warwick, and University of Alberta. A brief summary of main conclusions of this research is presented in this section.

Culver et al[7] tested a two-span continuous beam with a small amount of longitudinal slab reinforcement to establish the feasibility of designing continuous composite beams on the bases of ultimate strength. The results of the investigation concluded that only the steel section is effective in the negative moment region, and an expansion joint in the slab should be provided in the negative moment region to permit large rotation.

Barnard [8][9] tested a series of four continuous three-span beams in order to study the behavior of the most highly strained critical sections and the effect of their combined action on the behavior of the beam as a whole. Two beams failed by crushing of concrete in the positive moment region and the other two failed due to lateral buckling of the steel section in the negative moment region. The results indicated that continuous composite beams can be designed by the conventional plastic hinge method, if the positive moment hinge is the last to form; that the presence of slip strain does not significantly change the moment-curvature relationships from those obtained by assuming no slip strain; and that longitudinal slab reinforcement strengthens the negative moment regions, provided that buckling and shear failure can be avoided.

Johnson, Van Dalen and Kemp[10] conducted tests on fifteen simply-supported beams in negative bending and six two-span continuous beams. The continuous beams were loaded in such a manner that they were affected by transverse bending in the slab. The slabs were reinforced with various amounts of longitudinal reinforcement. The results indicated that complete interaction occurred in negative moment regions where the concrete slab was cracked due to longitudinal tension. The actual ultimate loads for the continuous beams exceeded theoretical values by 11 to 31 percent.

Daniel and Fisher[11] tested to failure four continuous beams which had been previously fatigue tested. The beams contained longitudinal reinforcement in the negative moment region. In each beam crushing of the concrete at the load points occurred at maximum load except in the beam with the largest amount of reinforcement where local buckling also occurred at ultimate load. Furthermore the longitudinal slab reinforcement in the negative moment regions attained its yield stress at ultimate load. It was concluded that plastic analysis adequately predicted ultimate loads.

Park[12] tested four two-span continuous beams with various amounts of longitudinal slab reinforcement in the negative moment region. It was concluded that continuous beams with longitudinal slab reinforcement in the negative moment regions can be satisfactorily analyzed by simple plastic theory. Very little redistribution of bending moments was required in the test beams to develop an ultimate condition, since there was little difference between the distribution of elastic and ultimate bending moments in spite of the large variations in the longi-

tudinal reinforcement content. Shear connectors, designed on the basis of ultimate capacity, performed adequately.

Extensive research on the behavior of stud shear connectors in a negative moment region was conducted by Van Dalen et al[10][13][14]. As a result, it was recommended that the design load for connectors in a negative moment region should be taken as 80 percent of the design values in a positive moment region.

In 1970 Climenhaga[15][16] investigated theoretical and experimental post-buckling behavior of composite beams in negative moment regions. His proposed approximate method, based on the upper-bound plastic limit theorem, gave a reasonable prediction of the moment-rotation characteristics for I-shape sections after local buckling.

Daniel et al[17][18][19] tested beams connected to columns simulating part of a multi-story frame. It was concluded that the ultimate strength of a composite section adjacent to the column face and sujected to positive bending can be conservatively based on the strength of the steel section plus a portion of the concrete slab whose width equals the column width. Results indicated that ultimate strength of a composite section in negative bending can be based on the steel section plus the longitudinal slab reinforcement. Test beams exhibited sufficient rotation capacity in the vicinity of the joint so as to develop a mechanism at ultimate load.

1.3 Previous Investigations at the University of Alberta

Research on continuous composite beams at the University of Alberta was initiated in 1965 by Ferrier[20] with behavioral studies of

composite beams under positive moment. The slab dimensions used in Ferrier's test beams were chosen so that in one beam the neutral axis was in the slab whereas in the other the neutral axis was below the slab. It was found the beams deflected more at working loads than predicted by usual analysis. This difference was likely due to residual stresses in the steel section; however residual stress did not influence the ultimate strength. Ultimate concrete slab strains in excess of 0.005 were developed. Slip between the concrete and steel section did not prevent the beams from developing their theoretical ultimate moment values, provided that the total strength of the shear connectors supplied the required horizontal shear resistance.

The second investigation, by Piepgrass[4] in 1968, was concerned with the behavior of composite beams in an isolated negative moment region. The main variables in this investigation were the amount of longitudinal reinforcement and slab width. Compression flanges of some steel sections were reinforced with cover plates in order to prevent premature local buckling. Beams without cover plates failed in local buckling in the flange and web whereas beams with cover plates failed in lateral buckling. Ultimate moments ranged from 98 to 107 percent of the theoretical plastic moment values. The average stress in the longitudinal slab reinforcement at ultimate moment was less than the yield stress, which implied little rotation capacity. It was therefore suggested that the use of steel sections defined as compact under the provisions of CSA Standard S16 may not necessarily guarantee adequate rotation capacity for the formation of a plastic hinge in a composite beam in negative bending.

Extensive tests of composite beams under negative moment were conducted by Davison[5] in 1969 and Lever[6] in 1970. The main variables in these tests were size of steel section, amount of longitudinal slab reinforcement and slab width. All beams failed in local buckling of the compression flange. It was concluded that significant increases in the negative moment capacity of composite beams can be achieved by the addition of longitudinal reinforcement, but these increases are not directly proportional to theoretical simple plastic moment values. For a given steel section, an increase in amount of longitudinal slab reinforcement results in a significant reduction in the rotation capacity. Therefore, to ensure the formation of a mechanism in beams where the negative hinge is first to form, it may be necessary to limit the amount of longitudinal slab reinforcement.

1.4 Object and Scope

This dissertation consists of both theoretical and experimental studies of the behavior of continuous composite beams. The experimental study provides further information on deformations, moment redistributions and failure modes for continuous beams. Since relatively little analytical investigation has been conducted into local and lateral buckling in negative bending, an objective of this investigation is a theoretical determination of ultimate strength and rotation capacity in a negative moment region. A further objective is the prediction of ultimate load and failure modes for continuous composite beams. The study also includes a theoretical analysis for the deformation of continuous composite beams. Finally design criteria for continuous composite beams are proposed.

CHAPTER II

STRENGTH OF COMPOSITE BEAMS

2.1 Introduction

Characteristics of composite sections are different in positive and negative moment regions. In a positive moment region the concrete slab or a portion thereof is in compression and contributes significantly to the moment resistance of the section as in Figure 2.1(a). Behavior under positive moment therefore is related to characteristics of the steel section, concrete slab and shear connectors.

Since concrete cracks when subjected to relatively small tensile stress, a beam under negative moment essentially consists of the steel section and longitudinal reinforcement in the slab with the concrete acting as a transfer medium. For usual amounts of longitudinal slab reinforcement the shear force transferred by the concrete slab through the shear connectors to the steel section is small in a negative moment region compared with that in a positive moment region. The behavior of a composite beam under negative moment is essentially related to the characteristics of the steel section, the longitudinal slab reinforcement and the shear connectors. In a negative moment region the lower flange is subjected to compressive stress, and local flange buckling may be a factor in the ultimate moment capacity. A number of composite beams tested under negative moment at the University of Alberta[5][6]

and the University of Cambridge[10][15][21] failed in local flange buckling. It was observed in the University of Alberta[4] tests that composite beams with a cover plate on the compression flange failed in lateral buckling because of increased resistance to local flange buckling.

2.2 General Behavior of Composite Beams

2.2.1 Positive Moment

Since in a positive moment region the concrete slab is subjected to compressive stress, the composite section is similar to a steel section with a cover plate on the compression flange. Stress distributions for a composite section are illustrated in Figure 2.2 for three conditions, namely, prior to yielding, prior to strain-hardening and after strain-hardening. A typical moment-curvature relationship is shown in Figure 2.3.

In order to evaluate elastic stiffness for composite sections, it is customary to transform the concrete slab area into an equivalent area of steel by reducing the slab width by a factor, $n = E_s/E_c$. The bending moment derived from the idealized stress distribution shown in Figure 2.4 is defined as the theoretical ultimate moment capacity. At ultimate conditions the stress in the steel section is equal to the yield stress and the stress in the concrete slab is in terms of a Whitney stress block[22]. The ultimate bending moment M_u for a beam with the neutral axis in the slab as in Figure 2.4(1) is therefore defined by

$$M_u = A_s\sigma_y(d/2 + t_c - a/2) \qquad 2.1$$

where $a = A_s\sigma_y/0.85f'_cb_c$

M_u for a beam with its neutral axis below the slab, as in Figure 2.4(b) is defined by

$$M_u = C_1e_1 + C_2e_2 \qquad 2.2$$

where $C_1 = 0.85f'_cA_c$

and $C_2 = (A_s\sigma_y - C_1)/2$

Effective interaction between concrete slab and steel section can be achieved by providing adequate shear connectors. Inadequate amounts or inadequate stiffness of shear connectors produces incomplete interaction. In the case of incomplete interaction two netural axes exist due to slippage as illustrated in Figure 2.5. The ultimate moment capacity for a beam with inadequate shear connectors is obtained in a manner similar to that for a beam with adequate shear connectors. Since inadequate shear connectors cannot transmit the required force, the maximum compression force in the concrete is limited to the ultimate strength of the shear connectors, ΣQ_u. Therefore a stress distribution at ultimate moment is as shown in Figure 2.6 and

$$M_u = C_1e_1 + C_2e_2 \qquad 2.3$$

where $C_1 = \Sigma Q_u$

and $C_2 = (A_s \sigma_y - C_1)/2$

The values of e_1 and e_2 in the above equations are dependent on the geometry of the beam section.

Equations 2.2 and 2.3 form the basis for Figure 2.7 which represents the relationship between the ratio of the shear strength $\Sigma Q_u/C$, and moment capacity[23][24].

2.2.2 Negative Moment

When a composite beam with longitudinal reinforcement and shear connectors in the slab is subjected to negative moment, such as in the vicinity of interior supports in a continuous span, the beam section may be considered to consist of the steel section and the longitudinal reinforcement, since concrete cannot resist appreciable tensile stress. The behavior is similar to that of a plain steel beam, if slippage does not occur between the slab and the steel section. Typical stress distributions are illustrated in Figure 2.8 for conditions before yielding, before strain-hardening and after strain-hardening of the steel. Typical moment-curvature relationships obtained from University of Alberta tests[5][6] are shown in Figure 2.9.

The simple plastic moment for negative moment conditions may be expressed as

$$M_p = A_r \sigma_{ry} e_1 + T e_2 \qquad 2.4$$

where e_1 and e_2 are defined in Figure 2.10. The simple plastic moment M_p for a section, which has no longitudinal reinforcement, is the same as that for the steel section alone.

Davison[5] and Lever[6] observed that the principal failure mode for composite beams subjected to negative bending was local flange buckling. Piepgrass[4] observed lateral buckling failures in tests of composite beams with cover plates on the compression flanges. Figure 2.11, based on University of Alberta tests, indicates that the ratio of the experimental ultimate moment to the theoretical ultimate moment decreases with an increase in the amount of longitudinal reinforcement.

2.3 Properties of Material

2.3.1 Steel

Mechanical properties of steel significantly affect the behavior of composite beams. The typical stress-strain curve for a structural steel in tension consists of an elastic range, a plastic range and a strain-hardening range as shown in Figure 2.12(a)[25]. The stress-strain relationship has been idealized by bilinear or multilinear functions as illustrated in Figure 2.12(b). Function (1), which idealizes the material as elastic and perfectly plastic, is employed in the simple plastic theory. Functions (2) and (3) express the stress-strain relationship by means of multilinear functions known as elasto-plastic strain-hardened functions. Function (2) is widely employed for structural analysis; however, since the tangent modulus after strain-hardening is defined as the initial tangent modulus at a

strain ε_{st}, significant differences in strain occur between the approximation and actual condition at higher stresses. In order to reduce the difference Lay and Smith[26] proposed function (3) which approximates the strain hardening range by two straight lines.

For purposes of the present investigation the stress-strain relationship after strain-hardening is idealized by function (4), which is a second order curve defined by three conditions; namely, the coordinates at the onset of strain-hardening (ε_{st},σ_y), the coordinates at ultimate stress (ε_u,σ_u) and the slope at the onset of strain-hardening E_{st}. The stress-strain relationship may be expressed as follows:

$$\sigma = E\varepsilon \qquad \text{for } \varepsilon < \varepsilon_y \qquad 2.5(a)$$

$$\sigma = \sigma_y \qquad \text{for } \varepsilon_y < \varepsilon < \varepsilon_{st} \qquad 2.5(b)$$

$$\sigma = a + \sqrt{b + c\varepsilon} \qquad \text{for } \varepsilon_{st} < \varepsilon \qquad 2.5(c)$$

where

$$a = \frac{\sigma_u^2 - \sigma_y^2 - 2E_{st}\sigma_y(\varepsilon_u - \varepsilon_{st})}{2\{\sigma_u - \sigma_y - E_{st}(\varepsilon_u - \varepsilon_{st})\}}$$

$$b = (\sigma_y - a)(\sigma_y - a - 2E_{st}\varepsilon_{st})$$

$$c = 2E_{st}(\sigma_y - a)$$

For example G40.12 structural steel with σ_y = 44ksi, σ_u = 68ksi, E_{st} = 750ksi,

ε_{st} = 0.0146 and ε_u = 0.20, Equation 2.5(c) is defined by

$$\sigma = 41.5 + \sqrt{-48.5 + 3720\varepsilon}$$

The same relationship is assumed in compression.

2.3.2 Concrete

The stress-strain relationship for concrete, which has been the subject of extensive research related to the development of ultimate strength of concrete members, consists of an ascending portion and a descending portion as shown in Figure 2.13.

In order to define the stress-strain relationship, various approximations have been proposed. Hognestad[27] proposed a parabolic equation for the ascending portion and a linear equation for the descending portion.

$$f_c = f_c' \left\{ 2\frac{\varepsilon_c}{\varepsilon_c'} - \left(\frac{\varepsilon_c}{\varepsilon_c'}\right)^2 \right\} \qquad \text{for ascending portion 2.6(a)}$$

$$f_c = f_c' \left[1.0 - \frac{0.15\varepsilon_c}{\varepsilon_{cu} - \varepsilon_c'} \right] \qquad \text{for descending portion 2.6(b)}$$

Smith and Young[28] proposed a single exponential function in the form of

$$f_c = K\,\varepsilon_c^m \qquad 2.7$$

where K is a constant and m is an exponent related to the concrete strength. A simple expression for the stress-strain relationship proposed by Desayi and Krishnan[29] has the form

$$f_c = \frac{E_i \varepsilon_c}{1 + (\varepsilon_c/\varepsilon_c')^2} \qquad 2.8$$

where E_i is the initial tangent modulus such that $E_i = 2f_c'/\varepsilon_c'$. This expression is well fitted to the ascending portion as well as descending portion.

Ultimate concrete strain based on results of axial compression tests of plain concrete and beam tests of reinforced concrete has been discussed by many researchers. Chambaud[30] reported an ultimate concrete strain of 0.0036 for cube strengths ranging from 3,000 to 7,000 psi. Billet and Appleton[31] observed ultimate strains in beam tests varying from 0.0028 to 0.0040 with an average of 0.0038. Ros[32], Brandtzaeg[33], Jensen[34] and Hognestad et al[35] found that ultimate strain varied with concrete strength and proposed

$$\varepsilon_{cu} = 0.004 - f_c'/(6.5 \times 10^6) \qquad 2.9$$

from axial compression tests. A constant value $\varepsilon_{cu} = 0.003$ is given in ACI Standard 318-71[36][37][38] for design purposes and is considered conservative.

In contrast to the ultimate strain, the strain ε_c' at maximum stress appears to be independent of concrete strength. Liebenberg[39] observed values of ε_c' in the order of 0.002 in compression tests.

2.3.3 Shear Connectors

Shear connectors are provided for two purposes in composite beams, i.e., transmission of horizontal shear between the concrete slab and the steel section and prevention of uplift of the concrete slab. Various types of shear connectors which fulfill these functions have been developed. Some types are rigid and give expectations of complete interaction. However, widely used types such as stud and channel connectors are flexible and permit slippage between the concrete slab and steel section. This slippage is due to deformation of the connectors and deformation of the concrete in the region of the connectors.

Push-out tests have been widely used to determine the shear strength and load-slip characteristics of shear connectors. The strength and load-slip relationship for connectors may be correlated with concrete strength. However, if load is expressed as a function of the static ultimate load, load-slip curves appear to be independent of concrete strength as shown in Figure 2.14[40].

Yam and Chapman[41] represented the load-slip curve by the exponential function

$$q_s = a \{1 - \exp(-b\Delta_s)\} \qquad 2.10$$

where q_s is the ratio of shear force Q to ultimate strength Q_u, and a and b are constants. By choosing two points on the exponential curve so that $\Delta_{s2} = 2\Delta_{s1}$ as in Figure 2.14, the constants may be defined as

$$a = \frac{q_{s1}^2}{2q_{s1} - q_{s2}}$$

$$b = \frac{1}{\Delta_{s1}} \ln \frac{q_{s1}}{q_{s2} - q_{s1}}$$

In order to investigate the behavior of shear connectors in a negative moment region, push-out tests on studs set in reinforced slabs as shown in Figure 2.15 have been conducted by Johnson and Van Dalen[10][13][14]. Ultimate push-out strengths obtained varied between 64 and 108 percent of the strengths obtained in conventional push-out tests, and slip at the failure load was approximately double that at 80 percent of the failure load, although the load-slip curves were widely scattered. The behavior of studs was found to mainly depend on the location of cracks on the slab surface which influence the load-slip relationship and the tensile force in the stud, resulting from the separation of the steel and concrete sections which influence the ultimate strength of shear connectors.

2.4 Flange Local Buckling

2.4.1 Previous Research

Research on inelastic flange local buckling of plain steel beams has been conducted by various investigators, including Haaijer[42][43], Lay[44] and Climenhaga[15][21]. All these studies began with a consideration of buckling of an isolated plate in a region of yielding.

Haaijer[42] analyzed local buckling by plate theory. The differential equation for an orthogonal anisotropic plate subjected to edge compression, as in Figure 2.16, has the form

$$D_x \frac{\partial^4 w}{\partial x^4} + 2H \frac{\partial^4 w}{\partial x^2 \partial y^2} + D_y \frac{\partial^4 w}{\partial y^4} = - \frac{t\sigma_x}{I} \frac{\partial^2 w}{\partial x^2} \qquad 2.11$$

where $2H = D_{xy} + D_{yx} + 4G_t$. The moduli D_x, D_y, D_{xy} and G_t were suggested from the incremental theory of plasticity taking the second invariant of the deviatoric stress tensor as the loading function. These moduli are functions of stress and strain, and Haaijer selected for his analysis the following values: $D_x = 3{,}200$ ksi, $D_y = 32{,}800$ ksi, $D_{xy} = D_{yx} = 8{,}100$ ksi and $G_t = 2{,}400$ ksi.

Lay[44] analyzed local buckling by employing torsional theory as shown in Figure 2.17(a). The torsional buckling equation is in the form of

$$E_t I_\omega \frac{\partial^4 \theta}{\partial z^4} - G_t J \frac{d^2\theta}{dz^2} + k\theta = - \frac{P_z}{r^2} \frac{d^2\theta}{dz^2} \qquad 2.12$$

Lay evaluated G_t on the basis of slip band theory which recognizes the basic discrimination of the behavior of steel in the region of yielding. This characteristic is not considered in the incremental theory. The ratio of inelastic to elastic shear moduli G_t/G, was determined as

$$\frac{G_t}{G} = \frac{2}{1 + \frac{h}{4(1+\nu)} \tan^2\alpha} \qquad 2.13$$

where α is the angle of slip plane as in Figure 1.17(b). Lay proposed the angle of slip plane is 45°, and Equation 2.13 becomes

$$\frac{G_t}{G} = \frac{2}{1 + \frac{h}{4(1 + \nu)}} \qquad 2.14$$

The warping constant I_ω and spring constant due to web buckling k were estimated as

$$I_\omega = \frac{7}{16}\left(\frac{b^3t^3}{144}\right) \qquad 2.15$$

$$k = \frac{G_t w^3}{3(d - 2t)} \qquad 2.16$$

Using these values for G_t, I_ω and k, the critical buckling load P_{cr} is determined as

$$P_{cr} = \frac{1}{r^2}\left\{G_t J + \left(\frac{n\pi}{L}\right)^2 EI_\omega + \left(\frac{L}{n\pi}\right)^2 k\right\} \qquad 2.17$$

By differentiating the critical load, P_{cr}, with respect to length L, the minimum buckling length is obtained as

$$\frac{L}{n} = \pi \sqrt[4]{\frac{E_t I_\omega}{k}} \qquad 2.18$$

Since the local buckling shape is one full wave, the ratio L/b is obtained from Equation 2.18 as

$$\frac{L}{b} = 0.713 \frac{t}{w}\left(\frac{A_f}{A_w}\right)^{\frac{1}{4}} \qquad 2.19$$

There is some question as to the validity of this expression, since it indicates that the minimum buckling length increases as the web thickness decreases, which is contrary to what might be expected.

Based on their respective analyses, Haaijer[42] and Lay[44] proposed maximum flange width-thickness ratios required to prevent local buckling.

Haaijer proposed

$$\frac{b}{2t} = \begin{cases} 8.16 & \text{for } \beta = 0.0 \\ 8.91 & \text{for } \beta = 0.1 \end{cases} \qquad 2.20$$

where β is a constant for web restraint.

Lay proposed

$$\frac{b}{2t} = 1.026\sqrt{G_t/\sigma_y} \qquad 2.21$$

In his study of local buckling of composite beams, Climenhaga [15][21] derived a relationship between the elastic-inelastic modular ratio, $h = E/E_t$, and the ratio of ultimate stress to yield stress, σ_u/σ_y, on the basis of tests. He proposed

$$\frac{b}{2t} = 0.348/\sqrt{\varepsilon_y(3.18 - \sigma_u/\sigma_y)} \qquad 2.22$$

An approximate method for obtaining the moment-rotation relationship after local buckling was proposed by Climenhaga[15], based on yield line theory developed for limit analysis of concrete slabs. A local buckling wave was first assumed as a series of straight lines

derived from yield lines as shown in Figure 2.18, and the web deformation was derived from a geometrical relationship for flange deformation. The moment-rotation relationship was then obtained by applying the principle of virtual work. Subsequent composite beam test results showed reasonable agreement, although the theory is quite conservative for stocky sections.

2.4.2 Proposed Analysis

In the past considerable attention has been concentrated on establishing flange proportions for plain steel beams which guarantee that local flange buckling does not occur prior to the onset of strain-hardening. It is necessary in the present study to develop a moment curvature relationship which extends into the strain-hardening range.

The basic equation for torsional buckling of a plate supported by a spring at its centerline[45] is expressed as

$$\frac{d^2}{dz^2}\left(EI_\omega \frac{d^2\theta}{dz^2}\right) - \frac{d}{dz}\left(GJ\frac{d\theta}{dz}\right) + k\theta = \frac{d}{dz}\left(r^2P\frac{d\theta}{dz}\right) \qquad 2.23$$

in which the warping rigidity EI_ω, St. Venant's torsional rigidity GJ, web restraint k and normal force P are all functions of z for a beam under varying moment.

Figure 2.19 indicates the variation in tangent modulus E_t with regard to strain. For a parabolic stress-strain relationship E_t decreases with increase in strain as shown in Figure 2.19(b). The strains measured in the plastic region in a tension test represent over-all

strains, as would be measured over the gage length of a strain measuring device. Based on the theory of Lüders lines, the plastic region is composed of an elastic zone, slip lines and a strain-hardened zone[42][43][46][47]. Therefore the tangent modulus in the plastic region is indeterminate.

The value of the inelastic shear modulus G_t in compression has been proposed by Bijlaard[48], Haaijer[42], Lay[44] and others on the basis of deformation theory, incremental theory and slip band theory. Various expressions for G_t are tabulated in Table 2.1.

The finite difference equation equivalent of Equation 2.23 at an arbitrary point i may be written as

$$a_{-2}\theta_{i-2} + a_{-1}\theta_{i-1} + a_0\theta_i + a_1\theta_{i+1} + a_2\theta_{i+2} =$$

$$b_{-1}\theta_{i-1} + b_0\theta_i + b_1\theta_{i+1} \qquad 2.24$$

where $a_{-2} = \lambda^2 c_{i-1}$

$$a_{-1} = -2\lambda^2(c_{i-1} - c_i) - (d_{i-1} + d_i)/2$$

$$a_0 = \lambda^2(c_{i-1} + 4c_i + c_{i+1}) + (d_{i-1} + 2d_i + d_{i-1})/2$$

$$a_1 = -2\lambda^2(c_i + c_i + 1) - (d_i + d_{i+1})/2$$

$$a_2 = \lambda^2 c_{i+1}$$

$$b_{-1} = (P_{i-1} + P_i)r^2/2$$

$$b_0 = (P_{i-1} + 2P_i + P_{i+1})r^2/2$$

$$b_1 = (P_i + P_{i+1})r^2/2$$

and $$c_i = (E_t I_\omega)_i,\ d_i = (G_t J)_i$$

The boundary conditions for a flange plate as shown in Figure 2.20(a) may be considered as torsionally simple supports, that is, the rotation θ and the second derivative of rotation θ'' are equal to zero. However, the boundary conditions for a flange plate with multiple bearing stiffeners as in Figure 2.20(b) may be taken as a torsionally fixed support, i.e., $\theta = \theta' = 0$.

The warping constant I_ω for a thin rectangular section is equal to $b^3t^3/144$[149][150] and Saint-Venant's torsional constant J for a thin rectangular section is approximately $bt^3/3.0$ or more accurately $bt^3(1 - 0.63t/b)/3.0$[51]. The web restraint constant k according to Lay is $G_t w^3/3.0(d - 2t)$.

2.5 Lateral Buckling

2.5.1 Introduction

If the compression flange is reinforced with a cover plate, the resistance to local buckling is increased and lateral buckling may

occur prior to local buckling. Piepgrass[4] observed lateral buckling under negative moment in composite beams with a cover plate on the compression flange. The ultimate moment for the beams tested by Piepgrass was 3 to 7 percent higher than the plastic moment, and the curvature at lateral buckling was about five times the curvature at initial yielding. To simulate conditions in composite beams in negative bending, Climenhaga[15] tested steel beams with a cover plate on the tension flange in place of a concrete slab with longitudinal reinforcement. Lateral buckling occurred in beams where 5 x 3 RSJ steel sections were used.

The lateral buckling configuration for a composite beam is illustrated in Figure 2.21. This configuration indicates that only the inverted tee section need be considered in a lateral buckling analysis. Elastic torsional buckling of a tee section with lateral restraint at the end of the stem has been analyzed for the case of axial load by Bleich[52] on the basis of thin-walled beam theory and Bulson[53] on the basis of plate theory.

Lateral buckling of an inverted tee section in a composite beam due to axial force and bending may occur in the elastic-plastic range. Since plate theory is complicated in a plastic region, thin-walled beam theory is used in the elastic-plastic range. General equations for thin-walled beams have been developed by Vlasov[49], Oden[50] and others. Vlasov's theory, later modified by Rajasekaran and Murray[54], is applied herein. Based on the assumption that a cross section remains plane, a lateral configuration for an inverted tee section is idealized in Figure 2.21(b).

2.5.2 Lateral Buckling Analysis

The stress distribution in a composite section under negative moment is shown in Figure 2.22(a). It is assumed that concrete can not transfer tensile stress, but the longitudinal slab reinforcement is effective in tension. Isolating the inverted tee section, when lateral buckling occurs, an external force T_k must be applied along the end of the stem to balance the forces in the reinforcement and the upper flange as shown in Figure 2.22(b). The stress resultant in the inverted tee section may be separated into components due to normal force N_z and due to bending moment M_x for the principal coordinates shown in Figure 2.22(c). When the section rotates about the hinge C, i.e., when the section buckles, additional indeterminate forces denoted as q_x^* and q_y^* in the x and y directions in Figure 2.22(b) occur at the hinge location C, because of restraint in the x and y directions.

For the above-mentioned conditions, buckling equations can be obtained from the general equations derived in Appendix A as follows:

$$(EI_x\xi'')'' - \{N_z(\xi' + a_y\theta')\}' + (M_x\theta')' + T_k x_k + (M_k\theta')' = q_y^* \qquad 2.25(a)$$

$$(EI_y\eta'')'' - \{N_z(\eta' - a_x\theta')\}' + T_k y_k = q_y^* \qquad 2.25(b)$$

$$(EI_\omega\theta'')'' - (GJ\theta')' - \{N_z(-a_x\eta' + a_y\xi')\}' + (M_x\xi')' - (M_\rho\theta')' + T_k\omega_k - (M_k\xi')' = q_y^*(c_x - a_x) - q_x^*(c_y - a_y) \qquad 2.25(c)$$

where c_x and c_y are x and y coordinates of the hinge location, and a_x and a_y are coordinates of the shear center, which is located at the junction of the web and the bottom flange.

The coordinates c_x, a_x, x_k and ω_k are zero, since the section is symmetrical about the y axis. Displacements ξ_c and η_c are zero in the x and y directions at the location C. Therefore displacements ξ and η become functions of θ as defined by

$$\xi = (c_y - a_y)\theta \qquad 2.26(a)$$

$$\eta = -(c_x - a_x)\theta \qquad 2.26(b)$$

The coordinates a_x, c_x, x_k and ω_k are zero as shown in Figure 2.22(b). Substituting Equations 2.26 into Equations 2.25, the lateral buckling equation can be expressed as a function of θ by

$$(EI_{\omega c}\theta'')'' - (GJ\theta')' = (M_\rho\theta')' \qquad 2.27$$

where $I_{\omega c} = I_\omega + (c_y - a_y)^2 I_y$, which is a warping constant with respect to the hinge location C, and M_ρ is defined as

$$M_\rho = \int\sigma_z\{x^2 + (y - c_y)^2\}dA \qquad 2.28$$

The local buckling equation, Equation 2.23, is developed as a particular case of Equation 2.27 by setting c_y=a_y and a constant stress σ_z,

and by adding a term for torsional restraint by web. The hinge location for local flange buckling is assumed to be at the junction of the lower flange and the web.

The warping constant $I_{\omega c}$ with respect to hinge location C, shown in Figure 2.22(b), is given by $b^3(d_w + t/2)^2/12$ from thin-walled beam theory. The warping constant $I_{\omega c}$ for an inverted-tee section with a cover plate on the flange is evaluated as

$$I_{\omega c} = \{b^3(d_w + t/2)^2 t + b_p^3(d_w + t + t_p/2)^2 t_p\}/12 \qquad 2.29$$

The torsional constant J for a flange with a cover plate is defined as

$$J = \{1 - 0.63(t + t_p)/b_n\} b_n (t + t_p)^3/3.0 +$$

$$\{1 - 0.63t_w/(b_n - b_w)\}(b_n - b_w)t_w^3/3.0 \qquad 2.30$$

where b_n and b_w are the smaller and the larger of the widths of the flange and cover plate, and t_w is the thickness of the plate corresponding to b_w.

For the case where the difference between b_n and b_w is small, the second term may be neglected. For example, the ratio of the second term to first term is 2.7 percent for Piepgrass' test beams. The torsional constant may be expressed for such cases as

$$J = \{1 - 0.63(t + t_p)/b_n\, b_n (t + t_p)^3\}/3.0$$

TABLE 2.1 VALUES OF INELASTIC SHEAR MODULUS

SOURCE	INELASTIC SHEAR MODULUS G_t
BLEICH[52]	$\frac{E}{2(1+\nu)\sqrt{h}}$
KAUFMANN[55]	$\frac{E}{(1+\nu)(h+1)}$
BIJLAARD[48]	$\frac{E_{sec}}{3}$
HANDELMAN AND PRAGER[56]	$\frac{E}{2(1+\nu)}$
HAAIJER[42]	2400 Ksi
LAY[44]	$\frac{E}{(1+\nu) + h/4}$

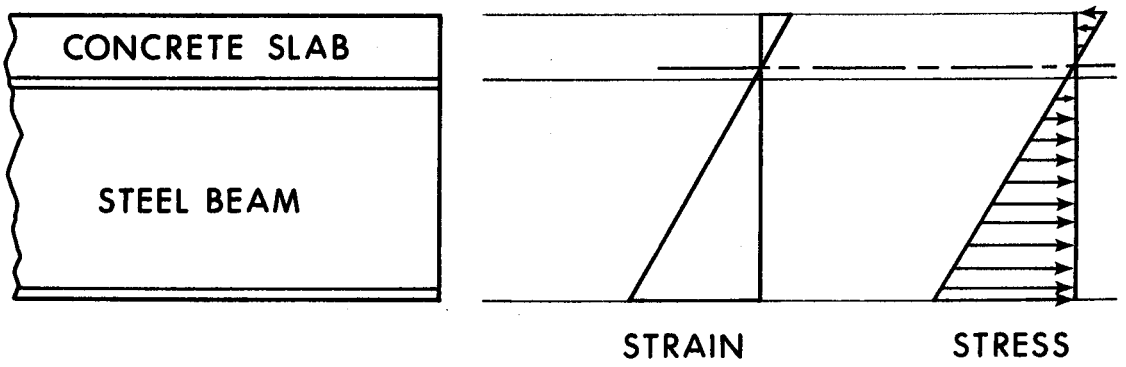

POSITIVE MOMENT REGION

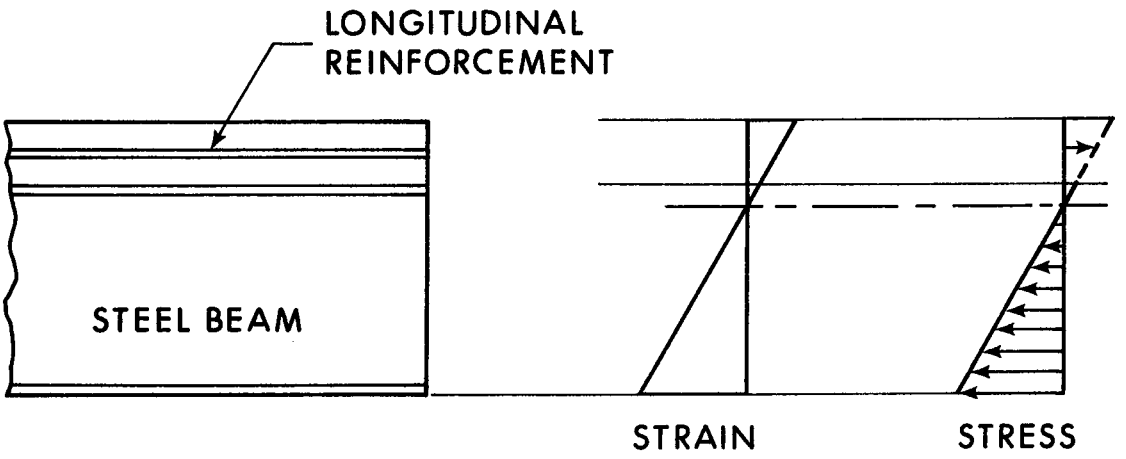

NEGATIVE MOMENT REGION

FIGURE 2.1 ELASTIC STRAIN AND STRESS DISTRIBUTIONS FOR COMPOSITE BEAMS

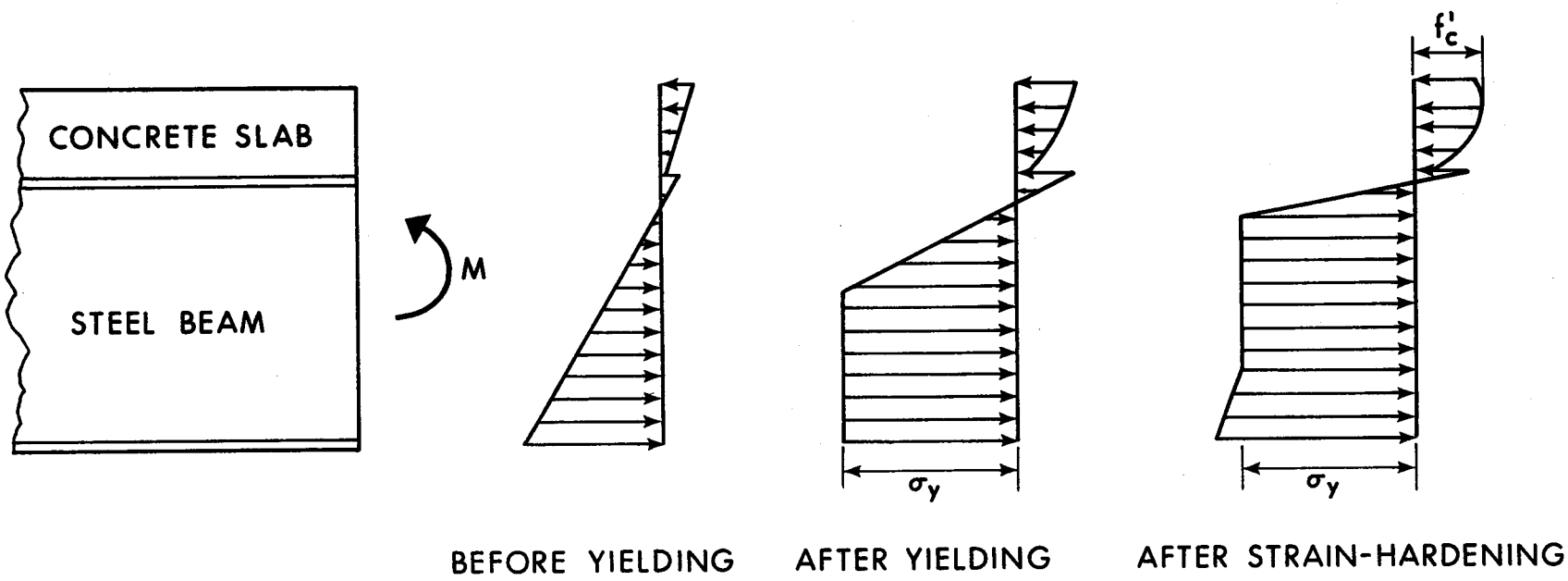

FIGURE 2.2 STRESS DISTRIBUTIONS IN A POSITIVE MOMENT REGION

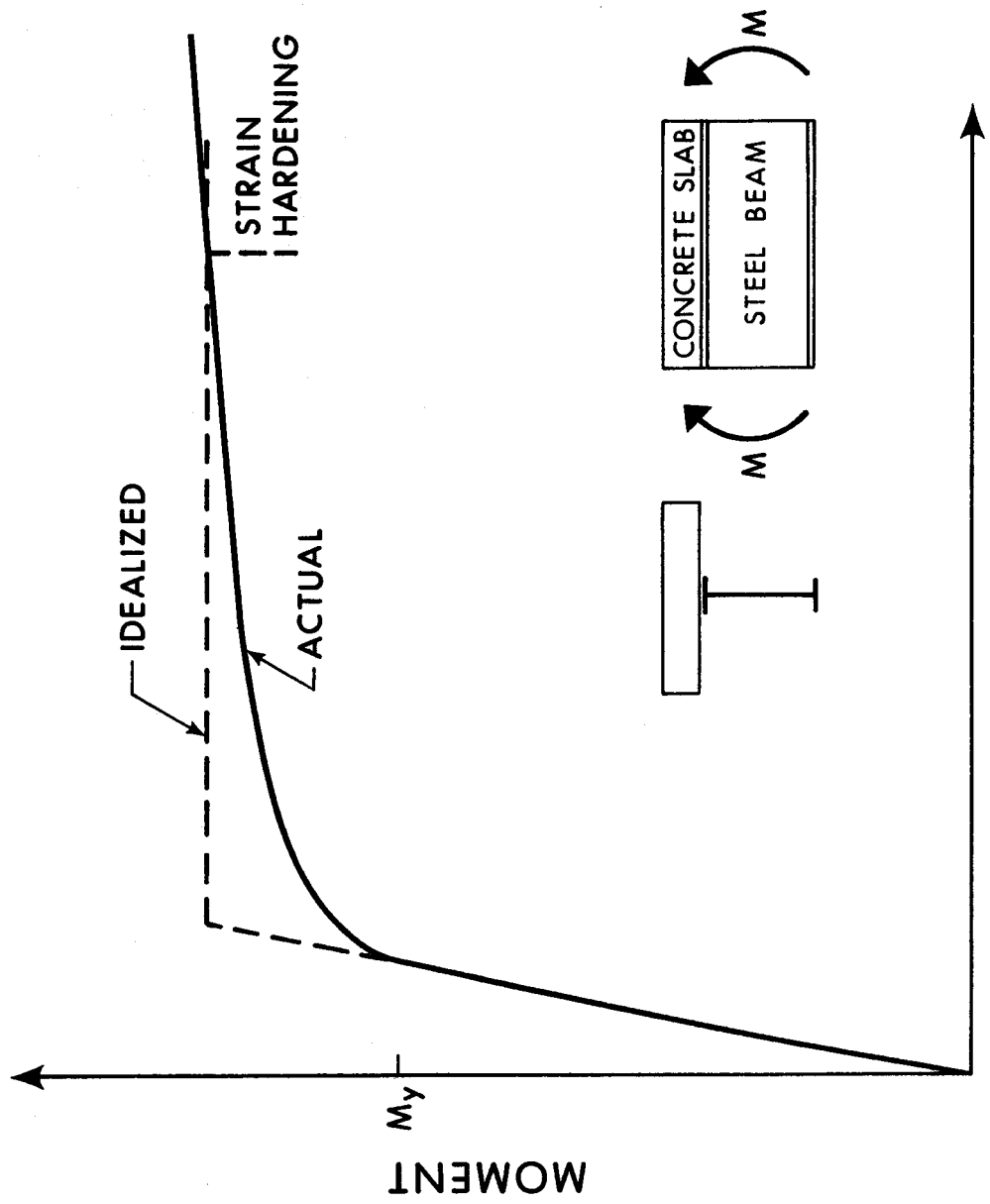

FIGURE 2.3 MOMENT-CURVATURE RELATIONSHIP FOR POSITIVE MOMENT

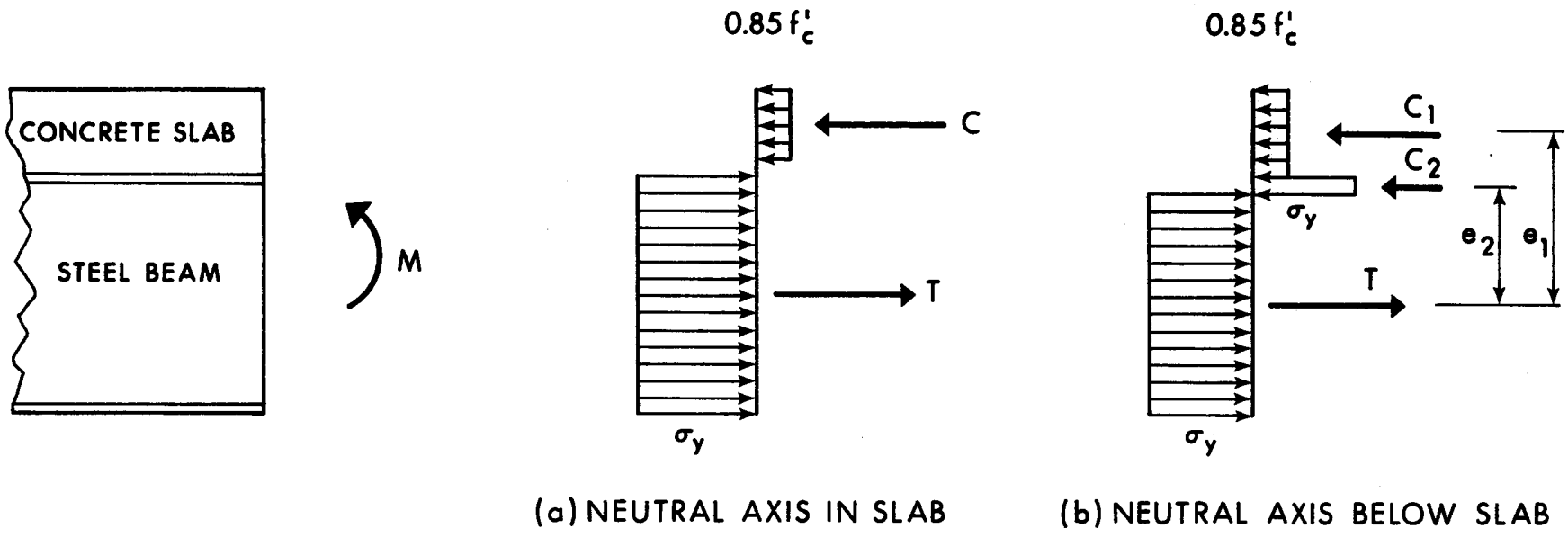

FIGURE 2.4 IDEALIZED STRESS CONDITIONS AT ULTIMATE MOMENT IN POSITIVE BENDING

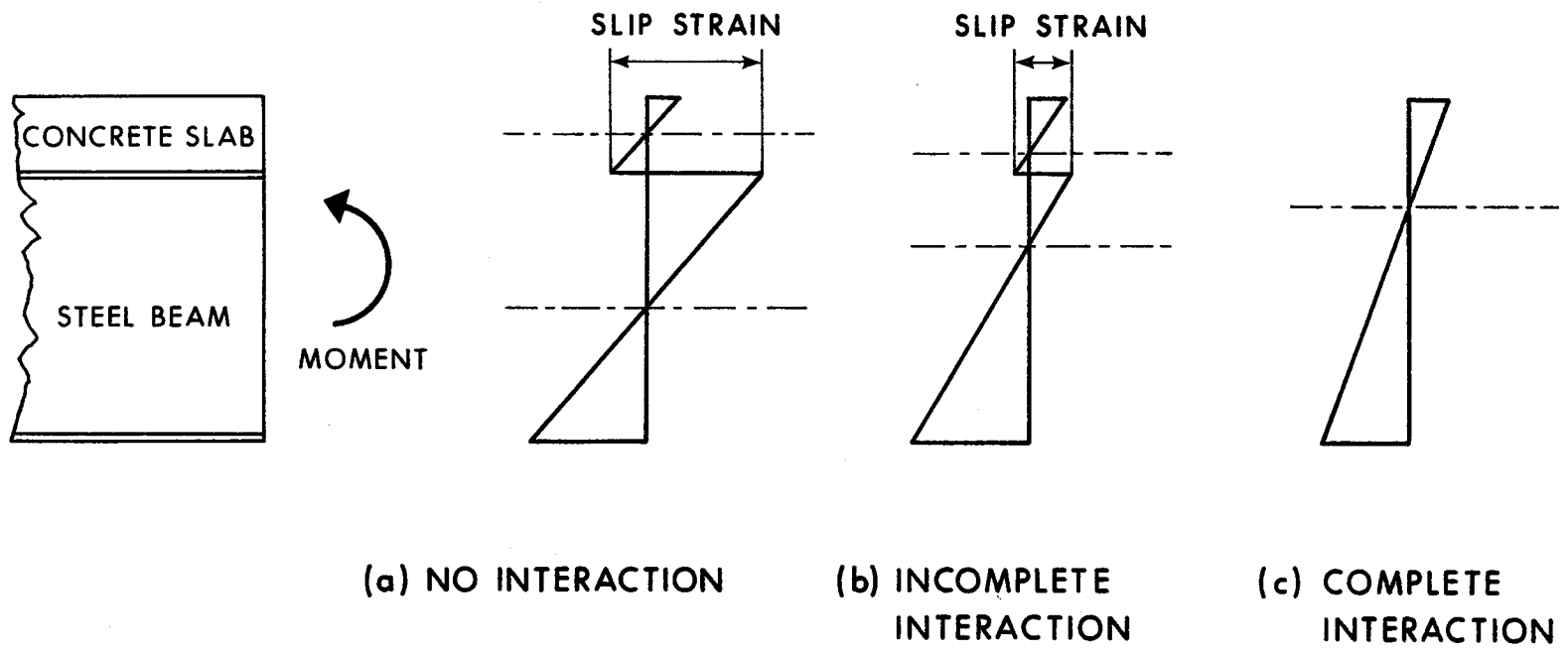

FIGURE 2.5 EFFECT OF INTERACTION ON STRAIN DISTRIBUTION

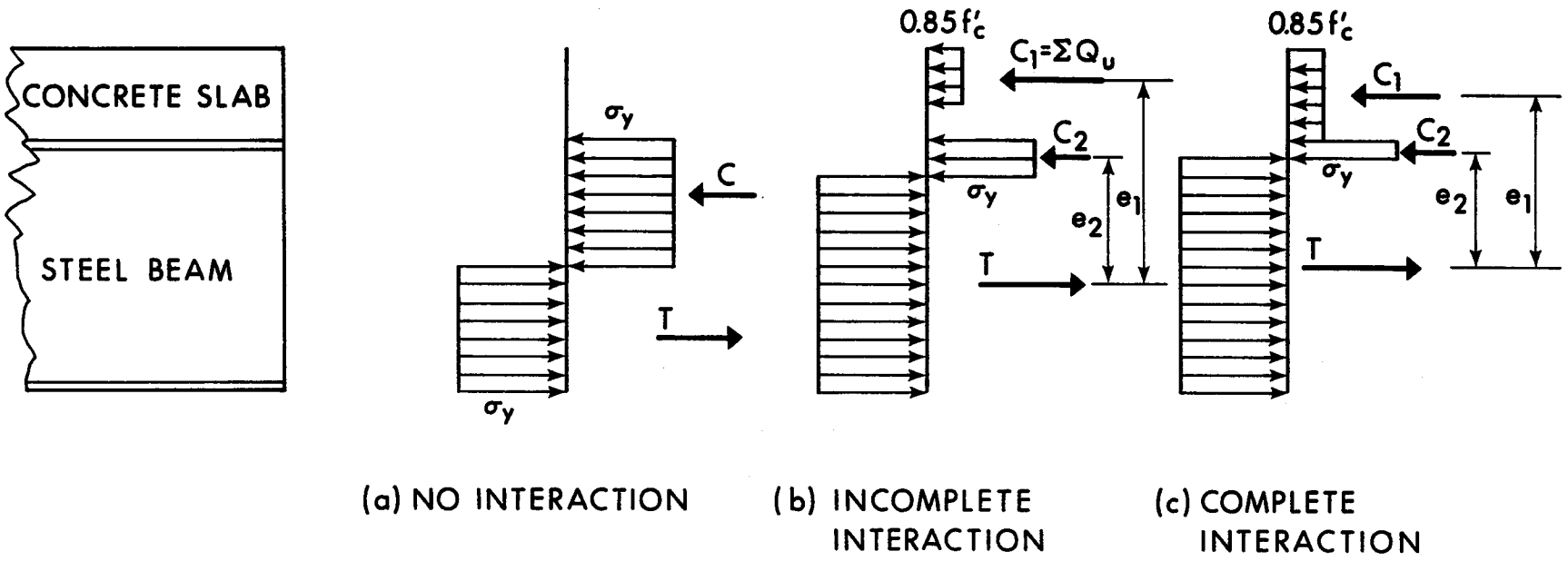

FIGURE 2.6 EFFECT OF INTERACTION ON IDEALIZED STRESS DISTRIBUTION AT ULTIMATE MOMENT

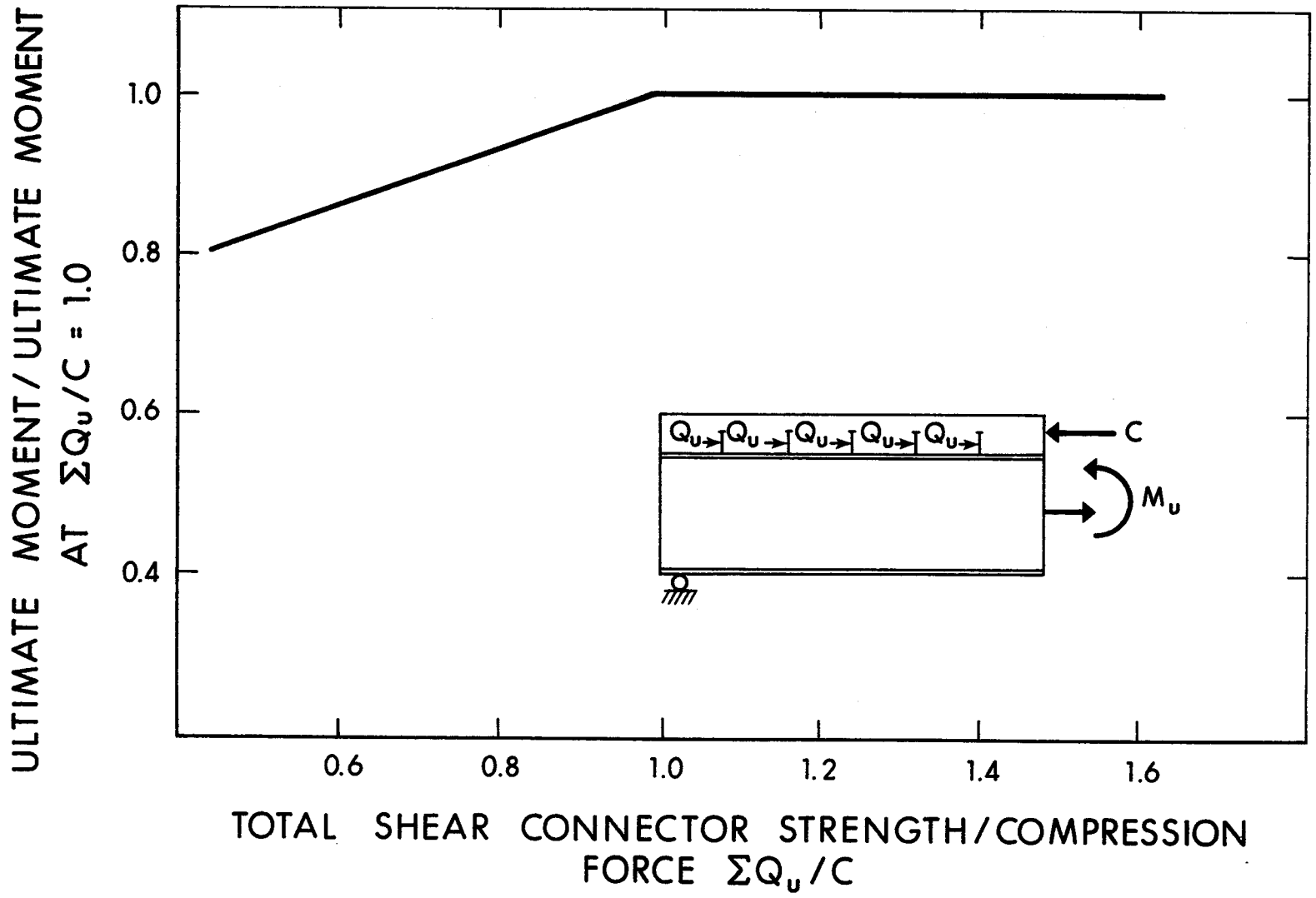

FIGURE 2.7 RELATIONSHIP BETWEEN SHEAR STRENGTH AND MOMENT CAPACITY (AFTER SLUTTER AND DRISCOLL[24])

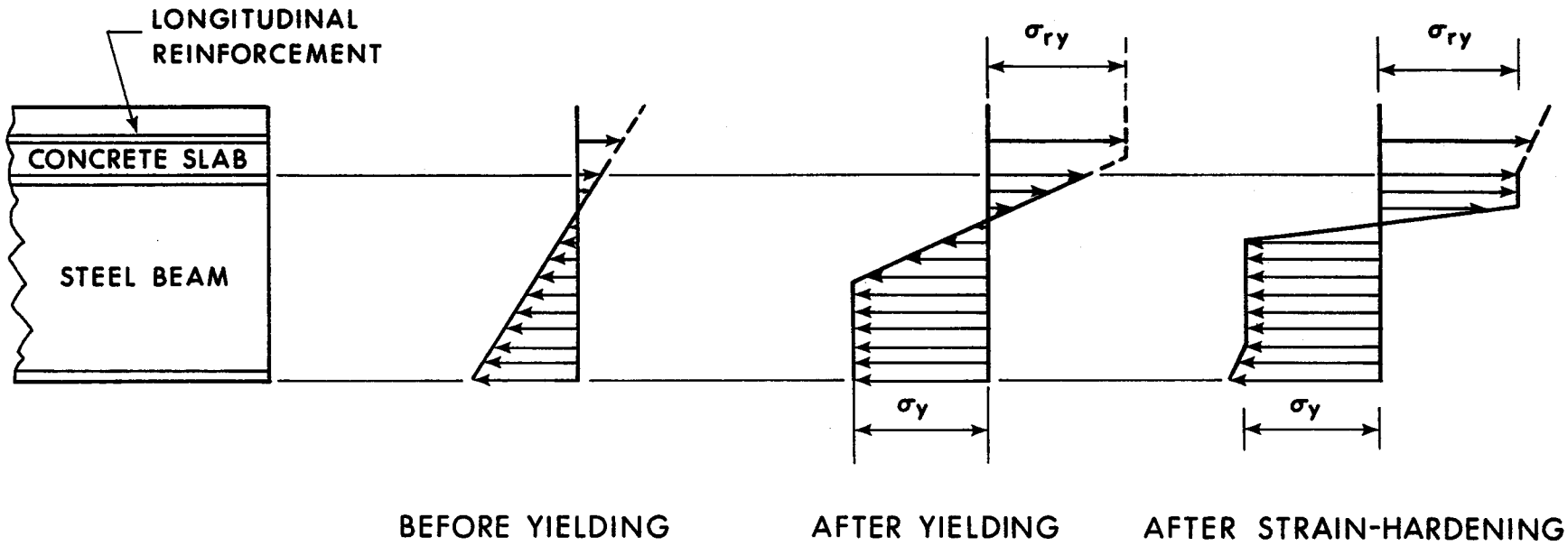

FIGURE 2.8 STRESS DISTRIBUTION IN A NEGATIVE MOMENT REGION

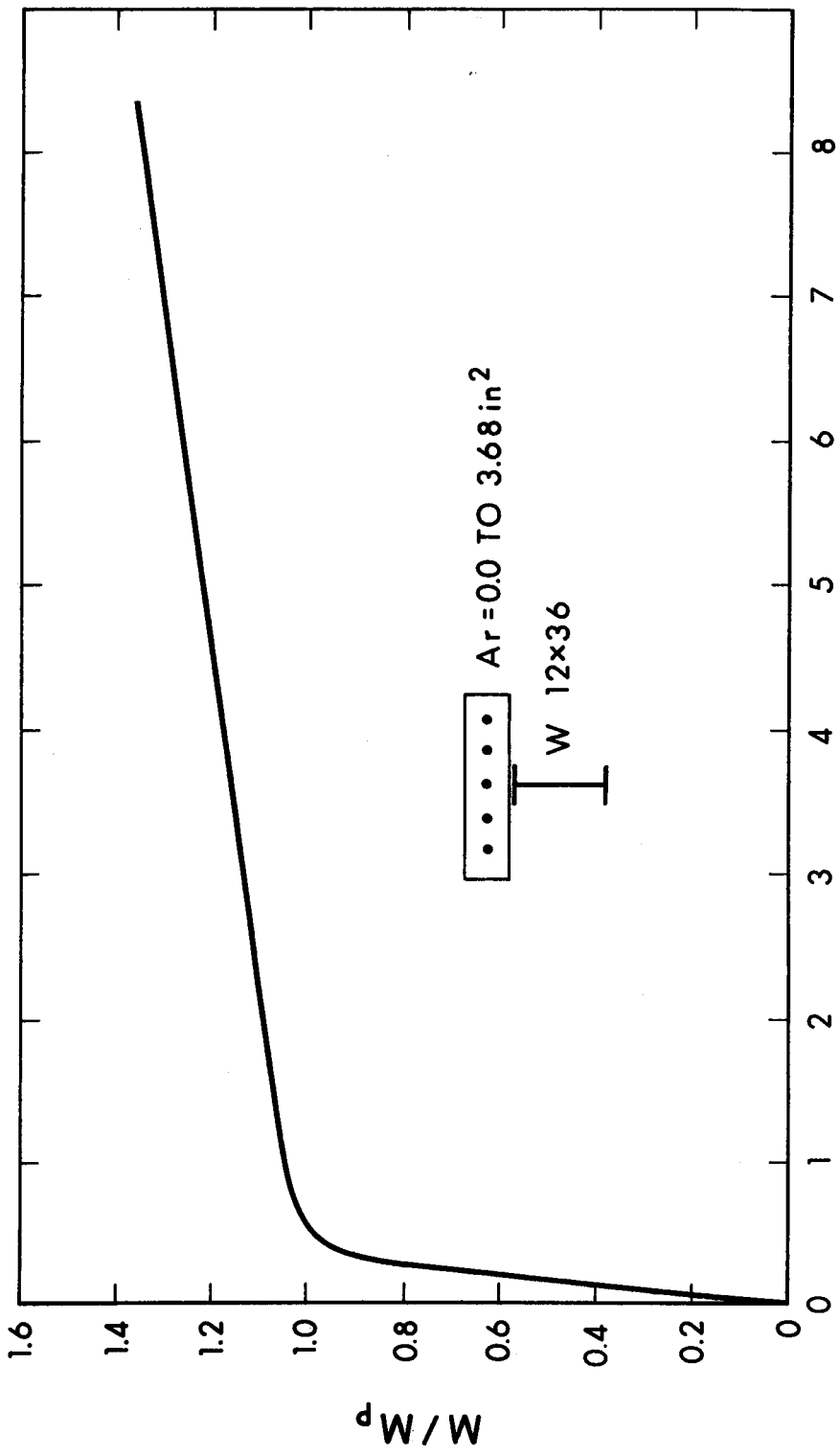

FIGURE 2.9 MOMENT-CURVATURE RELATIONSHIP IN NEGATIVE BENDING (AFTER DAVISON[5])

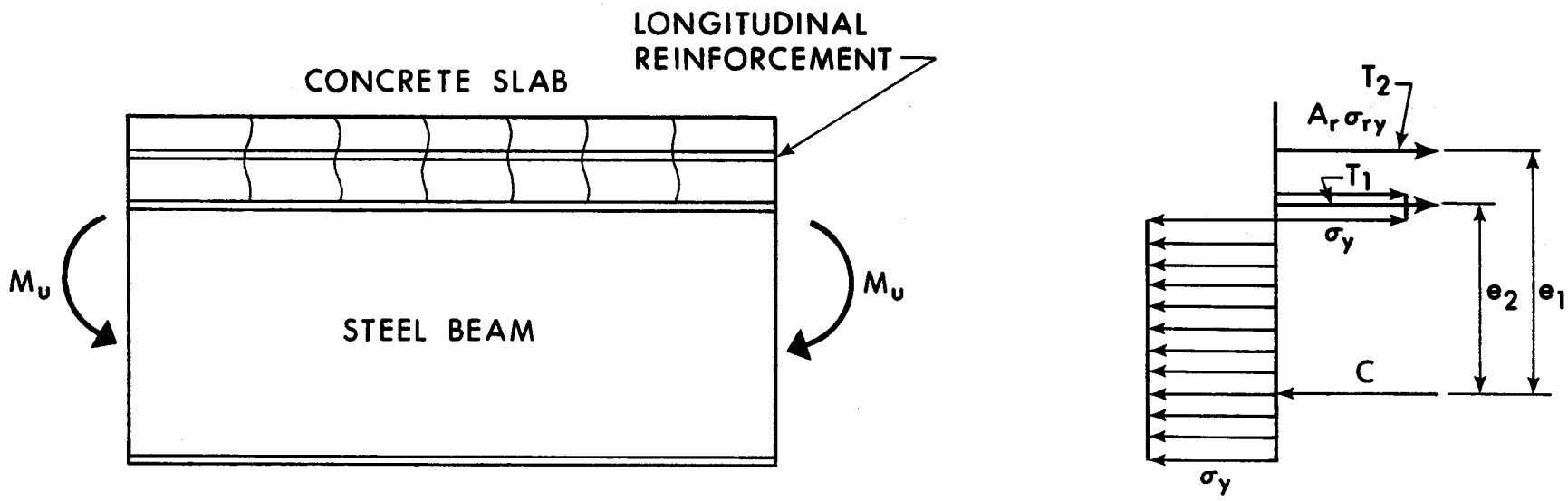

FIGURE 2.10 IDEALIZED STRESS DISTRIBUTION AT ULTIMATE MOMENT IN NEGATIVE BENDING

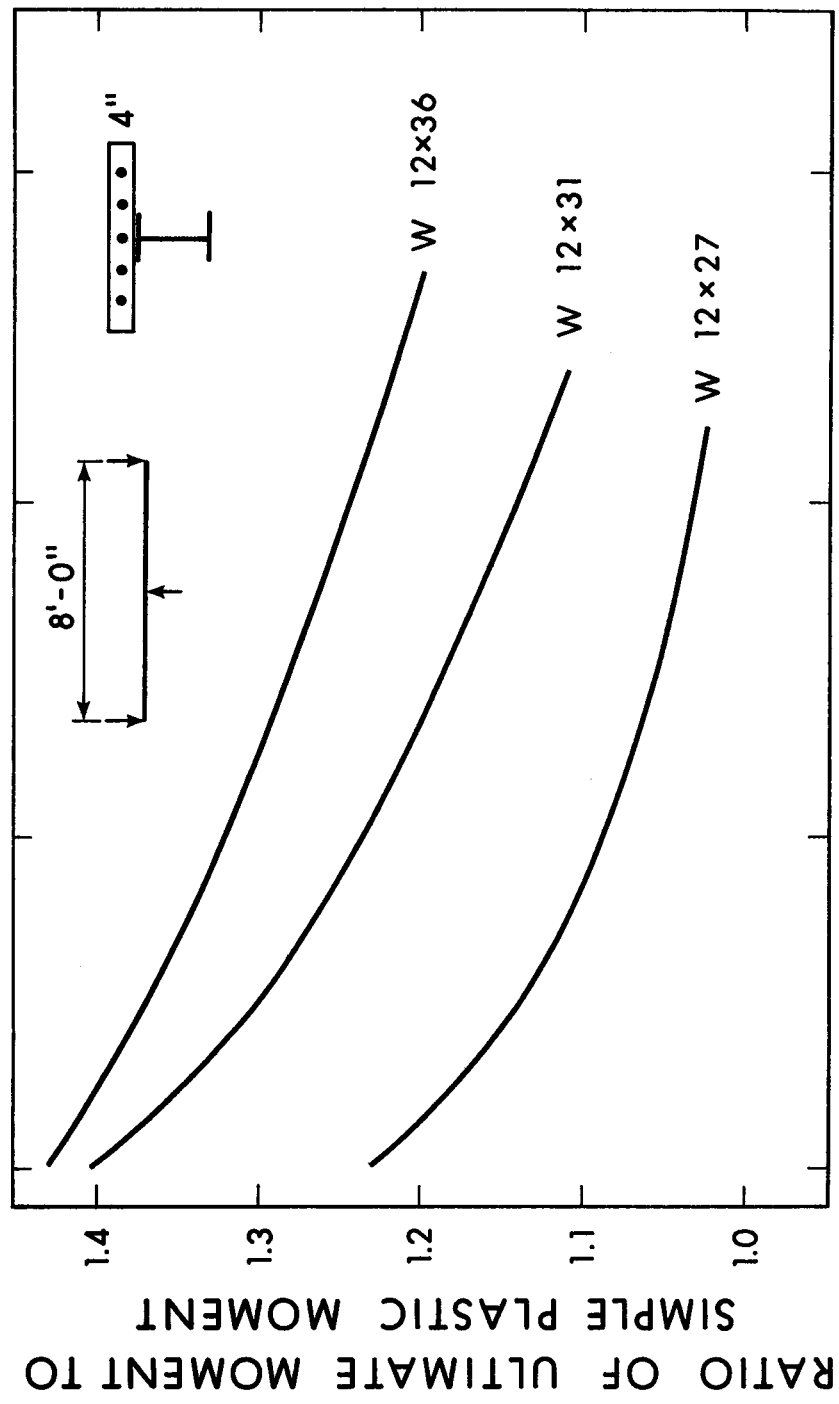

FIGURE 2.11 RELATIONSHIPS BETWEEN ULTIMATE MOMENT AND AREA OF LONGITUDINAL REINFORCEMENT (AFTER LEVER[6])

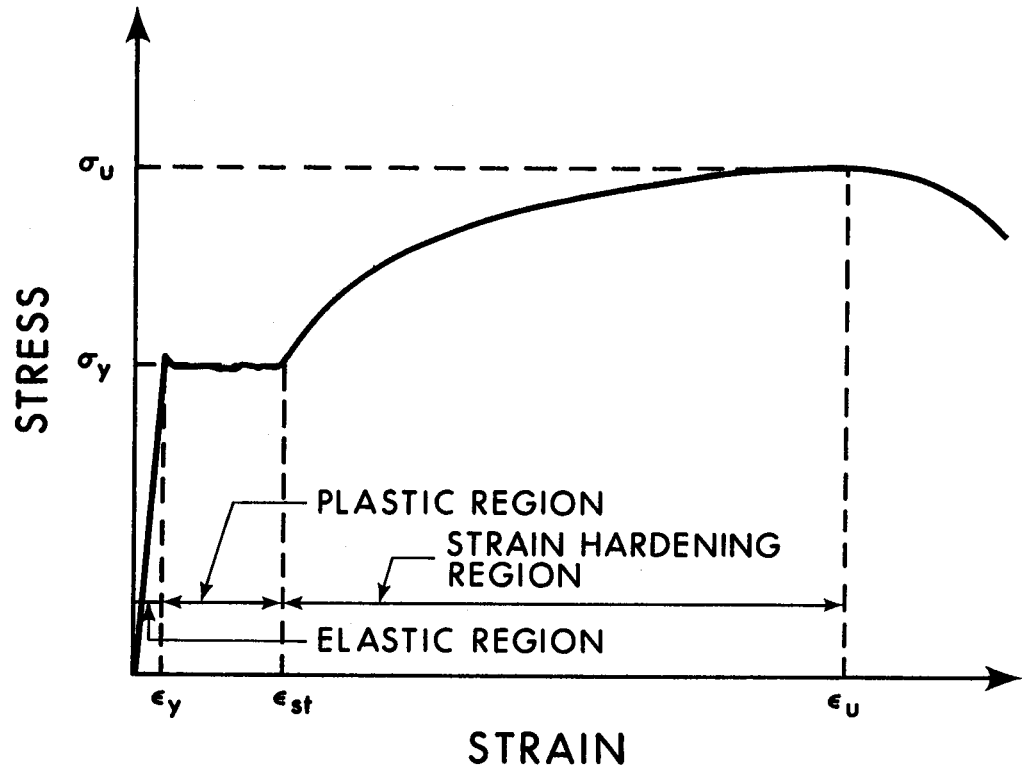

(a) TYPICAL STRESS-STRAIN RELATIONSHIP

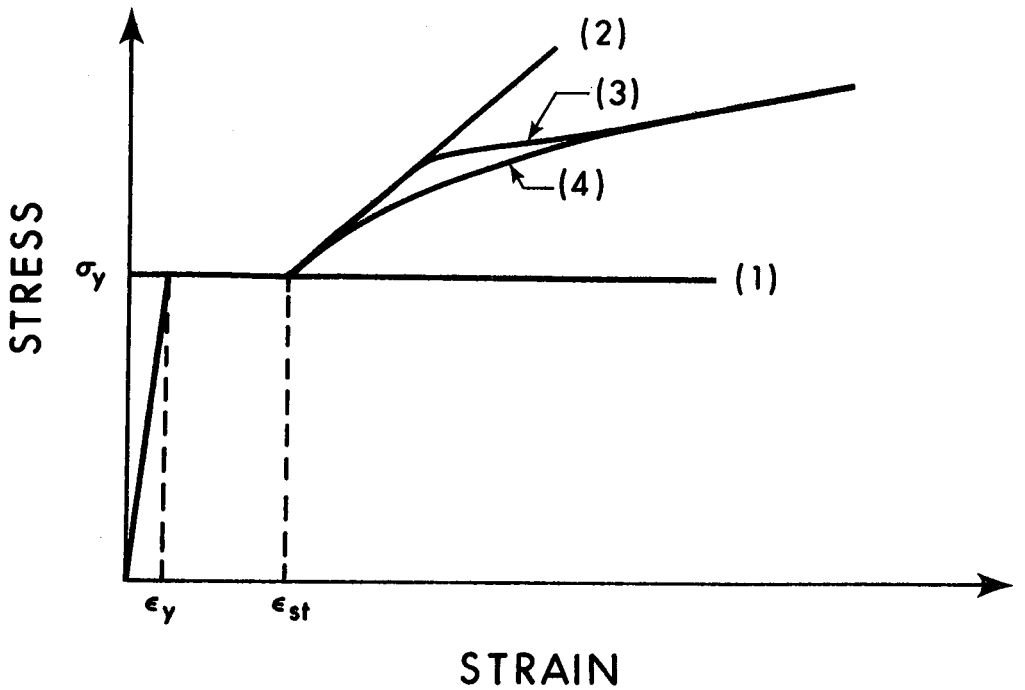

(b) IDEALIZED STRESS-STRAIN REALTIONSHIPS

FIGURE 2.12 STRESS-STRAIN RELATIONSHIPS FOR STRUCTURAL STEEL

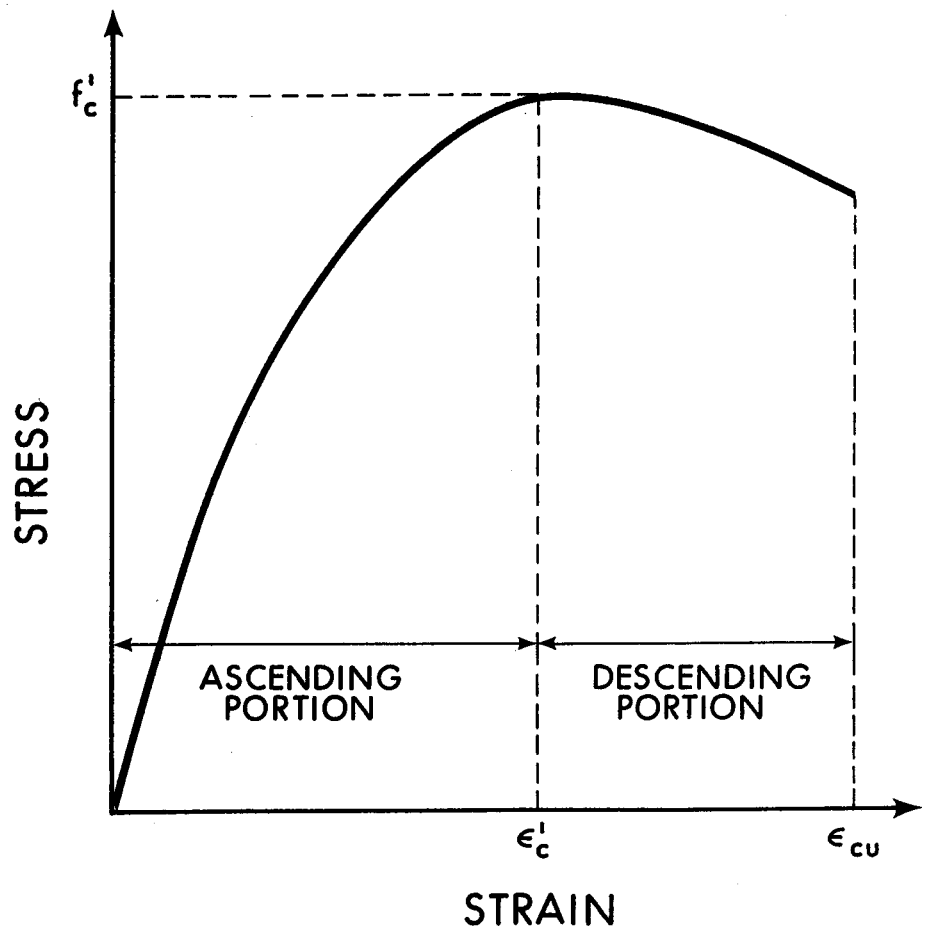

FIGURE 2.13 TYPICAL STRESS-STRAIN RELATIONSHIP FOR CONCRETE

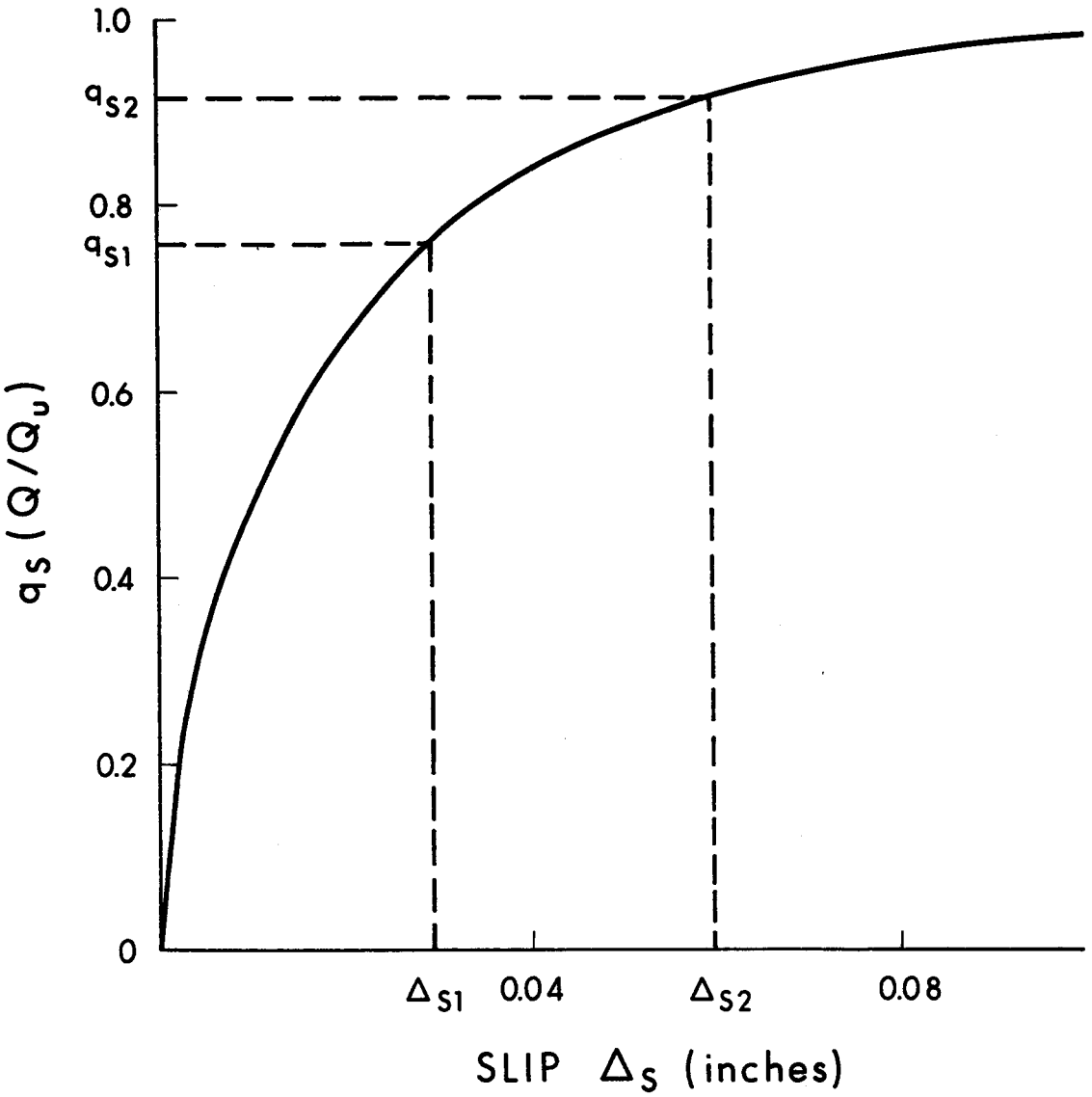

FIGURE 2.14 TYPICAL LOAD-SLIP RELATIONSHIP FOR STUD SHEAR CONNECTORS (AFTER MAINSTONE ET AL[40] AND YAM ET AL[41])

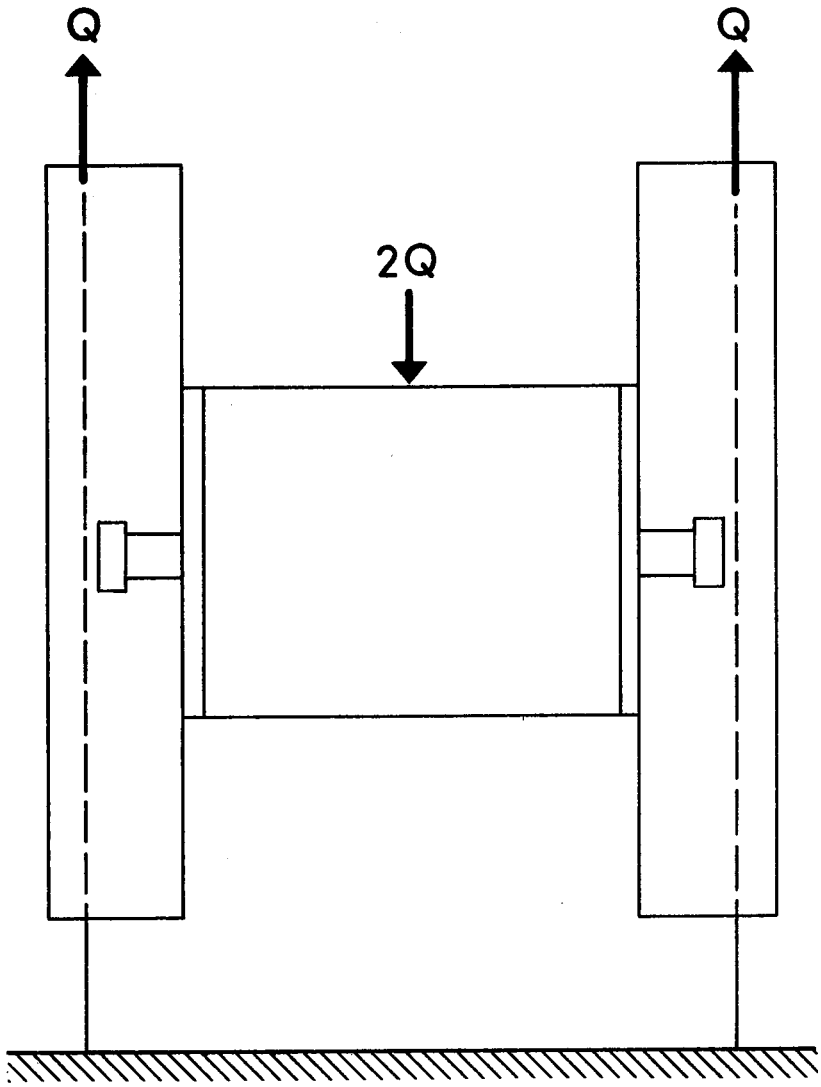

FIGURE 2.15 PUSH-OUT TEST FOR CONNECTORS SET IN SLABS IN TENSION (AFTER VAN DALEN[13])

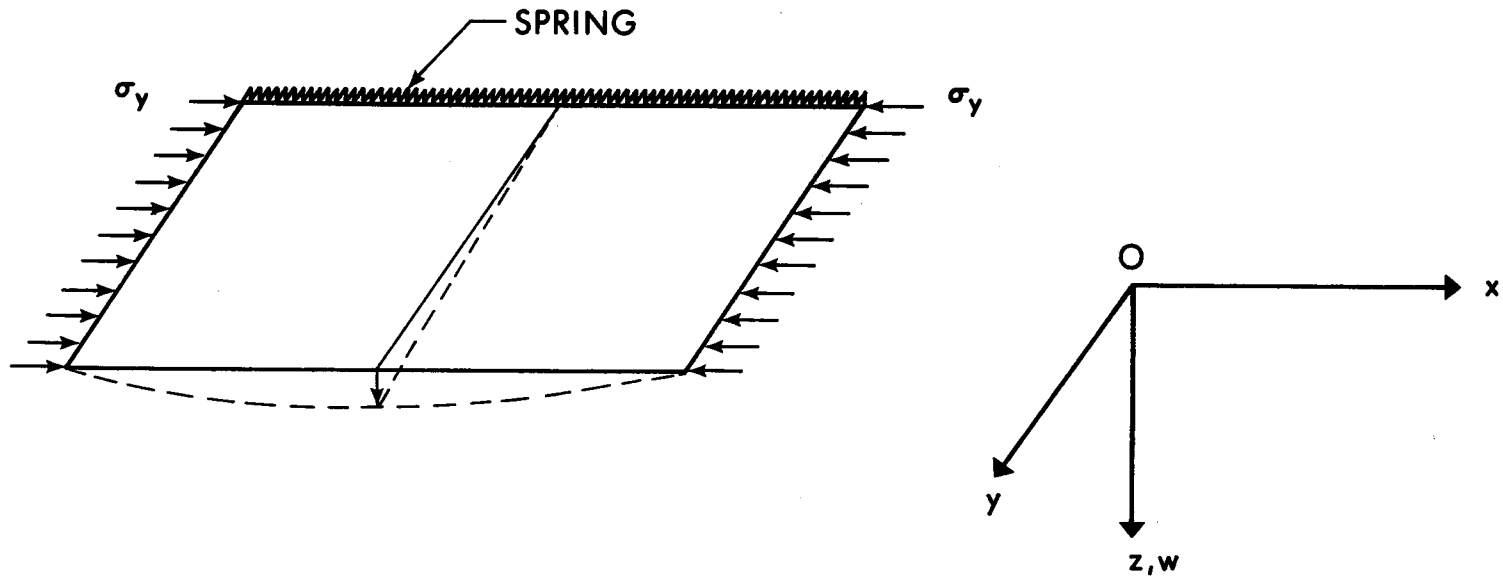

FIGURE 2.16 IDEALIZED PLATE BUCKLING MODEL (AFTER HAAIJER[42])

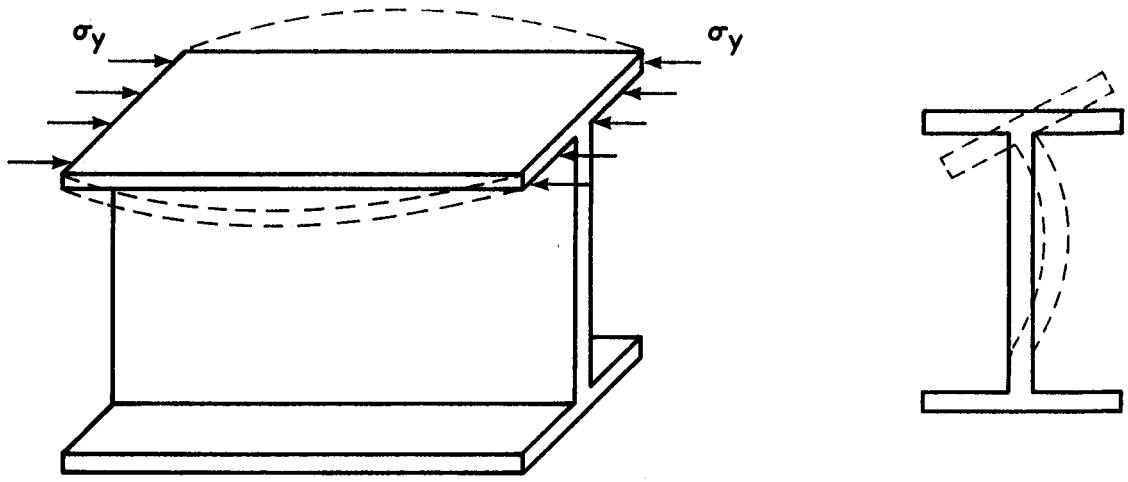

(a) DEFORMED SHAPE

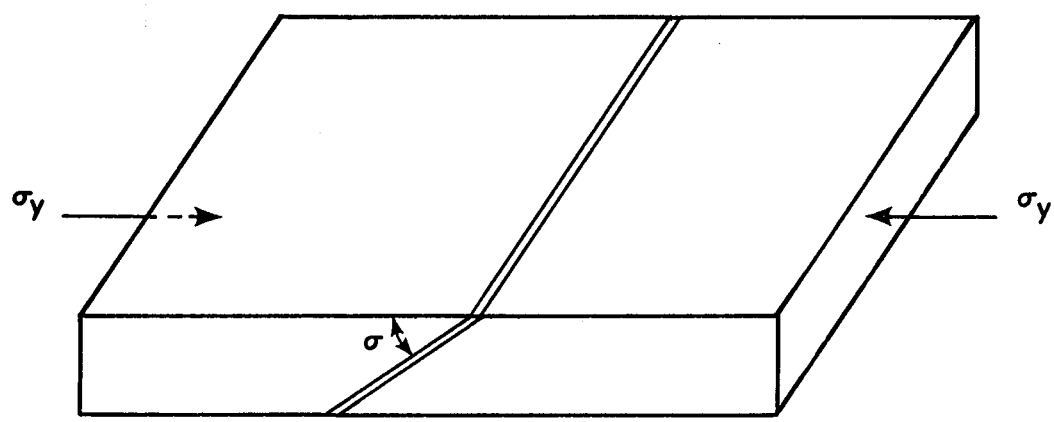

(b) SLIP PLANE

FIGURE 2.17 LOCAL BUCKLING CONDITIONS (AFTER LAY[44])

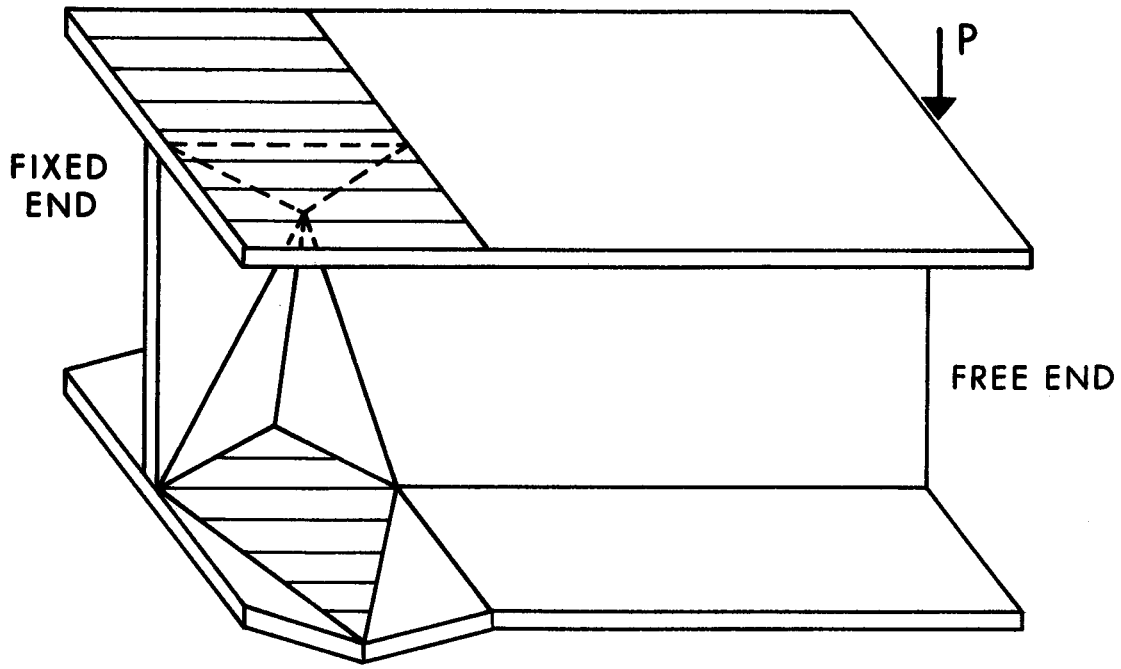

COMPLETE CONFIGURATION

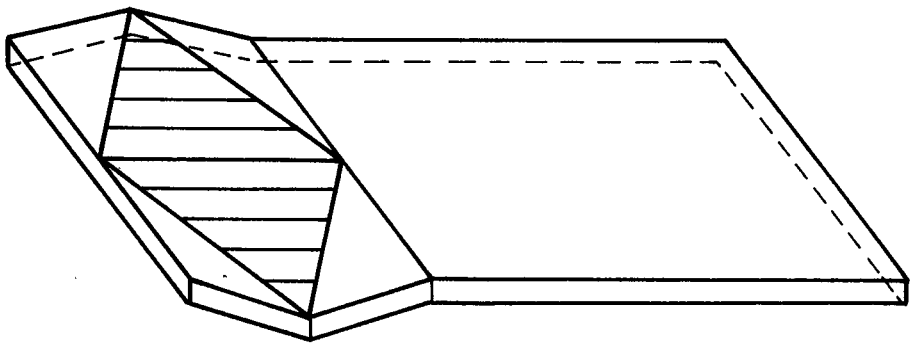

COMPRESSION FLANGE CONFIGURATION

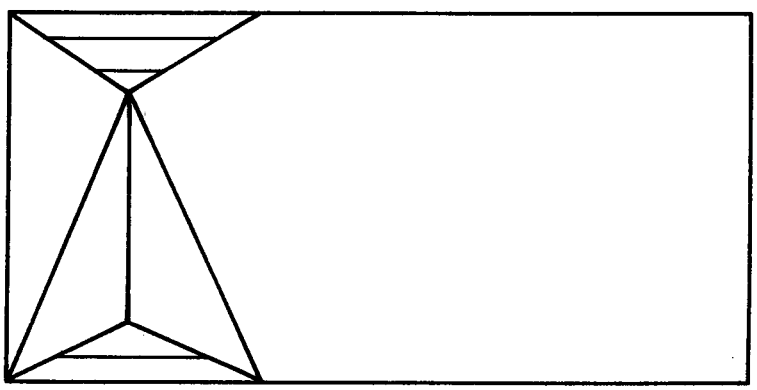

WEB CONFIGURATION

FIGURE 2.18 IDEALIZED SHAPE OF LOCAL BUCKLE (AFTER CLIMENHAGA[15])

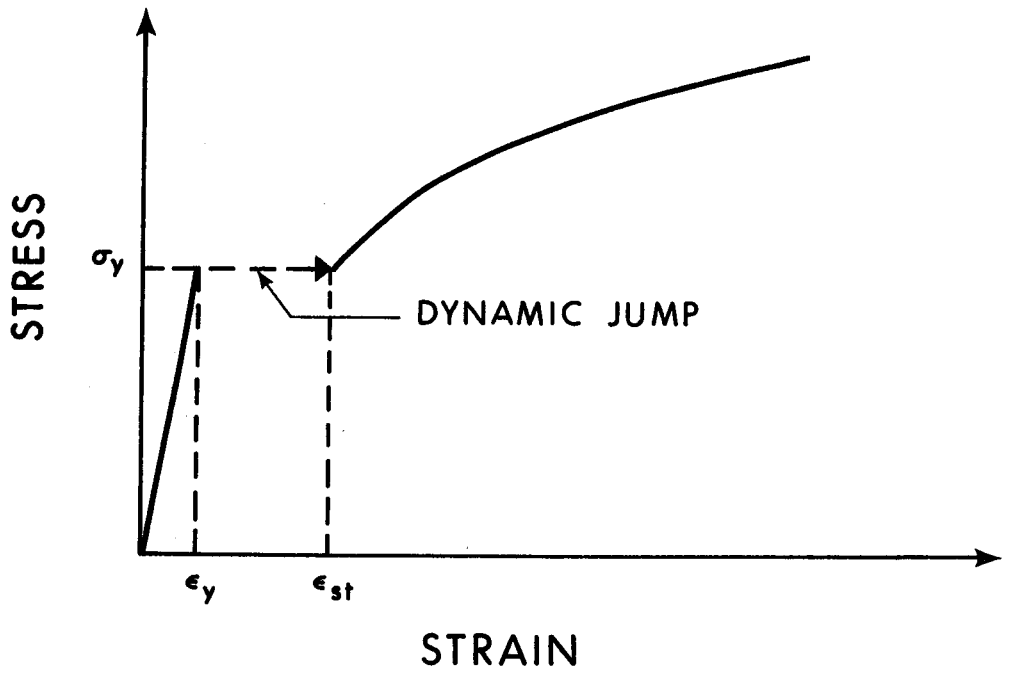

(a) STRESS - STRAIN RELATIONSHIP

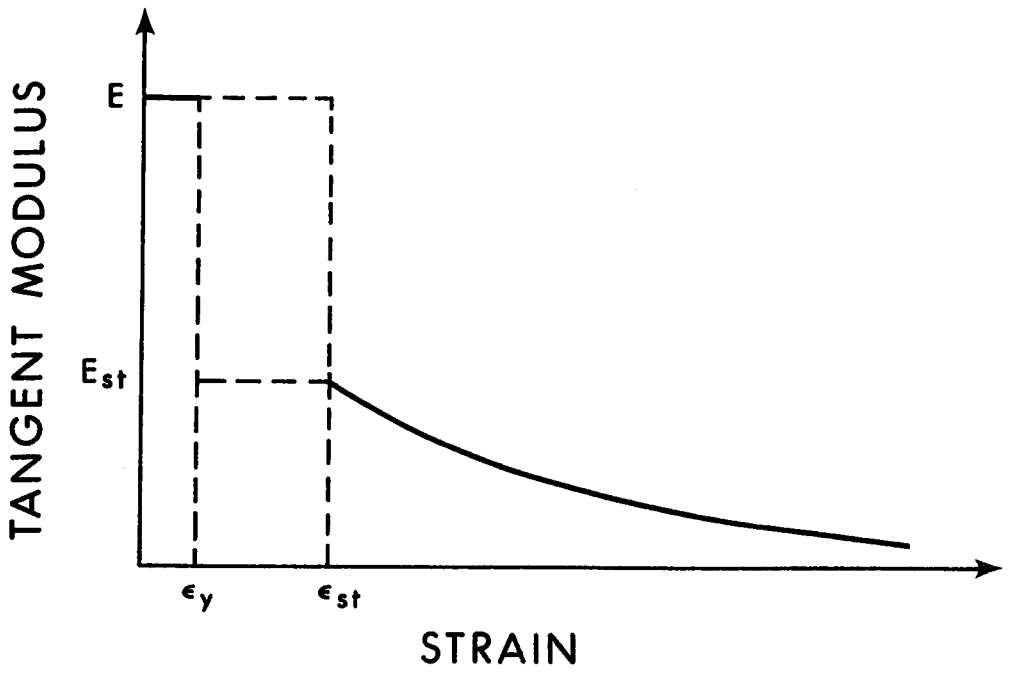

(b) TANGENT MODULUS - STRAIN RELATIONSHIP

FIGURE 2.19 RELATIONSHIP BETWEEN TANGENT MODULUS AND STRAIN

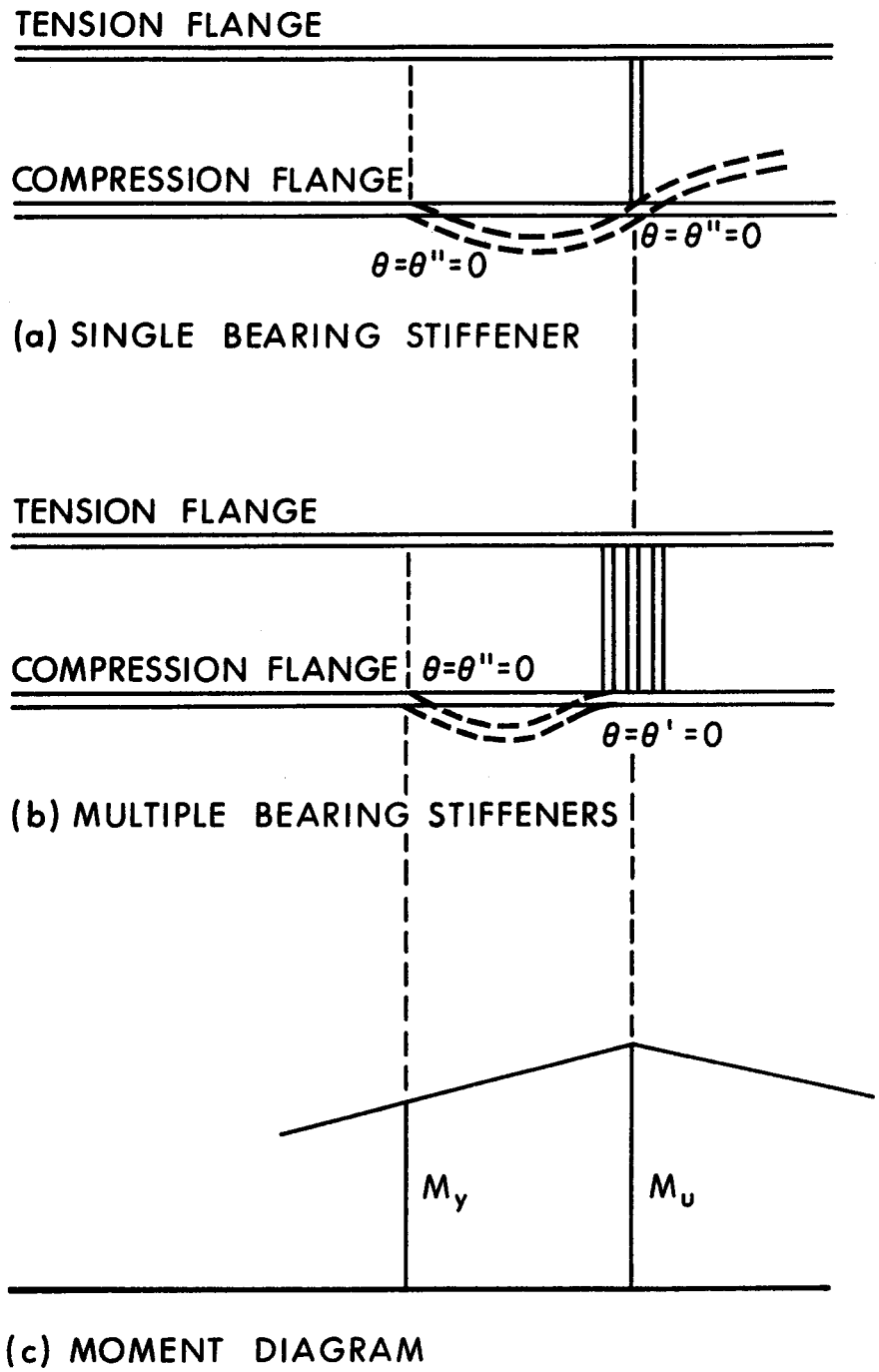

FIGURE 2.20 BOUNDARY CONDITIONS FOR LOCAL BUCKLING AT AN INTERIOR SUPPORT IN A CONTINUOUS BEAM

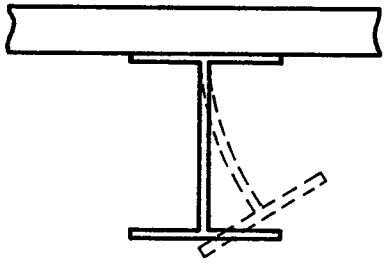

(a) ACTUAL BUCKLING CONFIGURATION

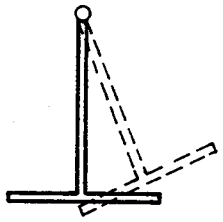

(b) BUCKLING MODEL USED IN ANALYSIS

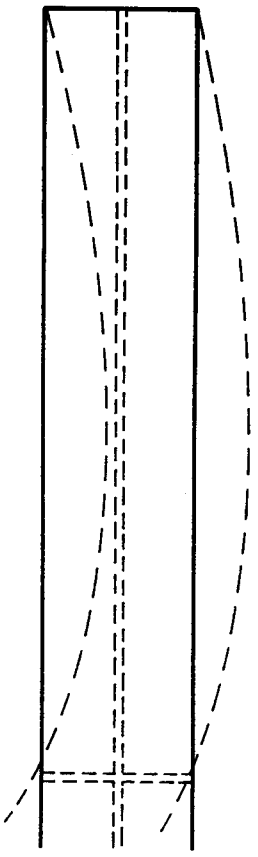

(c) PLAN VIEW OF LATERAL BUCKLING

FIGURE 2.21 LATERAL BUCKLING CONFIGURATION

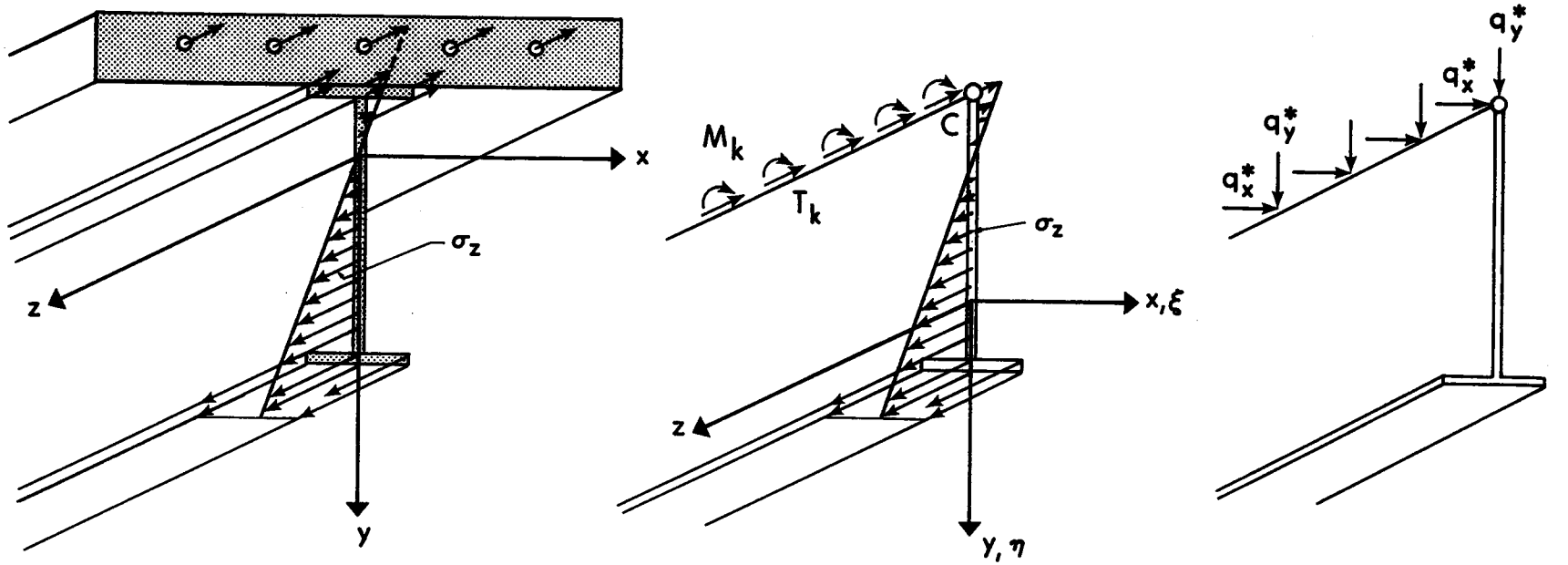

(a) FORCES ON COMPOSITE SECTION

(b) FORCES ON INVERTED TEE SECTION

(c) HINGE REACTIONS FOR INVERTED TEE SECTION

FIGURE 2.22 CO-ORDINATE SYSTEMS AND STRESS RESULTANTS FOR LATERAL BUCKLING ANALYSIS

CHAPTER III

DEFORMATION OF COMPOSITE BEAMS

3.1 Introduction

Beam deformations are produced by bending and shear. Deformation in composite beams is affected by slip along the interface between the concrete slab and steel section.

Bending deflections are dependent on the moment-curvature relationship. This relationship is obtained by direct integration for a linear elastic stress-strain relationship. For non-linear stress-strain relationships a numerical integration procedure may be used. Several such procedures have been proposed, and most of them are based on dividing a cross section into a number of segments. Numerical integration herein is based on the assumption of a linear stress variation in a segment. This assumption will provide adequate accuracy for a small number of segments. Since the stress varies in two directions for a section with residual stresses, the section is divided into segments in two directions.

Bending deformations may be calculated by means of such methods as the conjugate beam method, the finite difference method, the Newmark's method and the finite element method. The finite difference method modified herein has several advantages for analyzing inelastic beam deformation. The method does not require the solution

of a large number of equations in each iteration since the number of unknowns equals the number of redundants. Although the conventional finite difference method produces second order errors $O(\lambda^2)$[57], where λ is spacing, this error may be reduced appreciably by modification of the load term.

Shear deformation can be evaluated independent of bending deformation, since it does not affect bending deformation, and in a continuous beam can be evaluated independently in each span. One of the simplest methods for evaluation of shear deformation in an inelastic beam is based on the principle of virtual work. This method is employed in the present study.

The basic equation for slip deformation has been derived by Newmark[58], Yam[41] and others. The equation derived by Yam can be applied to the deformation in an inelastic beam. However, the solution of the equation requires considerable computation time, especially for continuous beams. The solution is simplified if we assume that slip strain, i.e., the derivative of slip with respect to length, is constant throughout the span.

3.2 Moment-Curvature Relationships

The stress resultants for a section, i.e., normal force N_z and bending moment M_x are defined by

$$N_z = \int_A \sigma dA \qquad 3.1(a)$$

$$M_x = \int_A \sigma y dA \qquad 3.1(b)$$

where the origin of the coordinates is the neutral axis as shown in Figure 3.1(a).

Integration of Equations 3.1(a) and (b) can be performed for a linear stress-strain relationship without difficulty. However, a numerical method must be applied to more complex stress-strain relationships such as those for concrete and for steel after yielding. Conventionally the integration of Equations 3.1 has been performed by a summation procedure

$$N_z = \int_A \sigma dA = \Sigma \sigma_j dA_j \qquad 3.2(a)$$

$$M_x = \int_A \sigma y dA = \Sigma \sigma_j y_j dA_j \qquad 3.2(b)$$

where σ_j, y_j and A_j are the stress, coordinate of the centroid of dA_j and area, respectively, as shown in Figure 3.1(b).

Equations 3.2 do not provide sufficient accuracy for certain stress distributions. Accuracy is improved if y_j is defined as the coordinate of the center of the gravity for the stress block suggested by Barnard[8] and shown in Figure 3.1(c).

It is also possible to perform numerical integration by Newmark's method[59]. Assuming a linear stress distribution in a segment as shown in Figure 3.2(a), the integration of Equations 3.1(a) and (b) results in

$$N_z = \int_A \sigma dA = \frac{1}{6} \sum_{j=1}^{n} \left\{ \sigma_{j-1} dA_{j-1} + 2\sigma_j (dA_{j-1} + dA_j) + \sigma_{j+1} dA_j \right\} \qquad 3.3(a)$$

$$M_x = \int_A y dA = \frac{1}{6} \sum_{j=1}^{n} \left\{ \sigma_{j-1} dA_{j-1} + 2\sigma_j (dA_{j-1} + dA_j) + \sigma_{j+1} dA_j \right\} y_j \qquad 3.3(b)$$

For equal areas of segments, the stress resultants N_z and M_x can be simplified as

$$N_z = \frac{dA}{6} \Sigma(\sigma_{j-1} + 4\sigma_j + \sigma_{j+1}) \qquad 3.4(a)$$

$$M_x = \frac{dA}{6} \Sigma(\sigma_{j-1} + 4\sigma_j + \sigma_{j+1})\, y_j \qquad 3.4(b)$$

It may be necessary to expand these expressions for normal force and bending moment to two dimensions for sections with residual stress. Denoting the equal intervals in the x and y directions by λ_x and λ_y and the stress at a mesh point by σ_{ij} as shown in Figure 3.2(b), Equations 3.4(a) and (b) become

$$N_z = \int_A \sigma dA = \iint \sigma dx dy$$

$$= \frac{\lambda_x}{6} \int \Sigma(\sigma_{i-1,j} + 4\sigma_{i,j} + \sigma_{i+1,j}) dy$$

$$= \frac{\lambda_x \lambda_y}{36} \sum_{ij} \sum \left\{ (\sigma_{i-1,j-1} + 4\sigma_{i,j-1} + \sigma_{i+1,j-1}) \right.$$

$$\left. + 4(\sigma_{i-1,j} + 4\sigma_{i,j} + \sigma_{i+1,j}) \right.$$

$$+ (\sigma_{i-1,j+1} + 4\sigma_{i,j+1} + \sigma_{i+1,j+1})\Big\} \qquad 3.5(a)$$

$$M_x = \frac{\lambda_x \lambda_y}{36} \Sigma\Sigma \Big\{ \sigma_{i-1,j-1} + 4\sigma_{i,j-1} + \sigma_{i+1,j-1}$$

$$+ 4(\sigma_{i-1,j} + \sigma_{i,j} + \sigma_{i+1,j})$$

$$+ \sigma_{i-1,j+1} + 4\sigma_{i,j+1} + \sigma_{i+1,j+1} \Big\} y_j \qquad 3.5(b)$$

3.3 Effect of Residual Stresses on Bending

Residual stresses occur in rolled sections as a result of plastic deformation during the cooling process after rolling. Usually compression occurs at the tips of the flanges and tension occurs at the junction of flange and web in a wide flange shape[61][62][63]. Idealized residual stress patterns have been proposed by various investigators. The two examples shown in Figures 3.3 have been employed for analysis of torsional column buckling by Galambos[63] and Lee et al[64].

Any residual stress pattern must satisfy equilibrium conditions, therefore the following equations must be satisfied[54].

$$\int_A \sigma_r dA = 0 \qquad 3.6(a)$$

$$\int_A \sigma_r y dA = 0 \qquad 3.6(b)$$

$$\int_A \sigma_r x \, dA = 0 \qquad 3.6(c)$$

$$-\left(\int \sigma_r \omega dA\right)' + M_{ttr} + M_{\rho r}\theta' = 0 \qquad 3.6(d)$$

In Equation 3.6(d) relating to twisting moment, the terms represent warping torque, Saint Venant's torque and a stress resultant which is defined by Equation A.25. If residual stresses are assumed constant along the member, the warping torque must be zero. Therefore Equation 3.6(d) can be rewritten as

$$M_{ttr} + M_{\rho r}\theta' = 0 \qquad 3.6(e)$$

which shows that twisting moment due to $M_{\rho r}\theta'$ balances Saint Venant's torque due to residual shear stress. If the twist is zero, that is, $\theta' = 0$, Saint Venant's torque must be zero.

3.4 Bending Deformation

The differential equation for bending deformation of a beam subjected to distributed load q_z is expressed as

$$(EIy'')'' = q_z \qquad 3.7$$

Equation 3.7 can be divided into two parts

$$EIy'' = -M \qquad 3.8(a)$$

$$M'' = -q_z \qquad 3.8(b)$$

The finite difference equations for Equations 3.8 are expressed in matrix form as

$$[EI][B]\{y\} = -\{M\} \qquad 3.9(a)$$

$$[B]\{M\} = -\{q_z\} \qquad 3.9(b)$$

For a simply supported beam, the matrix $[B]$ for equal segments λ can be established as

$$[B] = \frac{1}{\lambda^2}\begin{bmatrix} -2 & 1 & . & . \\ 1 & -2 & 1 & . \\ . & . & . & . \\ & & 1 & -2 \end{bmatrix} \qquad 3.10$$

The inversion of the matrix $[B]$ is of the form,

$$[B]^{-1} = \lambda^2[b_{ij}] \qquad 3.11$$

where the elements of the n x n matrix $[B]^{-1}$, b_{ij} are

$$b_{ij} = \begin{cases} i(n-j)/n & \text{for } i \geq j \\ ij/n & \text{for } i < j \end{cases} \qquad 3.12$$

By multiplying by $[B]^{-1}$, Equations 3.9 are expressed as

$$\{y\} = -[B]^{-1}[EI]^{-1}\{M\} \qquad 3.13(a)$$

$$\{M\} = -[B]^{-1}\{q_z\} \qquad 3.13(b)$$

where $[EI]^{-1}$ is a diagonal matrix with diagonal elements $1/EI_i$.

Conventionally Equation 3.13(b) is substituted directly into Equation 3.13(a); however this procedure may yield second order errors $O(\lambda^2)$. As shown in Figure 3.4, constant moment is assumed in each segment, rather than varying moment as produced by loads. However the moment which is introduced into Equation 3.13(a) must be related to the actual bending moment diagram. By assuming a linear moment variation between pivotal points i and (i+1), an equivalent moment at the point i may be given by $\frac{1}{6}(M_{i-1} + 4M_i + M_{i+1})$. This may be expressed in matrix form by introducing co-efficient matrix $[C]$ as

$$[C] = \frac{1}{6}\begin{bmatrix} 4 & 1 & . & . \\ 1 & 4 & 1 & . \\ . & . & . & . \\ . & . & 1 & 4 \end{bmatrix} \qquad 3.14$$

Since this procedure is also applied to a distributed load, the equivalent distributed load q_{eq} and bending moment M_{eq} are defined as

$$\{q_{eq}\} = [C]\{q_z\} \qquad 3.15(a)$$

$$\{M_{eq}\} = [C]\{M\} \qquad 3.15(b)$$

By using Equations 3.15 and substituting Equation 3.13(b) into 3.13(a), the deflection for a beam subjected to distributed loads is obtained as

$$\{y\} = [B]^{-1}[EI]^{-1}[C][B]^{-1}[C]\{q_z\} \qquad 3.16$$

Since a concentrated load P may be expressed as a distributed load equal to P/λ, the bending moment $\{M\}$ for a beam subjected to external moments $\{M_{ex}\}$, concentrated loads $\{P/\lambda\}$ and distributed loads $\{q_z\}$ is expressed as

$$\{M\} = \{M_{ex}\} - [B]^{-1}(\{P/\lambda\} + [C]\{q_z\}) \qquad 3.17$$

The corresponding deflection is

$$\{y\} = [B]^{-1}[EI]^{-1}[C]\left[-\{M_{ex}\} + [B]^{-1}(\{P/\lambda\} + [C]\{q\})\right] \qquad 3.18$$

Once the deflection $\{y\}$ and moment $\{M\}$ are obtained, the slope and shear can be evaluated by differentiating $\{y\}$ and $\{M\}$ respectively. The shear $V_{i+\frac{1}{2}}$ at the pivotal point $(i+\frac{1}{2})$ is expressed in finite difference form as

$$V_{i+\frac{1}{2}} = (M_{i+1} - M_i)/\lambda \qquad 3.19$$

The shear V_i at the location i is obtained by adding to the shear force $V_{i+\frac{1}{2}}$, the additional shear ΔV_i produced between i and $(i+\frac{1}{2})$, resulting in

$$V_i = V_{i+\frac{1}{2}} + \Delta V_i$$

$$= (M_{i+1} - M_i)/\lambda + \frac{\lambda}{6}(2q_i + q_{i+1}) \qquad 3.20$$

where the second term is the shear at i for linearly distributed loads between i and (i+1). Similarly the slope can be evaluated as

$$\theta_i = (y_{i+1} - y_i)/\lambda + \frac{\lambda}{6}\left(\frac{2M_i}{EI_i} + \frac{M_{i+1}}{EI_{i+1}}\right) \qquad 3.21$$

Since the conventional finite difference equation does not include the co-efficient matrix [C], it implies that a unit matrix [E] is the co-efficient matrix, which is equivalent to a rectangular integration.

3.5 Shear Deformation

Shear deformation is often neglected, since it is not usually significant when compared with bending deformation. However, it is significant for short beams and for beams with small shear resistance.

A composite beam has relatively large bending stiffness, but may not have large shearing stiffness, since the web of the steel

section provides the major shear resistance. The ratio of shear deformation to bending deformation also depends on the boundary conditions, and the type of loading. Bending deformation varies significantly for different boundary conditions. Shear deformation, however, is the same for all boundary conditions except for those at a free end or a yielding support. Shear deformation at z for the beam shown in Figure 3.5 may be expressed as $K_{sh} \frac{z(l-a)}{GAl}$ where k_{sh} is the shear correction factor defined by

$$k_{sh} = \frac{A}{I^2}\int_A \left(\frac{N_q}{b}\right)^2 dA \qquad 3.22$$

where N_q is the first moment of the section A_1 shown in Figure 3.6(b) with respect to the neutral axis. The shear correction factor is 1.2 for a rectangular section, 2.94 for a W12x36 section, 6.63 for a composite beam consisting of a W12x36 and a 5"x60" concrete slab, and 3.1 for a composite beam consisting of a W12x36 section and 3.6 in^2 of longitudinal reinforcement in a negative moment region. Generally k_{sh} is close to unity for wide-flange sections if only the web is considered to resist shear.

Shear deformation should not be neglected for an indeterminate structure. For a beam with fixed supports the ratio of shear deformation to bending deformation is approximately 4 times that for a simply supported beam.

Elastic shear deformation can be obtained by the virtual work method. Shear deformation is defined as

$$\delta_{sh} = \int_{Vol} \bar{\tau}\gamma dVol \qquad 3.23$$

where the virtual shear stress $\bar{\tau}$ equals to $\bar{V}\tau/V$, and $\bar{V}$ and V are the virtual shear and real shear. Therefore shear deformation δ_{sh} is represented by

$$\delta_{sh} = \int_{Vol} \frac{\bar{V}}{V} \tau\gamma dVol$$

$$= \int_{\ell} \frac{\bar{V}}{V} \int_{A} \tau\gamma dA \qquad 3.24$$

$\int_A \tau\gamma dA$ in Equation 3.24 can be derived from the normal stress σ_z due to bending at any location in the beam, since shear stress τ is given by

$$\tau = \frac{1}{w} \int_{A_1} \frac{\partial \sigma_z}{\partial z} dA \qquad 3.25$$

The shear strain γ is obtained from the stress-strain relationship which is similar in shape to the normal stress-strain relationship. The integration may be performed numerically by the same method as that explained in Section 3.2. The computation of shear deformation is relatively simple, once $(\int \tau\gamma dA)/V$ is calculated at intervals throughout the span.

3.6 Effect of Slip

Analytical studies of composite beams with incomplete interaction were first undertaken by Newmark[58], who assumed linear stress-strain relationships for steel and concrete and a linear force-deformation relationship for shear connectors. The basic equation for the compression force C in the slab was expressed as

$$C'' + \frac{s\gamma}{k_s}(f_1 M - f_2 C) = 0 \qquad 3.26$$

where s is spacing, k_s is a constant related to the shear connectors, and

$$f_1 = \frac{y_s}{E_c I_c + E I_s} \qquad 3.27$$

$$f_2 = \frac{1}{E_c A_c} + \frac{1}{E A_s} + f_1 y_s \qquad 3.28$$

where y_s is the distance between the centroids of the slab and steel section.

In an analysis involving non-linear stress-strain relationships and a non-linear force-slip relationship, Yam and Chapman[41] derived two first order simultaneous equations with two independent variables C and Δ_s (Figure 3.7) as

$$C' = \frac{dC}{dz} = \frac{a}{s\gamma}\left\{1 - \exp(-b\Delta_s)\right\} \qquad 3.29(a)$$

$$\Delta_s' = \frac{d\Delta_s}{dz} = -f(M,C) \qquad 3.29(b)$$

where a and b are constants defined in Section 2.3.3. Yam solved Equations 3.29 by means of the predictor-corrector method which is used for numerical integration. For a simply supported beam a value of slip is assumed. However, for an indeterminate structure the bending moment must also be assumed. Since two assumed values are required for continuous beams, more iterations must be carried out to obtain correct values.

Yam's approach requires considerable computational time. However, computational time may be significantly reduced by making an assumption that the slip strain, which is the differentiation of slip, is constant along the shear span. The slip distribution based on this assumption is linear as shown in Figure 3.8. The conditions in a shear span are illustrated in Figure 3.9 with all shear connectors in the shear span acting to resist the concrete compression force. The slip strain is defined as $\varepsilon_d = \Delta_s/L_s$, where Δ_s is obtained from the force-slip relationship and L_s is the shear span. There are two neutral axes in a section due to slip, and the distance between them is defined by ε_d/ϕ, where ϕ is curvature. The moment-curvature relationship can be obtained for this condition by employing numerical integration as discussed in Section 3.2. Presumably the moment-curvature relationship depends on the shear span and shear connector spacing. For the case of linear stress-strain relationships for steel and concrete and a linear force-slip relationship for shear connectors, the equivalent moment of inertia, accounting for slip, is derived in Appendix B.

Expressions for force-slip relationships in negative moment regions have not been proposed. Davison[5] measured strains in longitudinal slab reinforcement, and evaluated the ratio of measured strains to calculated strain, which he defined as an interaction factor. The interaction factor for the beams tested by Davison was approximately equal to 0.6.

3.7 Deformations in Continuous Beams

Stiffness in a negative moment region is usually smaller than that in a positive moment region, since in a negative moment region the concrete slab cracks when subject to relatively small tension stresses. Therefore stiffness is dependent upon the bending moment, resulting in a material non-linear problem.

Several methods have been proposed for the analysis of continuous beams; however all methods require an iteration procedure for a non-linear problem. Finite difference and flexibility procedures are employed in the following. The flexibility matrix for finite difference can be readily obtained for simply-supported beams as discussed in Section 3.3. Continuous beams may be considered as a series of simply supported beams to which the flexibility method is applied.

If δ_{io} is the deformation at the support i of the primary structure, and $\overline{\delta}_{ij}$ is the deformation produced at i due to unit value of redundant X_j, where $\overline{\delta}_{ij}$ is also defined as the flexibility factor, the displacement Δ_i at the support i becomes

$$\Delta_i = \delta_{io} + \Sigma\overline{\delta}_{ij}X_j \qquad 3.30(a)$$

or $$\{\Delta\} = \{\delta_o\} + [F]\{X\} \qquad 3.30(b)$$

Generally, moments or reactions are selected as the redundants in continuous beams. If moments are taken as redundants, the primary structure consists of n simple beams for an n-span continuous beam. One of the advantages of selecting moment redundants is that less computation is required in Equation 3.18. For example, a continuous beam with each span divided into m segments provides $n[B]^{-1}$ with m x m elements for a beam where moments are selected as redundants, instead of a $[B]^{-1}$ matrix with n(m + 1) x n(m + 1) elements for a beam where reactions are selected as redundants.

The first step in the analysis procedure for continuous beams is to assume redundants $\{X\}$. The second step is to find $\{\delta_o\}$ and $[F]$ from Equations 3.18 and 3.26. Then redundants $\{X\}$ can be solved from Equation 3.30(b). The third step is to find the moment in the real structure. If bending moments are close enough to those previously assumed, then the assumed redundants $\{X\}$ are correct. If not, successive iteration must be carried out. The $i^{\underline{th}}$ assumption of $\{X\}_i$ is provided by

$$\{X\}_i = \{X\}_{i-2} + \alpha(\{X\}_{i-1} - \{X\}_{i-2}) \qquad 3.31$$

When the factor α is greater than unity, it is the so-called over-relaxation factor for elastic analysis. When it is less than unity, it is the so-called under-relaxation factor for inelastic analysis.

Several analytical methods have been proposed for an inelastic region. One of the methods is based on using the stiffness EI in Equation 3.18 as defined by the secant modulus in the moment-curvature relationship. This method requires the evaluation of Equation 3.18 in every iteration. As illustrated in Figure 3.9 , the total curvature for moment M can be divided into elastic and plastic curvature. Instead of changing the stiffness, an additional external moment, corresponding to plastic curvature is applied to the inelastic region. This additional external moment is given by $EI\phi_p$ where EI is elastic stiffness and ϕ_p is plastic curvature.

Since shear deformation does not affect redundants, shear deformation is determined after bending deformation. A computer program for deformation analysis is presented in Appendix D.

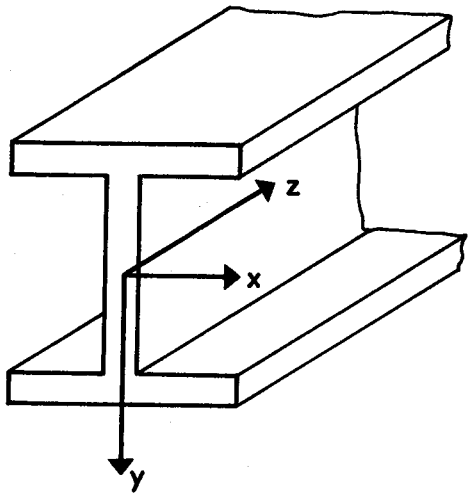

(a) COORDINATE SYSTEM

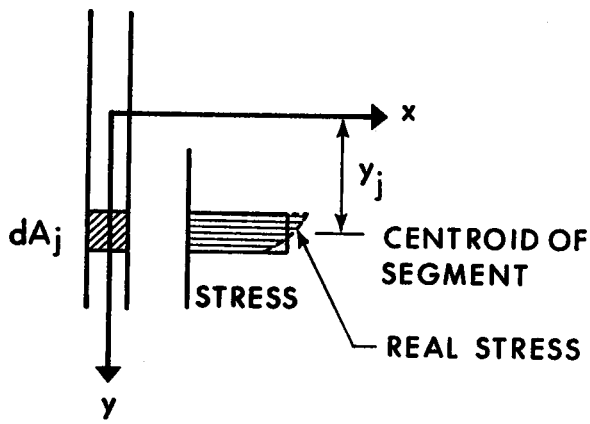

(b) CONVENTIONAL PROCEDURE

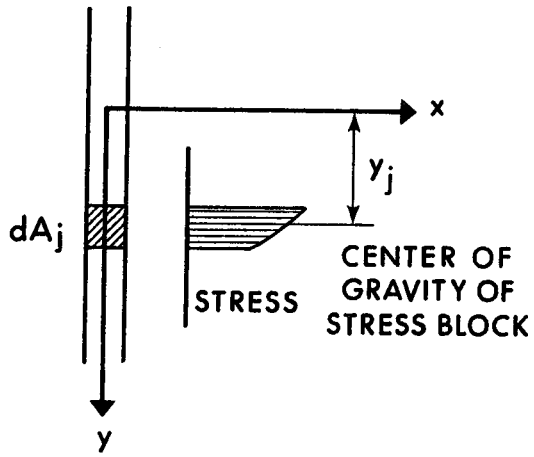

(c) BARNARD'S PROCEDURE

FIGURE 3.1 CO-ORDINATE SYSTEMS FOR NUMERICAL INTEGRATION PROCEDURES

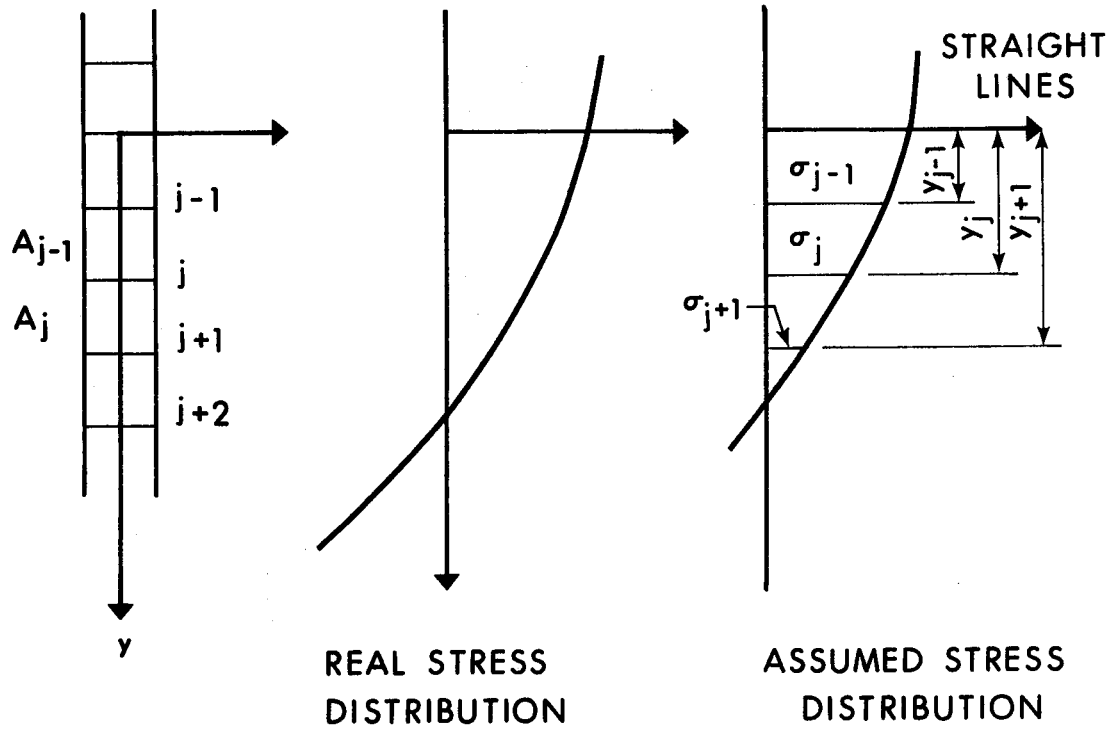

(a) COORDINATE SYSTEM FOR ONE DIMENSION

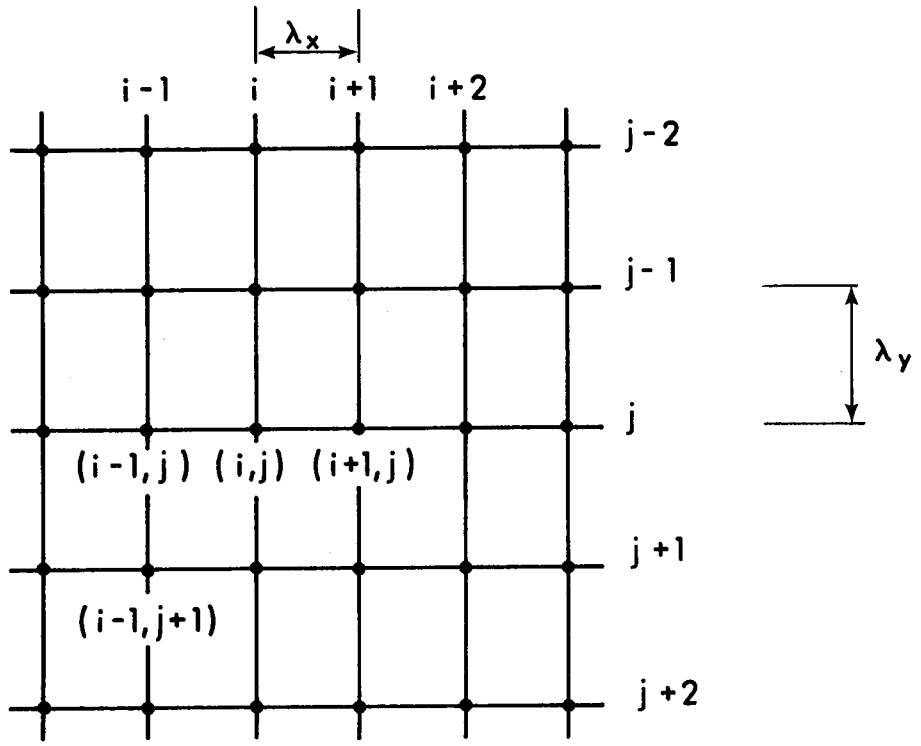

(b) COORDINATE SYSTEM FOR TWO DIMENSIONS

FIGURE 3.2 CO-ORDINATE SYSTEM FOR PROPOSED NUMERICAL INTEGRATION PROCEDURE

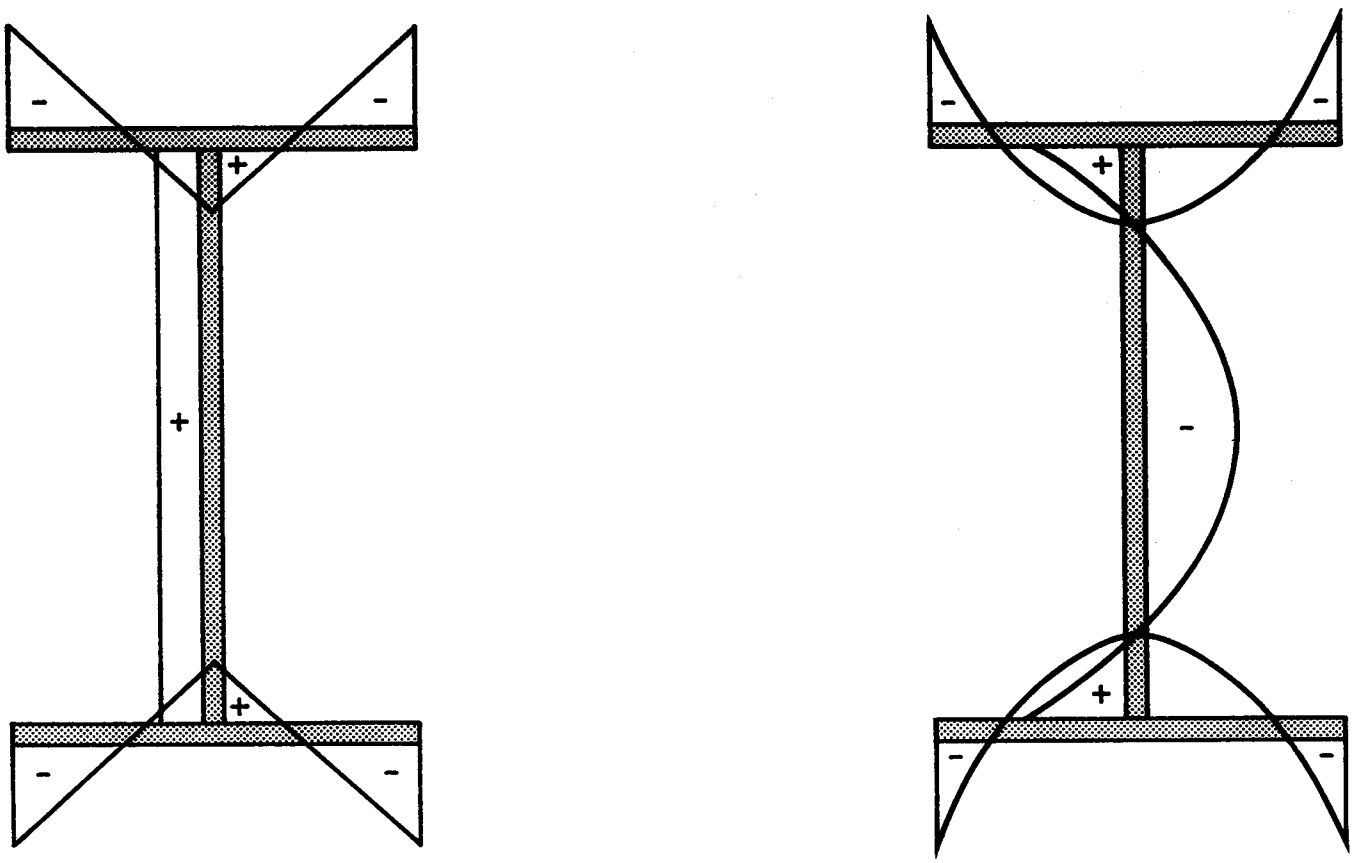

FIGURE 3.3 IDEALIZED RESIDUAL STRESS PATTERNS IN WIDE FLANGE BEAMS

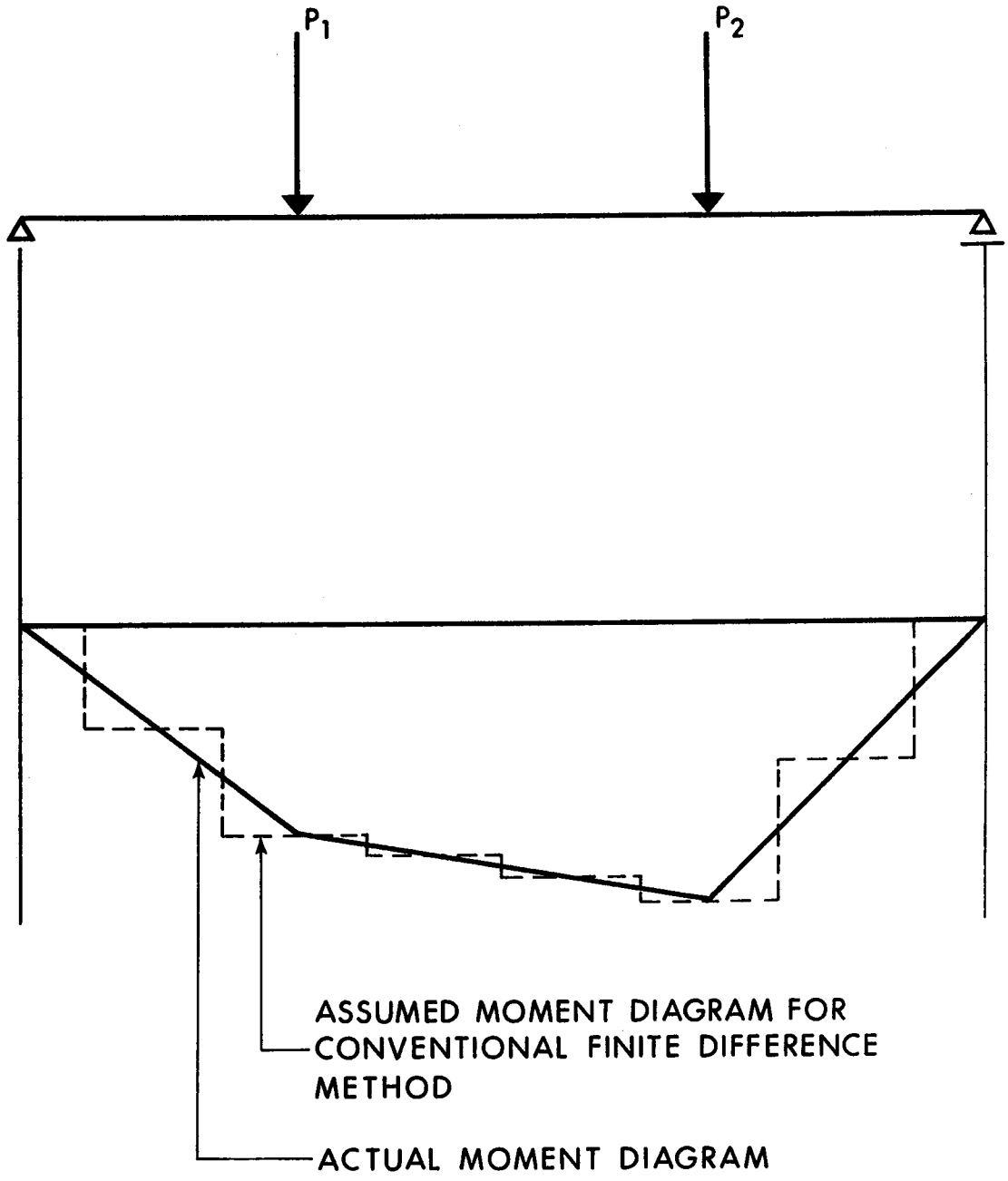

FIGURE 3.4 ASSUMED BENDING MOMENT DIAGRAM FOR CONVENTIONAL FINITE DIFFERENCE METHOD

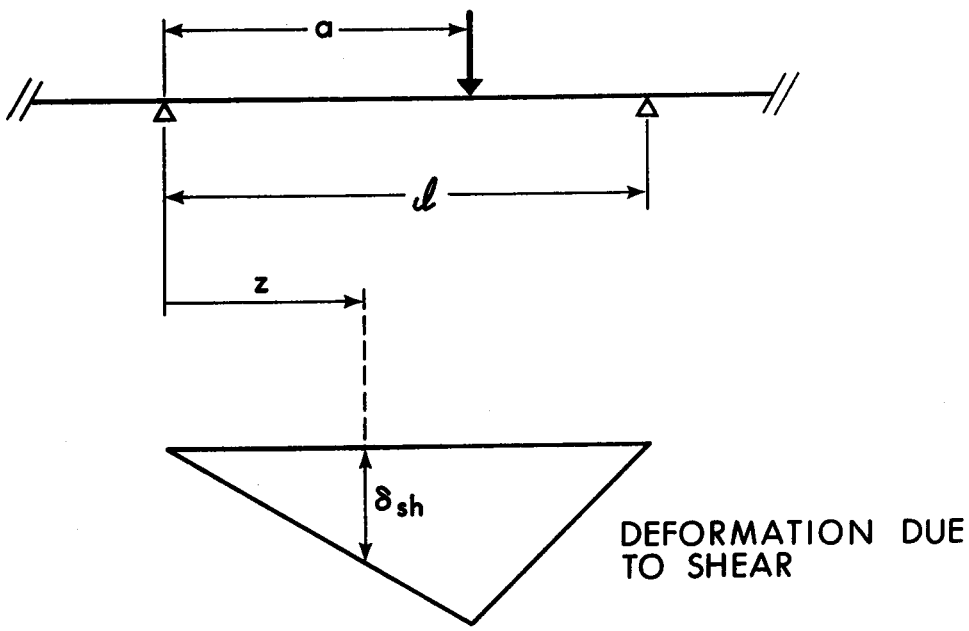

$$\delta_{sh} = \frac{k_{sh}\, z\, (\ell - a) P}{GA\, \ell} \qquad \text{for } z \leq a$$

$$= \frac{k_{sh}\, a\, (\ell - z)\, P}{GA\, \ell} \qquad \text{for } z \geq a$$

FIGURE 3.5 SHEAR DEFORMATION NOTATION

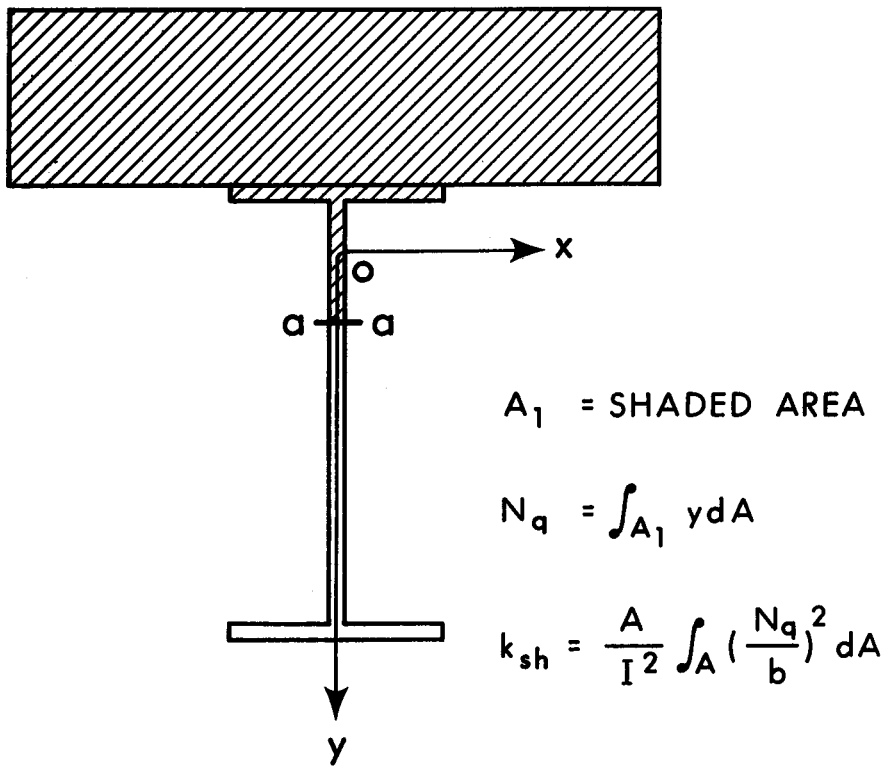

FIGURE 3.6 DEFINITION OF AREA A_1 REQUIRED FOR THE EVALUATION OF THE SHEAR CORRECTION FACTOR k_{sh}

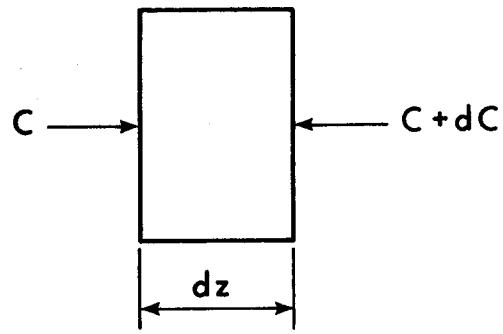

(a) SLAB ELEMENT

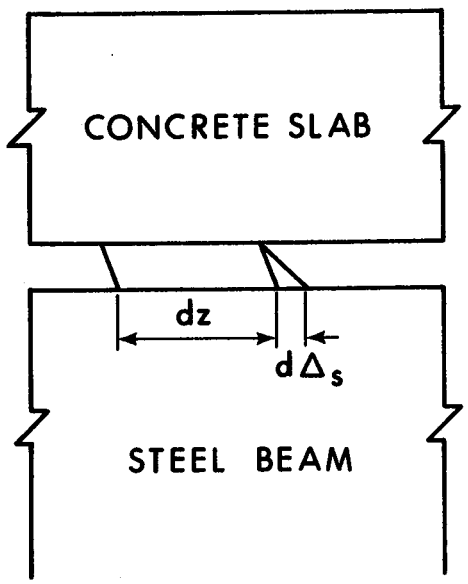

(b) COMPOSITE BEAM ELEMENT

FIGURE 3.7 SLIPPAGE MECHANISM (AFTER YAM AND CHAPMAN[41])

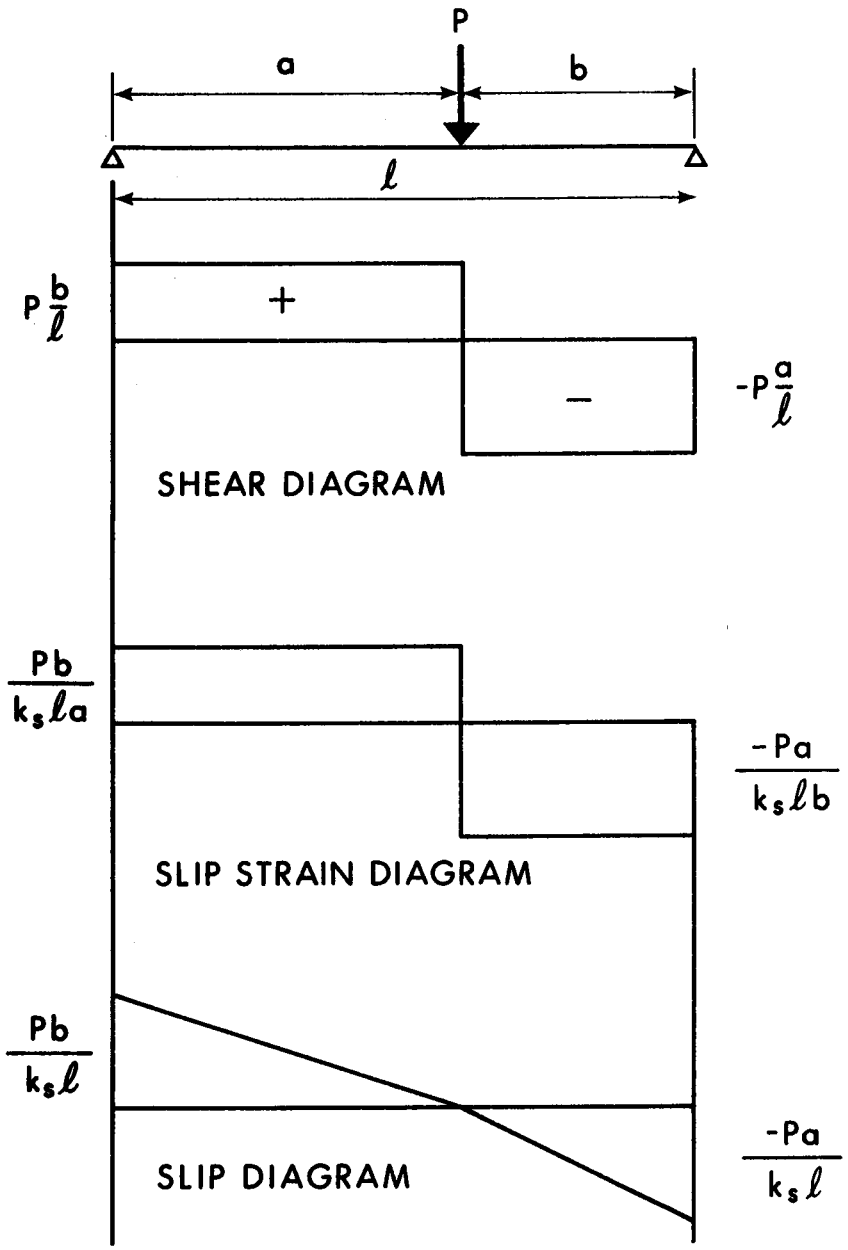

FIGURE 3.8 ASSUMED SLIP STRAIN AND SLIP DIAGRAMS

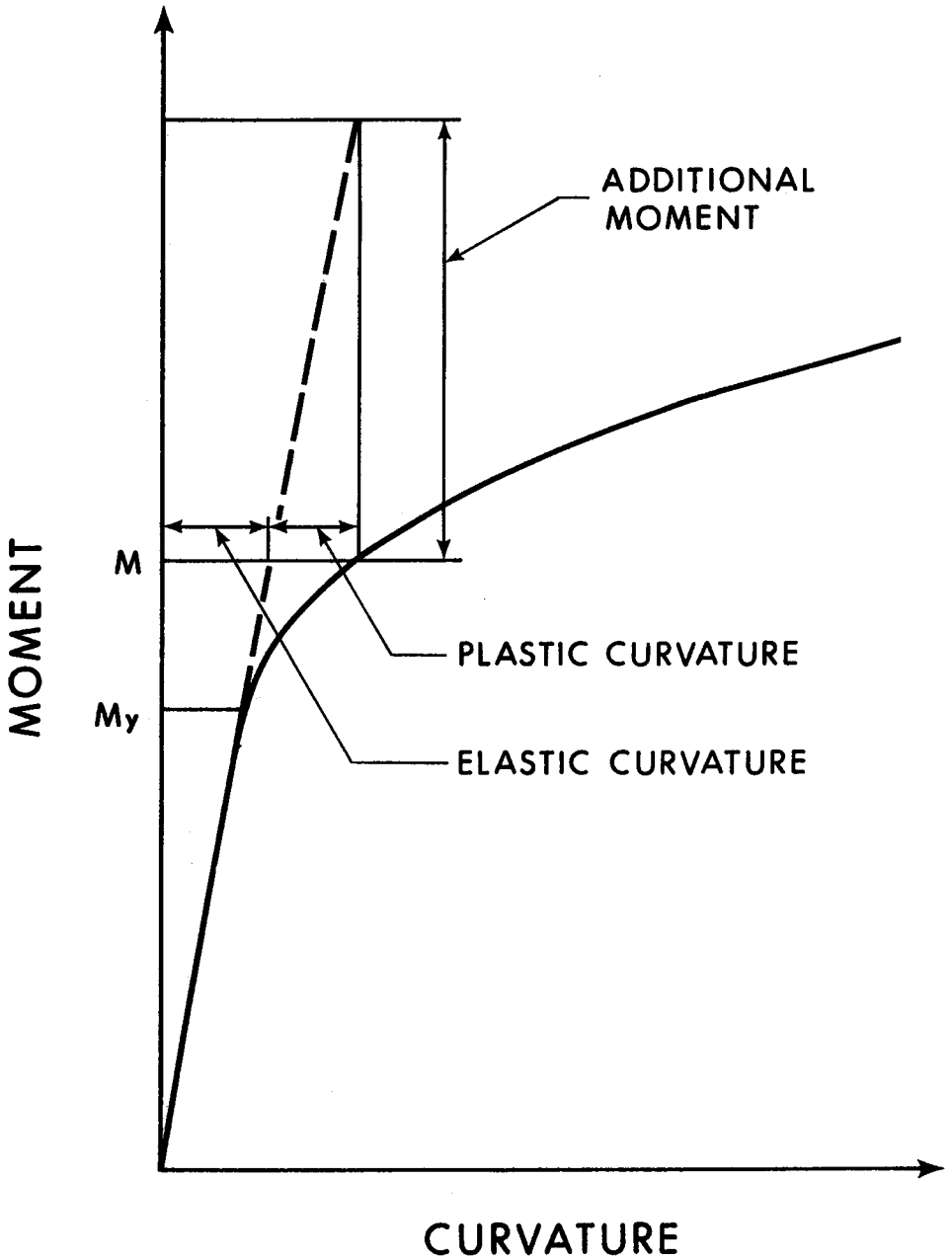

FIGURE 3.9 ADDITIONAL EXTERNAL MOMENT CORRESPONDING TO THE PLASTIC CURVATURE

CHAPTER IV

TESTS OF CONTINUOUS COMPOSITE BEAMS

4.1 Introduction

The object of the tests conducted as part of the present study was to provide additional information on the behavior of continuous composite beams. Although a number of tests have been conducted in the past by Barnard[8][9], Daniel et al[18] and Park[12], it was felt necessary to conduct further tests with particular emphasis on the effects of longitudinal slab reinforcement on ultimate strength, failure modes and general behavior. Three two-span beams were tested under concentrated loads applied at the midspans.

4.2 Test Program

4.2.1 Design of Specimens

The size of beam specimens was determined to a large extent by limitations imposed by laboratory facilities. W12 x 31 and W12 x 27 steel sections were selected, since these sizes have been used in previous tests at the University of Alberta[6]. CSA Standard S16-1969[1] limits width-thickness ratio of compression flanges and webs for sections used in plastic design, and the ratios for W12 x 31, W12 x 27 and W10 x 21 steel sections are approximately equal to these limitations. G40.12 steel was specified.

4.2.2 Fabrication

All steel sections were delivered to the laboratory complete with shear connectors and bearing stiffeners. Additional 3'-0" lengths of the W12 x 31, W12 x 27 and W10 x 21 sections were supplied for material property tests. The steel surface at locations for electrical resistance strain gages was ground smooth. 1½" x 1½" styrofoam blocks were placed at these locations and were subsequently removed after the concrete hardened.

The slab reinforcing bars were also ground smooth at the strain gage locations, and then tied together to form a grid. Styrofoam blocks were attached to the bars at gage locations. Plastic chairs held the reinforcement in place. Plate 4.1 shows details of the fabricated steel specimens, reinforcing grids and form work in position prior to casting.

Concrete was mixed in a 9 cubic foot Erich mixer in the University of Alberta Structural Engineering Laboratory. The mix proportions are shown in Table 4.4. One beam specimen together with 8 test cylinders was cast from 4 batches of concrete. The concrete was vibrated into place by a mechanical vibrator and was finished by means of a wooden screed and steel trowel. The beams were moist-cured for 5 days and removed from the formwork to cure under laboratory conditions for periods ranging from 69 to 72 days before testing.

After a beam was positioned in the testing apparatus and strain gages were connected to the indicators, the steel section was white-washed so that the development of yielding could be observed.

A 4" slab thickness and a 4'0" slab width were selected, since these dimensions had been used in previous tests at the University of Alberta. A concrete strength of 4500 psi, which is a common strength used in actual structures, was selected.

The amount of longitudinal slab reinforcement at the interior support significantly affects ultimate loads and failure modes. Local buckling may be the dominant failure mode in a beam with a relatively large amount of longitudinal reinforcement. On the other hand, crushing of concrete may be the dominant failure mode for a section with a small amount of longitudinal steel. The amount of longitudinal slab reinforcement as shown in Table 4.1 were selected to produce different failure conditions. The longitudinal bars were placed at mid-depth in the negative moment regions.

Shear connectors as shown in Figure 4.1 were provided according to provisions of CSA Standard S16-1969, which are based on ultimate connector strength. The shear connectors were 3/4 inch diameter, 3½ inches long,headed stud connectors.

Transverse reinforcement was introduced in order to control longitudinal cracking. Ferrier[20] encountered longitudinal cracking in beam specimens with transverse steel in the amount of 0.2 percent of the concrete area,which corresponds to temperature reinforcement requirements. The present beams were reinforced transversely with #3 bars placed at 4½" intervals throughout the length of the slab. This reinforcement is equal to 0.67 percent of the concrete slab area or three times the nominal temperature reinforcement.

Complete details of the test specimens are shown in Figure 4.1.

4.2.3 Test Equipment

Test specimens were supported at mid-length on a hinge reaction unit anchored to a concrete pedestal and at each end by a roller unit fitted with a rocker plate assembly seated on a concrete pedestal, as shown in Figure 4.2.

Two 100-ton Amsler hydraulic jacks were used as loading units centered on the longitudinal centerline of the specimen. Loads were transmitted to the concrete slab through 12" x 8" x 1½" spreader plates set in plaster of Paris to ensure uniform contact.

Details of the lateral support system are shown in Figure 4.3(a) and Plate 4.2(a). At each support, steel channels, attached to the web stiffeners and supported by vertical steel columns, resisted lateral rotation of the specimen as shown in Figure 4.3(b) and Plate 4.2(b). The slab was supported laterally by rollers on vertical guides near midspans.

4.2.4 Material Properties

Results of tension tests performed on samples of #3, #4 and #5 bars used as longitudinal and transverse reinforcement are shown in Table 4.2. Test coupons, two from each flange and three from the web, were cut from 3'-0" lengths of W12 x 31, W12 x 27 and W10 x 21 provided for this purpose. Results of coupon tests are shown in Table 4.3.

Eight concrete cylinders were cast for each beam and cured under laboratory conditions. Five cylinders were tested in compression and three were subjected to a splitting test at the time of the test on the corresponding beam. Test results are shown in Table 4.4.

4.2.5 Instrumentation

Measurements of strains in the steel sections, reinforcing bars and concrete slabs were obtained by means of KFC-5-C1-11 and SR4-A7 electrical resistance strain gages. Deflections, rotations and slip deformations were measured by mechanical means.

Deflections were measured by means of a precise level focused on graduated scales suspended from the bottom flange of the specimen. Deflection measurements were taken at the centers of the two spans and at locations 30 inches from the interior support in the vicinity of the points of inflection.

Rotations were measured by means of mechanical rotation meters at the beam ends and by means of sets of two dial gages at locations 30 inches from the interior support. These mechanical rotation meters consisted of a level tube, an extension dial and two arms connected by a hinge as shown in Figure 4.4. A vertical steel bar was welded to the steel section and two dial gages 24 inches apart were mounted by magnetic bases on the interior support as shown in Figure 4.4. Rotations were determined from the relationship

$$\theta = \left(\Delta_{d_1} - \Delta_{d_2}\right)/\ell_a$$

where Δ_{d_1} and Δ_{d_2} are displacements measured by the dial gages and ℓ_a is the distance between the gages.

Curvatures were measured at the interior support and the load points by means of electric resistance strain gages. For measuring

curvature, three gages were attached to the steel section, six gages were attached to the concrete slab in positive moment regions and three gages were attached to reinforcing bars in the negative moment region.

Points of inflection were determined from measurements obtained from sets of two electric resistance strain gages. Since inflection points were expected approximately 30 inches from the interior support, gages were positioned at 24" and 36" from the support. Assuming that strains in the flange vary linearly, the inflection point can be simply located from the measurements obtained from these two gages. Once inflection points are located, reactions and bending moments are easily evaluated from an analysis of a statically determinate structure.

Slip and slip strain measurements were obtained by means of dial gages and electric resistance strain gages, respectively. Six locations for these measurements were selected in the positive moment region. Slip strains are defined by the difference of strains in the steel section and concrete slab at the interface. Therefore two strain gages were required at each location. Slip was measured by means of dial gages attached to the steel sections by magnetic mounts, and reacting against a steel angle attached to the concrete slab.

Strains in the transverse reinforcing bars were measured at four locations.

Complete instrumentation details are shown in Figure 4.4 and Plate 4.3.

4.2.6 Testing Procedure

Prior to testing, the electric resistance strain gages were connected through switch boxes to strain indicators. Immediately prior

to loading all gages were balanced for initial reading and mechanical gages were positioned securely. A load of 5 Kips was applied through each jack and then removed before initial readings were taken. Existing cracks in the slab were marked at this time.

Load increments were different in each test. For steel strains less than the yield strain 10 Kips or 20 Kips increments were applied. After yielding began, load increments were gradually reduced to provide sufficient values to plot an accurate load-deflection relationship. For each load, strain and deflection measurements were recorded and cracks were marked. At each load sufficient time was allowed for stabilization of deflection and rotation. After maximum loading the test was continued in order to obtain the falling portion of the load deflection curve. When deflection approached the 5 inch maximum extension of the jacks, load was removed and additional 1 inch plates were positioned under the jacks and load was re-applied. Beams were tested well beyond ultimate load conditions to the point where concrete crushing and/or significant flange buckling at the interior support occurred. Failure modes and crack patterns were photographed before the specimen was removed.

4.3 Test Results

4.3.1 Introduction

All original data obtained from the beam tests is filed in the Department of Civil Engineering at the University of Alberta. Data presented herein is in tabular, graphical and photographic form.

4.3.2 General Behavior

4.3.2.1 Beam CB1

No visible cracks could be found in the concrete slab at the start of the test. At a load of 30 Kips, cracks appeared on the top surface of the slab in the negative moment region. These cracks extended to the bottom surface of the slab at a load of 50 Kips. Cracks appeared on the bottom surface in the positive moment regions at a load of 50 Kips. Spalling of the white-wash on the steel section began at a load of 80 Kips in the negative moment region and at a load of 100 Kips in the positive moment regions.

At a load of 100 Kips it required approximately 5 minutes to establish equilibrium, and more than 15 minutes were required to stabilize the load at 120 Kips. Cracking progressively spread throughout the slab and crushing began at the top surface at a load of approximately 131 Kips. At a load of 135 Kips it was still possible to stabilize conditions in the beam, though crushing extended over 15 inches. The load was then increased to 137 Kips. After 15 minutes the slab was crushed completely, and the load could not be held. After crushing of the concrete, local flange buckles formed and the load decreased. Crushing and local flange buckling failures are shown in Plate 4.4.

4.3.2.2 Beam CB2

This beam was the first beam tested in this program. It was loaded initially without a bracing system. However, at a load of 70 Kips the beam rotated transversely to such an extent that the test was terminated. After the bracing system was introduced, the beam was load to failure without any further difficulty.

The first cracks were observed at a load of 20 Kips in the negative moment region and at a load of 50 Kips in the positive moment regions. Local flange buckling initiated in the negative moment region at a load of 120 Kips and extended gradually with increasing load. Local buckling was completely formed at a load of 130 Kips. At this load crushing of concrete started at the load locations. Deflections were stabilized at a load of 133 Kips, but could not be stabilized at 136 Kips. The load decreased to 130 Kips at which point crushing was initiated. During unloading, web buckling occurred between the load point and the interior support at a load of 126 Kips. Finally a section of the concrete slab at a load point spalled off at a load of 116 Kips. The failure modes are shown in Plate 4.5.

4.3.2.3 Beam CB3

A visible crack existed on the top slab surface near the interior support prior to loading. Tension cracks began to appear in the negative moment region at a load of 10 Kips, and in the positive moment regions at 50 Kips. Local buckling initiated at a load of 87 Kips and slowly developed as the load increased. At a load of 92 Kips crushing of concrete occurred at a load point and at a load of 94 Kips the concrete was completely crushed. The flange buckles were completely formed at the interior support as the deflection increased. Failure modes are shown in Plate 4.6.

4.3.3 Load-Deflection and Load-Rotation Relationships

Load-deflection relationships are shown in Figures 4.5. Deflections were measured at midspans and at locations 30 inches from

the interior support. Rotations at the exterior support and at locations 30 inches from the interior support are plotted against load in Figures4.6.

4.3.4 Load-Reaction and Load-Moment Relationships

Inflection points were determined from strain data obtained at locations 24 inches and 36 inches from the interior support. Reactions were then calculated on the basis of a statically determinate structural analysis. Resulting load-reaction relationships are shown in Figures 4.7. Bending moments at the load locations and at the interior support were obtained from reactions and loads. Load-moment relationships are shown in Figures 4.8.

4.3.5 Moment-Curvature Relationships

Moment-curvature relationships at the midspans and at the interior support are shown in Figures 4.9. The maximum strain values obtained from electric resistance strain gages were 2 to 3 percent. This magnitude of strain was sufficient to establish moment-curvature relationships.

4.3.6 Slip Deformation and Slip Strains

Load-slip relationships are shown in Figures 4.10. Distribution of slip and slip strain are shown in Figures 4.11 and 4.12.

4.3.7 Strain Distribution Across Slab Width

Strains were measured at the slab edges and the longitudinal slab centerline. Figure 4.13 shows the ratio of slab edge strain to slab centerline strain at the load points for various load values.

4.3.8 Transverse Strains

Strains were measured in the transverse reinforcing bars at the longitudinal centerline and at various locations in the span. Load-strain relationships were shown in Figures 4.14.

4.3.9 Crack Patterns

Crack patterns in the concrete slabs are shown in the Figures 4.15.

4.4 Discussion of Test Results

4.4.1 General Behavior

Transverse rotation may occur as a result of warping of the slab or steel section prior to testing. Transverse rotation due to load was effectively resisted by the bracing system and by the reaction system described in Section 4.2.3.

Initial cracks were observed only in Beam CB3. This crack may have been due to shrinkage, or, since it was located over the interior support, it may have occurred during positioning in the test apparatus. The first transverse cracks appeared in the negative moment region. Later transverse cracks appeared on the bottom surface in the positive moment regions. Diagonal cracks developed at the approach of failure. Longitudinal splitting was effectively prevented by means of the transverse reinforcement. Although a few longitudinal cracks appeared near the load locations before failure, they did not appear to affect the ultimate moment capacity of the beam.

Failure of Beam CB1 was a concrete crushing failure. Local buckling followed as a result of reduced stiffness in the positive moment

regions. The amount of longitudinal reinforcement in Beam CB1 was 1.6 in^2 or 17 percent of the area of the steel section, which was the smallest amount in the three beams. Failure of Beam CB2 occurred as a result of local buckling followed by concrete crushing. The area of longitudinal reinforcement was 3.1 in^2, i.e., 38.9 percent of the area of the steel section which was the highest amount in the three beams. Failure of Beam CB3 resulted from concrete crushing followed by local buckling. Although local buckling initiated prior to crushing of concrete, it did not produce a sudden failure. The area of longitudinal reinforcement in Beam CB3 was 32.3 percent of the area of the steel section.

4.4.2 Load-Deflection and Load-Rotation Relationships

Load-deflection and load-rotation relationships have similar characteristics as indicated in Figures 4.5 and 4.6. They consist of three ranges, i.e., elastic, plastic and unloading ranges. The deflections at the maximum load were 2.6, 1.8 and 2.1 inches for Beams CB1, CB2 and CB3, respectively. These values indicate an increase in deflection with decrease in the ratio of the area of longitudinal reinforcement to the area of the steel section.

Rotation measurements at the ultimate load were not dependable. Since the rotation bars were welded to the web of the steel section, deformation of the web affected the rotation measurement. End rotations at ultimate load were approximately 5 times the rotations at initial yielding. The unloading portions of the load-rotation curves are different to those obtained for isolated simple beams under negative bending due to the fact that continuous beams have greater ductility than isolated simple beams.

4.4.3 Load-Reaction and Load-Moment Relationships

Reactions were determined from the location of points of inflection. The moment diagram is linear for concentrated loads. If the concrete slab does not have tensile cracks, the strain can be assumed to vary linearly along the span and the location of a point of inflection may be determined by linear interpolation between strains measured on both sides of the point of inflection. If the concrete slab has tensile cracks, the location of a point of inflection is related to the stiffness and the distance from the neutral axis to the gage location in positive and negative moment regions. However, the effect of cracking to moments is not significant. Strains 24 and 36 inches from the interior support did not exceed yield strain values in any of the beams. The points of inflection in each span were almost equidistant from the interior support and therefore the two exterior reactions and the moments at the load positions were almost equal in the elastic range. However, in the plastic and unloading portions they differed slightly as shown in Figures 4.7 and 4.8 probably due to imperfections in the beams affecting symmetry.

Bending moments are proportional to the applied load in the elastic range. Figures 4.8 show slight moment redistribution in Beams CB1 and CB2 for loads greater than 90 Kips and significant redistribution in Beam CB3 for loads greater than 50 Kips.

4.4.4 Moment-Curvature Relationships

Curvature values were obtained from strains at the top and bottom of the steel sections. The range of curvatures which could be measured by this means was limited because the strain gages were not

effective beyond strains of 2 to 3 percent. Therefore curvatures were not obtained for the unloading range.

Although moment-curvature relationships for Beam CB1 indicate that stiffness in the positive moment regions was greater than in the negative moment regions for elastic conditions, inelastic stiffness was approximately the same in both regions. Therefore the ratio of inelastic to elastic stiffness in the negative moment region is greater than that in the positive moment regions. This may be related to the descending portion of the stress-strain relationship for concrete. This effect is apparent in all beams tested.

4.4.5 Slip and Slip-Strain

Maximum slip occurred at locations near the load, as shown in Figures 4.10. This behavior is similar to that observed in simple span beams[20][40]. Since shear forces are in opposite directions on opposite sides of the load, slip deformations reverse at the load location. Load-slip relationships presented in Figures 4.9 include the unloading portion, which is not defined in the pushout test.

As shown in Figures 4.11, there is no particular trend in the slip-strain distribution.

4.4.6 Strains in Transverse Reinforcement

Strains were measured in the transverse reinforcing bars which were located 3 inches from the bottom of the slab in positive moment regions and 2¼ inches from the bottom of the slab in negative moment regions. Figures 4.14 indicate that strains in the transverse reinforcement exceeded yield strain in positive moment regions but not in the negative moment region.

4.4.7 Effective Slab Width

The effective slab width may be evaluated from the stress distribution. The ratio of strain at the edge of the slab to that at the center, γ_ε, was approximately 70 percent as shown in Figure 4.13. The theoretical strain distribution over the slab width is an exponential function[51]. Assuming the function as a parabola, the effective slab width, b_e, may be expressed as

$$b_e = b_c - \frac{2}{3}(1 - \gamma_\varepsilon)(b_c - b) \qquad 4.1$$

For the beams tested, b = 6.5 in., b_c = 48 in. and γ_ε = 0.7. Therefore the effective slab width is 39.7 inches. This results in $(b_e - b)/(b_c - b)$ equal to 0.81 or in $(b_c - b)/\ell$ equal to 0.23.

According to CSA Standard S16[7] the effective projection of the slab beyond the flange of the steel section is considered to be the smaller of: (i) one-sixth of the beam span and (ii) twelve times the slab thickness for a slab which is not supported along its edges, and the smaller of: (i) one-fourth of the beam span and (ii) sixteen times the slab thickness for a slab which is supported along its edges. The effective design width, therefore, is 30.5 inches for the former case and 40.5 inches for the latter case. The effective slab width for the test beams with unsupported slab edges was therefore greater than the Code value and was close to the Code value for a beam with supported slab edges.

4.4.8 Crack Patterns

Three crack patterns were developed in the slab, i.e.,

transverse cracking, longitudinal cracking and herringbone cracking as shown in Figures 4.15. Transverse cracks were developed in the negative moment regions due to tensile stress at relatively small loads. Longitudinal cracks at the load points were produced along the centerline of the beam at relatively large loads. Herringbone cracks were developed at large loads and the direction of the cracks was approximately 45° to the beam centerline near the ends of the beams. The angle decreased as the load point was approached. These two crack patterns, i.e., longitudinal and herringbone, are caused by the stresses produced around shear connectors[65,66] and by the relatively large tensile strain as a result of Poisson's ratio effect.

TABLE 4.1 TEST SPECIMENS

BEAM	STEEL SECTION	SLAB DIMENSION		LONGITUDINAL REIN-FORCEMENT	AREA OF LONGITUDINAL REIN-FORCEMENT (in^2)	RATIO OF LONGITUDINAL REINFORCEMENT AREA TO STEEL SECTION AREA	TRANSVERSE REINFORCEMENT	RATIO OF TRANSVERSE REINFORCEMENT AREA TO CONCRETE SLAB AREA
		WIDTH (inches)	THICKNESS (inches)					
CB1	W12x31	48	4	8 #4 BARS	1.6	0.176	#3 BARS @4.5"	0.0067
CB2	W12x27	48	4	10 #5 BARS	3.1	0.389	#3 BARS @4.5"	0.0067
CB3	W10x21	48	4	10 #4 BARS	2.0	0.323	#3 BARS @4.5"	0.0067

TABLE 4.2 PROPERTIES OF SLAB REINFORCEMENT

BAR SIZE	YIELD STRESS (ksi)	ULTIMATE STRESS (ksi)
#3	53.4	75.1
	52.6	76.0
	52.8	75.2
	Ave. 52.9	Ave. 75.4
#4	59.1	83.3
	59.3	84.1
	59.6	84.1
	Ave. 59.3	Ave. 83.8
#5	52.2	76.3
	49.4	76.6
	49.4	76.8
	Ave. 50.3	Ave. 76.6

TABLE 4.3 PROPERTIES OF STRUCTURAL STEEL

COUPON	YIELD STRESS (ksi)	ULTIMATE STRESS (ksi)	MODULUS OF ELASTICITY (ksi)	STRAIN AT STRAIN-HARDENING (inches/inch)	STRAIN-HARDENING MODULUS (ksi)
	40.4	66.3	29400	.0096	1330
W12x31	41.0	67.1	31700	.0070	1250
FLANGE	41.4	67.5	30000	.0126	1330
	39.1	66.3	30100	.0068	1360
Ave.	40.5	66.8	30200	.0090	1317
	46.7	73.8	30700	.0197	1050
W12x31	47.8	70.7	31600	.0200	1140
WEB	46.2	68.8	30500	.0176	1470
Ave.	46.9	71.1	30900	.0194	1220
	45.7	67.1	32200	.0065	1180
W12x27	43.3	65.8	29200	.0120	1160
FLANGE	45.4	68.0	32400	.0028	1000
	46.3	69.1	29500	.0128	1130
Ave.	45.2	67.5	31300	.0085	1160
	48.8	67.1	29800	.0192	1110
W12x27	48.9	66.3	30400	.0258	--
WEB	49.6	66.6	30400	.0232	890
Ave.	49.1	66.7	30200	.0226	1000
	43.4	68.7	32600	.0180	850
W10x21	43.7	69.5	31900	.0142	850
FLANGE	43.1	68.8	32200	.0158	700
	43.9	68.7	31500	.0177	750
Ave.	43.5	68.9	32100	.0164	790
	47.5	69.0	27800	.0242	--
W10x21	48.2	68.6	29000	.0252	--
WEB	47.3	68.7	27700	.0230	--
Ave.	47.7	68.8	28200	.0241	--

TABLE 4.4 PROPERTIES OF CONCRETE*

BEAM	AGE AT TEST (days)	COMPRESSIVE STRESS (psi)	SPLITTING TENSION STRESS (psi)
CB1	72	5358	486
		5340	407
		5500	--
		5924	--
		5924	--
		Ave. 5577	446
CB2	69	5553	354
		5641	433
		5447	451
		5535	--
		5128	--
		Ave. 5460	410
CB3	72	6012	487
		5588	442
		5659	--
		6118	--
		6366	--
		Ave. 5948	465

* MIX PROPORTIONS

CEMENT	133 lbs.
WATER	66 lbs.
SAND	344 lbs.
COARSE AGGREGATE	500 lbs.

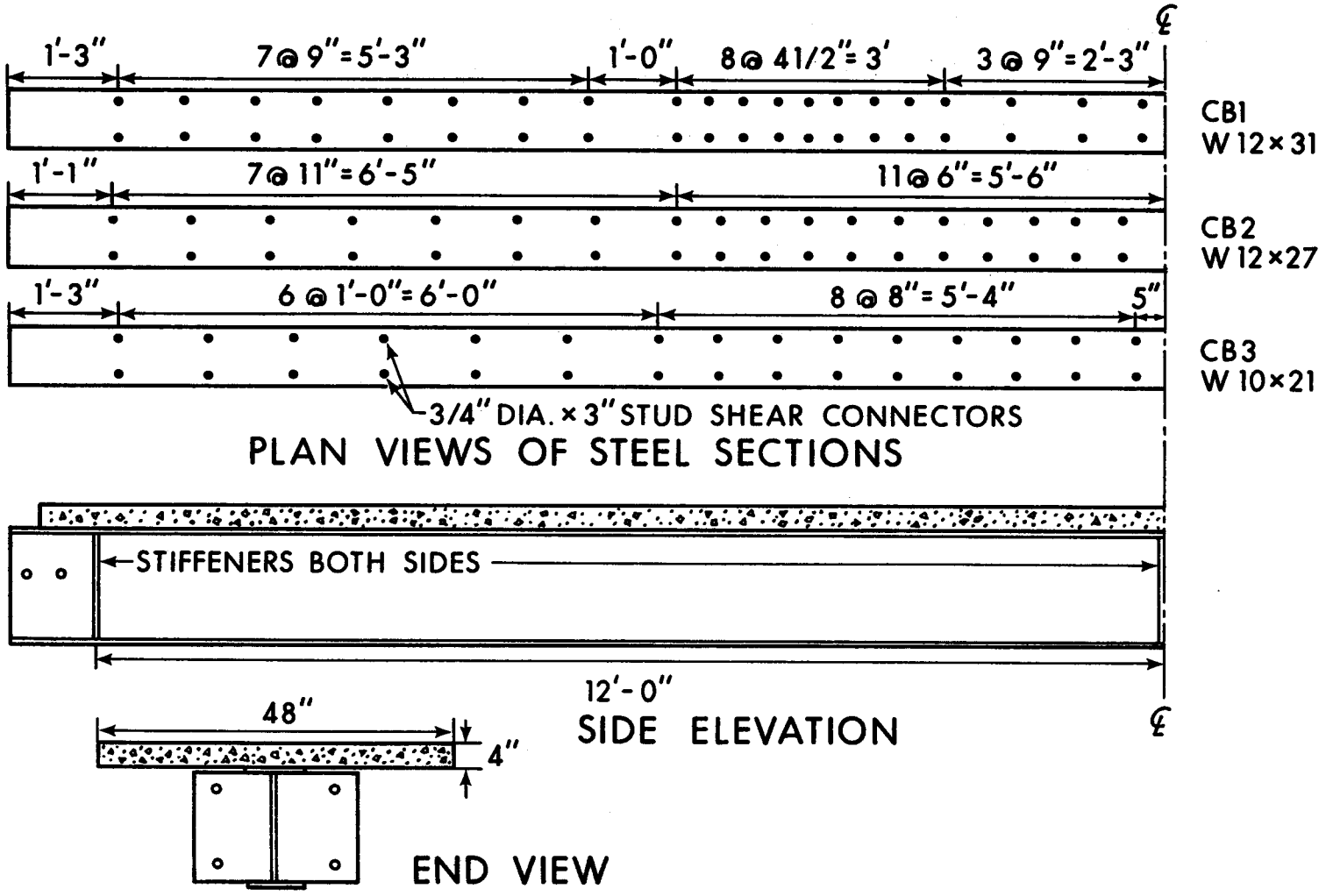

FIGURE 4.1 DETAILS OF TEST SPECIMENS

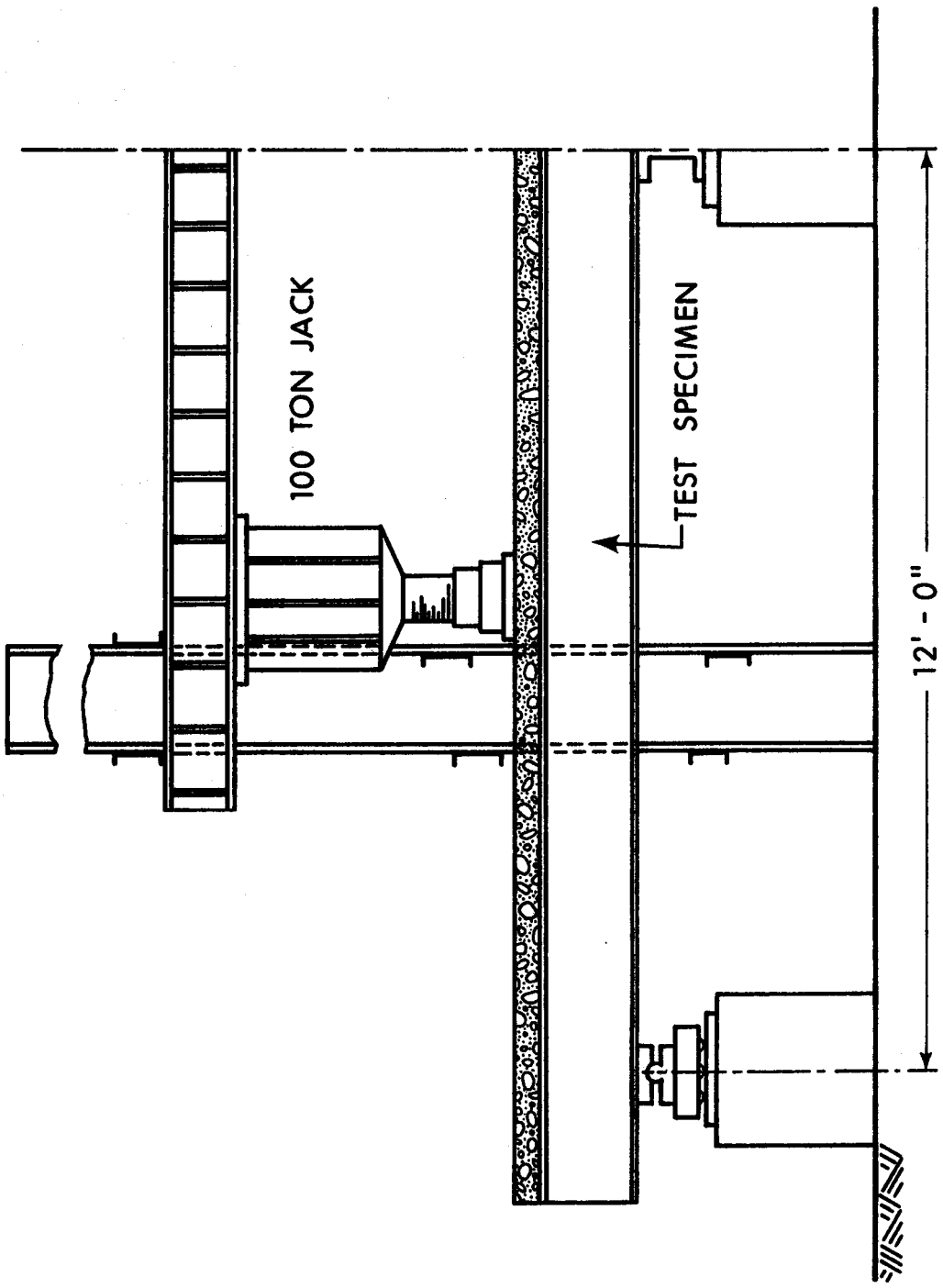

FIGURE 4.2 TEST SET-UP

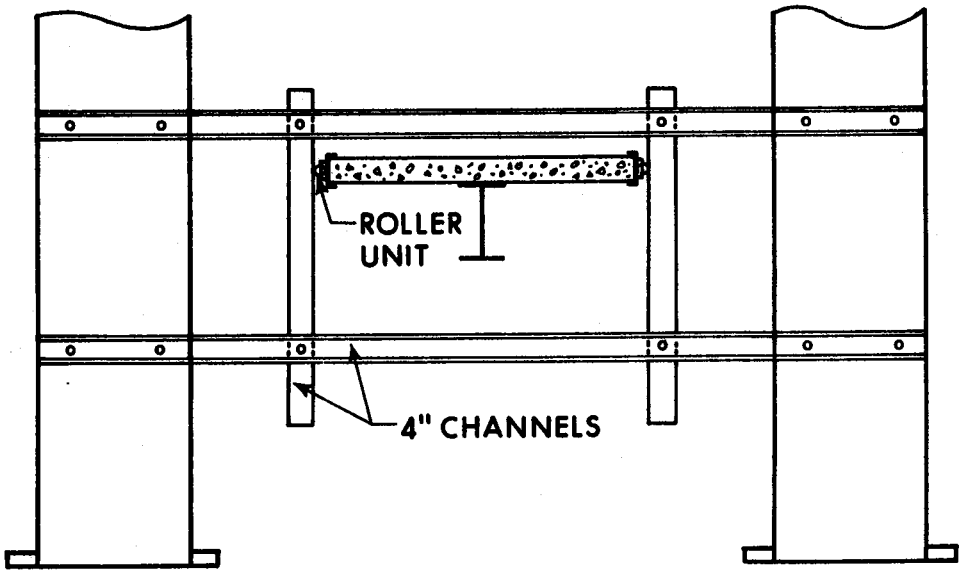

(a) LATERAL BRACING SYSTEM

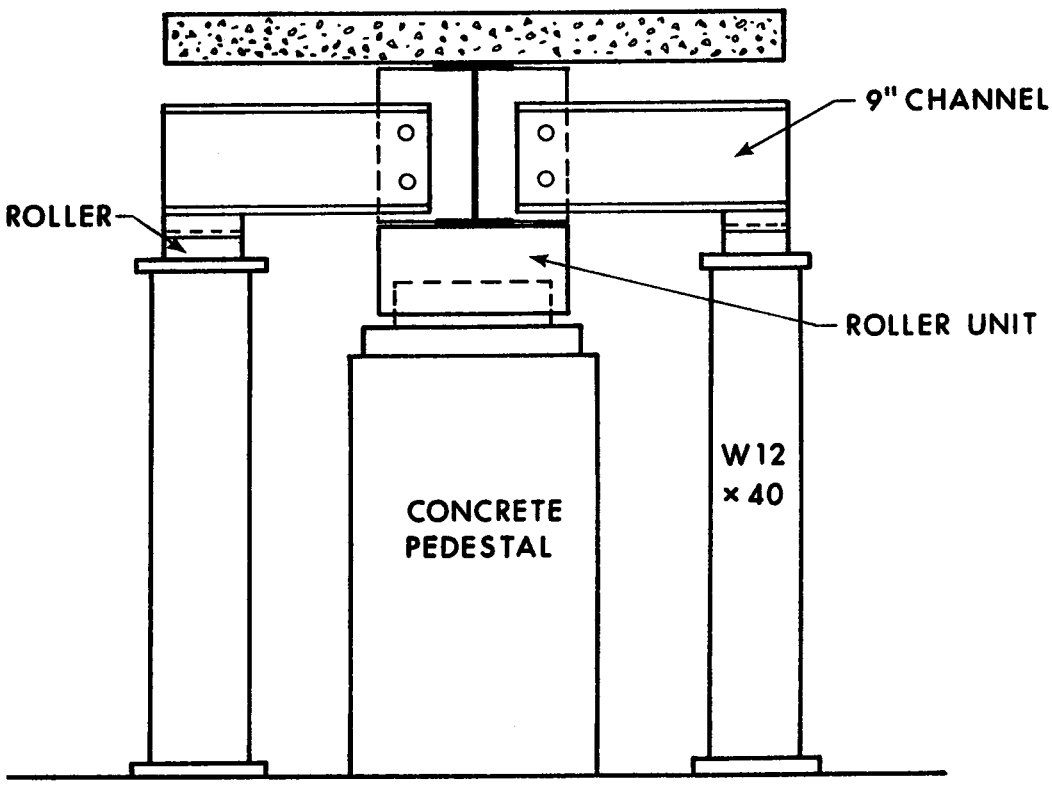

(b) REACTION SYSTEM

FIGURE 4.3 SUPPORT DETAILS

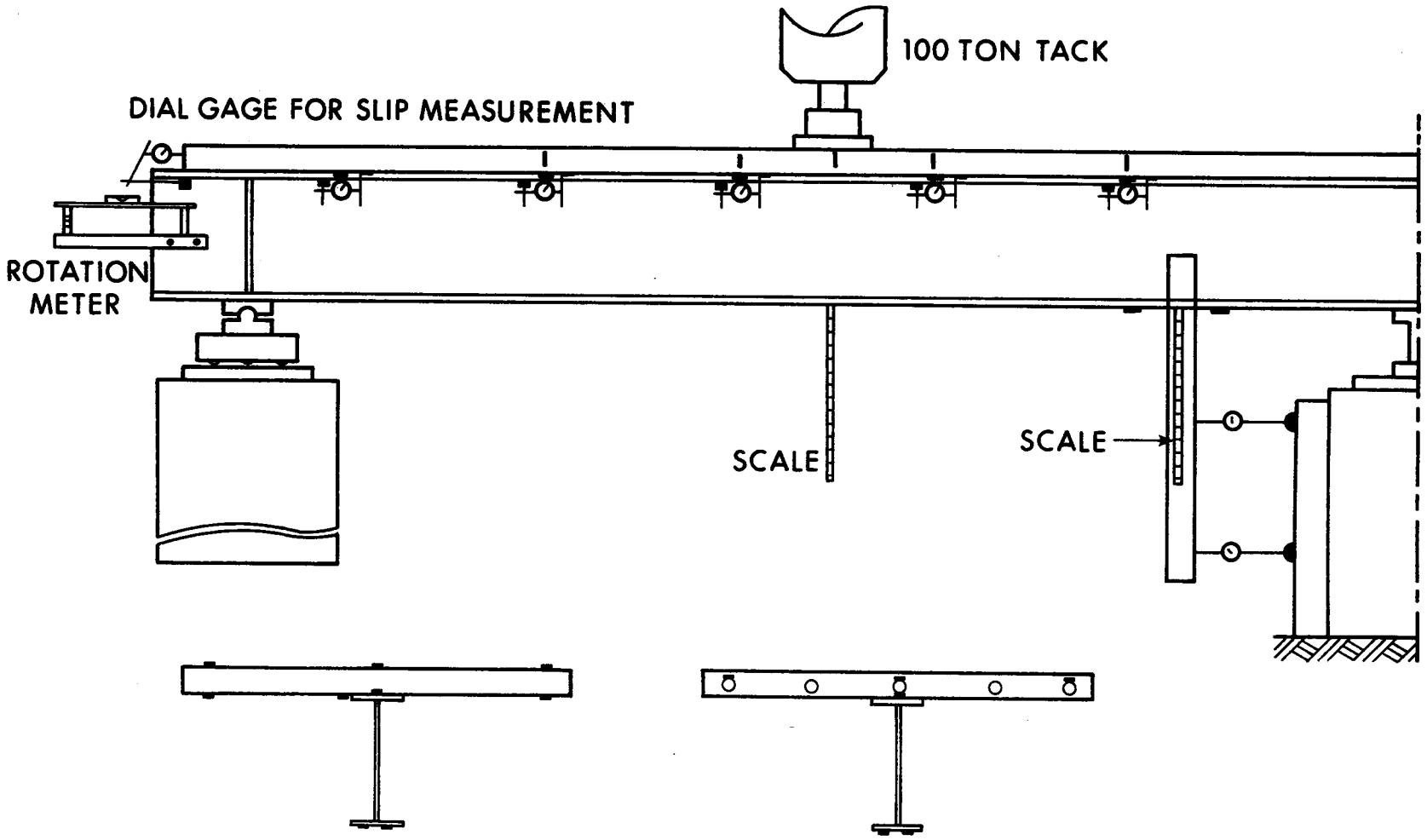

FIGURE 4.4 INSTRUMENTATION

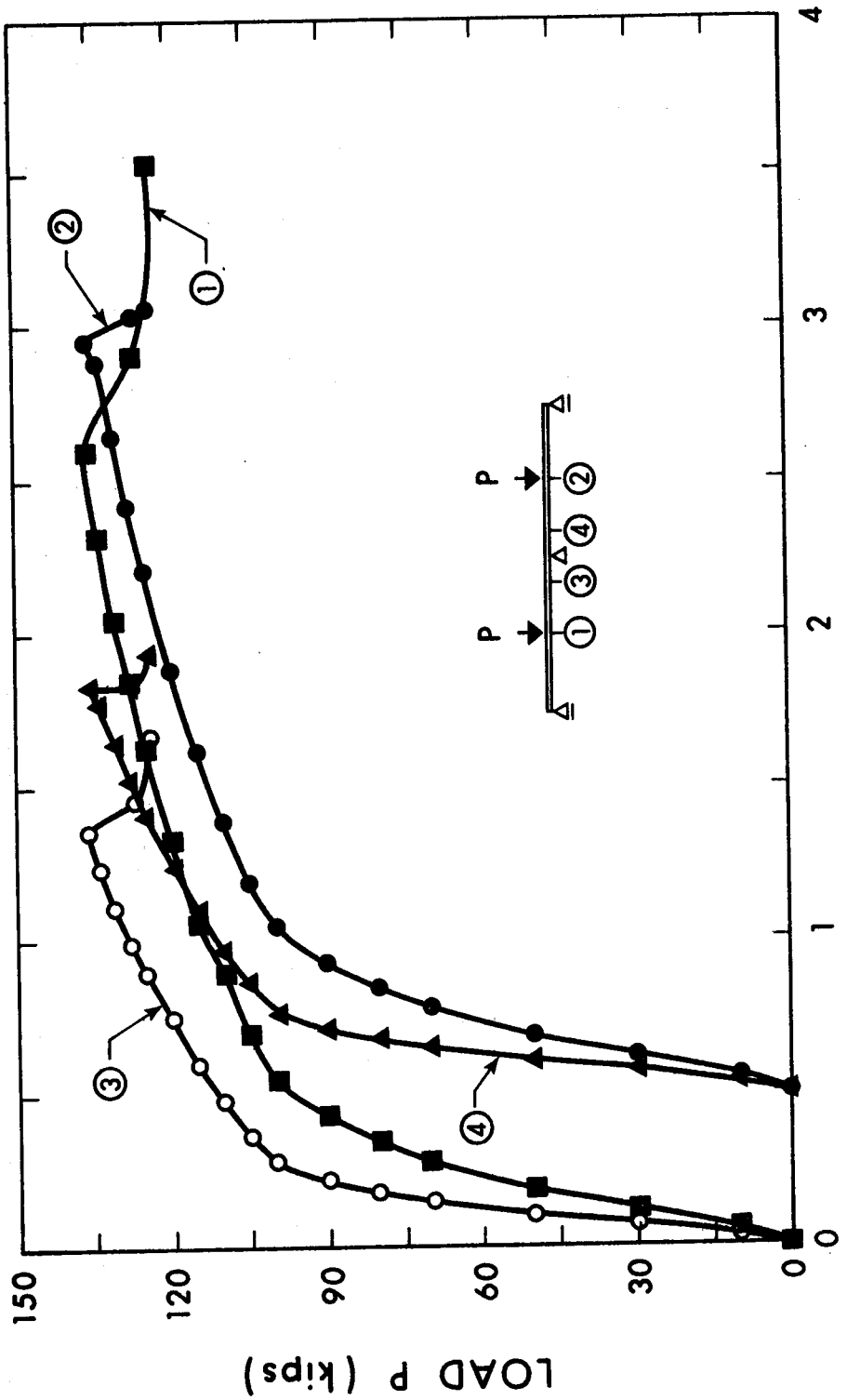

FIGURE 4.5(a) LOAD-DEFLECTION RELATIONSHIPS FOR BEAM CB1

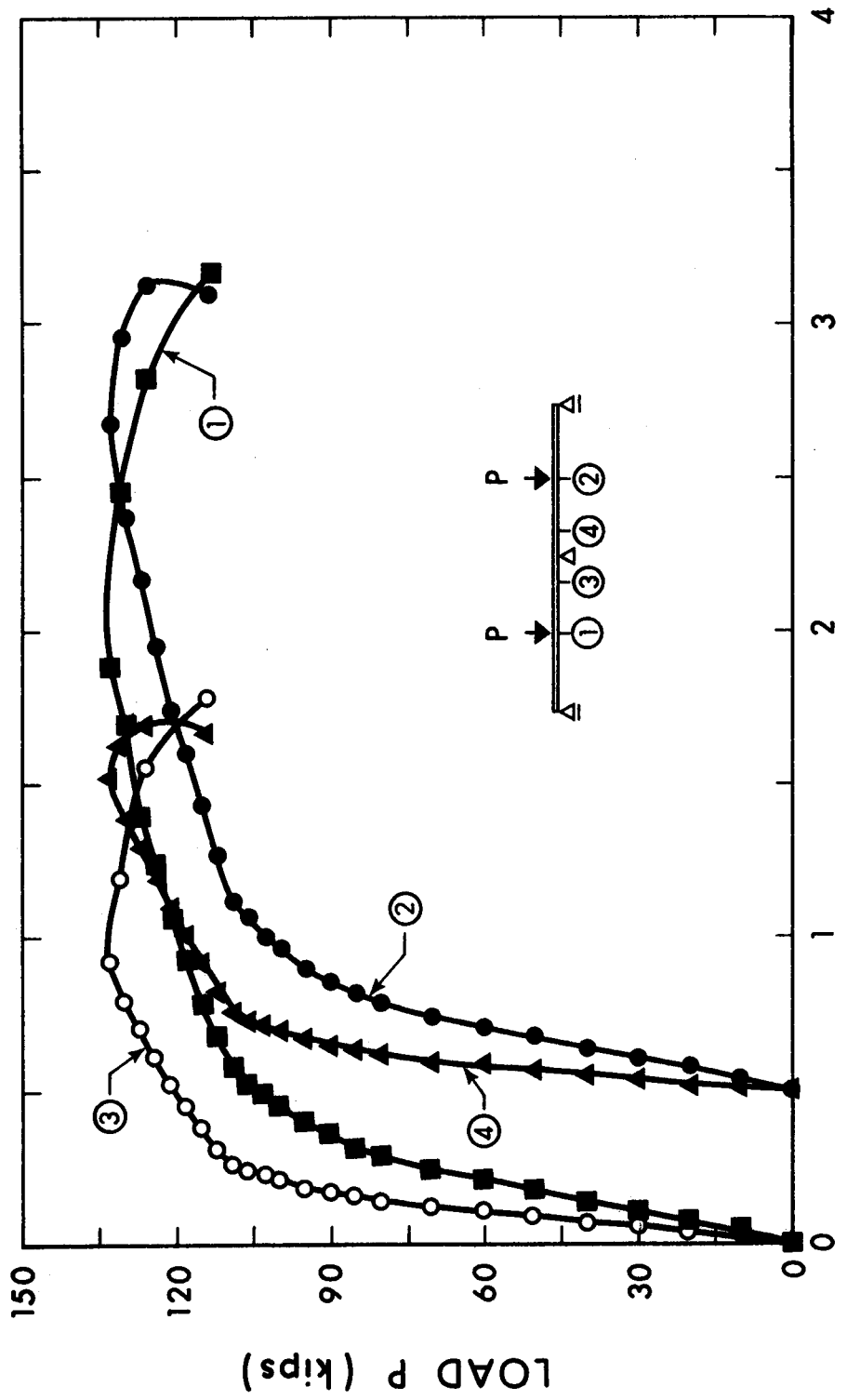

FIGURE 4.5(b) LOAD-DEFLECTION RELATIONSHIPS FOR BEAM CB2

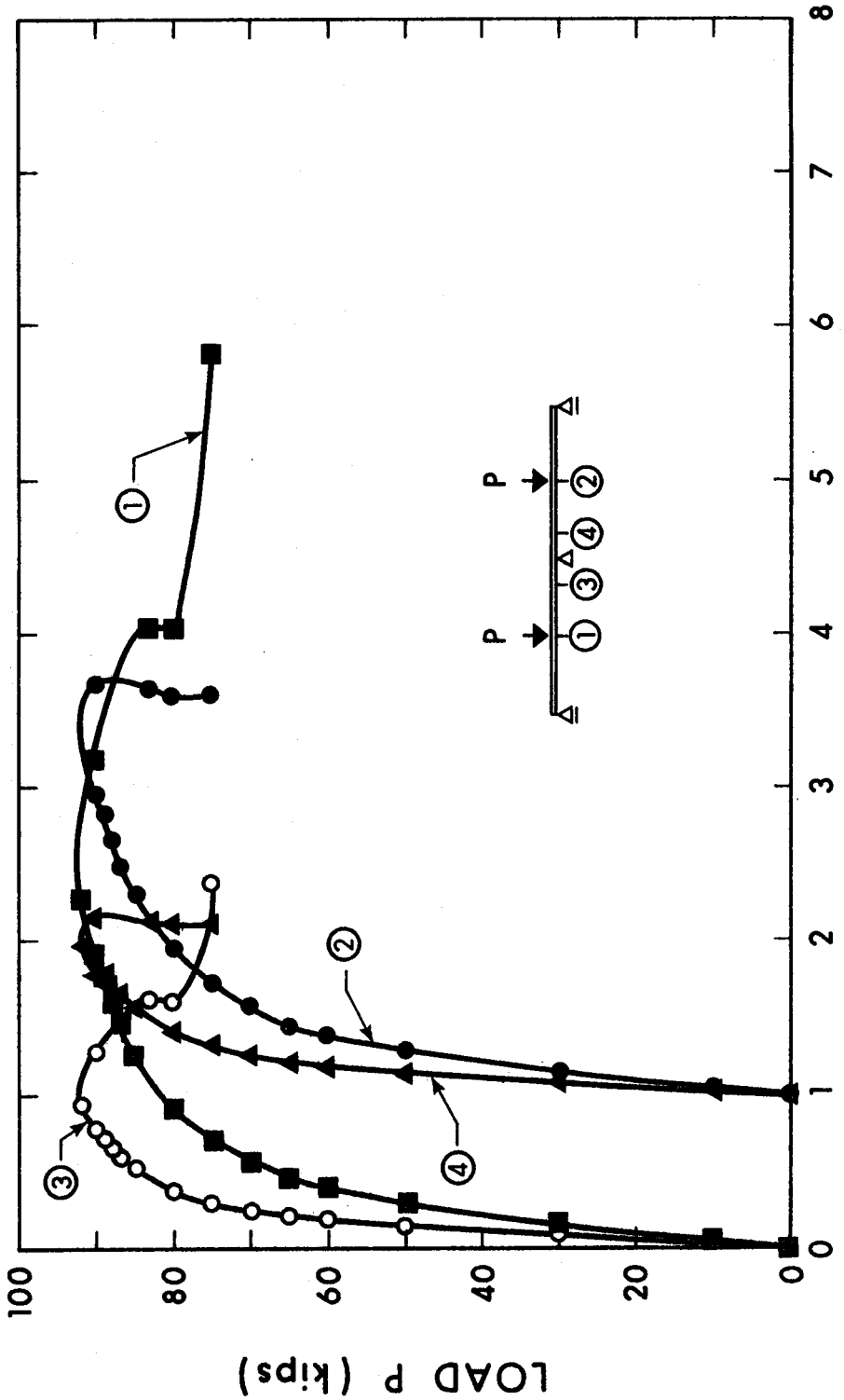

FIGURE 4.5(c) LOAD-DEFLECTION RELATIONSHIPS FOR BEAM CB3

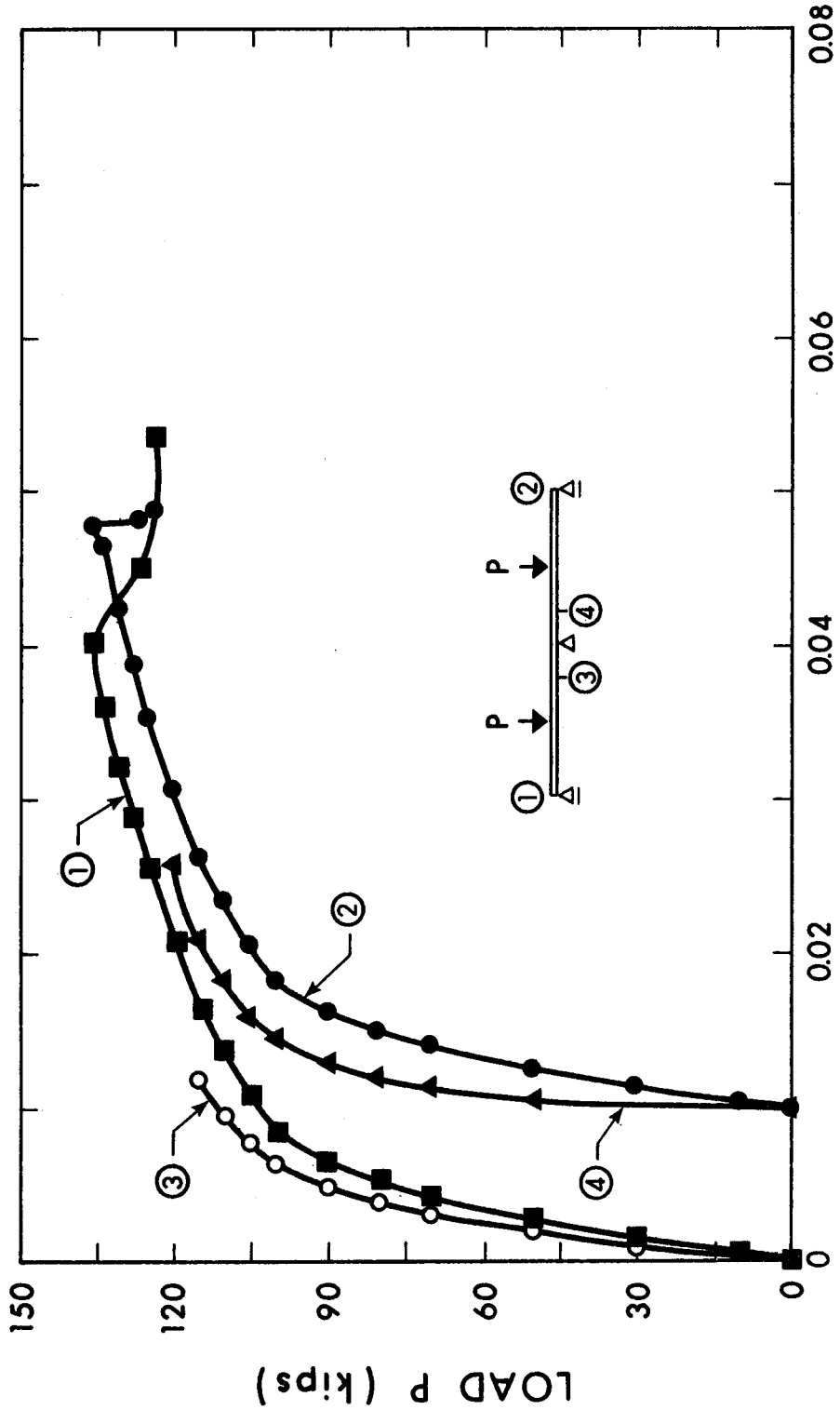

FIGURE 4.6(a) LOAD-ROTATION RELATIONSHIPS FOR BEAM CB1

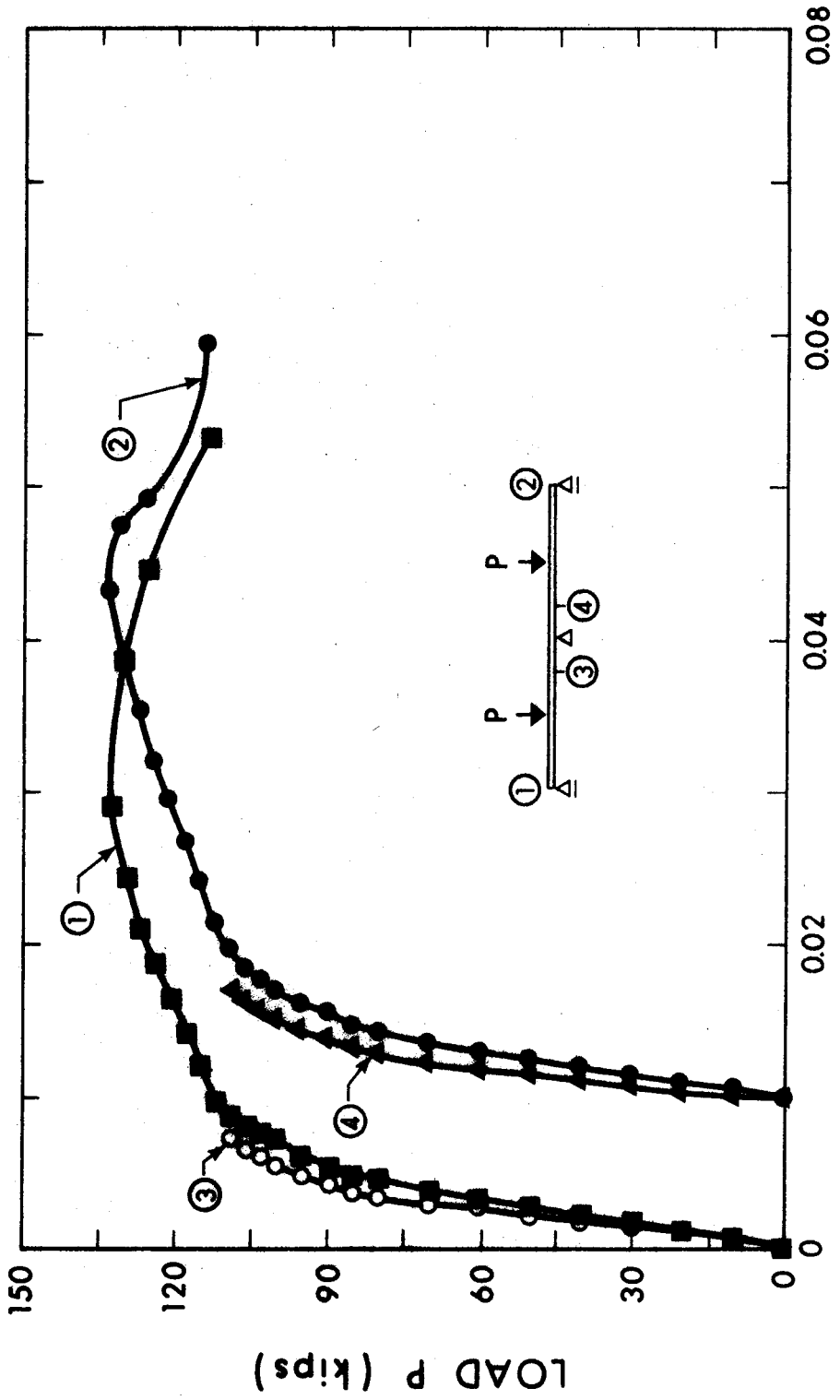

FIGURE 4.6(b) LOAD-ROTATION RELATIONSHIPS FOR BEAM CB2

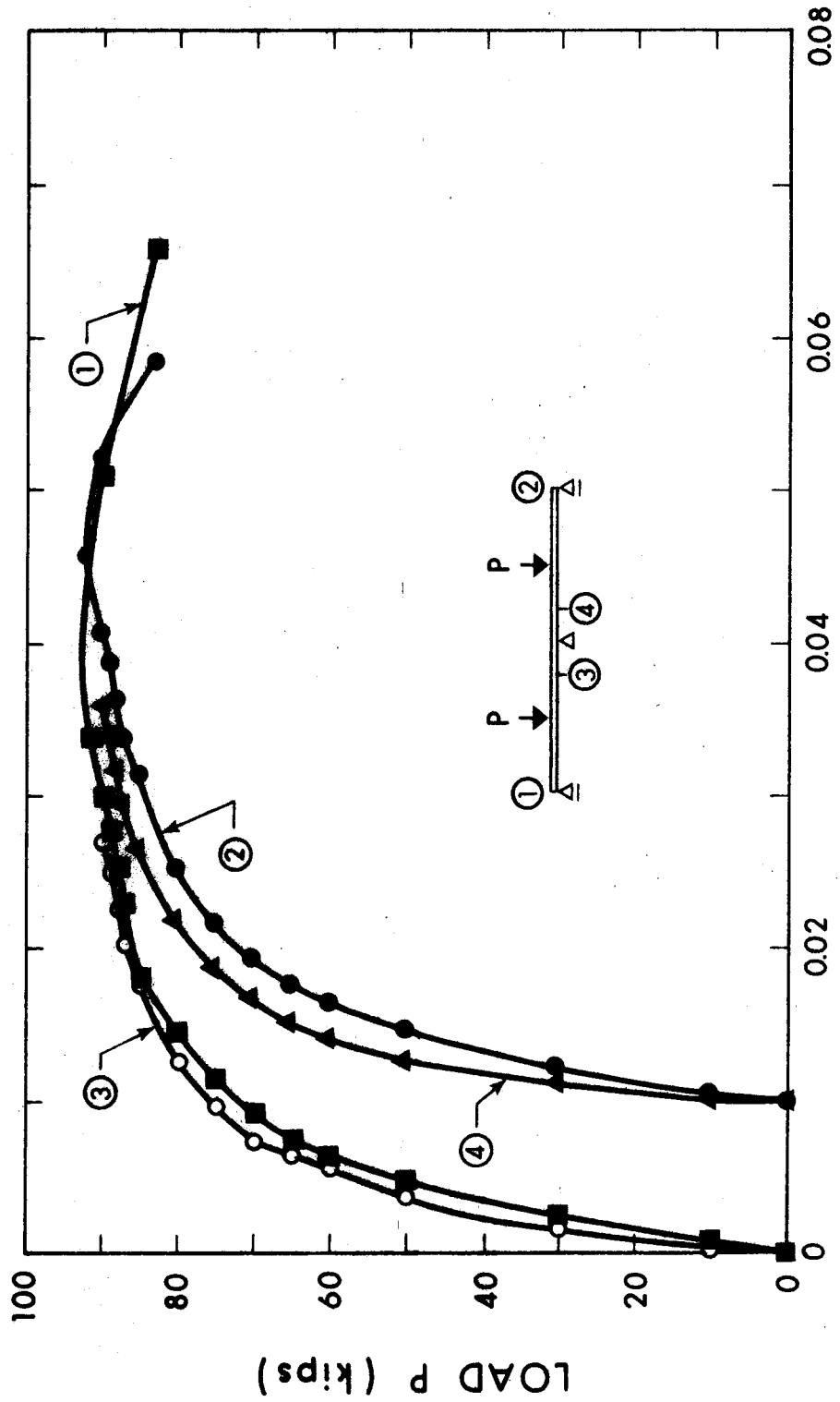

FIGURE 4.6(c) LOAD-ROTATION RELATIONSHIPS FOR BEAM CB3

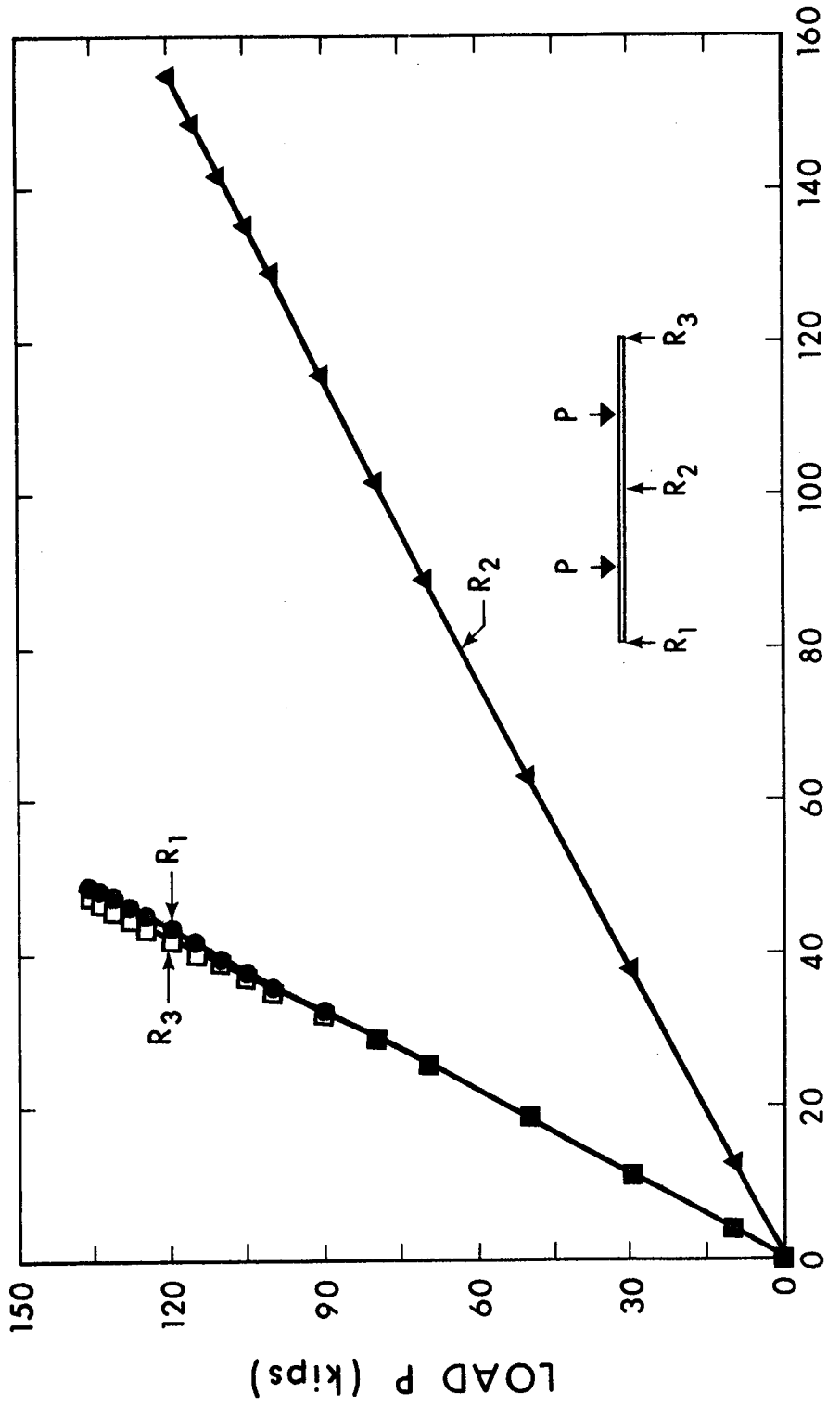

FIGURE 4.7(a) LOAD-REACTION RELATIONSHIPS FOR BEAM CB1

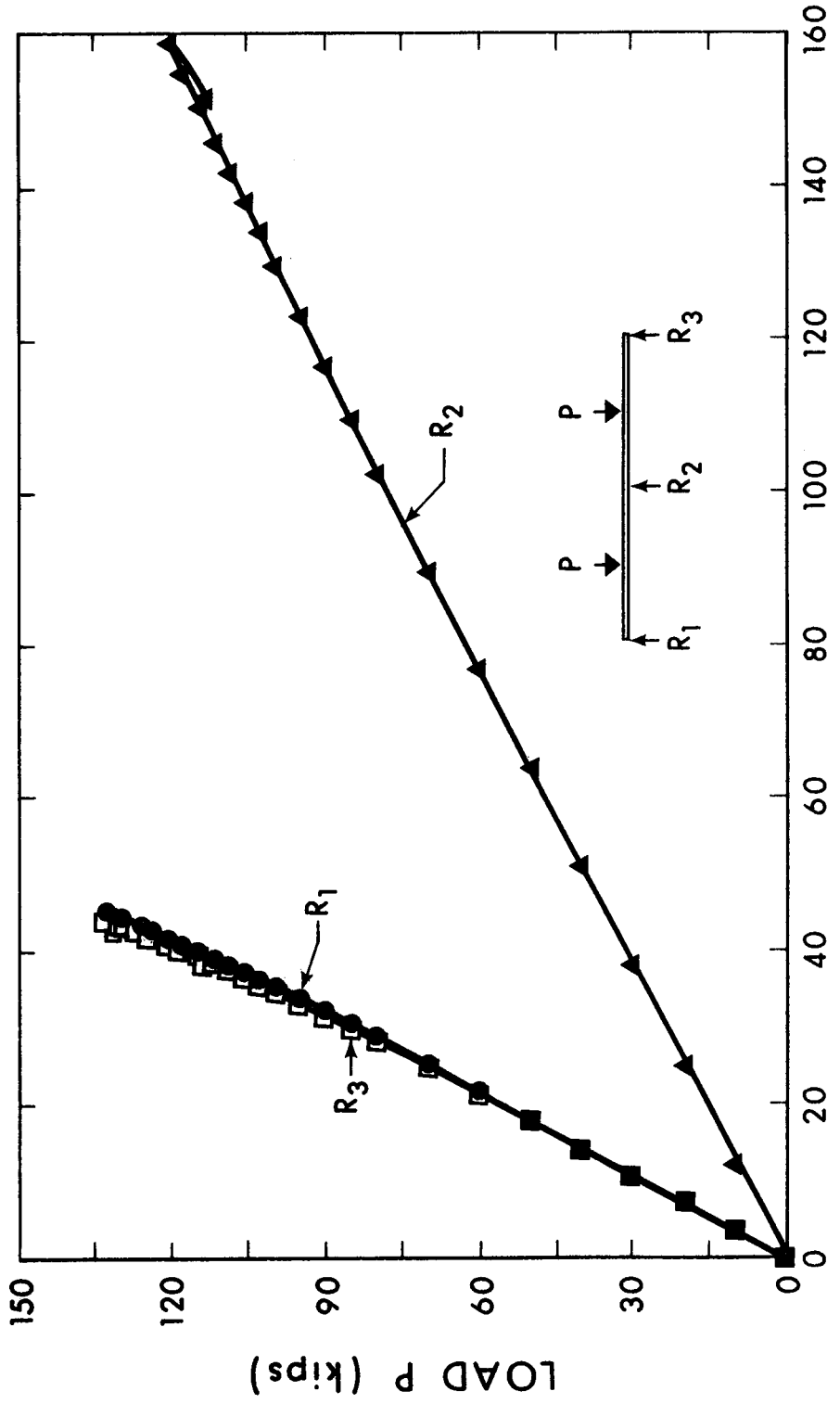

FIGURE 4.7(b) LOAD-REACTION RELATIONSHIPS FOR BEAM CB2

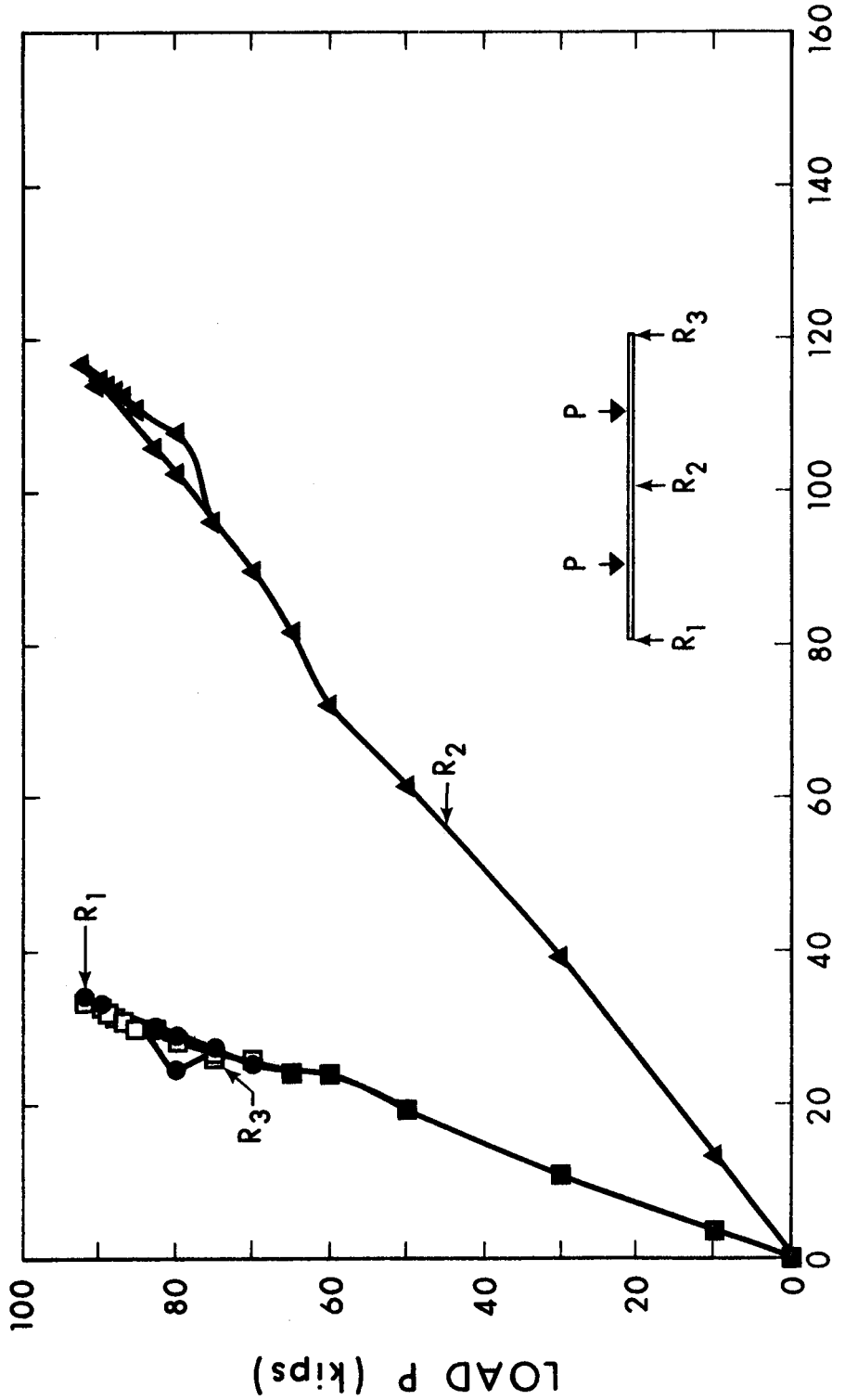

FIGURE 4.7(c) LOAD-REACTION RELATIONSHIPS FOR BEAM CB3

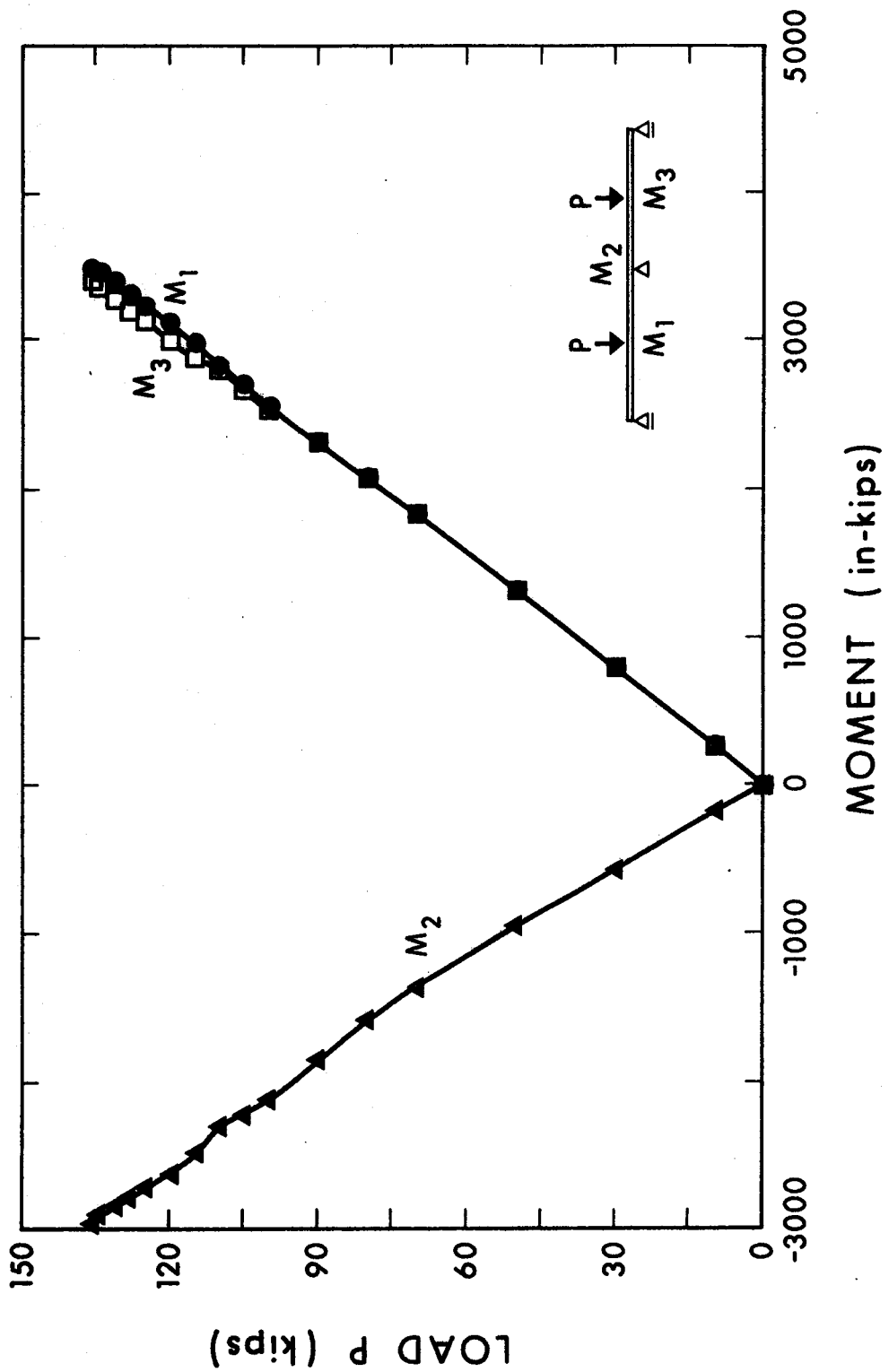

FIGURE 4.8(a) LOAD-BENDING MOMENT RELATIONSHIPS FOR BEAM CB1

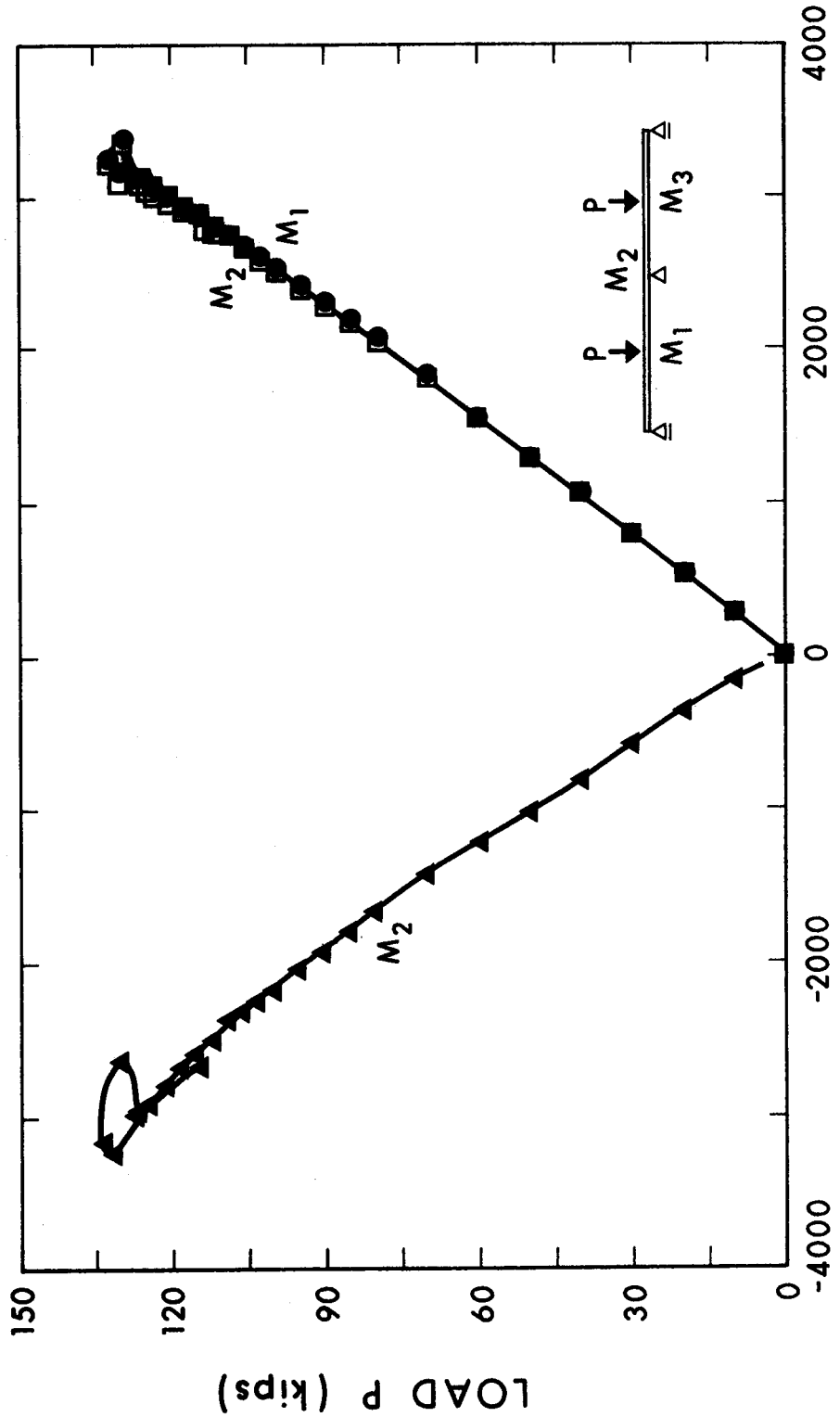

FIGURE 4.8(b) LOAD-BENDING MOMENT RELATIONSHIPS FOR BEAM CB2

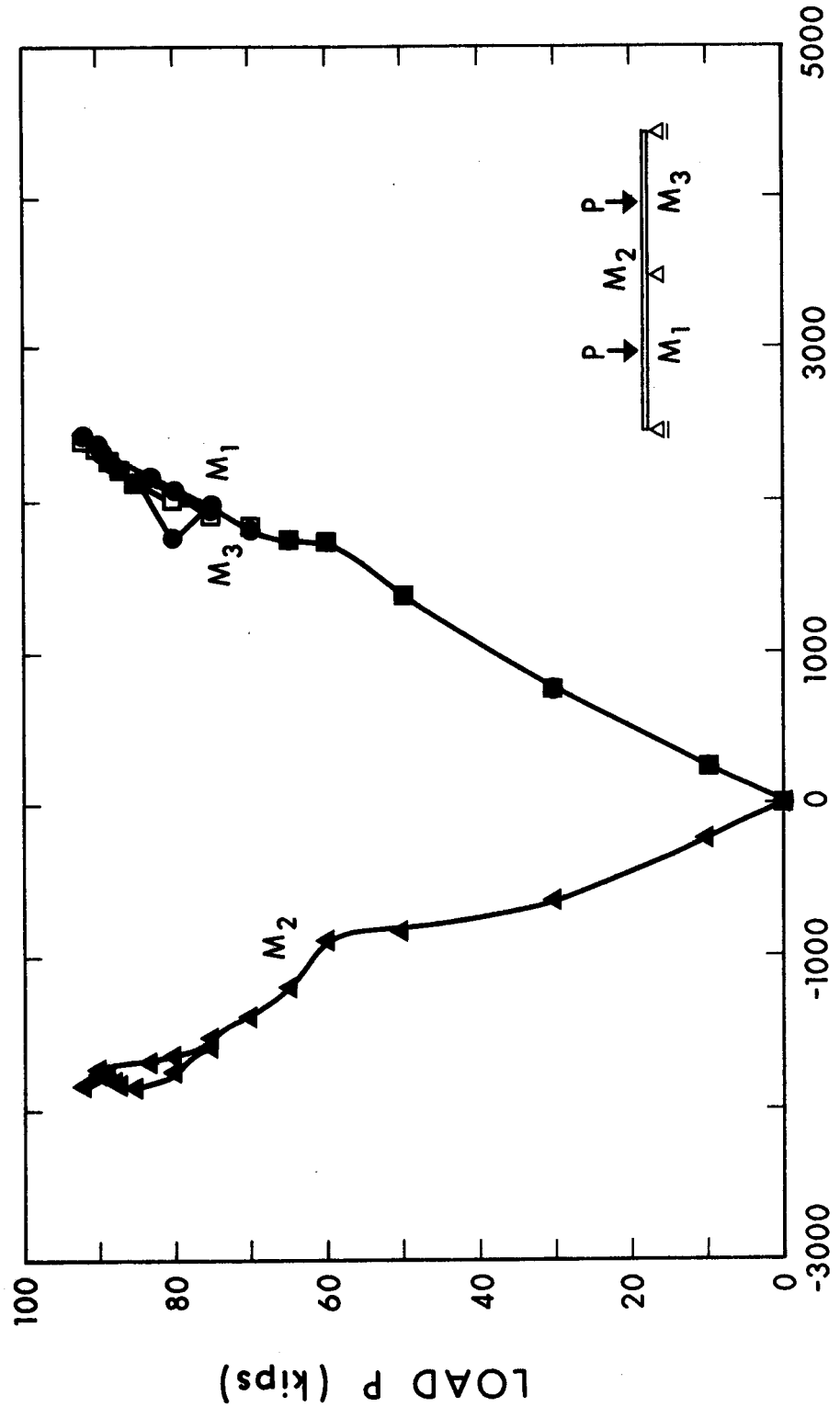

FIGURE 4.8(c) LOAD-BENDING MOMENT RELATIONSHIPS FOR BEAM CB3

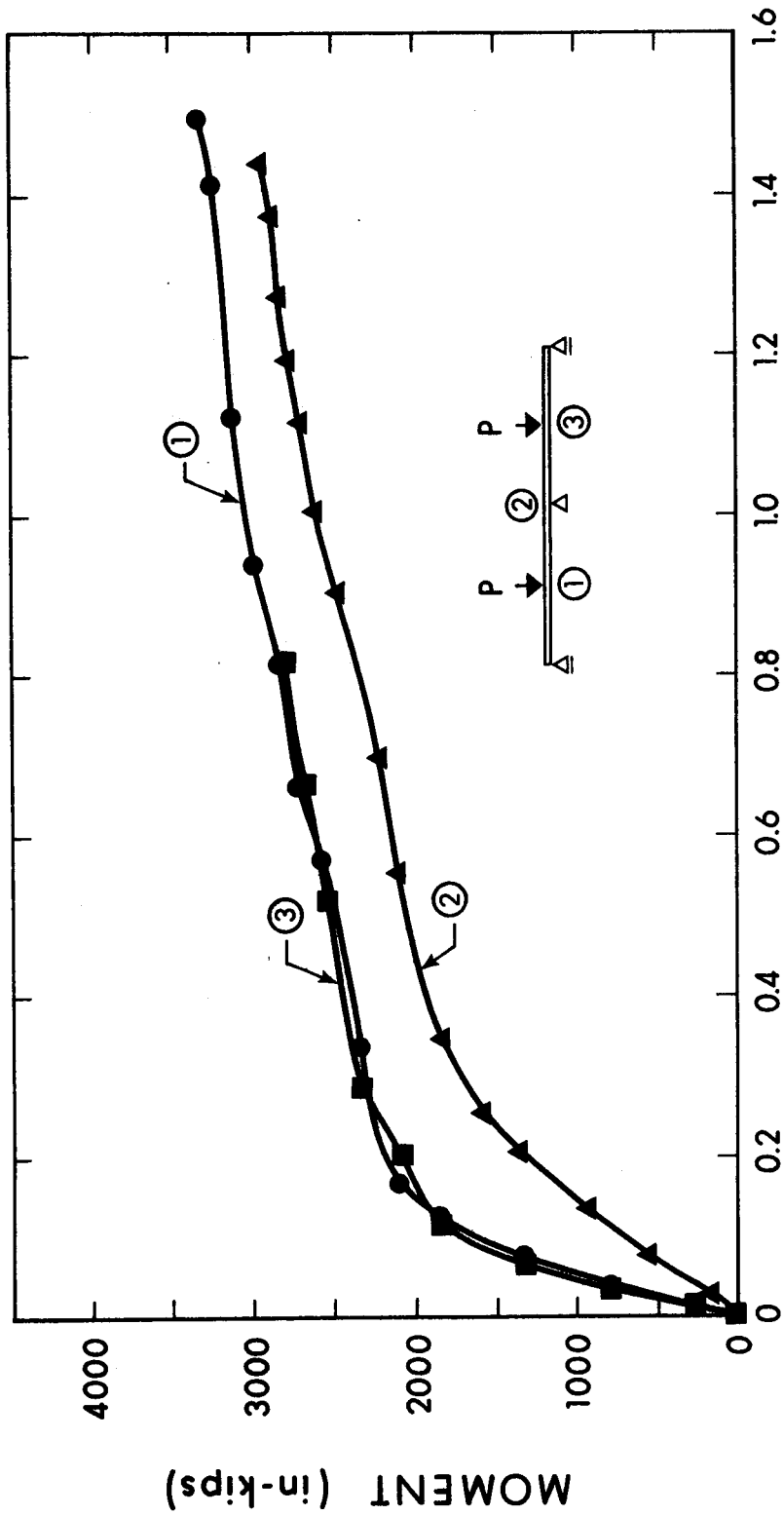

FIGURE 4.9(a) MOMENT-CURVATURE RELATIONSHIPS FOR BEAM CB1

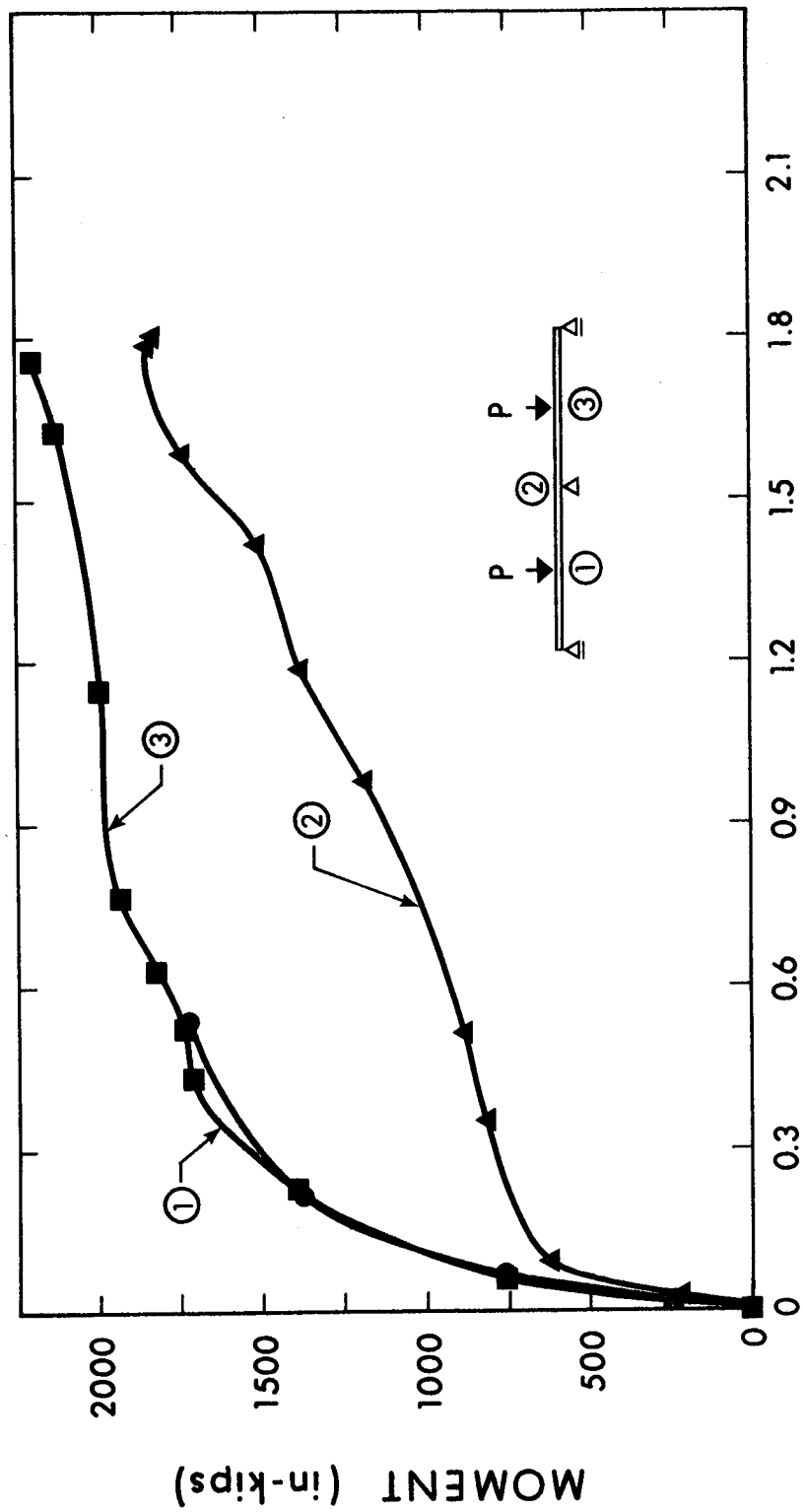

FIGURE 4.9(c) MOMENT-CURVATURE RELATIONSHIPS FOR BEAM CB3

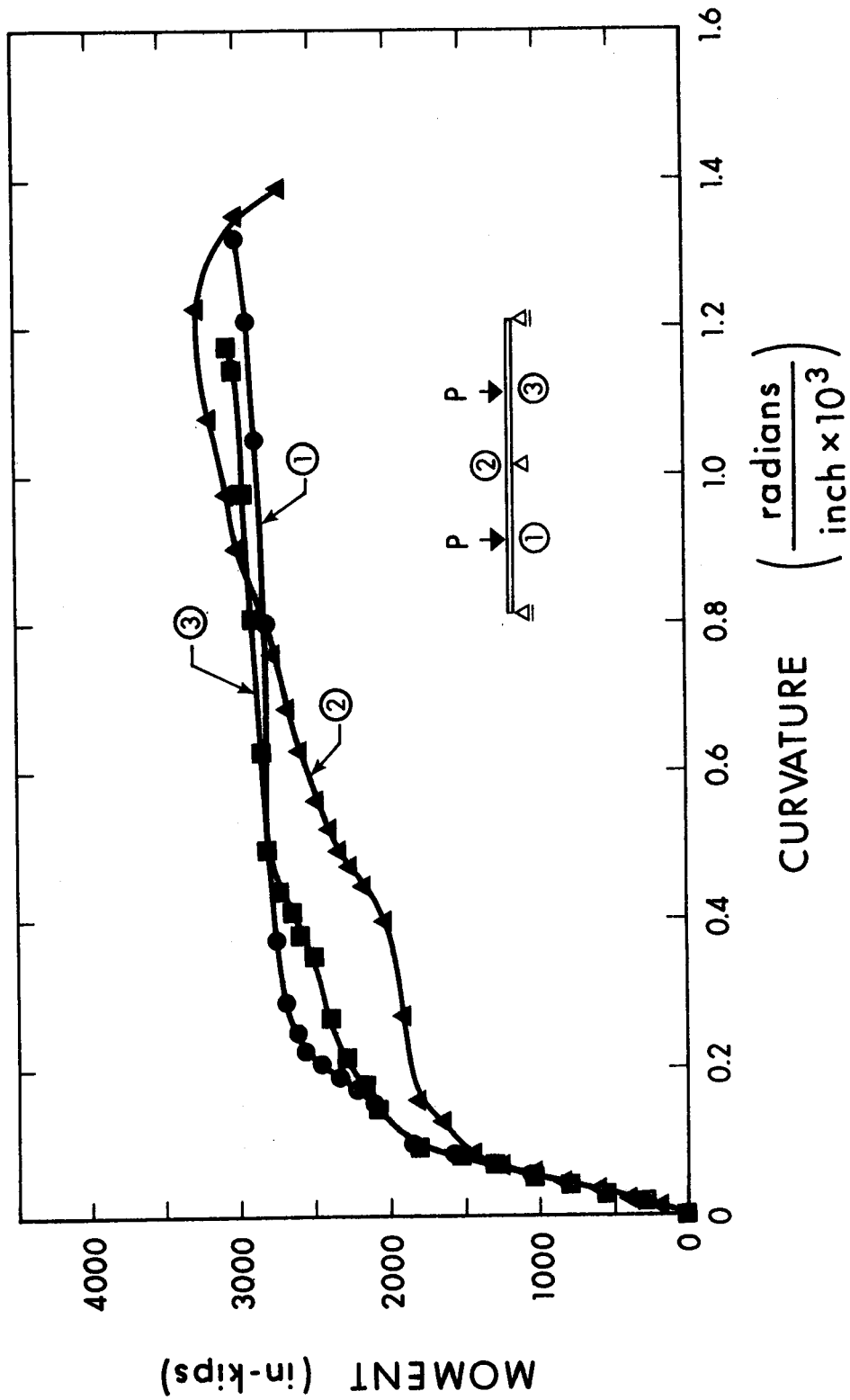

FIGURE 4.9(b) MOMENT-CURVATURE RELATIONSHIPS FOR BEAM CB2

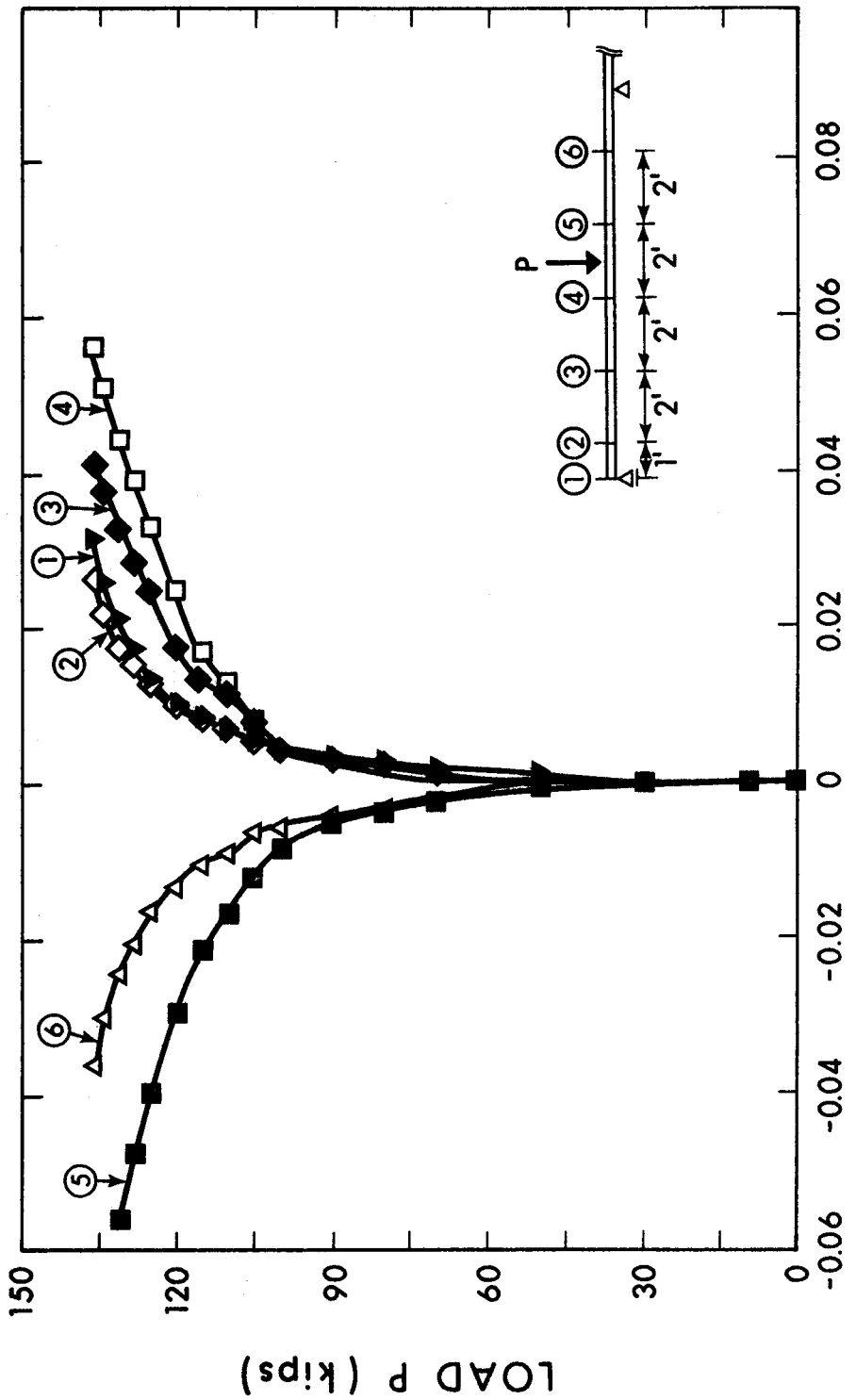

FIGURE 4.10(a) LOAD-SLIP RELATIONSHIPS FOR BEAM CB1

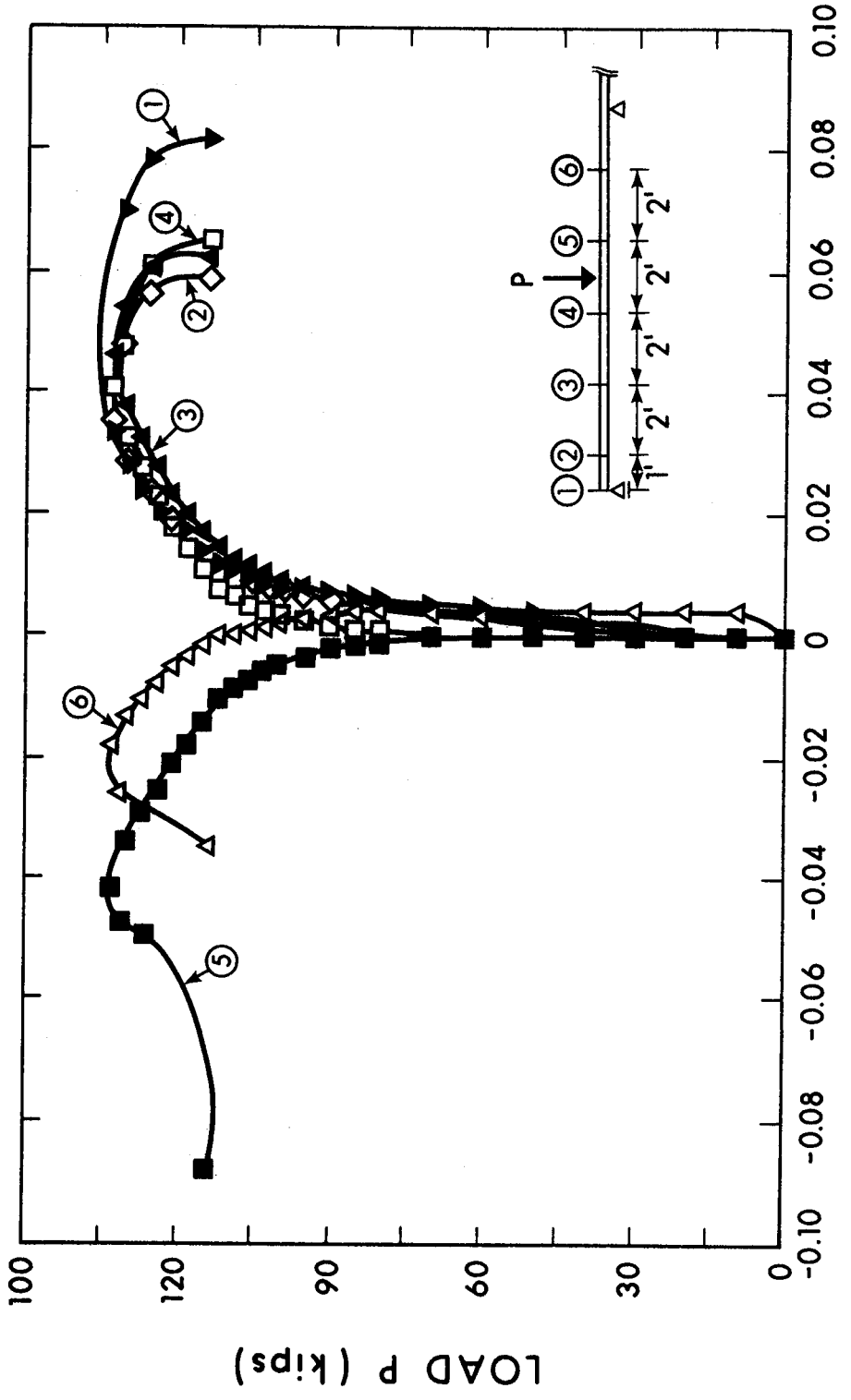

FIGURE 4.10(b) LOAD-SLIP RELATIONSHIPS FOR BEAM CB2

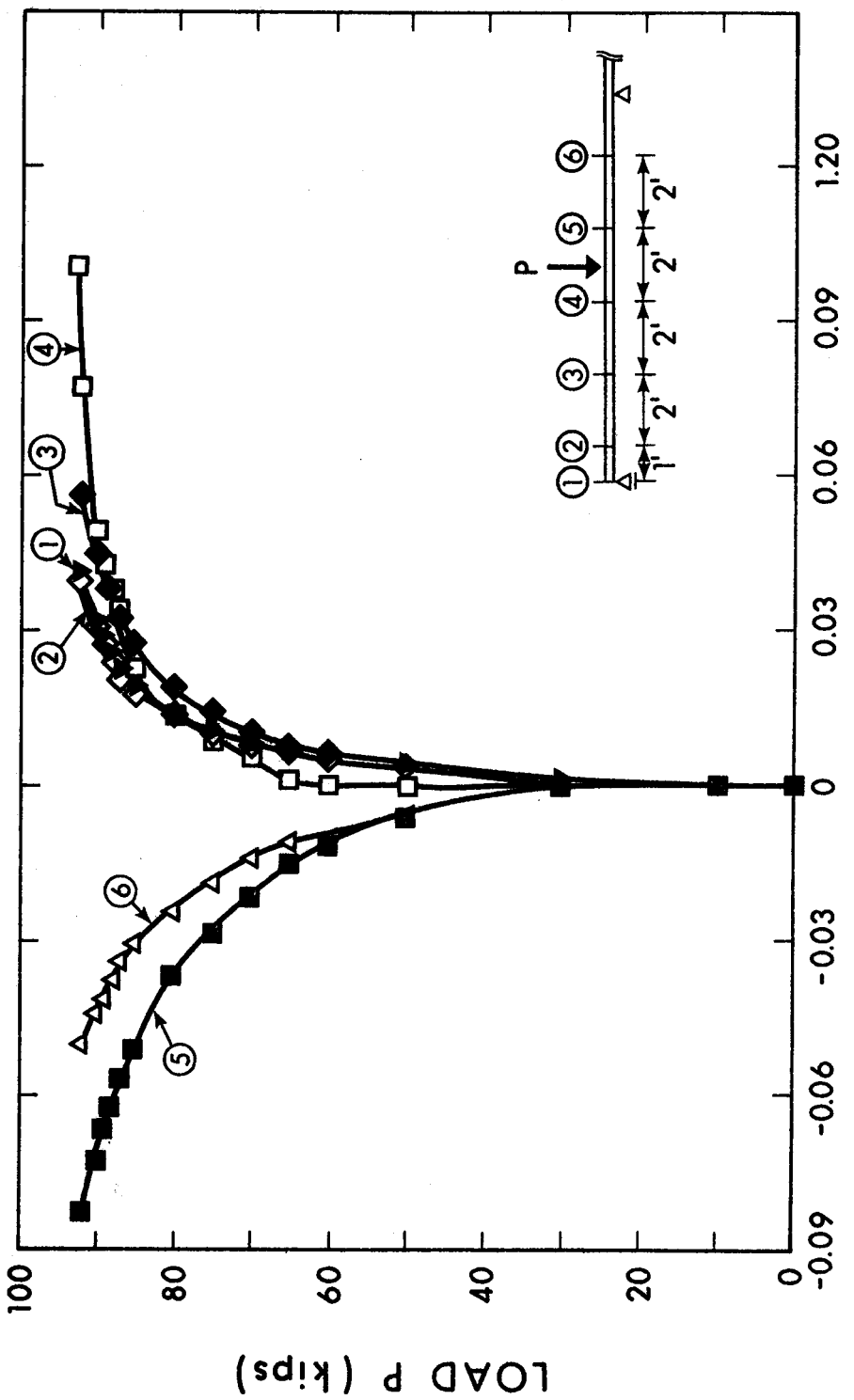

FIGURE 4.10(c) LOAD-SLIP RELATIONSHIPS FOR BEAM CB3

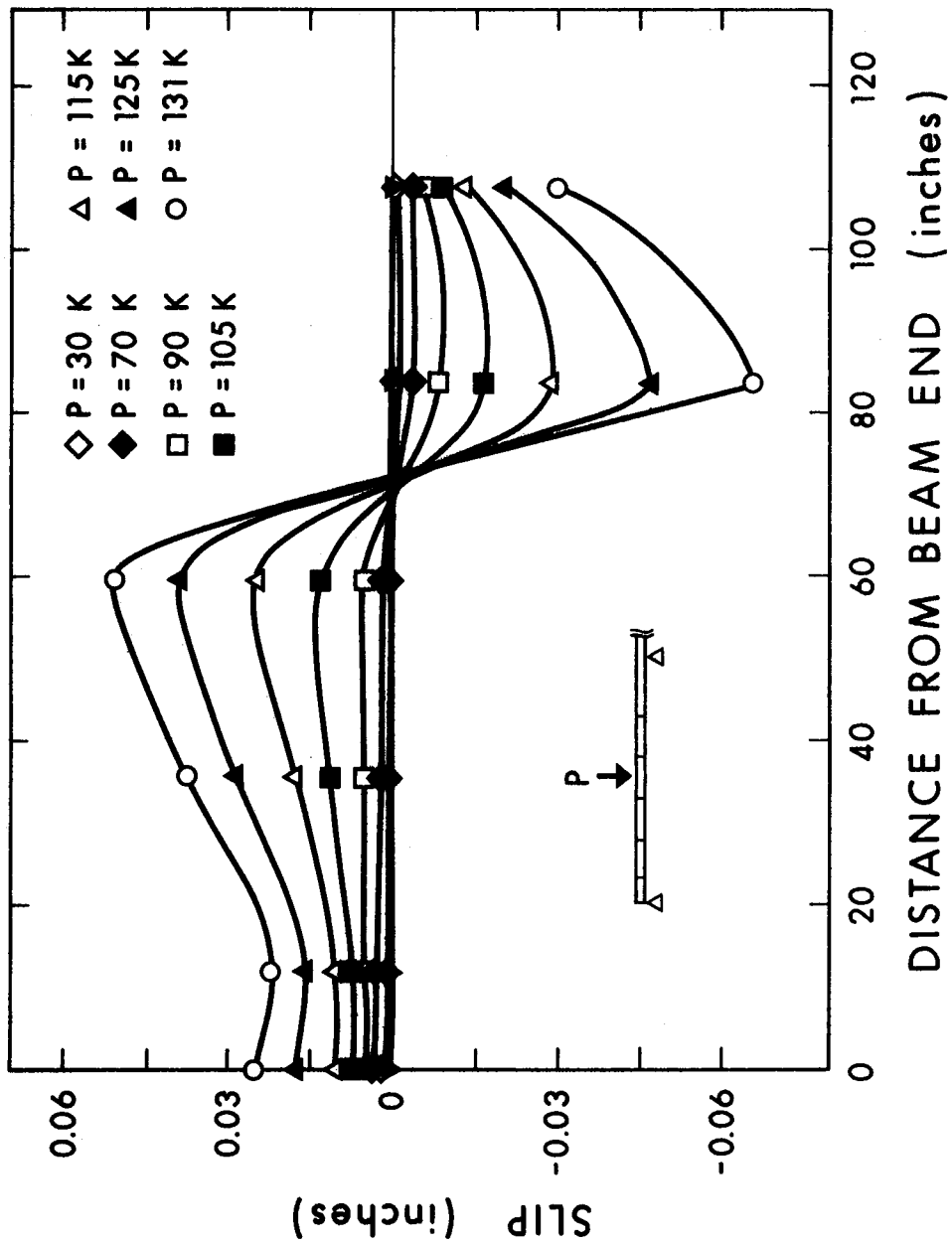

FIGURE 4.11(a) SLIP DISTRIBUTION FOR BEAM CB1

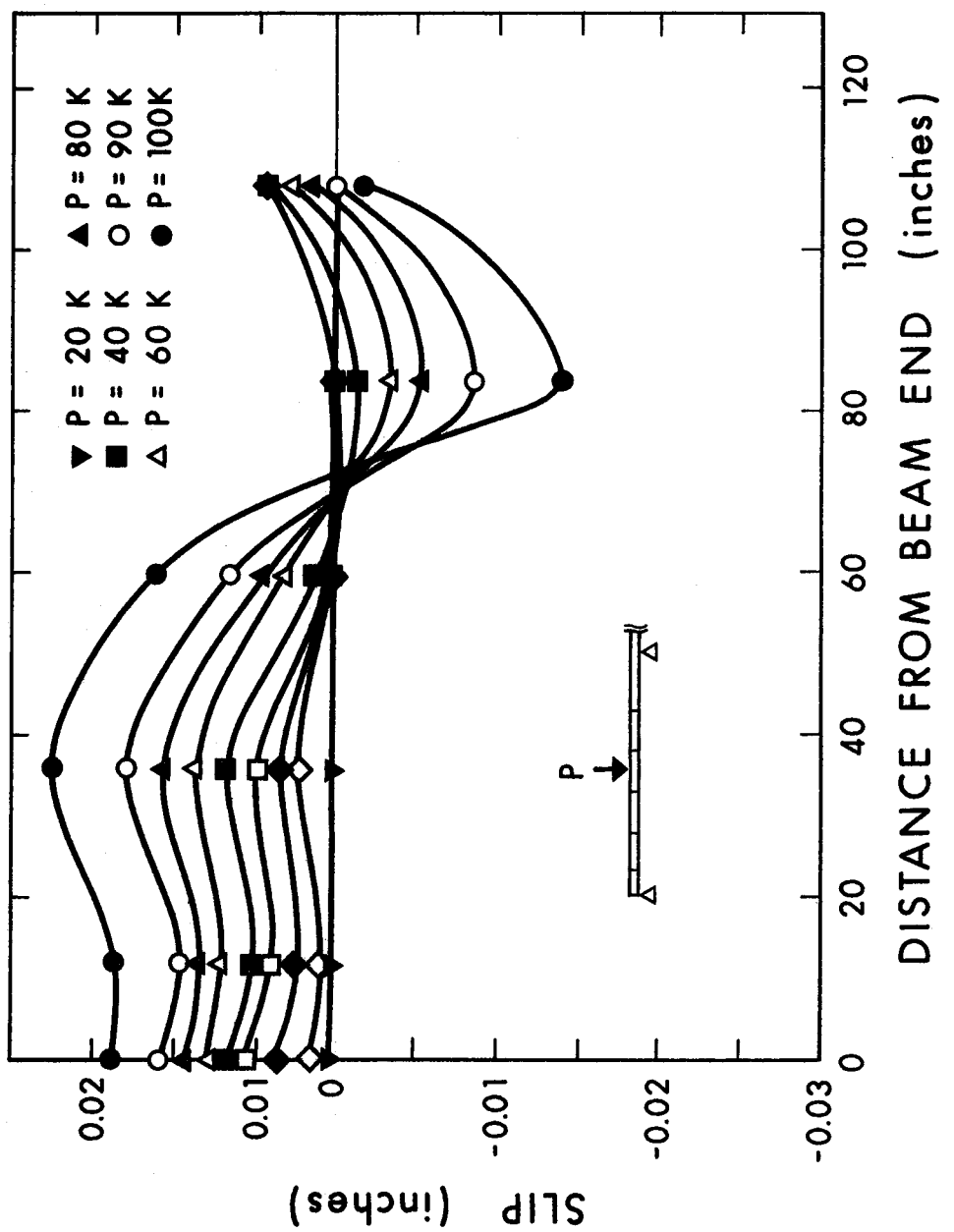

FIGURE 4.11(b) SLIP DISTRIBUTION FOR BEAM CB2

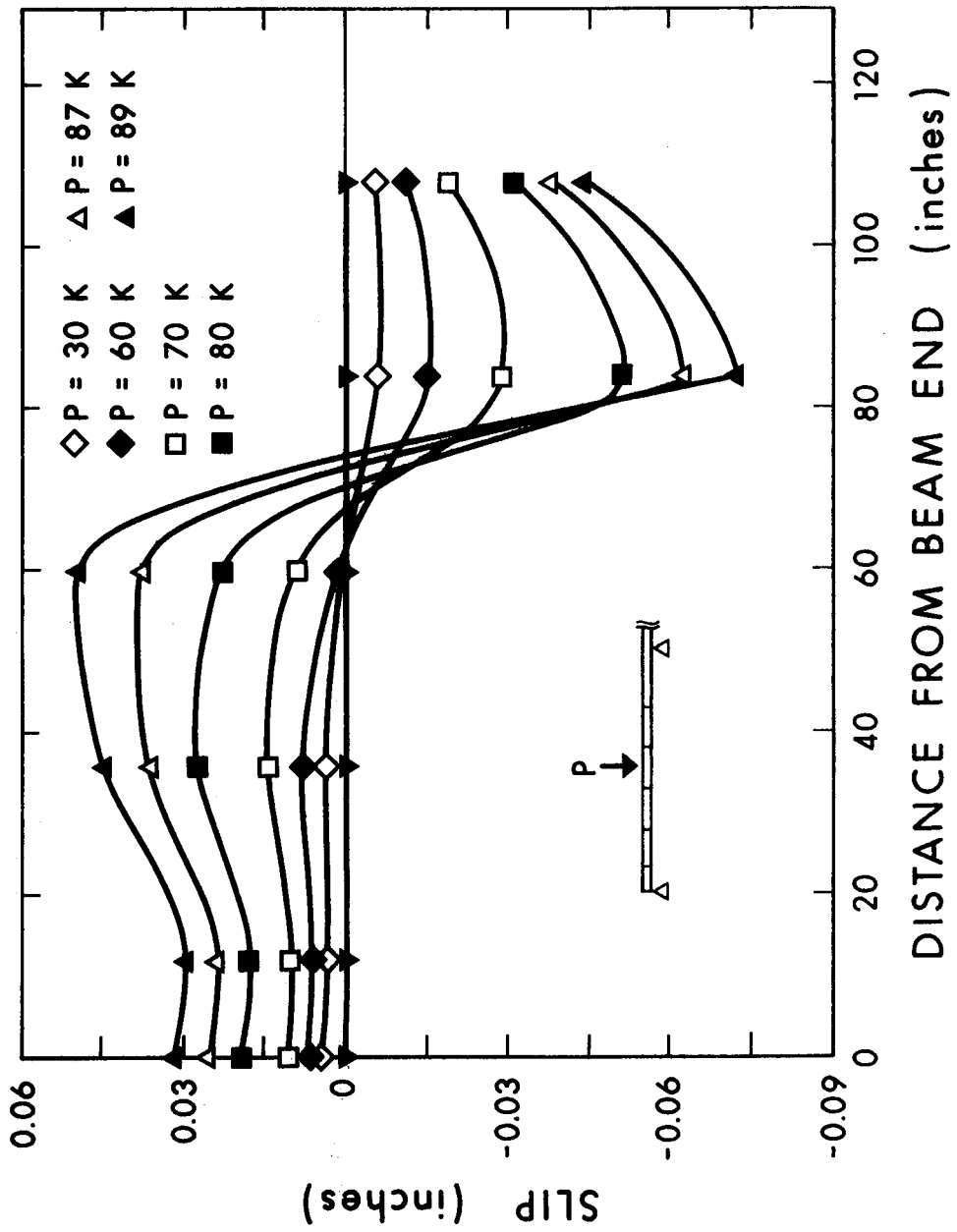

FIGURE 4.11(c) SLIP DISTRIBUTION FOR BEAM CB3

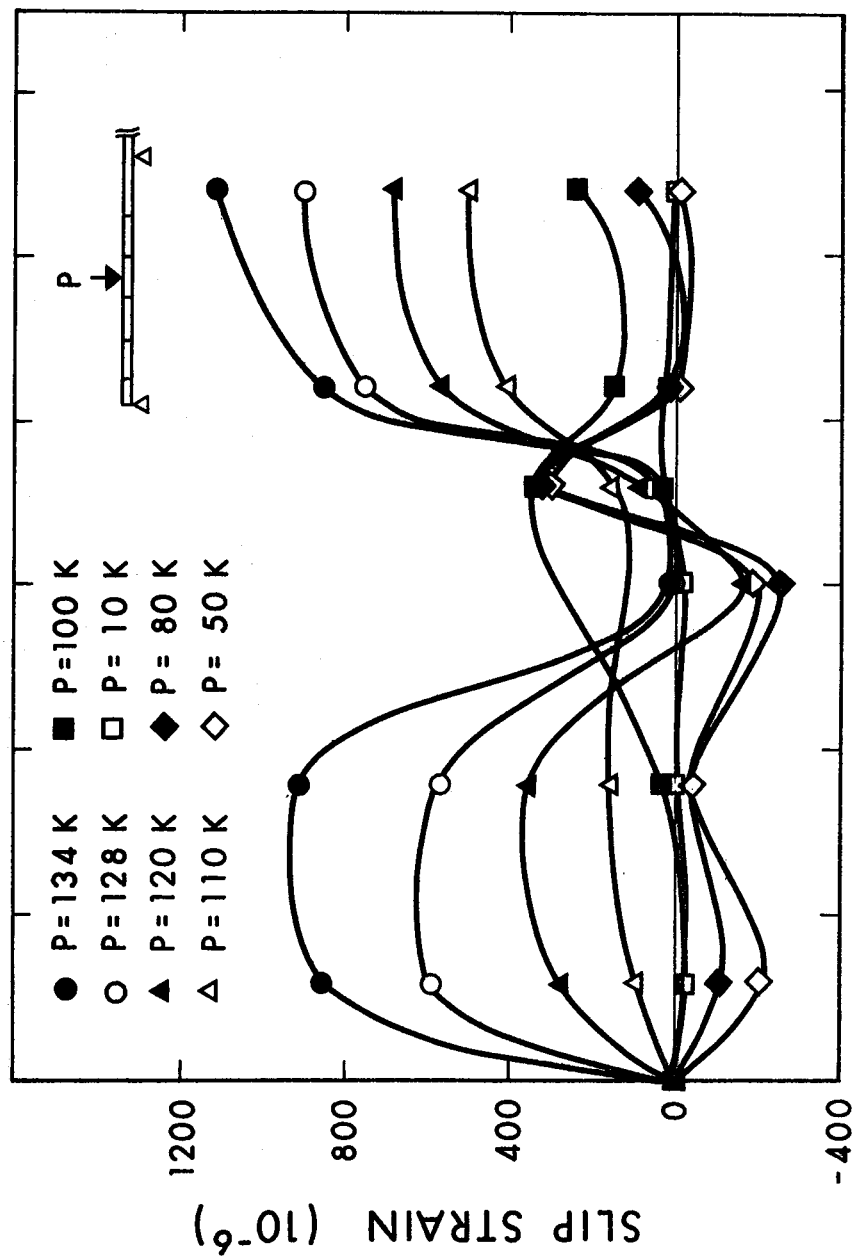

FIGURE 4.12(a) SLIP STRAIN DISTRIBUTION FOR BEAM CB1

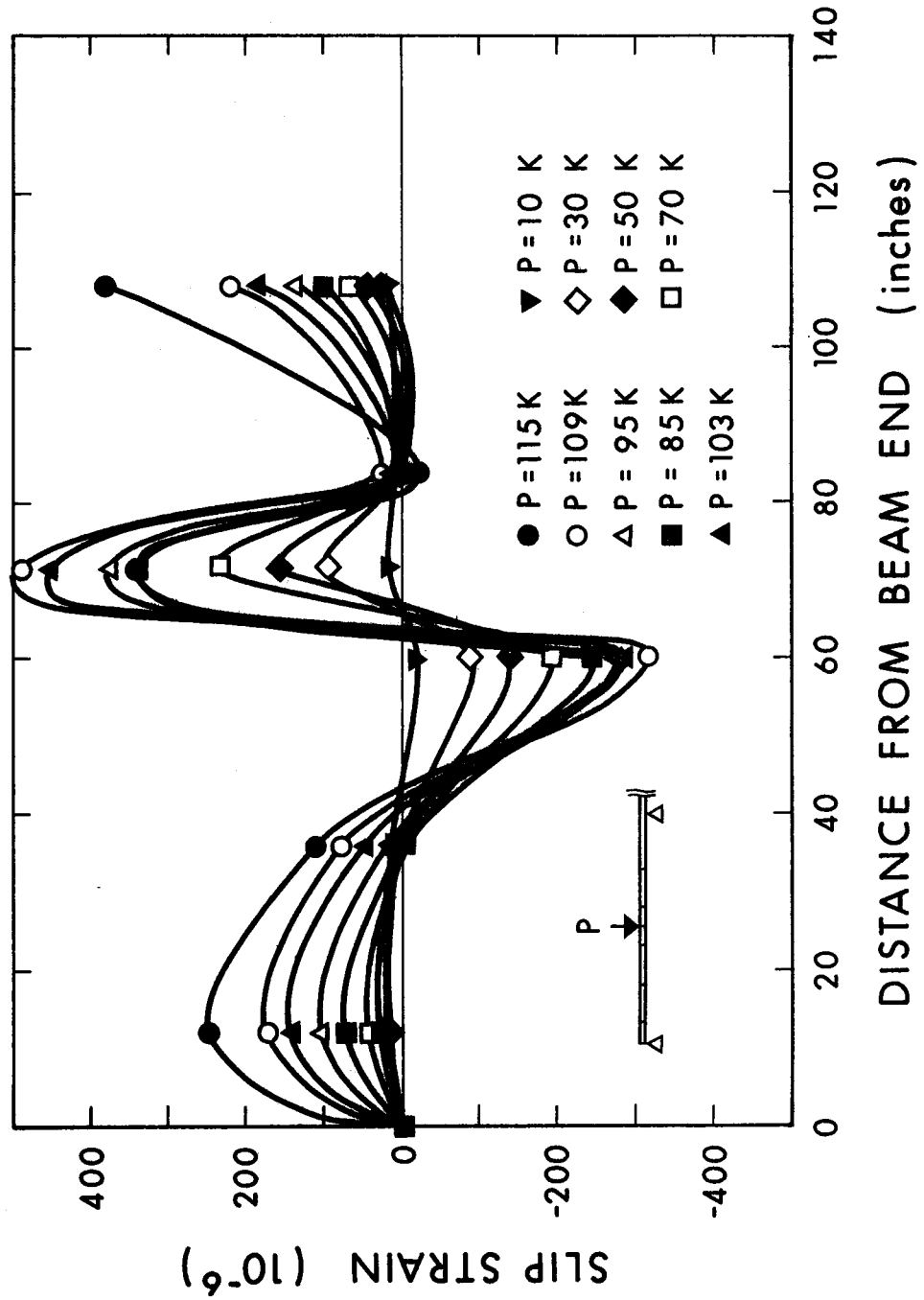

FIGURE 4.12(b) SLIP STRAIN DISTRIBUTION FOR BEAM CB2

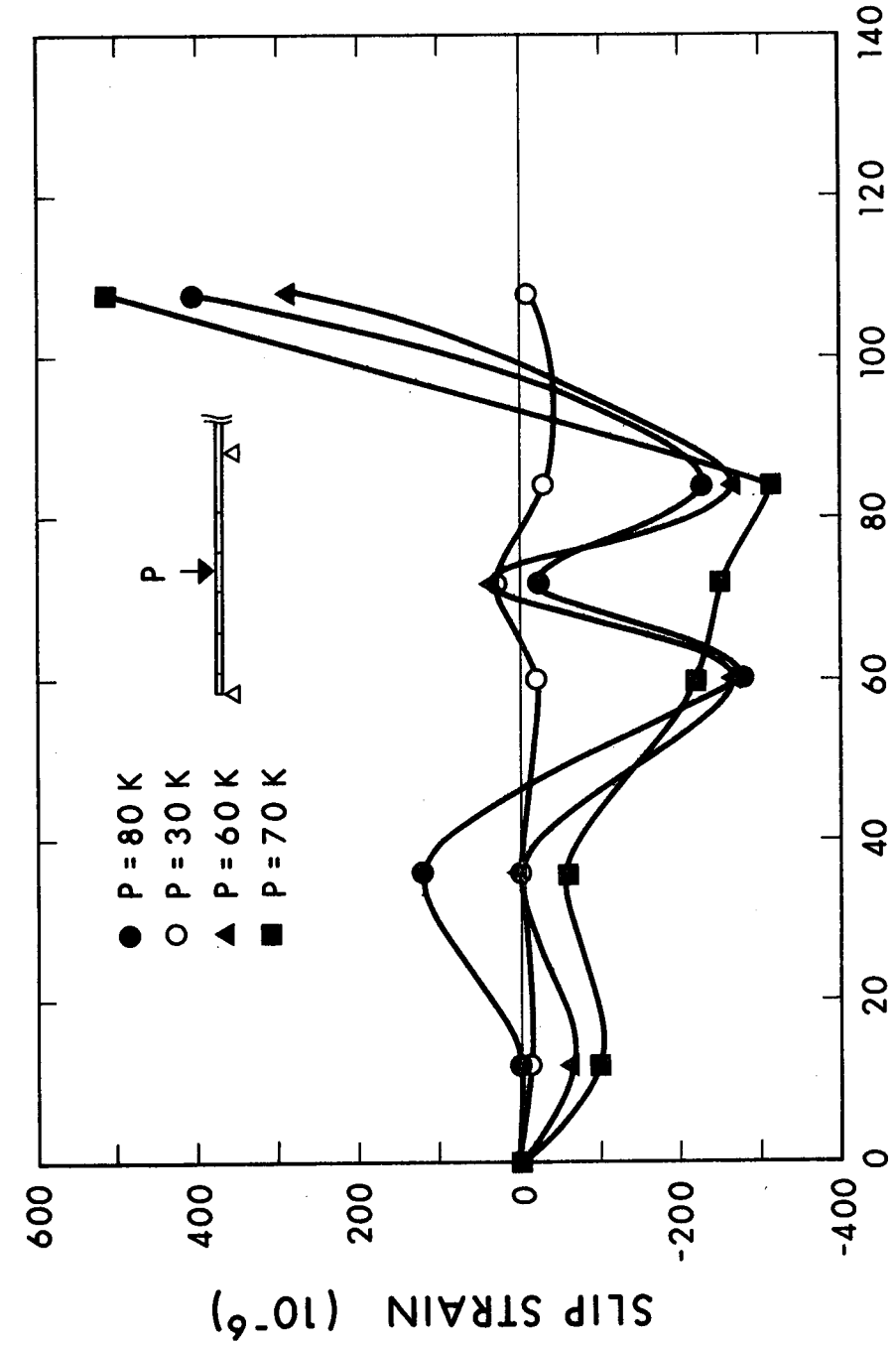

FIGURE 4.12(c) SLIP STRAIN DISTRIBUTION FOR BEAM CB3

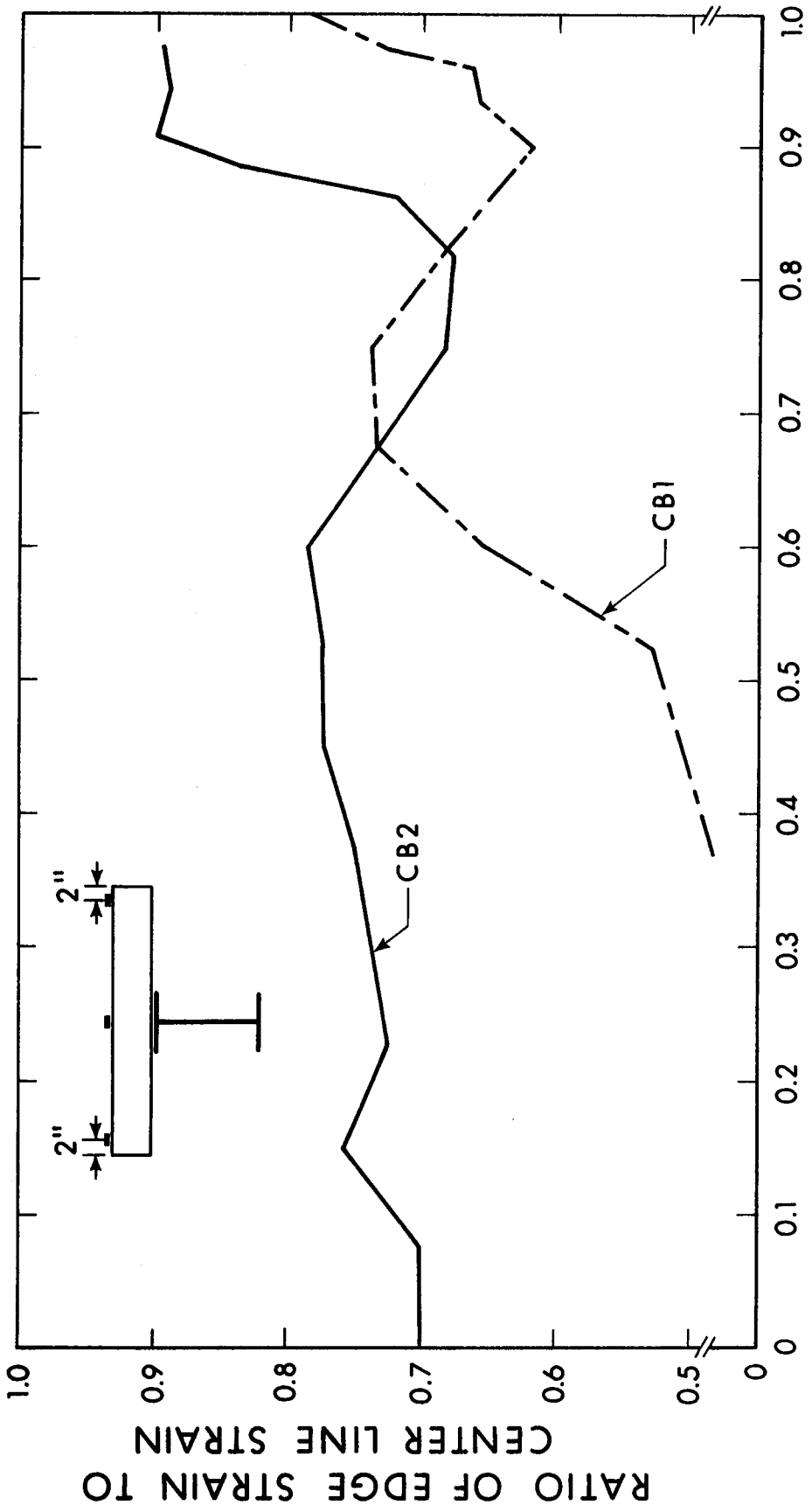

FIGURE 4.13 RATIO OF SLAB EDGE STRAIN TO SLAB CENTERLINE STRAIN

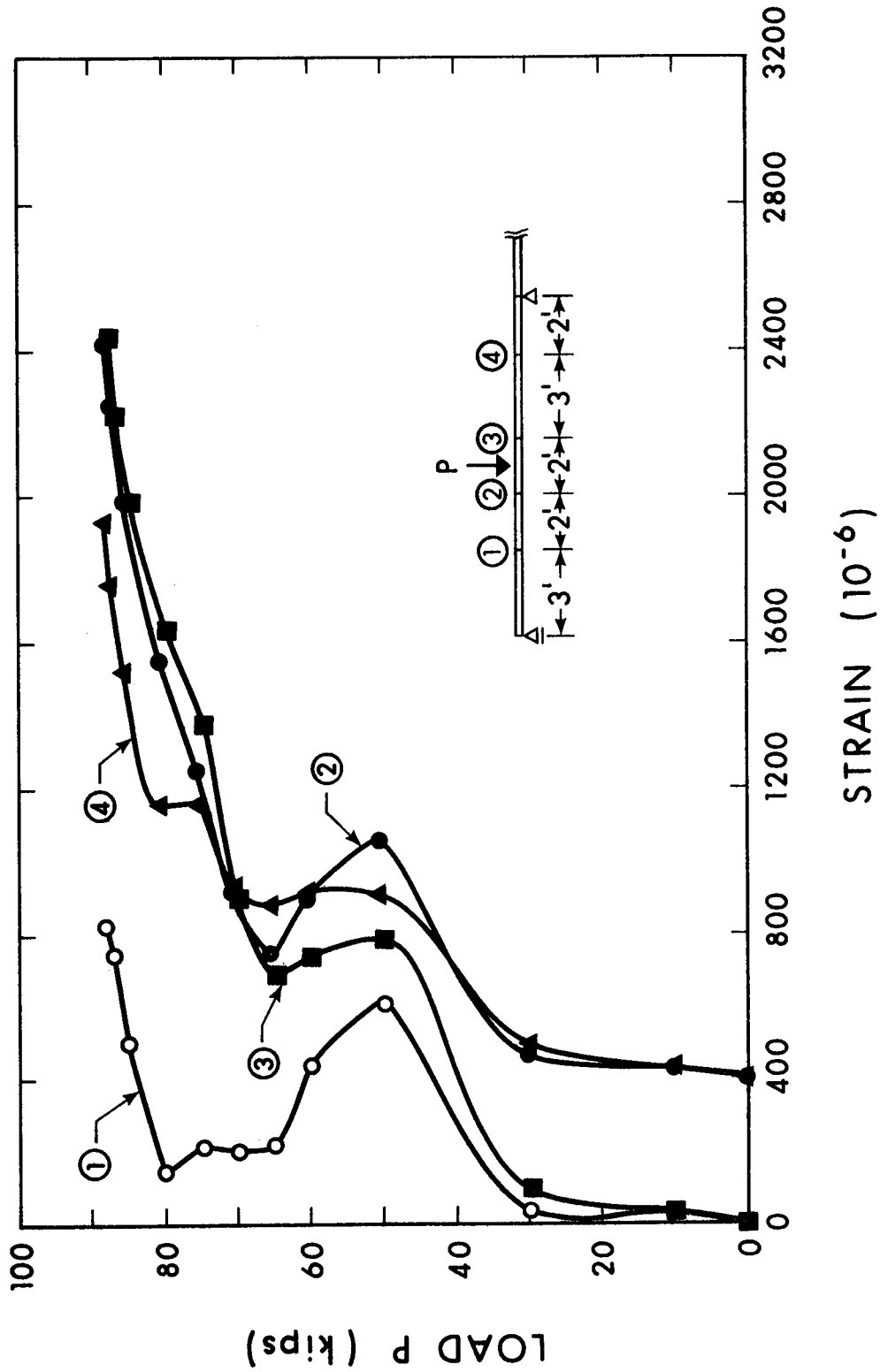

FIGURE 4.14(a) LOAD-TRANSVERSE STRAIN RELATIONSHIPS FOR BEAM CB1

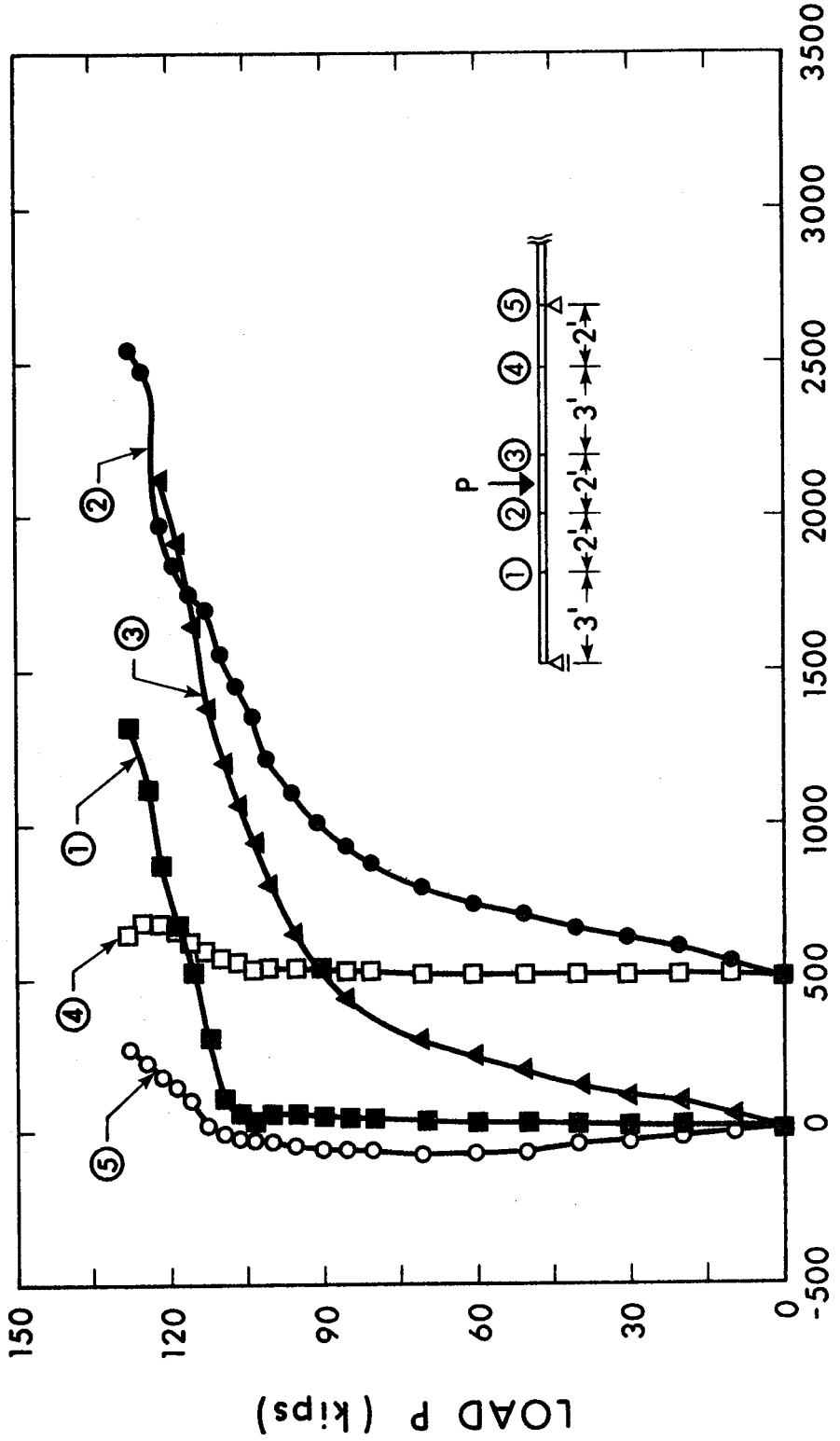

FIGURE 4.14(b) LOAD-TRANSVERSE STRAIN RELATIONSHIP FOR BEAM CB2

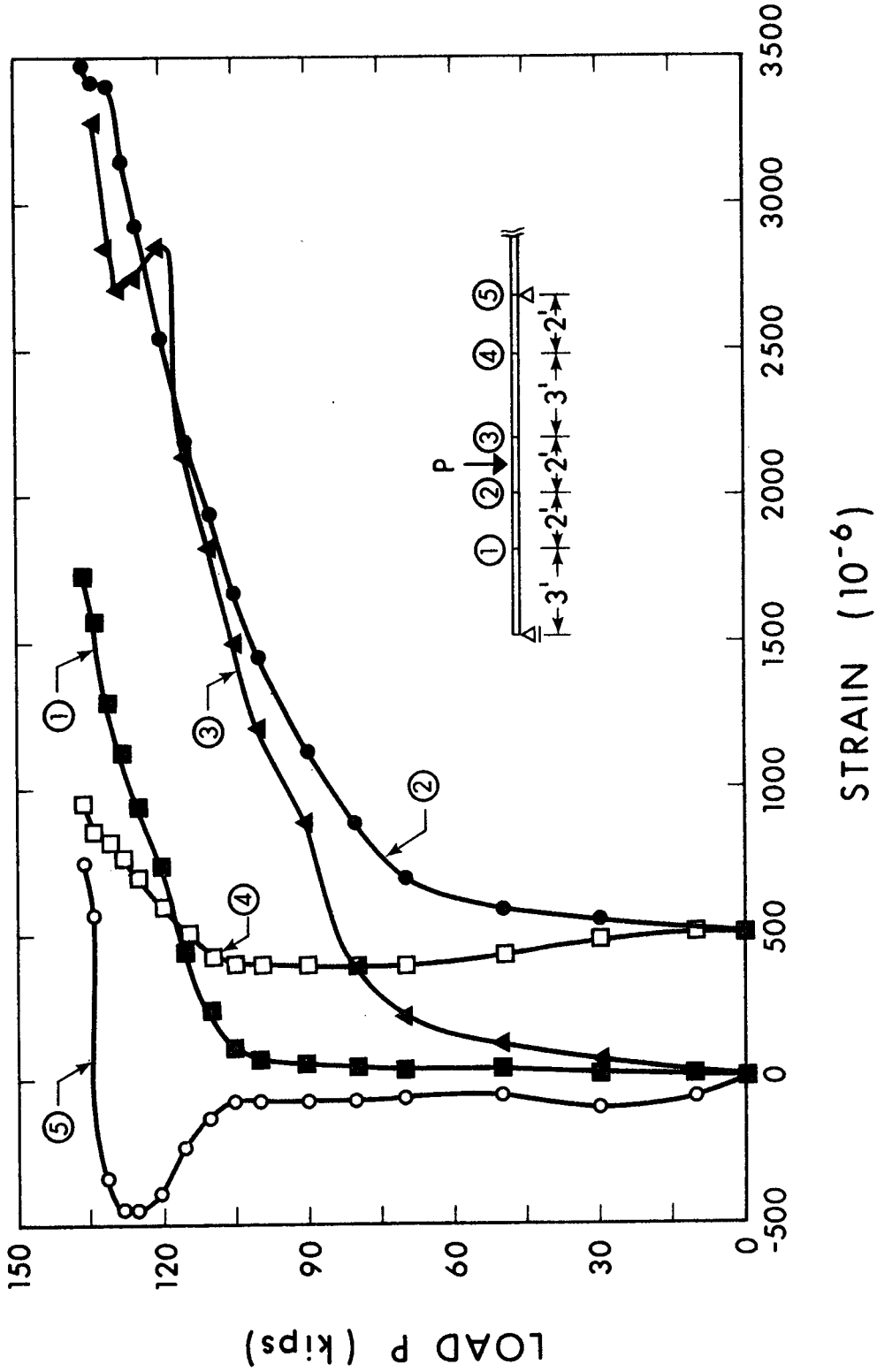

FIGURE 4.14(c) LOAD-TRANSVERSE STRAIN RELATIONSHIPS FOR BEAM CB3

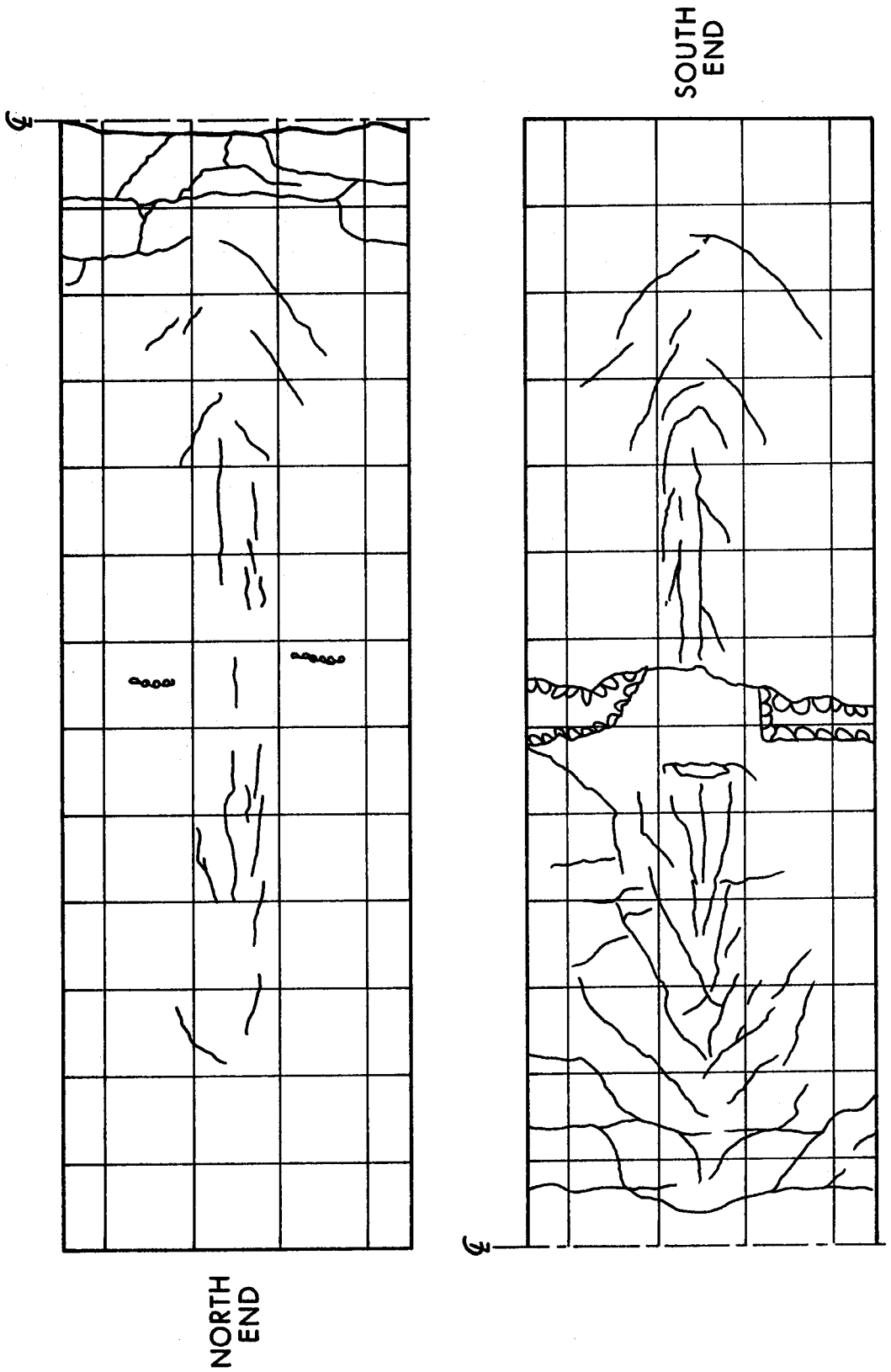

FIGURE 4.15(a) CRACK PATTERNS FOR BEAM CB1

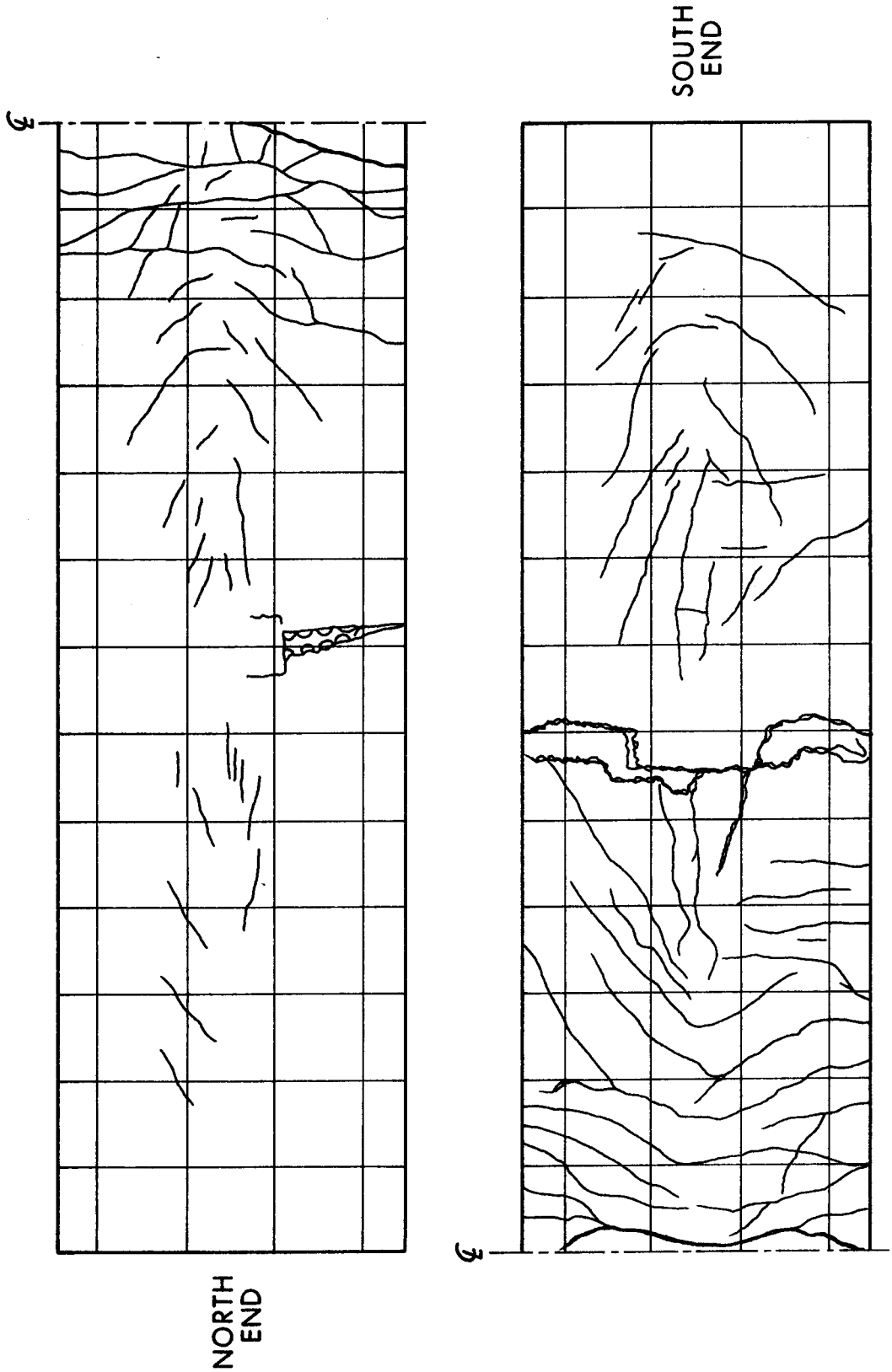

FIGURE 4.15(b) CRACK PATTERNS FOR BEAM CB2

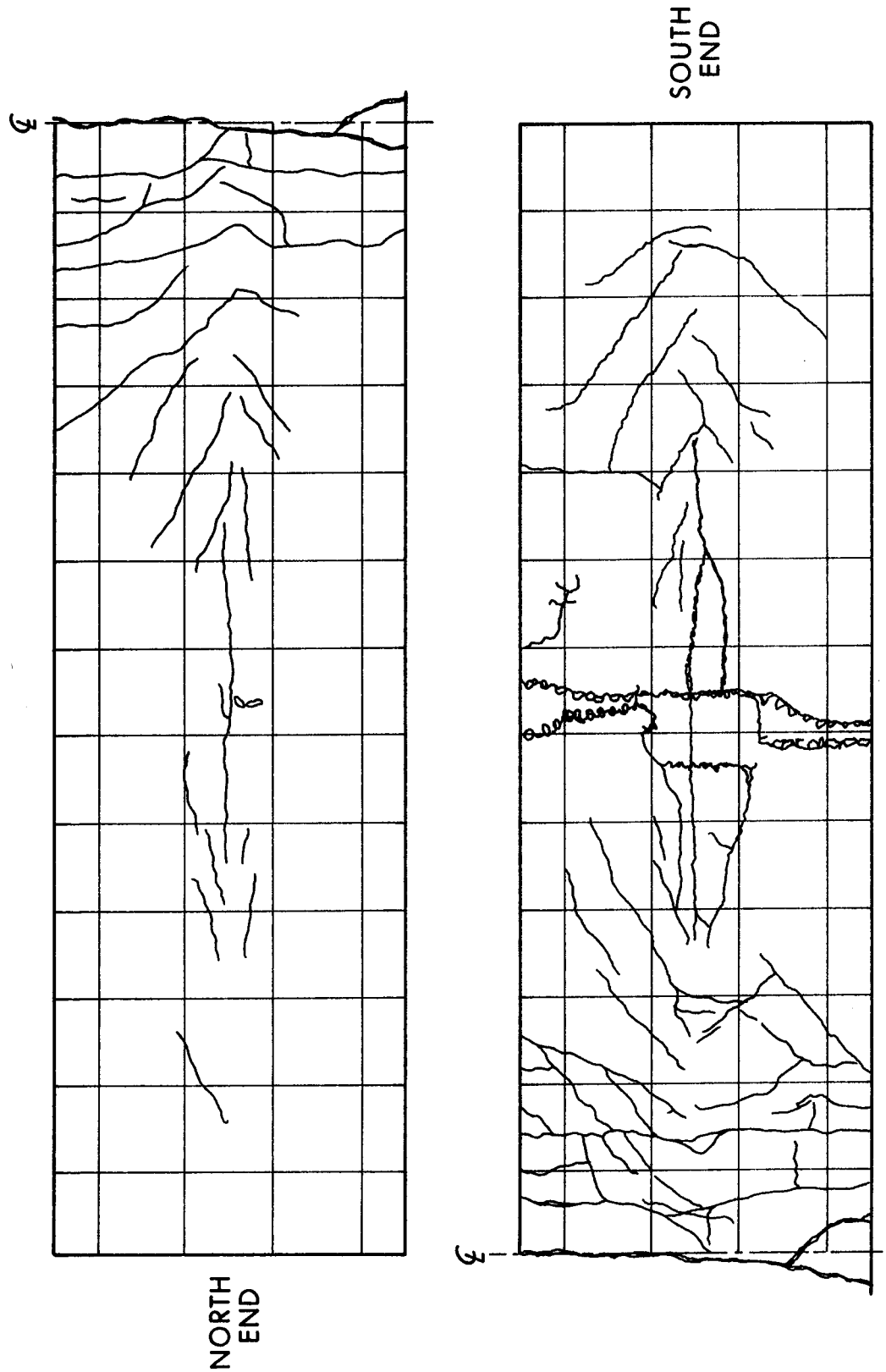

FIGURE 4.15(c) CRACK PATTERNS FOR BEAM CB3

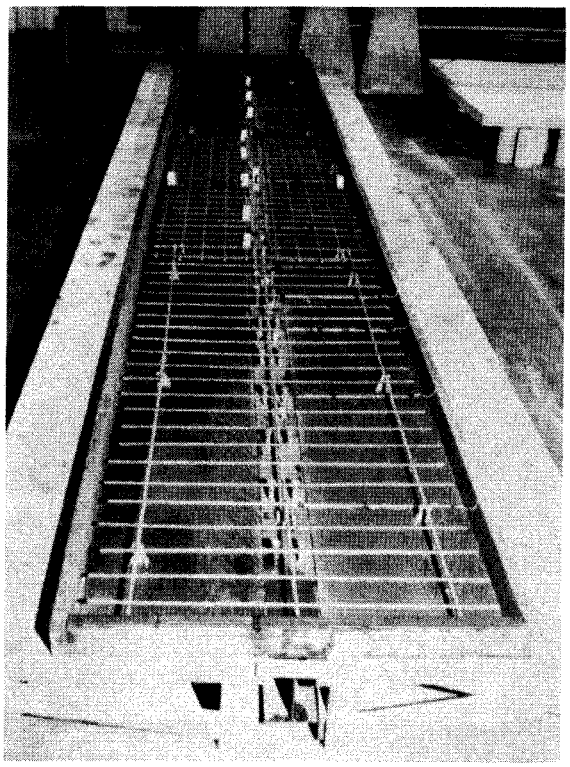

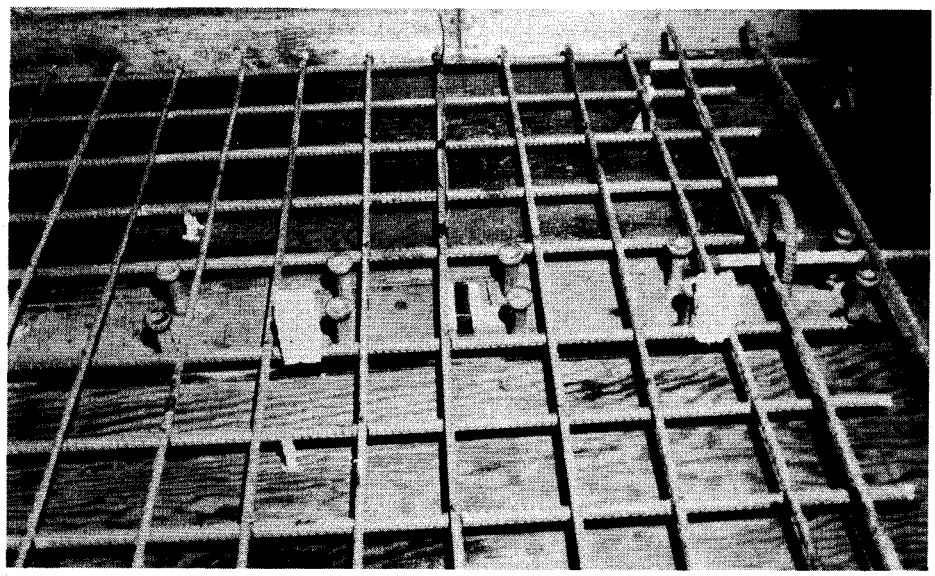

PLATE 4.1 FORMWORK AND REINFORCEMENT DETAILS

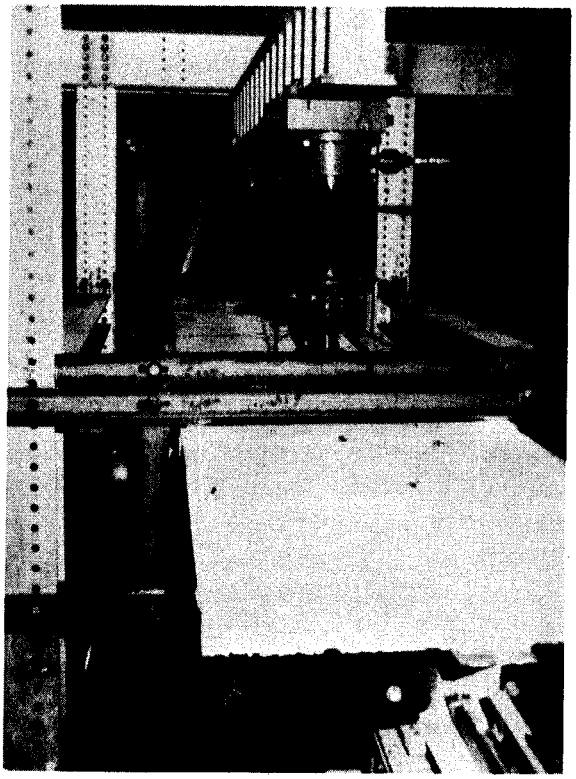

(a) LATERAL BRACING

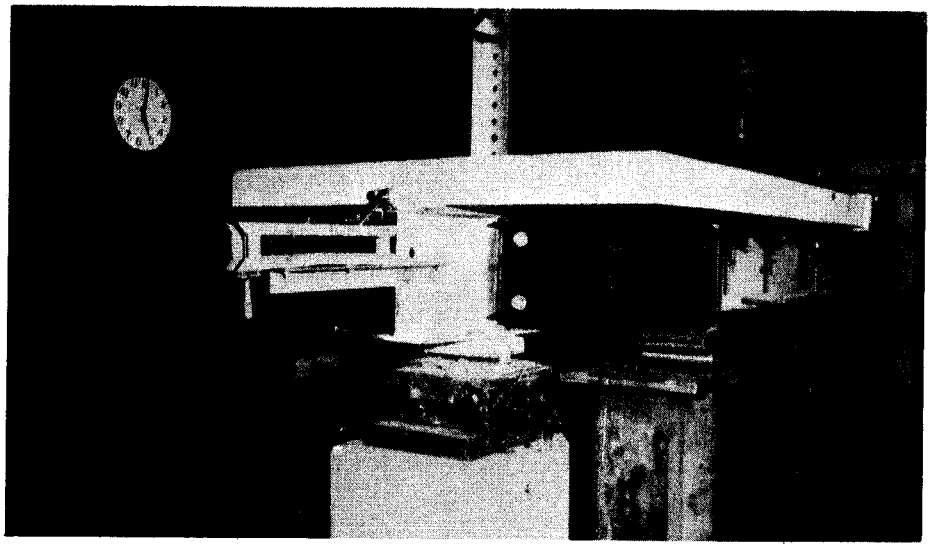

(b) SUPPORT SYSTEM

PLATE 4.2 LATERAL BRACING AND SUPPORT SYSTEM

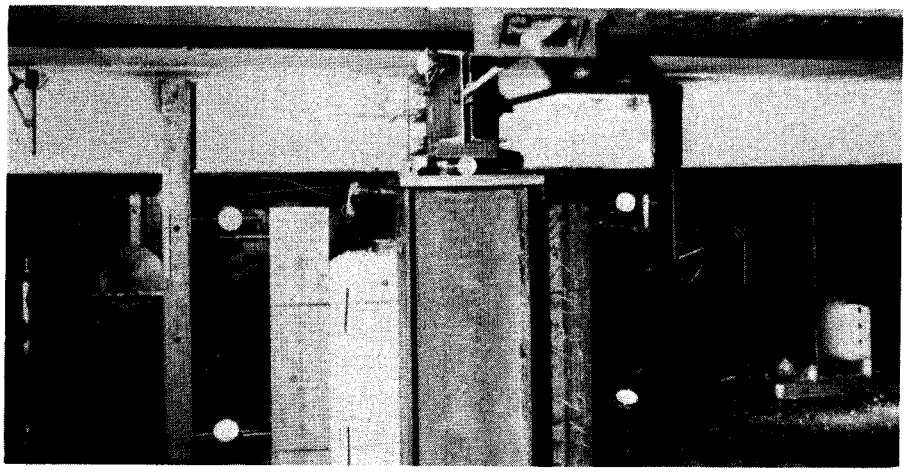

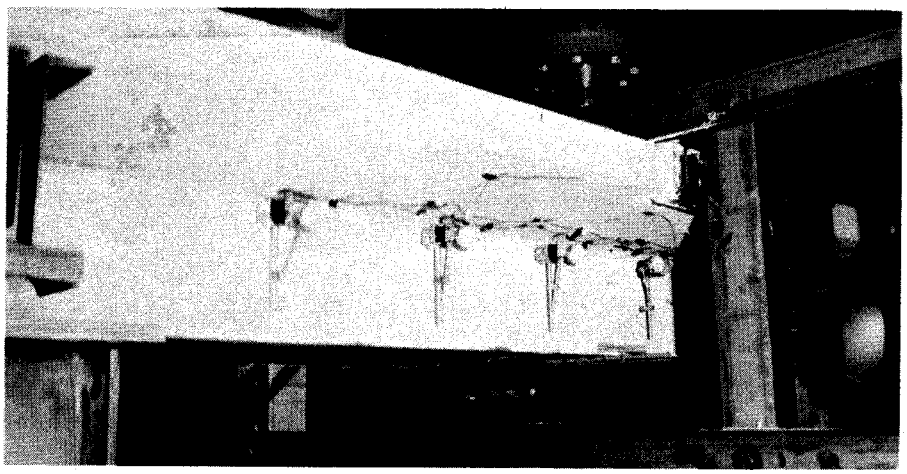

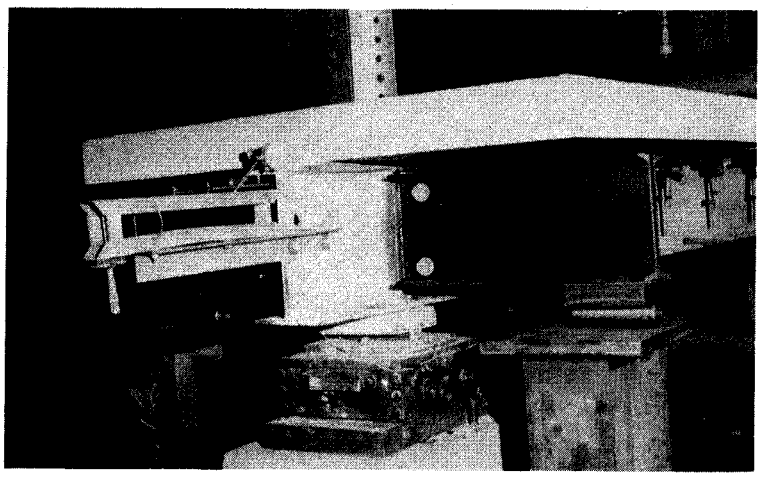

PLATE 4.3 INSTRUMENTATION

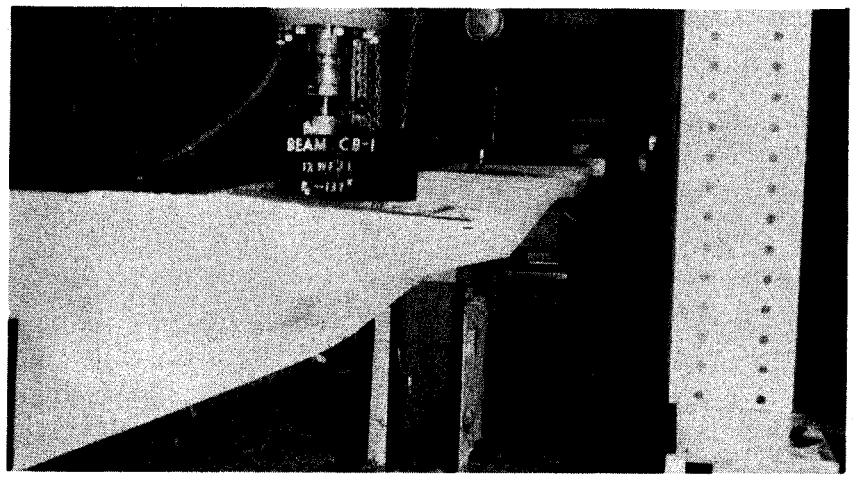

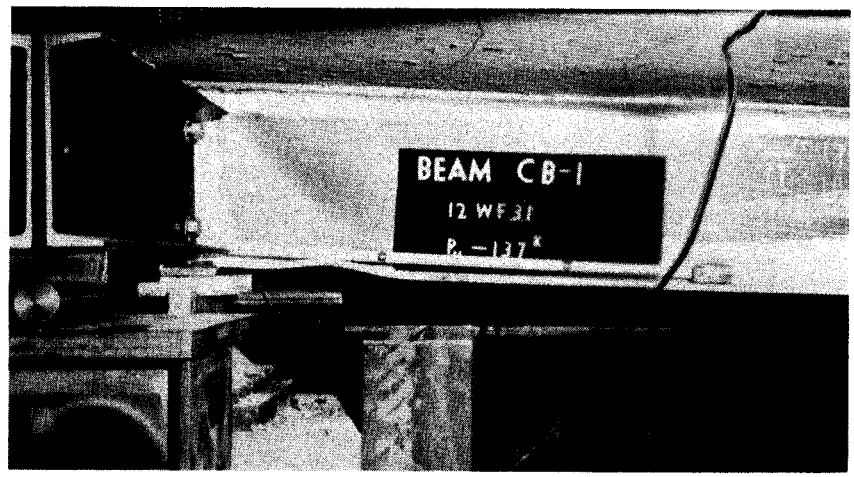

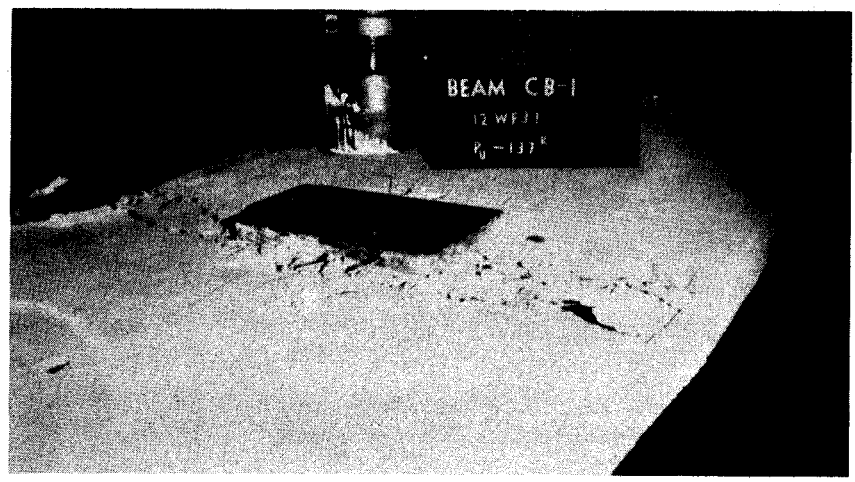

PLATE 4.4 FAILURE OF BEAM CB1

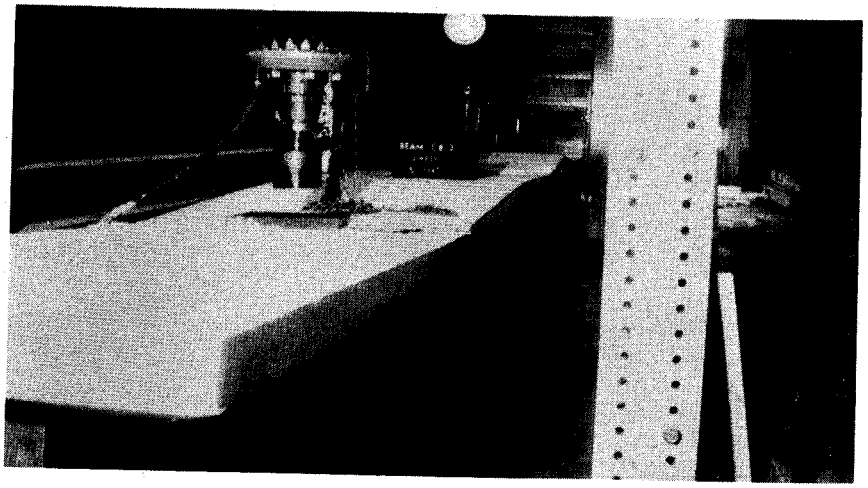

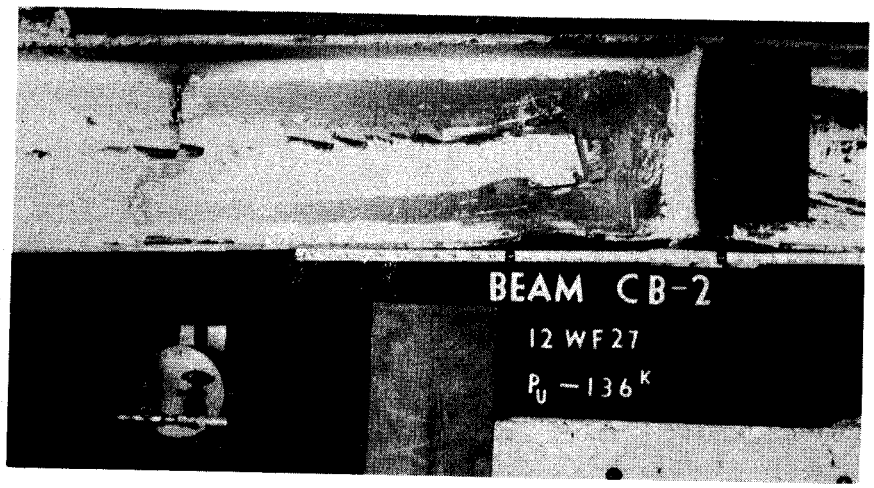

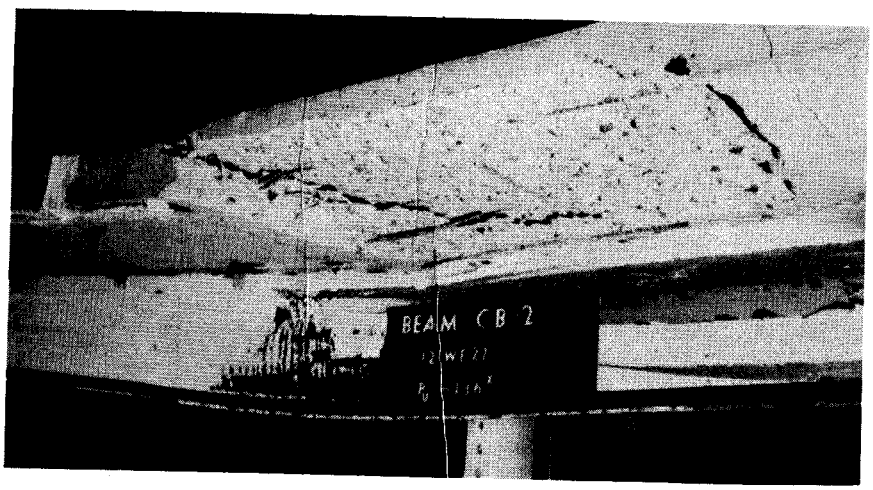

PLATE 4.5 FAILURE OF BEAM CB2

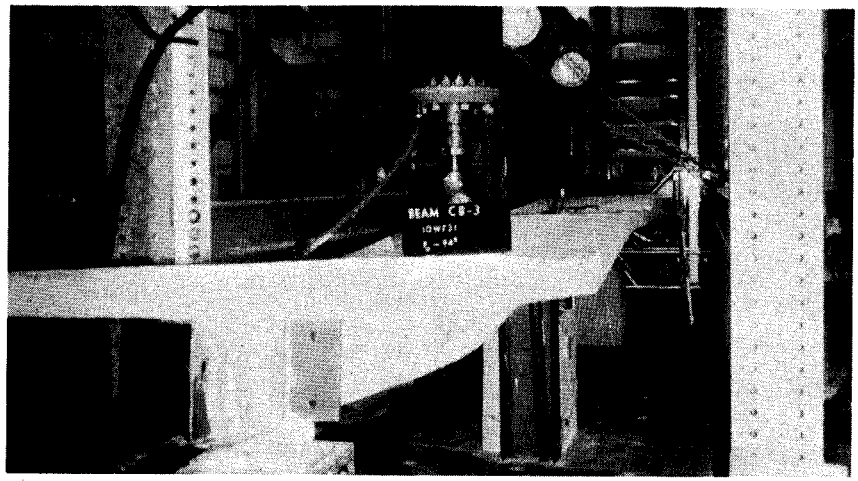

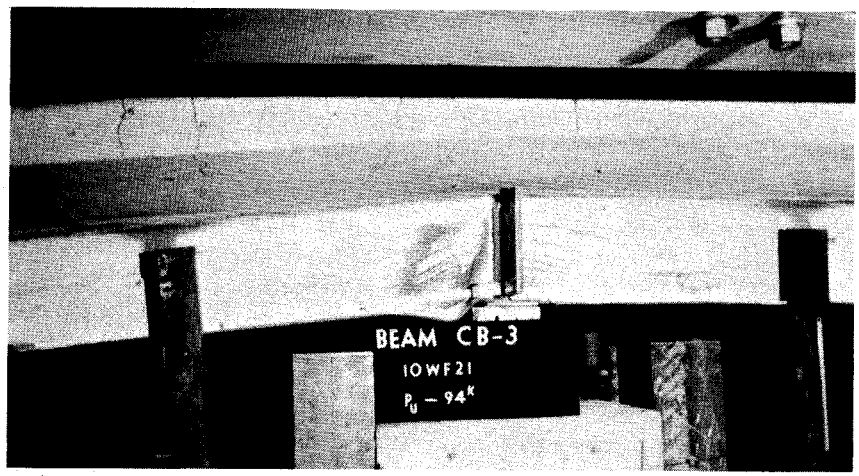

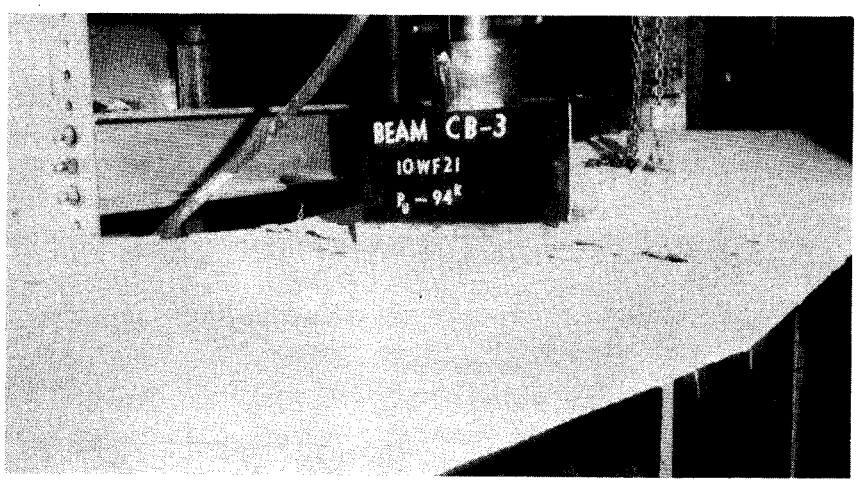

PLATE 4.6 FAILURE OF BEAM CB3

CHAPTER V

BEHAVIOR OF CONTINUOUS BEAMS

5.1 Introduction

The present chapter compares results of the proposed analysis with experimental data from tests conducted at the University of Alberta, the University of Cambridge and Lehigh University.

Deformations in continuous composite beams have received relatively little attention in the past. Deformations have been mainly analysed assuming elastic properties. Barnard[8] discussed deformation and moment-curvature relationships without consideration of moment redistribution. In the present chapter deformation behavior is discussed for both elastic and plastic ranges. The analysis includes the effect of slip and shear as well as bending. Moment redistribution, which occurs in the process of the formation of a mechanism, is taken into account.

Crushing of concrete in the positive moment region and local flange buckling in the negative moment region are the major failure modes. Shear connector failure and longitudinal splitting can be prevented by proper design provisions.

5.2 Local Flange Buckling

5.2.1 Presentation of Data

Davison's[5] and Lever's[6] beams were composed of W12 x 27,

W12 x 31 and W12 x 36 sections and concrete slabs with various amounts of longitudinal slab reinforcement. All beams failed in local flange buckling after ultimate moment capacity was achieved. Dimensions of test beams are shown in Figure 5.1.

Theoretical values shown in Table 5.1 are based on Lay's and Bijlaard's proposed shear modulus values. Figures 5.2(a), (b) and (c) compare test and analytical ultimate moment values with plastic moment values. They also illustrate the effect of longitudinal slab reinforcement on the ratio of test ultimate moment to the plastic moment values. Table 5.2 compares test and theoretical values of curvature at the onset of local flange buckling. Theoretical values are based on Lay's and Bijlaard proposed shear modulus. The relationships between curvature based on Lay's proposed shear modulus and the amount of longitudinal reinforcement are shown in Figure 5.3.

To simulate the effect of longitudinal slab reinforcement in a composite beam under negative moment, Clinenhaga [15] tested beams consisting of a steel section and a coverplate welded on the tension flange. Some beams contained longitudinal stiffeners welded on the web as indicated in Figure 5.4. Test and analytical results are tabulated in Table 5.3.

5.2.2 Discussion

For beams tested at the University of Alberta, experimental and theoretical values for local buckling moments are very similar. Lay's inelastic shear modulus results in higher moment values for stockier sections such as W12 x 31 and W12 x 36. Generally theoretical values

based on Bijlaard's shear modulus are higher than those based on Lay's shear modulus in the vicinity of the onset of the strain-hardening, and tend to decrease with increasing strain. Composite beams with W12 x 27 sections appear to buckle shortly after the onset of strain-hardening.

The difference between experimental moment values and theoretical moment values based on Lay's shear modulus for beams tested at the University of Alberta is within 15 per cent. The difference is large for beams with W12 x 27 and W12 x 31 sections and lower amounts of reinforcement, and also for beams with a W12 x 36 section with larger amounts of reinforcement as shown in Figures 5.2. The figures also indicate that theoretical values increase in proportion with the simple plastic moment values for increasing amounts of reinforcement. However experimental values do not increase as much with increased amounts of reinforcement. Values of M_u/M_p indicate this behavior as shown in the same figures. Although for beams with W12 x 36 sections experimental and theoretical values are fairly close, they still exhibit the same above-mentioned trend. This may be due to underestimating the web restraint for small amounts of longitudinal reinforcement, or due to the effect of lateral displacement for large amounts of longitudinal reinforcement. However, since the difference is not significantly large, the proposed analysis is considered acceptable for predicting local flange buckling.

Figures 5.2(a), (b) and (c) show that the ratio of ultimate moment to the simple plastic moment, M_u/M_p, for beams with W12 x 36 sections is larger than that ratio for beams with W12 x 31 and W12 x 27 sections. This is presumably due to the large flange torsional resistance of W12 x 36 sections. The width-thickness ratio of a W12 x 36 section

is 6.1 which is considerably larger than that specified in CSA Standard S16-1969(1).

Table 5.3 shows good agreement between theoretical and experimental ultimate moment values for Climenhaga's beams, except for beams with 5x3 RSJ sections and for beams with longitudinal stiffeners on the webs. The average ratio of test to theoretical moment values is 1.11. The shallowest sections (5 x 3 RSJ) exhibit the largest ratio of test to theoretical values. The presence of longitudinal web stiffeners increases the ratio M_u/M_p by approximately 10 percent for 16 x 5½ UB26 sections and by approximately 20 percent for an 8 x 5¼ UB17 section. A comparison of experimental and theoretical moment values for 8'-4" and 12'-4" spans indicates little difference, although theoretical ultimate moment values for the smaller span are about 2 percent higher.

Table 5.2 and Figure 5.3 show a significant difference between experimental and theoretical curvatures at local flange buckling for the University of Alberta tests. This may be partly due to the fact that curvature in the inelastic range is greatly affected by relatively small increase in moment, and partly due to the fact that there is a difference between the actual stress-strain relationship and that used in the analysis. A stress increment of 3 Ksi at a stress level of 60 Ksi for a yield stress of 44 Ksi may produce a strain increment of 0.01 based on an inelastic tangent modulus of 300 Ksi. This strain increment of 0.01 corresponds to the strain at the onset of the strain hardening, or to a curvature increment 0.00133 for a 12 inch depth section such as a W12 x 36 section. For example, a beam which buckled locally at a stress of 60 Ksi and a curvature of 0.0088, such as Beam 18 in Table 5.2, may show a 15 percent difference in curvature in spite of only a 5 percent difference in

moment.

As shown in Figure 5.3, curvatures at the onset of local buckling decrease fairly rapidly with increasing amounts of longitudinal slab reinforcement.

5.3 Lateral Buckling

5.3.1 Presentation of Data

As indicated in Chapter II, lateral buckling of composite beams under negative moment may occur for beams where local buckling is precluded. Beams tested by Piepgrass were composed of a W12 x 16.5 steel section with a 3" x 3/8" coverplate welded on the compression flange and a concrete slab with various amounts of longitudinal reinforcement as shown in Figure 5.5. Table 5.4 compares Piepgrass' test results with analytical values. Figure 5.6(a) shows analytical values of M_u/M_p for various span lengths and amounts of longitudinal reinforcement. The effect of varying size of coverplate is shown in Figure 5.6(b).

5.3.2 Discussion

The difference between experimental and theoretical ultimate moment values are within 5 percent as shown in Table 5.4. This agreement indicates that it is acceptable to assume a hinge located at the end of the stem of the inverted tee section.

The effect of span length on lateral buckling values is shown in Figure 5.6(a) for the section used in Piepgrass' test beams. The ratio M_u/M_p decreases with increasing span, and the ultimate moment

values become less than the plastic moment values in the span range of 115 to 165 inches with longitudinal slab reinforcement varying from 0 to 2.4 in^2. The length of the negative moment region for actual beams may vary from 50 to 150 inches. Therefore lateral buckling effects must be considered when designing continuous beams.

Figure 5.6(a) shows the effect of coverplate size on lateral buckling. A wider coverplate produces a lower value of M_u/M_p.

Figures 5.6(a) and (b) and Table 5.4 show that the ratio M_u/M_p is influenced by the amount of longitudinal slab reinforcement.

5.4 Moment-Curvature Relationships

Moment-curvature relationships for various beam sections are shown in Figures 5.7 to 5.13. Figures 5.7 and 5.8 show the effect of residual stress patterns on moment-curvature relationships in a positive moment region. Residual stresses at flange tips are assumed 0, 0.3 and $0.5\sigma_y$. Residual stress pattern I, which is a linear stress pattern, produces little effect on the moment-curvature relationships. However, residual stress pattern II, which is a parabolic pattern, produces considerable effect on the relationships as shown in Figure 5.8. Test results shown in these figures are those obtained by Ferrier and Davison. The test results for a plain W12 x 36 section compares favorably with the analytical results based on pattern II with $\sigma_r = 0.3\sigma_y$. The experimental moment-curvature relationships for composite sections do not fit the analytical relationships in the plastic range, but they compare favorably in the elastic range. The presence of residual stresses decreases the

stiffness of the composite sections in positive bending as shown in Figures 5.7 and 5.8.

Figures 5.9 and 5.10 show the effect of residual stress on moment-curvature relationships in a negative moment region. These figures include results of Davison's tests for comparison. With increasing amounts of longitudinal reinforcement, the actual stiffness of the composite section decreases in comparison with theoretical stiffness. This may be due to the effect of slip. According to Davison's test[5], the interaction factor, which is discussed in Chapter III, was approximately equal to 0.6 when the longitudinal reinforcement reached yield strain. From a comparison of theoretical and test results, the interaction factor appears to decrease with increasing stress in the longitudinal slab reinforcement, since theoretical values based on the interaction factor agree with test values in the elastic range, but not in the plastic range. Presumably this difference may also relate to the behavior of shear connectors.

The effect of residual stresses on the moment-curvature relationship in a negative moment region differs from that in a positive moment region. Since the stress in the bottom flange is compression in negative bending and tension in positive bending, residual stresses have a different effect on moment in positive and negative bending. The stiffness is increased by residual stresses after yielding in a negative moment region as shown in Figures 5.9 and 5.10.

Figures 5.11 to 5.13 show experimental and theoretical moment-curvature relationships for beams tested in the present study. Theoretical relationships are in good agreement with experimental rela-

tionships in positive moment regions. However the agreement is not good in negative moment regions, except for Beam CB1 which has the smallest amount of longitudinal slab reinforcement. In the elastic range, the difference is large with the actual stiffness approximately two times the theoretical stiffness. Strain-hardening begins shortly after initial yielding of the steel in the negative moment regions. All three beams tested attained ultimate moments greater than simple plastic moments as shown in Figures 5.11 to 13.

5.5 Deformation

5.5.1 Deflection

Load-deflection relationships obtained in previous investigations and in the present study are compared with theoretical relationships in Figures 5.14 to 5.19. Figure 5.14 compares theoretical and experimental load-deflection relationships for a simple span tested by Yam and Chapman[41]. Yam's analysis includes the effect of slip. The load-deflection relationship based on the writer's proposed analysis discussed in Chapter III is also shown. In the elastic region the proposed analysis agrees well with Yam's analysis. As ultimate load is approached, the proposed method results in deflections larger than those obtained in Yam's analysis. This difference is due to the fact that the stress-strain relationship for concrete employed by Yam is an idealized elasto-plastic relationship whereas that employed in the proposed analysis is based in Desayi's approximate formula as given in Equation 2.8. The latter relationship has a falling portion after maximum stress, causing reduced

stiffness at high loads. Both Yam's analysis and the proposed analysis yield values close to experimental results.

Some complete load-deflection relationships for continuous beams have been reported in previous investigations [7][11][12]. Test results presented by Culver et al[7] are compared with theoretical values in Figure 5.15. Theoretical values are in good agreement with the test values.

Figure 5.16 compares results of tests on continuous beams conducted at Lehigh University by Daniels et al[11] with theoretical values. Since the beam span was comparatively long, the effect of shear on the deflection is relatively small. However, it still amounts to 17 per cent of the bending deflection. Theoretical results are in fairly good agreement with experimental results. In the simple plastic analysis hinges form almost simultaneously at the interior support and load points. The load point hinges form first, followed closely by the formation of the hinge at the interior support.

Deflection at the load point at the formation of the last hinge is determined by the slope-deflection method. The coefficients of the beam stiffness matrix for a composite beam are related to the ratio of the stiffness in positive bending to that in negative bending and are also related to the ratio of the length of the positive moment region to that of the negative moment region. Appendix C includes tables of values for stiffness matrix coefficients for the slope-deflection method. The load-deflection relationships for beams tested in the present investigation are compared with theoretical relationships in Figures 5.17 to 5.19. The effect of shear on deflection is appreciable, since the beams

are relatively short. As indicated in the previous section there is a relatively large difference in the moment-curvature relationships in negative moment regions for Beam CB2 and Beam CB3. However, the analytical load-deflection relationships are in good agreement with the test relationships. In the analysis the effective width is taken as 40 inches as discussed in Chapter IV.

In the simple plastic analysis the first hinge forms at the interior support in all beams. The second hinges at the load points form immediately after the first hinge formation for Beams CB1 and CB3. For Beam CB2 the first hinge forms at a load of 95 Kips and the second hinge forms at a load of 121 Kips. Deflections in the elastic range, determined by simple plastic analysis, are small.

5.5.2 Rotation

Little load-rotation information for continuous composite beams is available in previous research. A certain amount of rotation data was obtained in the present study. As discussed in Chapter IV, rotations were measured at the ends of beams. Results are shown in Figures 5.20 to 5.22 together with analytical relationships. The characteristics of the load-rotation relationships are similar to those of load-deflection relationships. The effect of shear on the end rotation is not as significant as on the center deflection. The ratio of the center deflection due to shear to that due to bending is $12k_{sh}EI/AG\ell^2$ for a simply supported beam with span length ℓ and a concentrated P at the midspan, and the ratio of the end rotation due to shear to that due to bending is $8k_{sh}EI/AG\ell^2$. This implies that the effect of shear on end rotation is two-thirds of that on the center deflection.

5.6 Load-Moment Relationships

The theoretical load-moment relationship is linear up to initial yielding. After yielding begins the moment is redistributed and the relationship is no longer linear. Figure 5.23 shows experimental and theoretical load-moment relationships for beams tested in the present investigation.

The theoretical load-moment relationships are in good agreement with test results, with the theoretical values being slightly greater than the test values for positive moment in the elastic range. This indicates that the stiffness of the beam in a positive moment region was greater than theoretical stiffness, or the stiffness in the negative moment region was smaller than the theoretical stiffness.

For a two-span continuous beam with a load P at each midspan

$$M_1 - M_2/2 = PL/4 \qquad 5.1$$

where M_1 and M_2 are bending moments at the load point and the interior support, respectively. The increment in positive moment, ΔM, therefore, produces an increment in negative moment equal to $2\Delta M$. The difference between the theoretical and the test load-moment relationships is large in the negative moment region.

The experimental values of the negative moment M_2 in Beam CB2 began to increase fairly rapidly at a load of 100 Kips and to approach the positive moment M_1. This implies that the ratio of stiffness in the negative moment region to that in the positive moment region increased for

loads greater than 100 Kips. This condition can also be seen in the moment-curvature relationships for Beam CB2 in Figure 5.12.

The moment redistribution in Beam CB3 commenced at a load of 50 Kips and thereafter negative moment ceased to increase proportionally with the load due to a decrease in stiffness. This behavior can be explained by the moment-curvature relationships for Beam CB3 shown in Figure 5.13. The test curve in the figure shows yielding at approximately 800 in-Kips which is equivalent to the load of 50 Kips as indicated in the load-moment relationships in Figure 5.23. Since the stiffness in the negative moment region is greater than that in the positive moment region after yielding, as shown in Figure 5.13, the negative moment increased at a higher rate when the load reached 60 Kips, when the positive moment at the load points reached the yield moment. Load-moment relationships based on simple plastic theory shows good agreement with the experimental relationships.

5.7 Failure Modes

Figures 5.24 show the relationships between the failure loads and the amounts of longitudinal slab reinforcement for beams tested in the present study. Failure modes are local buckling in the negative moment region and crushing of concrete in the positive moment region. The ultimate concrete strain at failure is determined by Equation 2.9 as 0.0032 for a concrete strength of 5.5 Ksi. Experimental and theoretical ultimate loads are shown in Table 5.5, Beam CB1 failed due to crushing of concrete at a load of 135 Kips, after which local buckling occurred at the interior support. The proposed analysis predicts crushing

of concrete at a load of 135 Kips, and local buckling at a load of 141 Kips which of course means that failure is predicted at a load of 135 Kips. Since the stiffness in the positive moment region decreased considerably after crushing of the concrete, local buckling occurred at a load lower than the ultimate load.

Beam CB2 failed in local buckling which initiated at a load of 120 Kips and completely formed at 130 Kips and subsequently in crushing of concrete at a load of 133 Kips. Figure 5.24(b) shows that analysis predicts local buckling at a load of 122 Kips and crushing of concrete at a load of 131 Kips. In a continuous beam the ultimate load can be greater than that causing local buckling because of redistribution of moment.

Beam CB3 failed in local buckling which began at a load of 85 Kips and completely formed at a load of 90 Kips, followed by crushing of concrete. The analysis predicts crushing of concrete at a load of 89 Kips and local buckling at a load of 90 Kips as indicated in Figure 5.24(c). As in the case of Beam CB2, local buckling was not the direct cause of failure.

Theoretical predictions for local buckling and crushing failures are in good agreement with experimental results for all beams. Although local buckling actually initiated at lower loads than predicted for Beams CB2 and CB3, the beams attained the predicted loads based on concrete crushing at an ultimate concrete strain of 0.0032. This may indicate that the beam stiffness was not significantly reduced by the initiation of local buckling. Crushing of concrete causes immediate failure and the beam cannot sustain additional load. All three beams tested in

the present study attained ultimate loads 8 to 12 percent greater than those predicted by simple plastic theory.

Ultimate loads based on simple plastic theory are not directly proportional to the amount of longitudinal slab reinforcement. Values of ultimate load do not change significantly for areas of longitudinal slab reinforcement in excess of $A_w\sigma_y/\sigma_{ry}$, since the plastic negative moment does not increase appreciably once the neutral axis reaches the tension flange. The limiting value $A_w\sigma_y/\sigma_{ry}$ is shown in Figures 5.24. Failure loads due to concrete crushing increase proportionally with the simple plastic ultimate loads. Ultimate loads based on local buckling are almost constant regardless of the amount of reinforcement, although local buckling loads for simply-supported beams are almost proportional to the simple plastic ultimate loads as discussed in Section 5.2. This is due to the fact that an increase in longitudinal slab reinforcement produces an increase in negative bending moment capacity because of increased stiffness.

5.8 Behavioral Study

Additional theoretical analyses were conducted for a number of composite beams with a steel section varying in depth from 10 and 16 inches and with flange width-thickness ratios less than $54/\sqrt{\sigma_y}$ which is a limitation for plastic design of plain steel sections. This limiting width-thickness ratio is 8.14 for G40.12 steel with a yield stress of 44Ksi. The beams were two-span continuous beams with each span equal to 20'-0". Slab thicknesses of 4 and 6 inches were chosen. A slab

width of 60 inches was used in all beams. The concrete strength was 3500 psi. The amount of longitudinal reinforcement was varied up to a maximum value equal to twice the area of the web of the steel section. Steel properties such as yield stress and strain-hardening modulus were the same for the steel section and the reinforcement for convenience. Details of the beams are shown in Figure 5.25.

Analytical results related to failure loads and failure modes are shown in Figures 5.26 and 5.27. The failure modes are local buckling at the interior support and crushing of concrete at the load points. Ultimate concrete strains of 0.003, 0.0035 and 0.004 are considered in determining ultimate loads based on a crushing failure. The ultimate loads are expressed by the ratio to the ultimate simple plastic load for the beam with no longitudinal slab reinforcement on the vertical co-ordinate and the amounts of longitudinal slab reinforcement are expressed by the ratio to the web area of the steel section on the horizontal coordinate in the figures.

The analyses indicate that the flange width-thickness ratio significantly effects the ultimate loads based on local flange buckling. W12 x 27 and W16 x 36 sections have b/t ratios equal to 8.14 which is equal to the upper limit of $54/\sqrt{\sigma_y}$. For these two sections the local buckling loads are very close to the simple plastic ultimate loads for longitudinal slab reinforcement greater than A_w and the local buckling loads are smaller than the simple plastic ultimate loads for amounts of longitudinal reinforcement equal to $2A_w$. The local buckling loads for such stocky sections are significantly greater than the simple plastic ultimate loads.

Ultimate loads based on concrete crushing increase almost proportionally with the increase in the simple plastic ultimate loads. Ultimate load based on an ultimate strain of 0.0035 is greater than the simple plastic ultimate load by more than 5 percent. Ultimate load based on a strain of 0.003, the value employed in the ACI 318-71 Building Code, is greater than the simple plastic ultimate load by only 2 to 3 percent.

The failure load curves for W12 x 27 in Figure 5.26 are quite similar to those in Figure 5.24(b), in spite of different beam length, different strength of concrete and different slab width. Results of the analysis for 4 inch and 6 inch slab thickness are very similar.

Ultimate loads for composite beams with W10 x 25 and W14 x 34 sections are greater than theoretical values based on simple plastic theory for an amount of longitudinal reinforcement equal to $2A_w$. The flange width-thickness ratios for W10 x 25 and W14 x 34 sections are 6.5 and 7.4, respectively, or 20 and 10 percent less, respectively, than the provision in CSA Standard S16-1969.

TABLE 5.1 COMPARISON OF EXPERIMENTAL AND THEORETICAL ULTIMATE MOMENT VALUES FOR BEAMS TESTED BY DAVISON[5] AND LEVER[6]

BEAM NO.	STEEL SECTION	AREA OF LONGITUDINAL REINFORCEMENT (in^2)	ULTIMATE MOMENT (in-kips)		
			EXPERIMENT	ANALYSIS	
				BASED ON LAY'S PROPOSED SHEAR MODULUS	BASED ON BIJLAARD'S PROPOSED SHEAR MODULUS
18	W12x36	0.0	2900	2891	2537
11		1.18	3320	3284	2950
12		1.96	3390	3449	3133
13		2.45	3420	3557	3233
14		3.68	3510	3742	3383
21	W12x31	0.0	2550	2246	2077
22		0.80	2860	2499	2354
23		1.86	2990	2749	2606
24		2.48	3010	2895	2698
25		3.72	2900	3005	2844
31	W12x27	0.0	2270	1915	1996
32		0.80	2400	2183	2244
33		1.60	2580	2425	2489
34		3.10	2700	2652	2740

TABLE 5.2 CURVATURE AT LOCAL FLANGE BUCKLING MOMENT FOR BEAMS TESTED BY DAVISON[5] AND LEVER[6]

BEAM NO.	STEEL SECTION	AREA OF LONGITUDINAL REINFORCEMENT (in^2)	CURVATURE (radians/inch$\times 10^3$)	
			EXPERIMENT	ANALYSIS BASED ON LAY'S SHEAR MODULUS
18	W12x36	0.0	8.80	6.92
11		1.18	8.00	5.41
12		1.96	6.00	4.31
13		2.45	4.90	4.02
14		3.68	2.50	3.09
21	W12x31	0.0	4.54	3.31
22		0.80	3.72	2.89
23		1.86	2.60	1.91
24		2.46	2.26	1.64
25		3.72	1.95	1.46
31	W12x27	0.0	4.20	4.50
32		0.80	3.78	3.90
33		1.60	2.87	3.06
34		3.10	2.29	2.41

TABLE 5.3 COMPARISON OF THEORETICAL AND EXPERIMENTAL RESULTS FOR BEAMS TESTED BY CLIMENHAGA[15]

STEEL SECTION	COVER PLATE	BEAM LENGTH	LONGITUDINAL STIFFENER ON WEB	ULTIMATE MOMENT (in-kips)		RATIO OF EXPERIMENTAL TO ANALYTICAL ULTIMATE MOMENT
				EXPERIMENT	ANALYSIS	
5x3RSJ	2½x½	12'-4"	NO	355	266	1.33
5x3RSJ	2½x½	8'-4"	NO	362	275	1.32
8x5¼UB17	4½x¾	12'-4"	NO	1040	956	1.09
8x5¼UB17	4½x¾	8'-4"	NO	1010	968	1.04
8x5¼UB20	4½x¾	12'-4"	NO	1235	1019	1.21
8x5¼UB20	4½x¾	8'-4"	NO	1275	1043	1.22
12x4UB16.5	3½x1	12'-4"	NO	1477	1566	.94
12x4UB16.5	3x¾	8'-4"	NO	1540	1502	1.03
14x5UB22	4½x1	12'-4"	NO	1930	2153	.90
14x5UB22	4½x½	8'-4"	NO	1877	1916	.98
16x5½UB26	4½x1	12'-4"	NO	2580	2504	1.03
16x5½UB26	4½x½	8'-4"	YES	2622	2295	1.14
8x5¼UB17	4½x¾	8'-4"	YES	1145	909	1.26
12x4UB22	3½x¾	8'-4"	NO	1730	1818	.95
16x5½UB26	4½x¾	12'-4"	YES	2808	2422	1.16

TABLE 5.4 LATERAL BUCKLING MOMENT FOR BEAMS TESTED BY PIEPGRASS[4]

STEEL SECTION	AREA OF LONGITUDINAL REINFORCEMENT (in^2)	SIMPLE PLASTIC MOMENT (in-kips)	ULTIMATE MOMENT (in-kips)		RATIO OF EXPERIMENTAL TO ANALYTICAL ULTIMATE MOMENT
			EXPERIMENT	ANALYSIS	
W12x16.5	1.20	1637	1920	1820	1.05
W12x16.5	2.48	1982	2112	2175	.97
W12x16.5	2.48	1982	2116	2175	.99
W12x16.5	3.10	2260	2260	2307	.98

TABLE 5.5 COMPARISON OF EXPERIMENTAL AND THEORETICAL VALUES OF ULTIMATE LOADS FOR BEAMS TESTED IN PRESENT INVESTIGATION

BEAM	IDEALIZED ULTIMATE LOAD BASED ON SIMPLE PLASTIC THEORY (kips)	PROPOSED ANALYSIS ULTIMATE LOAD (kips)		EXPERIMENT LOAD (kips)			
		CONCRETE CRUSHING	LOCAL BUCKLING	AT INITIAL CONCRETE CRUSHING	AT COMPLETE CONCRETE CRUSHING	AT INITIAL LOCAL BUCKLING	AT COMPLETE LOCAL BUCKLING
CB1	124	135	140	135	137	--	--
CB2	123	131	122	133	136	120	130
CB3	82	84	85	92	94	85	90

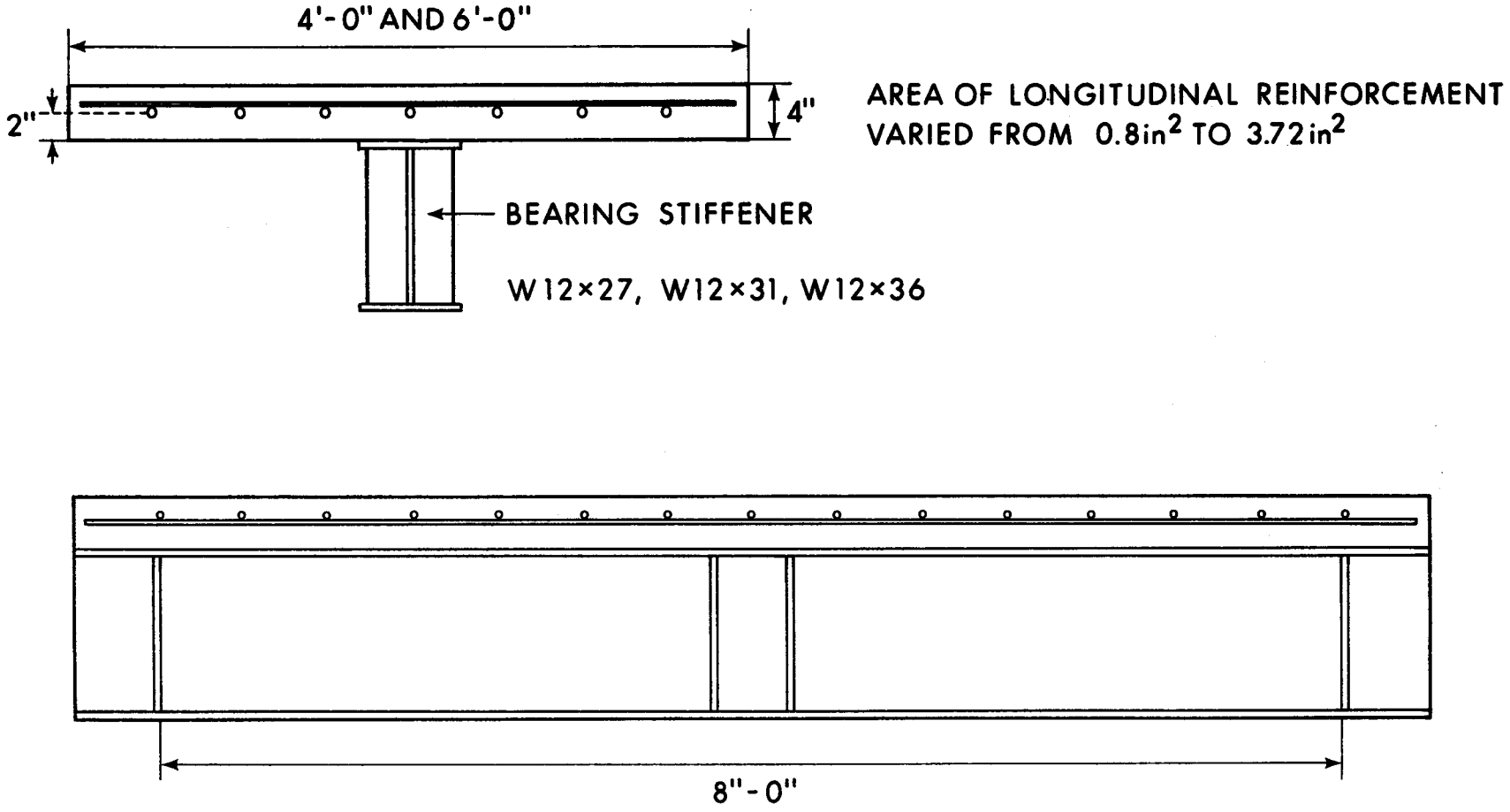

FIGURE 5.1 COMPOSITE BEAMS TESTED BY DAVISON[5] AND LEVER[6]

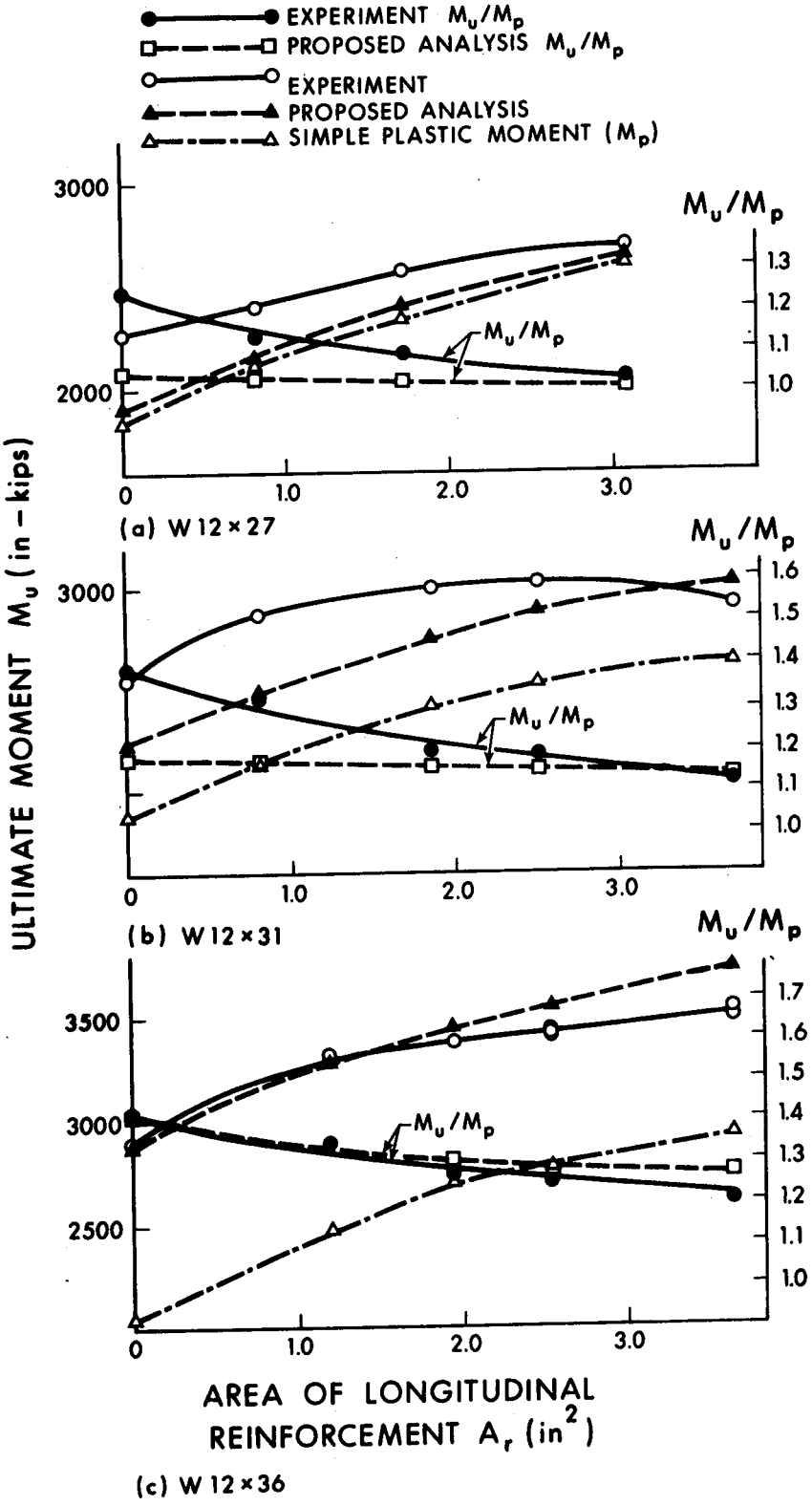

FIGURE 5.2 ULTIMATE MOMENT - AMOUNT OF LONGITUDINAL SLAB REINFORCEMENT RELATIONSHIPS

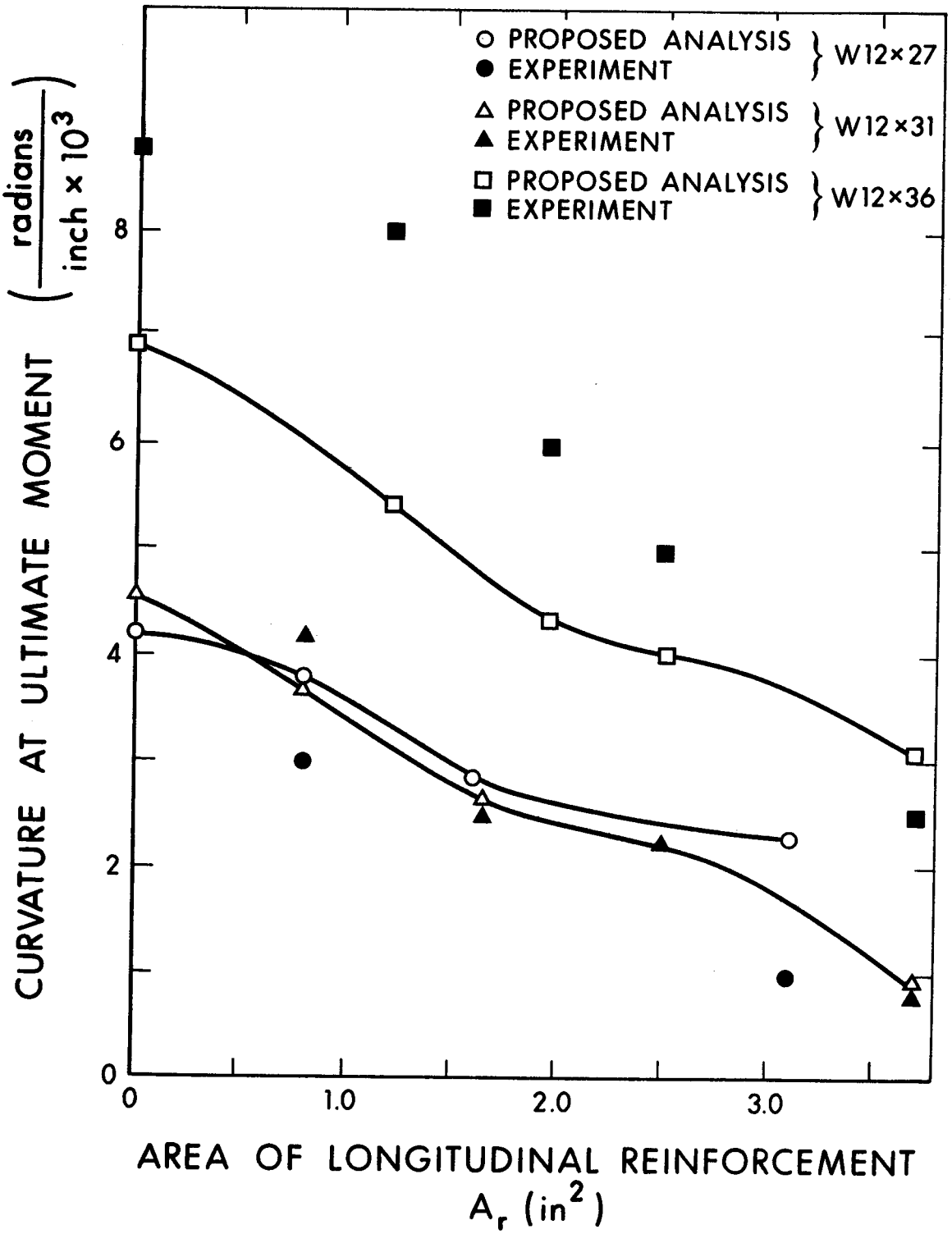

FIGURE 5.3 CURVATURE AT ULTIMATE MOMENT

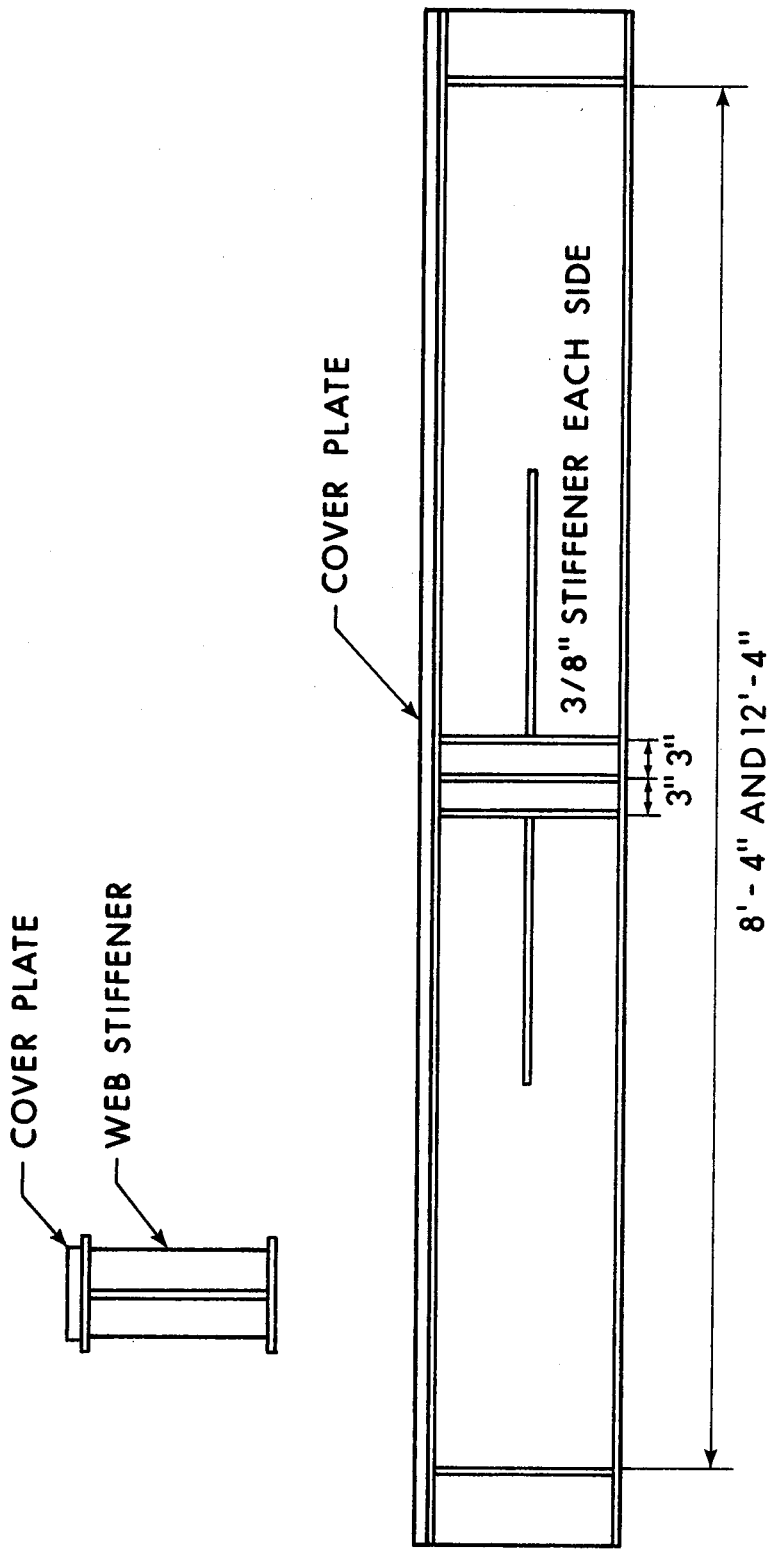

FIGURE 5.4 COMPOSITE BEAMS TESTED BY CLIMENHAGA

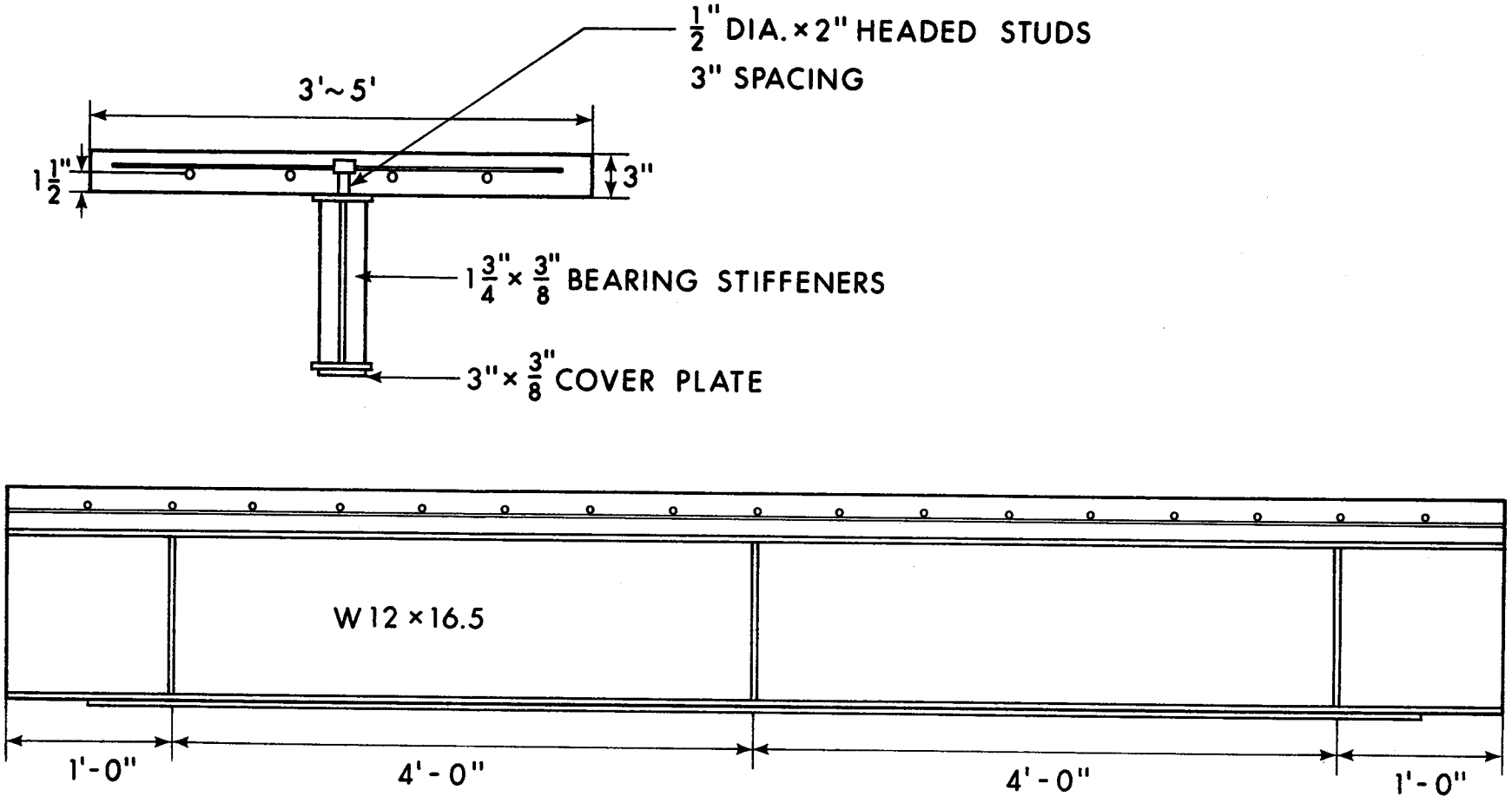

FIGURE 5.5 BEAMS TESTED BY PIEPGRASS

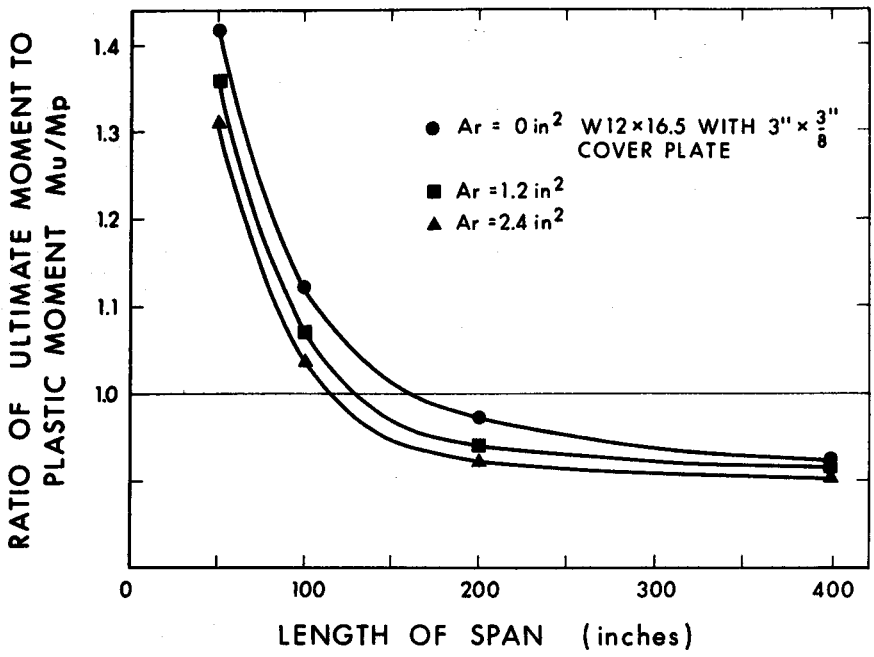

(a) EFFECT OF SPAN LENGTH ON Mu/Mp RATIO

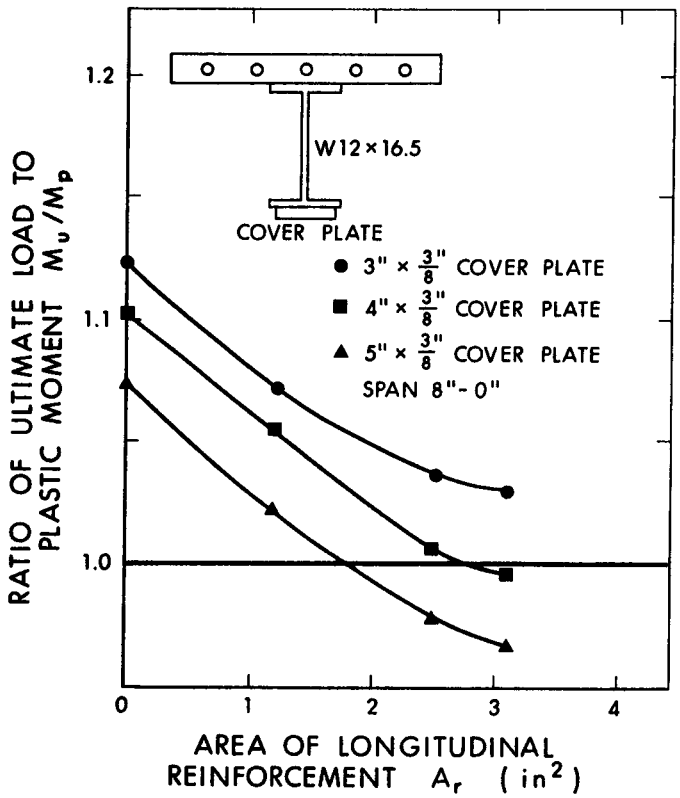

(b) EFFECT OF AREA OF LONGITUDINAL REINFORCEMENT ON Mu/Mp RATIO

FIGURE 5.6 FACTORS AFFECTING M_u/M_p RATIO

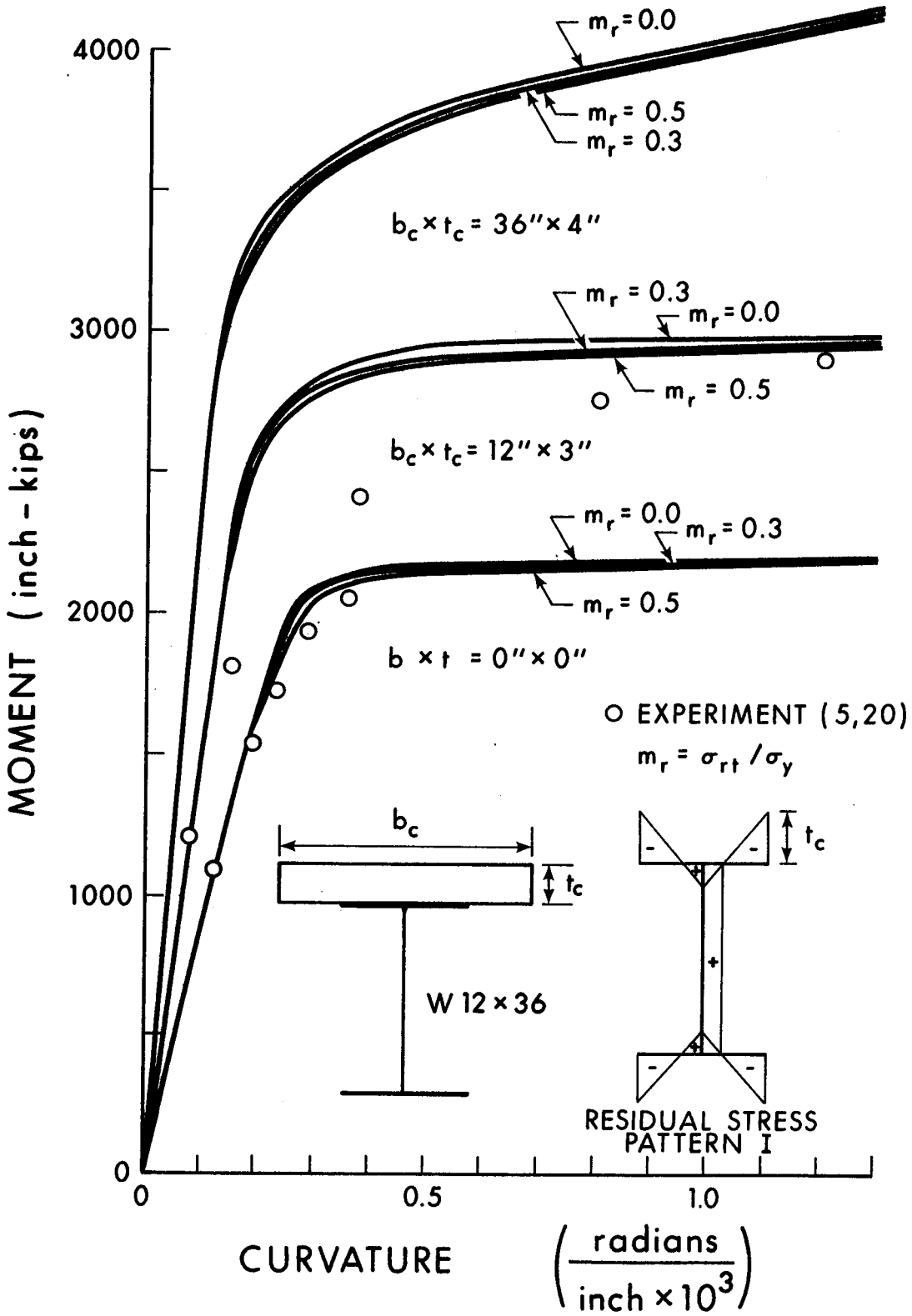

FIGURE 5.7 EFFECT OF RESIDUAL STRESSES ON MOMENT-CURVATURE RELATIONSHIPS IN A POSITIVE MOMENT REGION

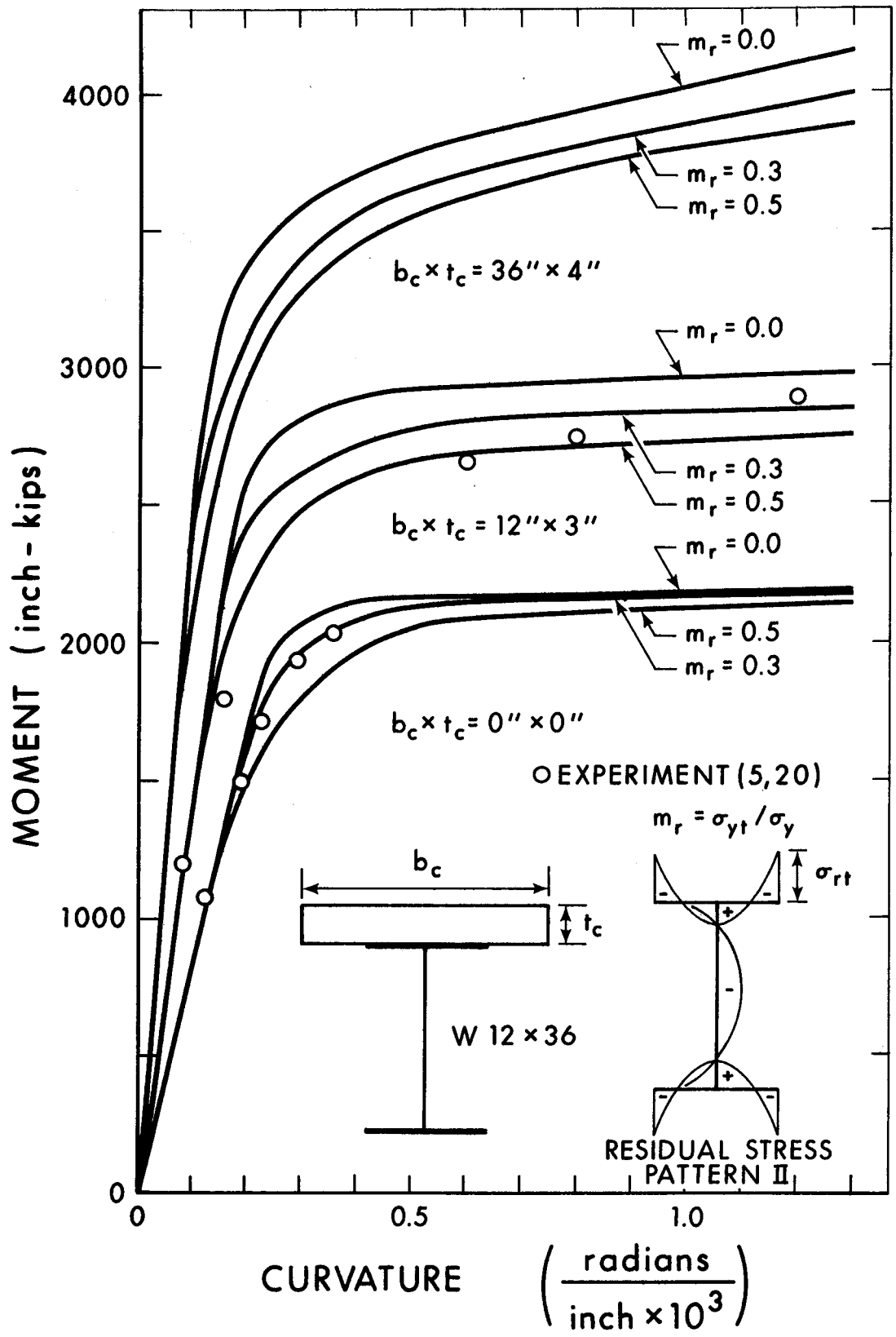

FIGURE 5.8 EFFECT OF RESIDUAL STRESSES ON MOMENT-CURVATURE RELATIONSHIPS IN A POSITIVE MOMENT REGION

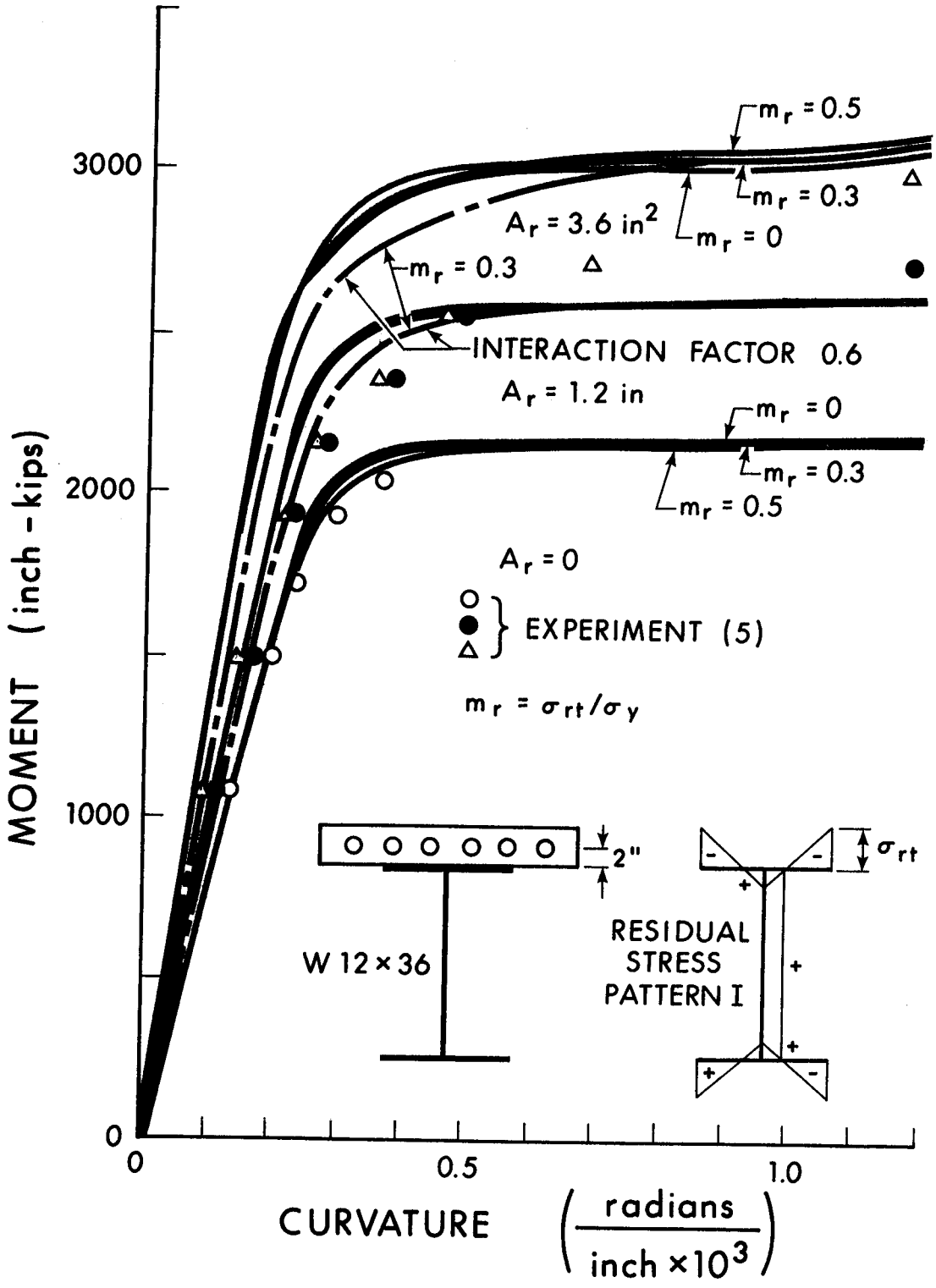

FIGURE 5.9 EFFECT OF RESIDUAL STRESSES ON MOMENT-CURVATURE RELATIONSHIPS IN A NEGATIVE MOMENT REGION

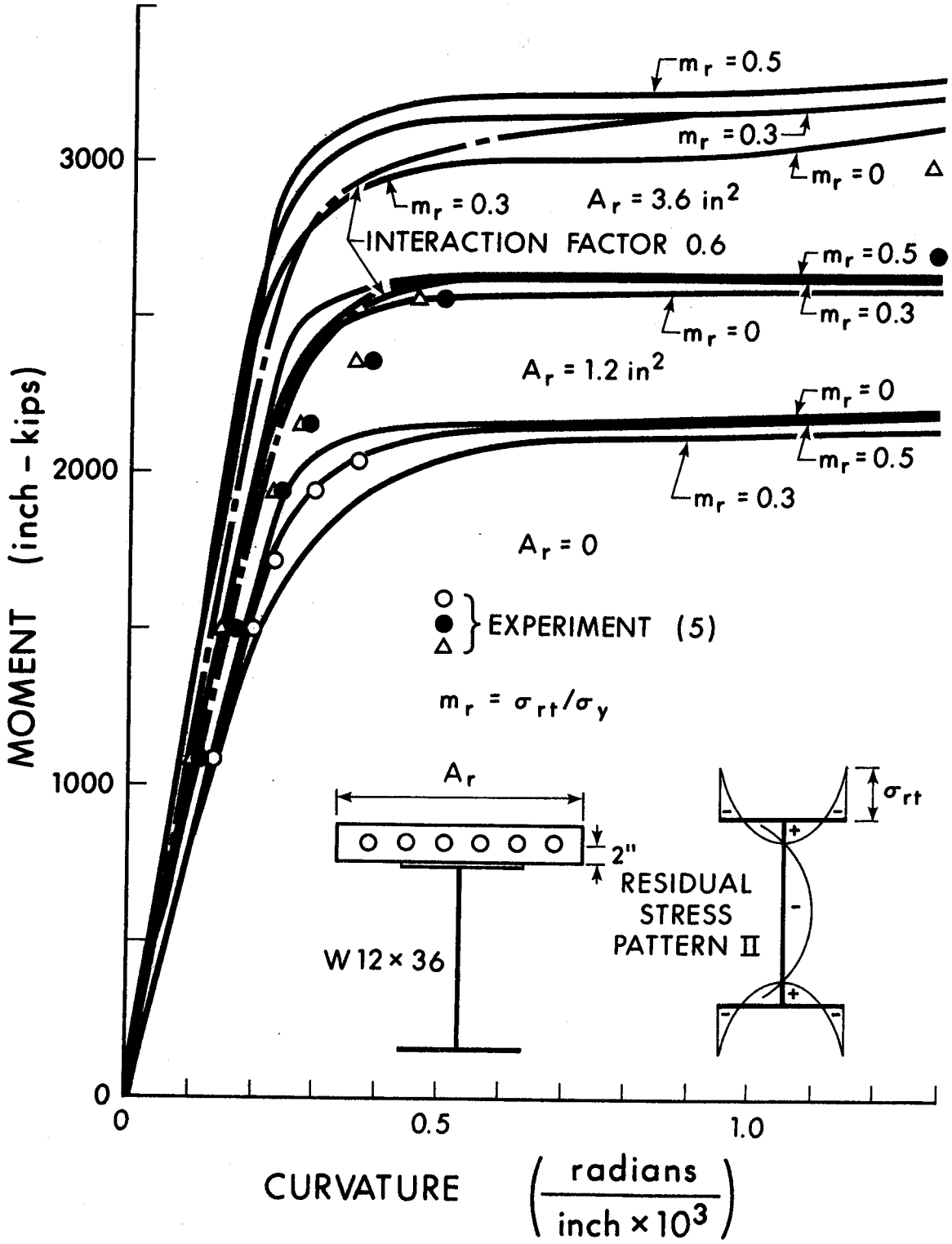

FIGURE 5.10 EFFECT OF RESIDUAL STRESSES ON MOMENT-CURVATURE RELATIONSHIPS IN A NEGATIVE MOMENT REGION

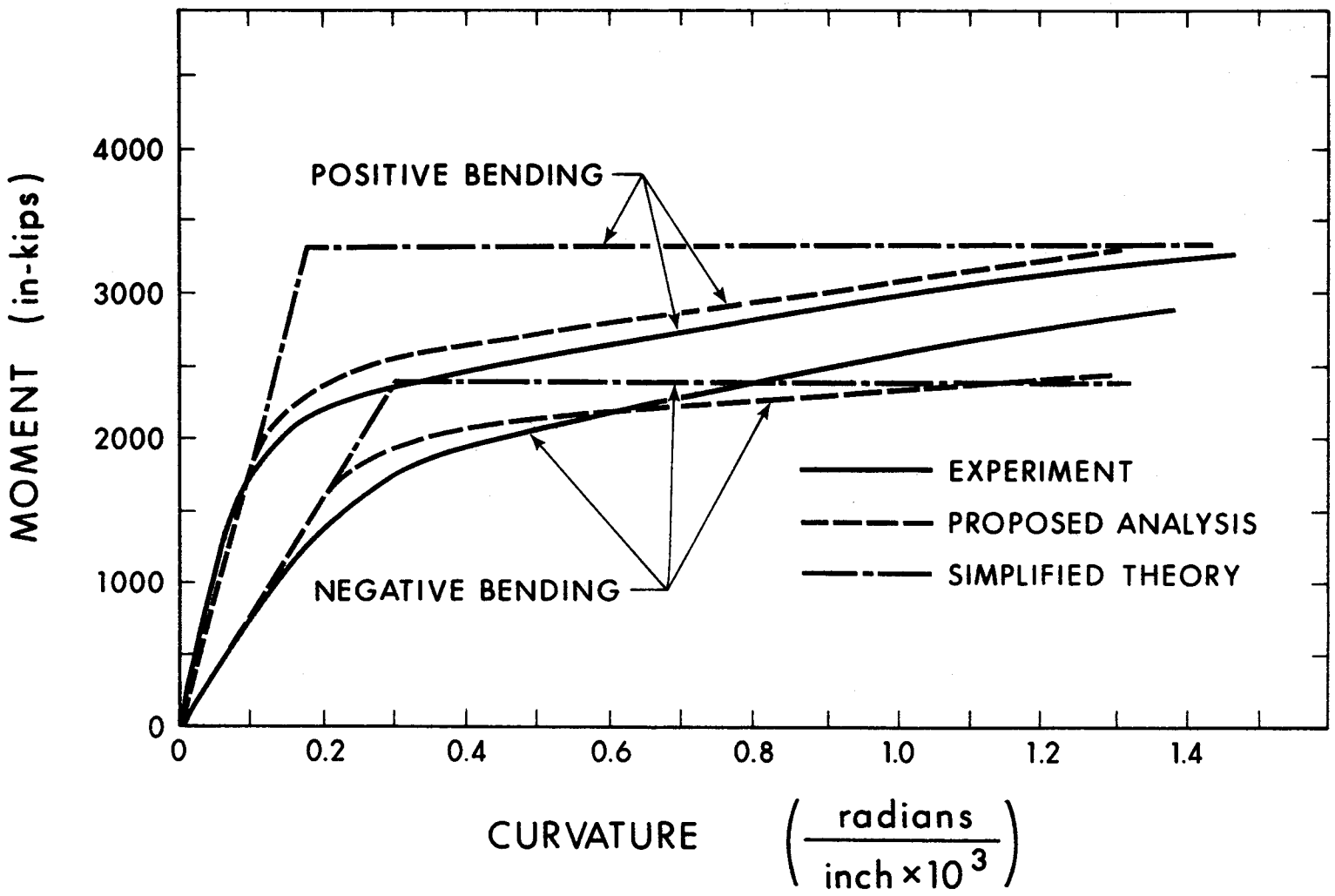

FIGURE 5.11 EXPERIMENTAL AND THEORETICAL MOMENT-CURVATURE RELATIONSHIPS FOR BEAM CB1

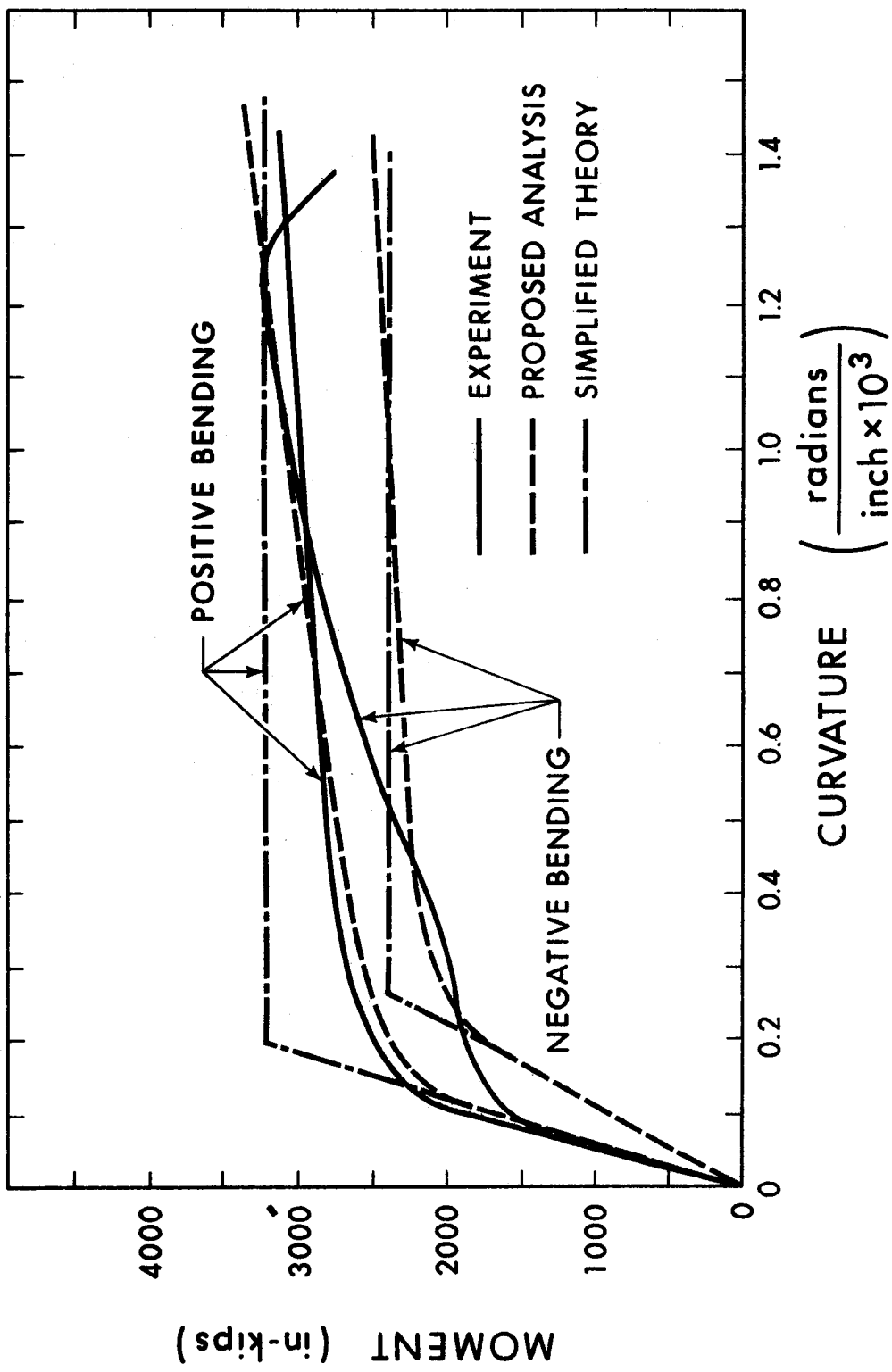

FIGURE 5.12 EXPERIMENTAL AND THEORETICAL MOMENT-CURVATURE RELATIONSHIPS FOR BEAM CB2

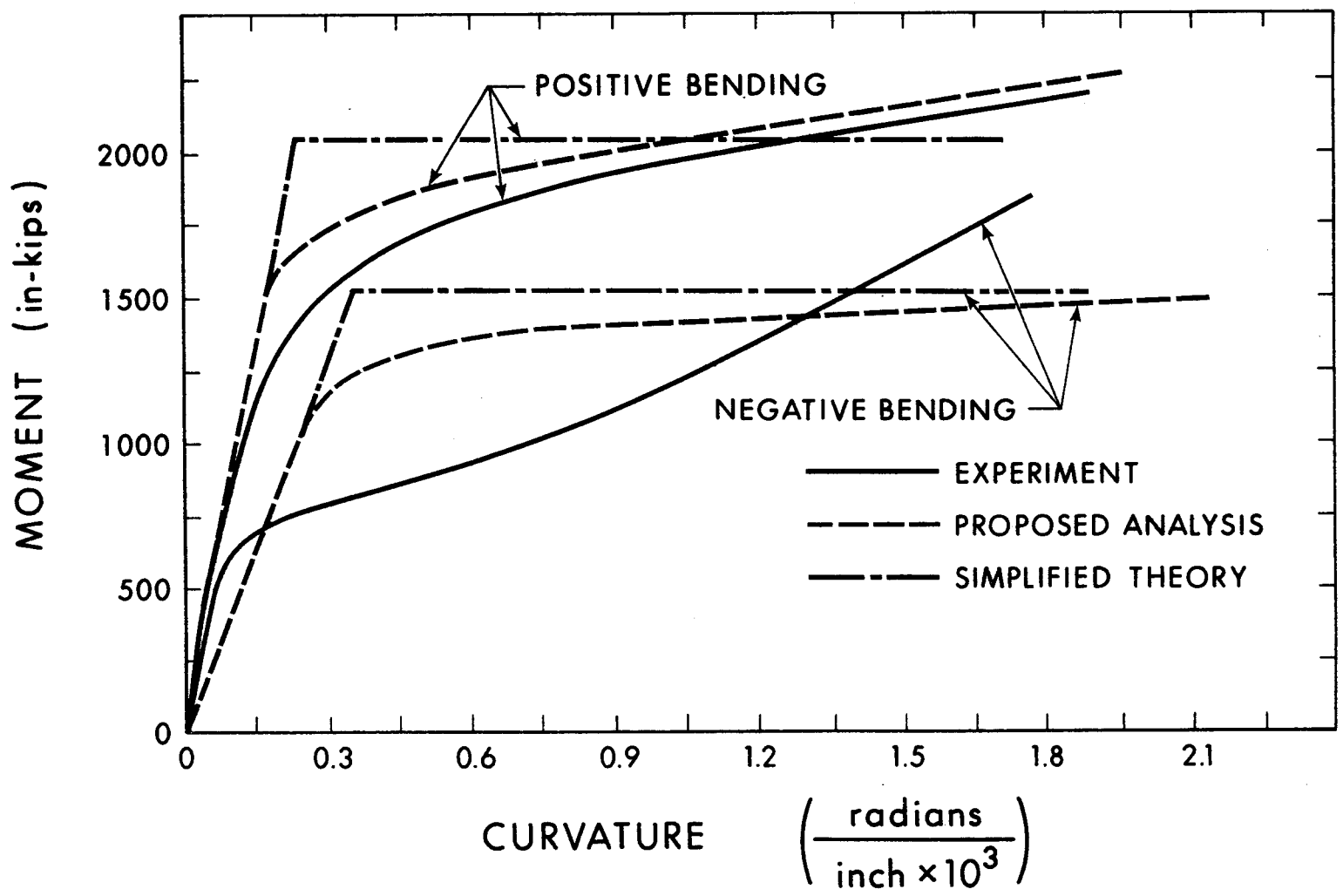

FIGURE 5.13 EXPERIMENTAL AND THEORETICAL MOMENT-CURVATURE RELATIONSHIP FOR BEAM CB3

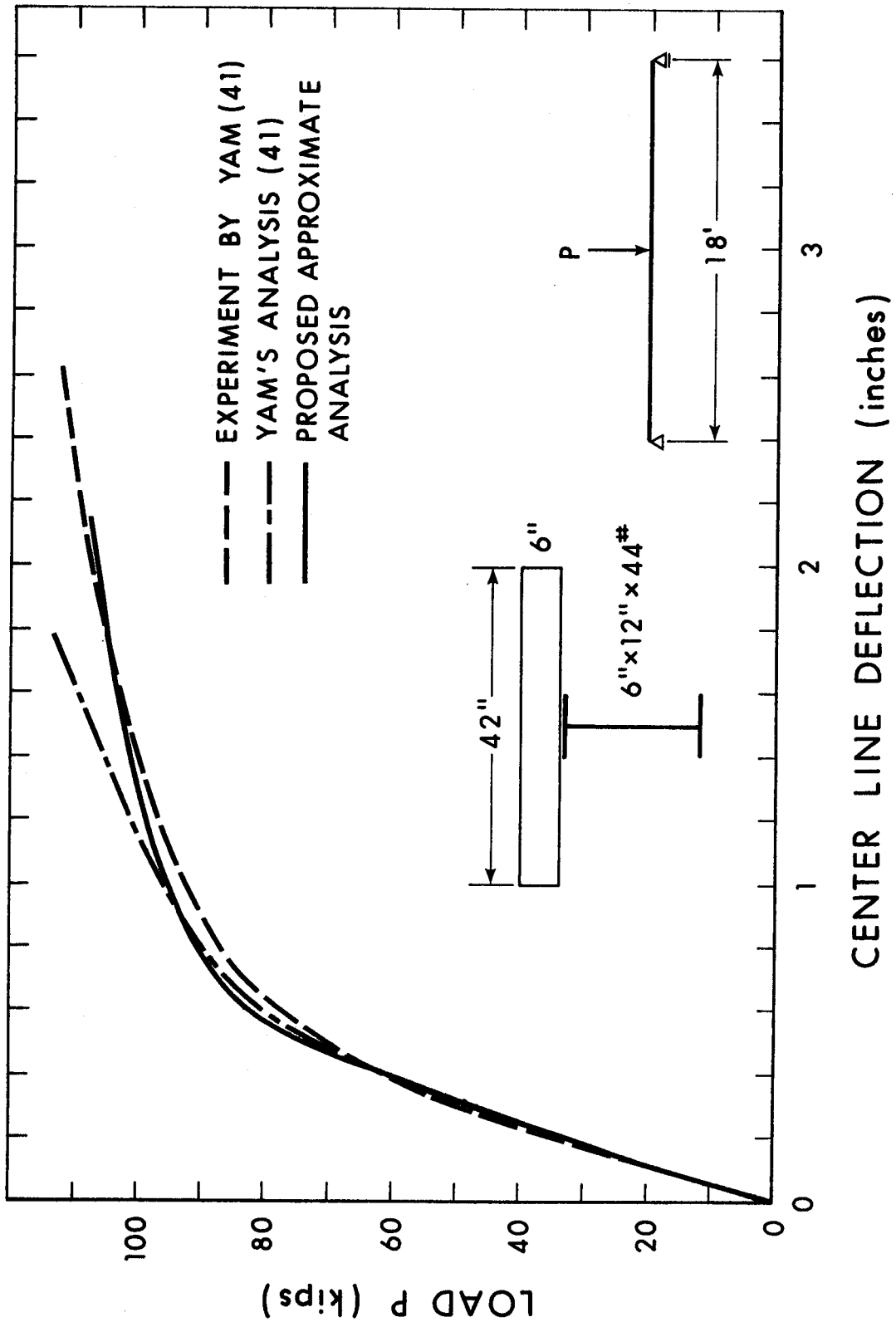

FIGURE 5.14 EFFECT OF SLIP ON DEFLECTION

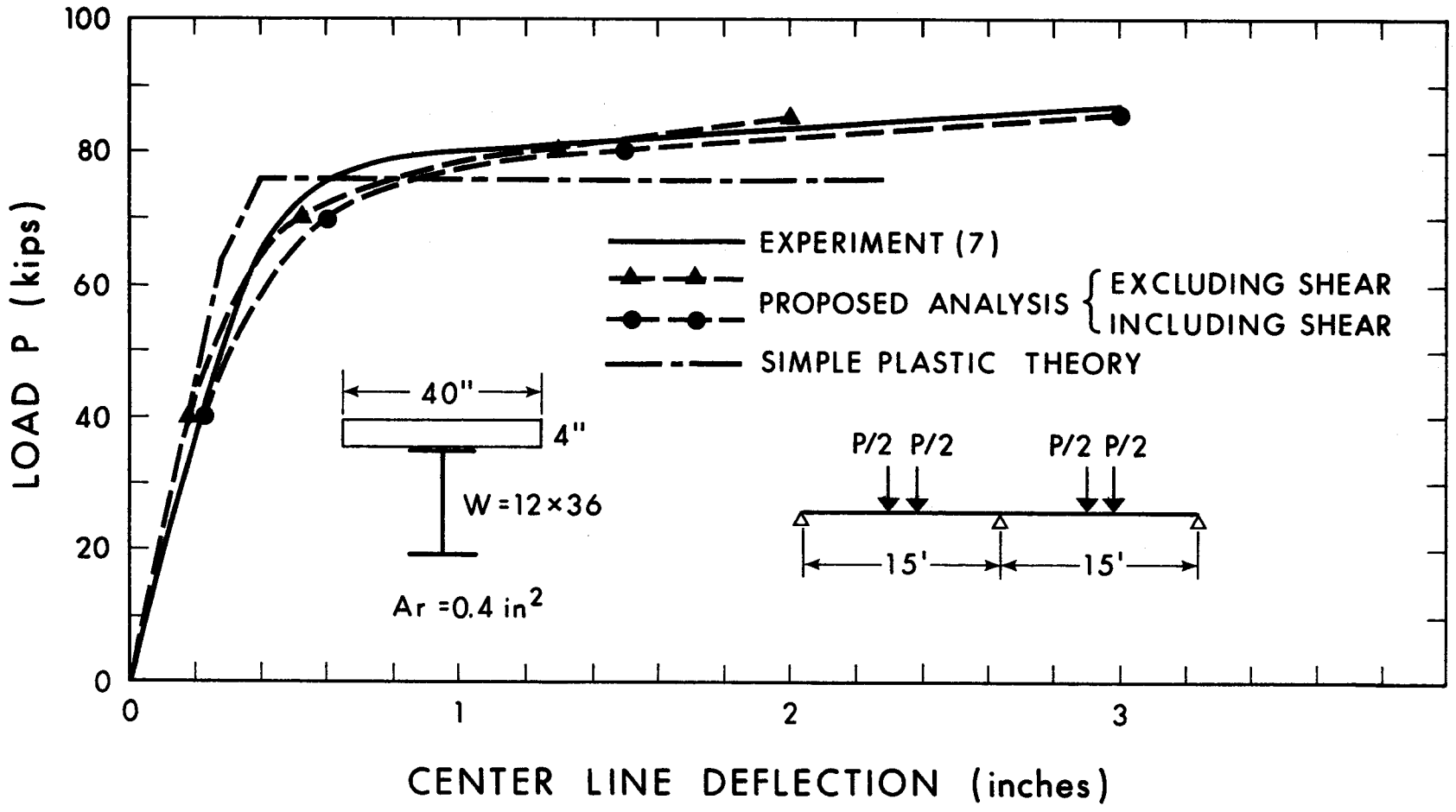

FIGURE 5.15 EXPERIMENTAL AND THEORETICAL LOAD-DEFLECTION RELATIONSHIPS

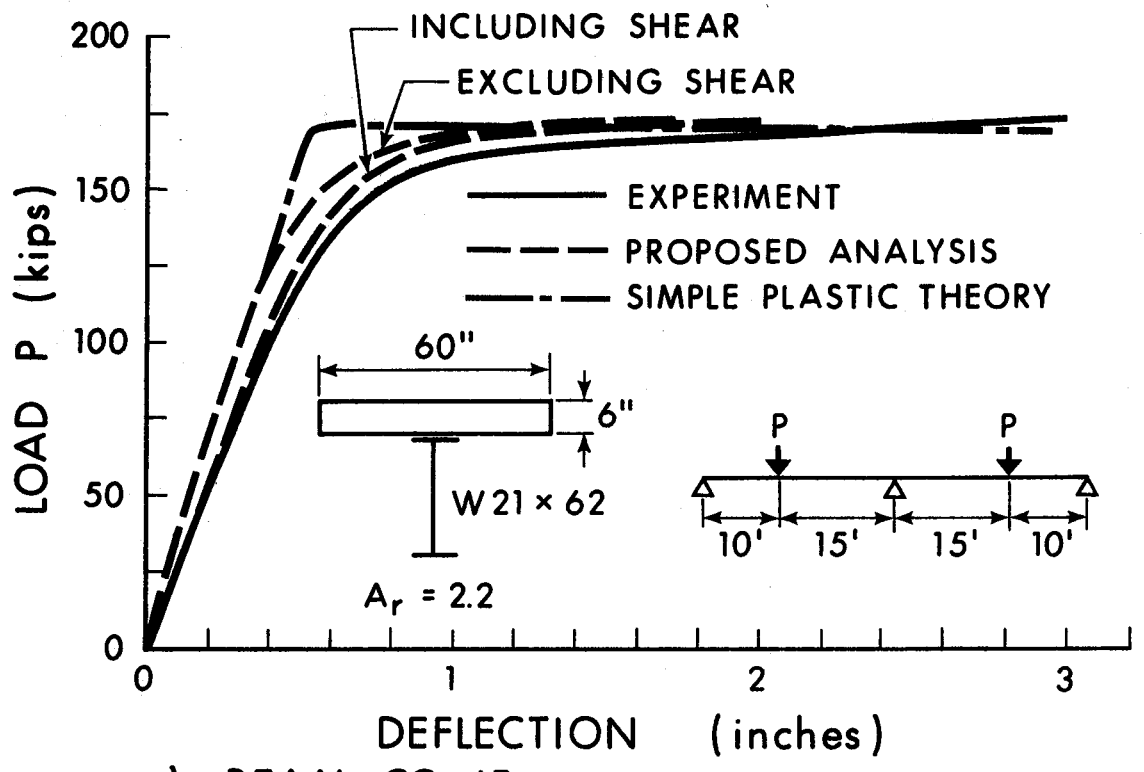

a) BEAM CC-1F

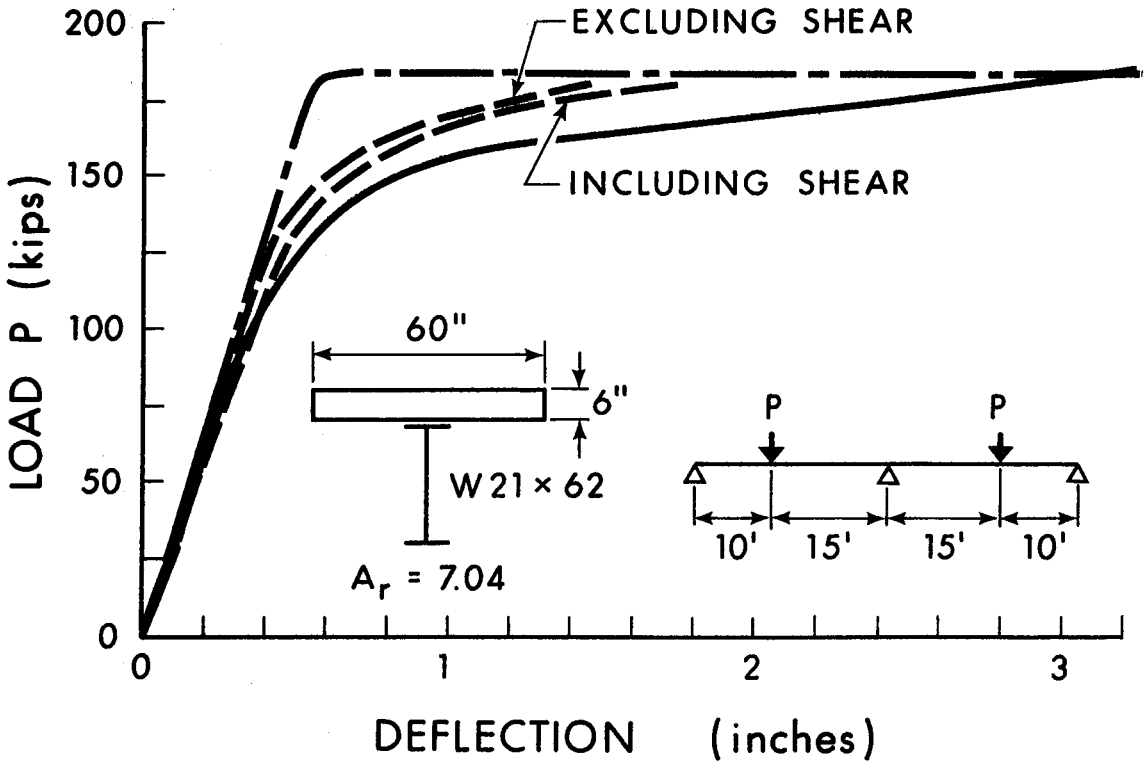

b) BEAM CC-3S

FIGURE 5.16 LOAD-DEFLECTION RELATIONSHIPS FOR BEAMS TESTED BY DANIELS AND FISHER[11]

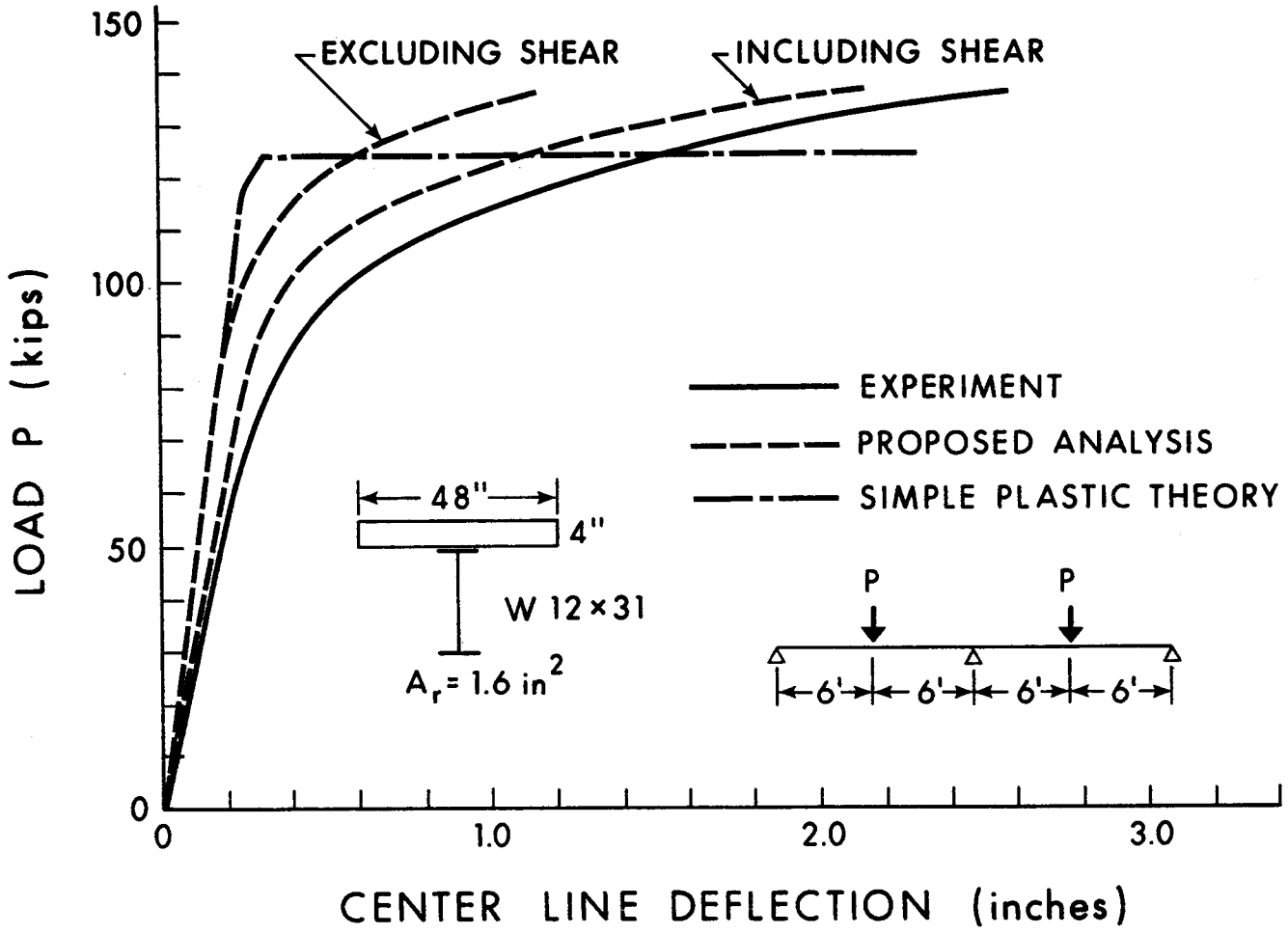

FIGURE 5.17 LOAD-DEFLECTION RELATIONSHIPS FOR BEAM CB1

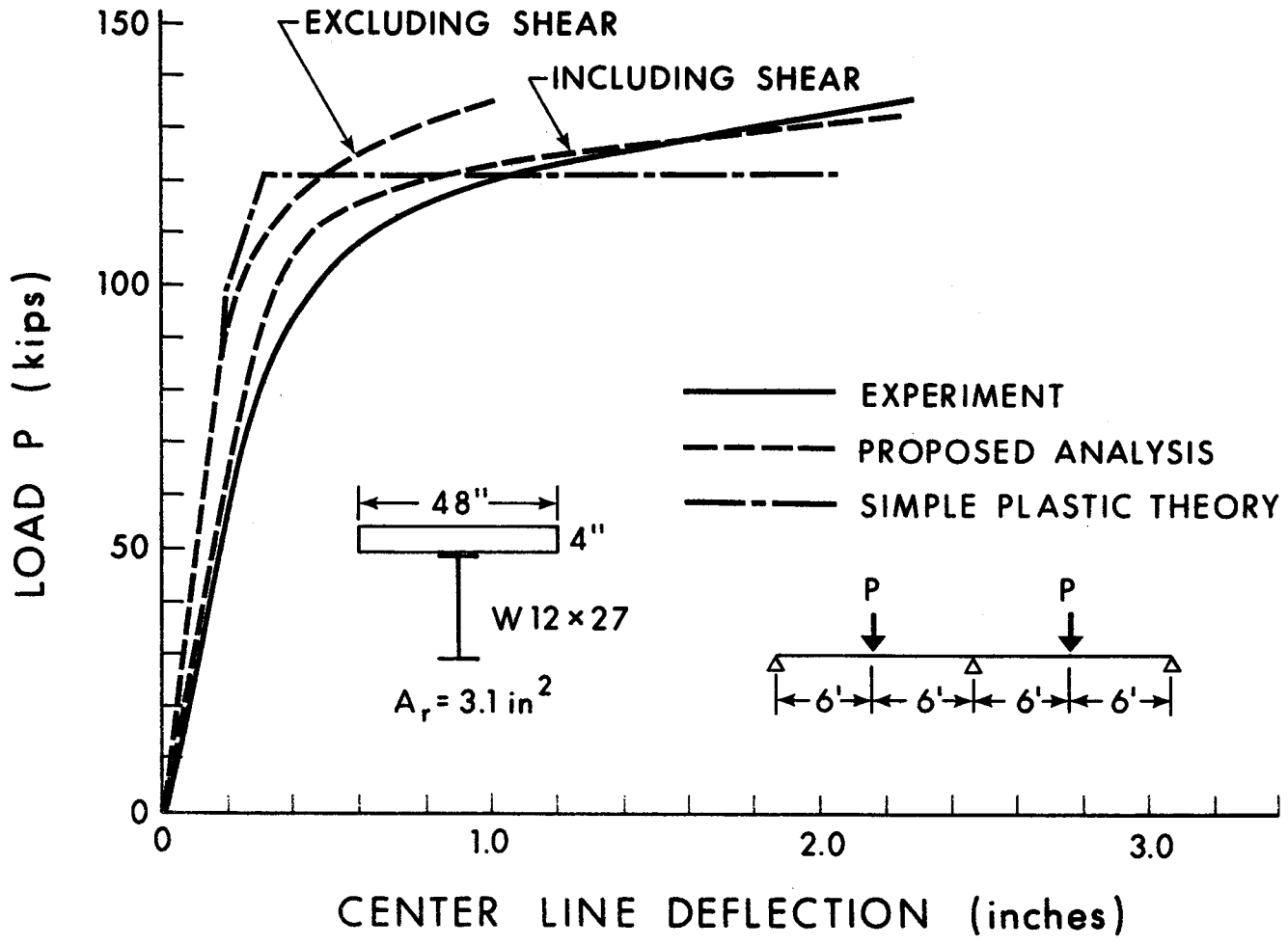

FIGURES 5.18 LOAD-DEFLECTION RELATIONSHIPS FOR BEAM CB2

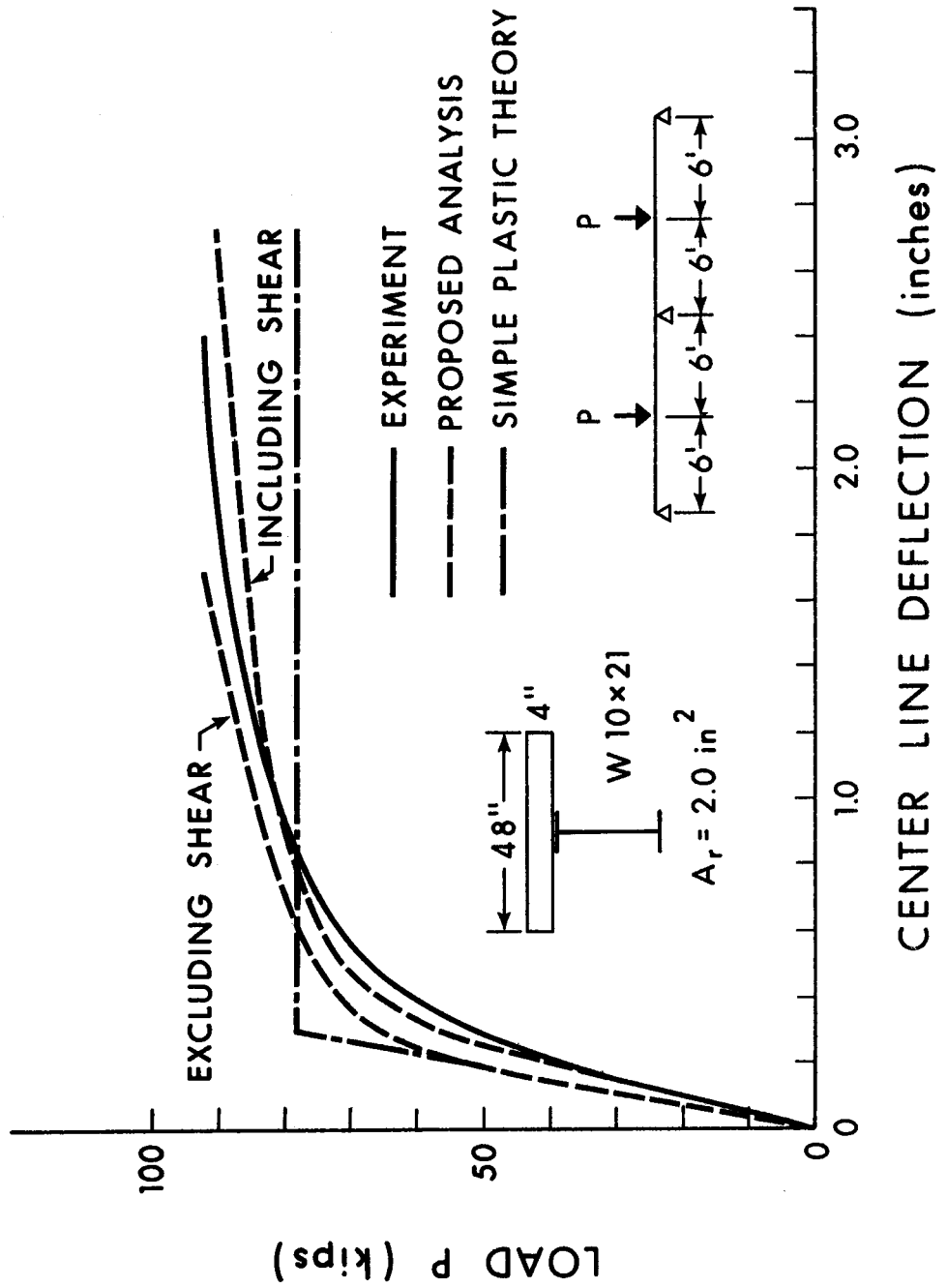

FIGURE 5.19 LOAD-DEFLECTION RELATIONSHIPS FOR BEAM CB3

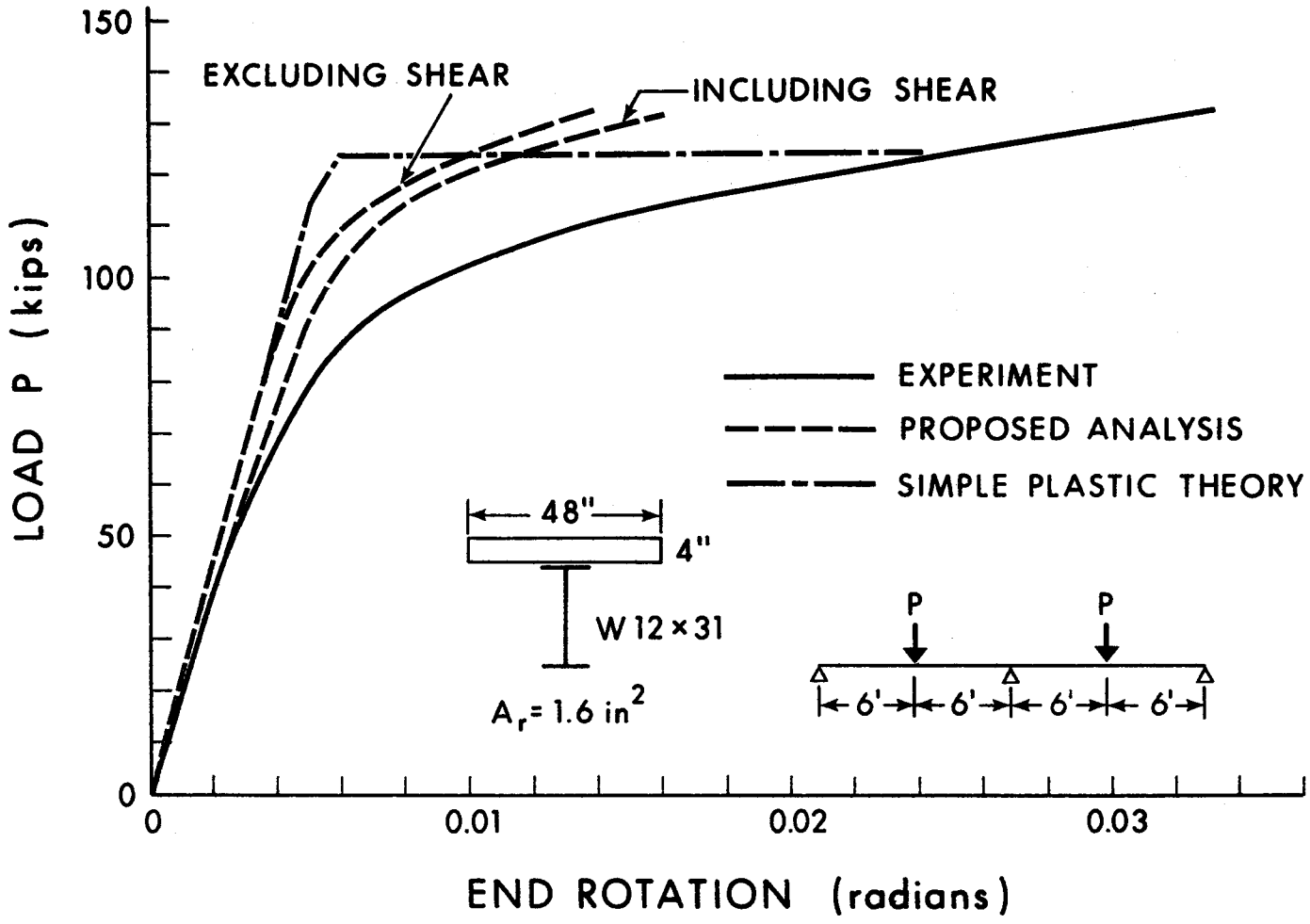

FIGURE 5.20 LOAD-ROTATION RELATIONSHIPS FOR BEAM CB1

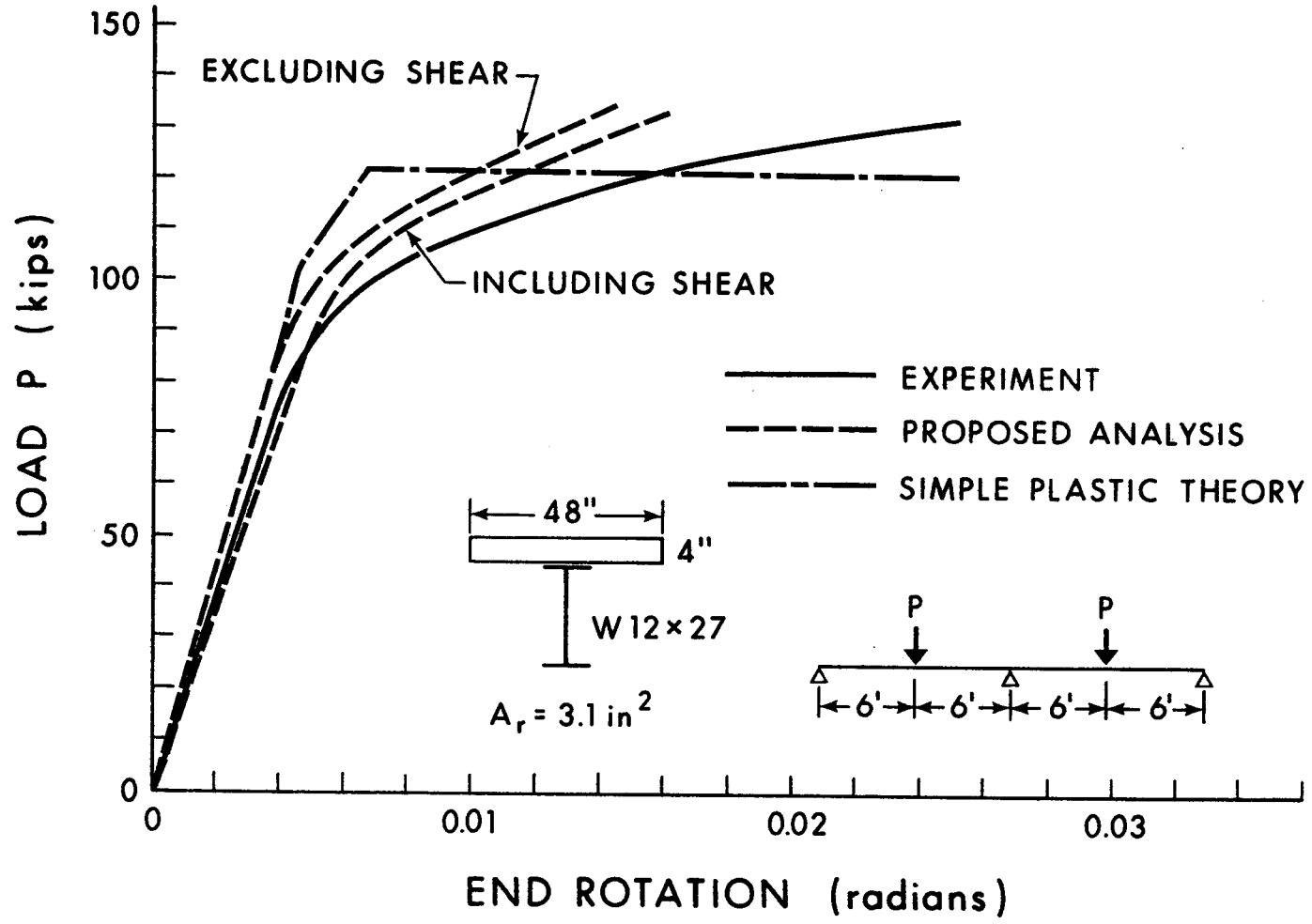

FIGURE 5.21 LOAD-ROTATION RELATIONSHIPS FOR BEAM CB2

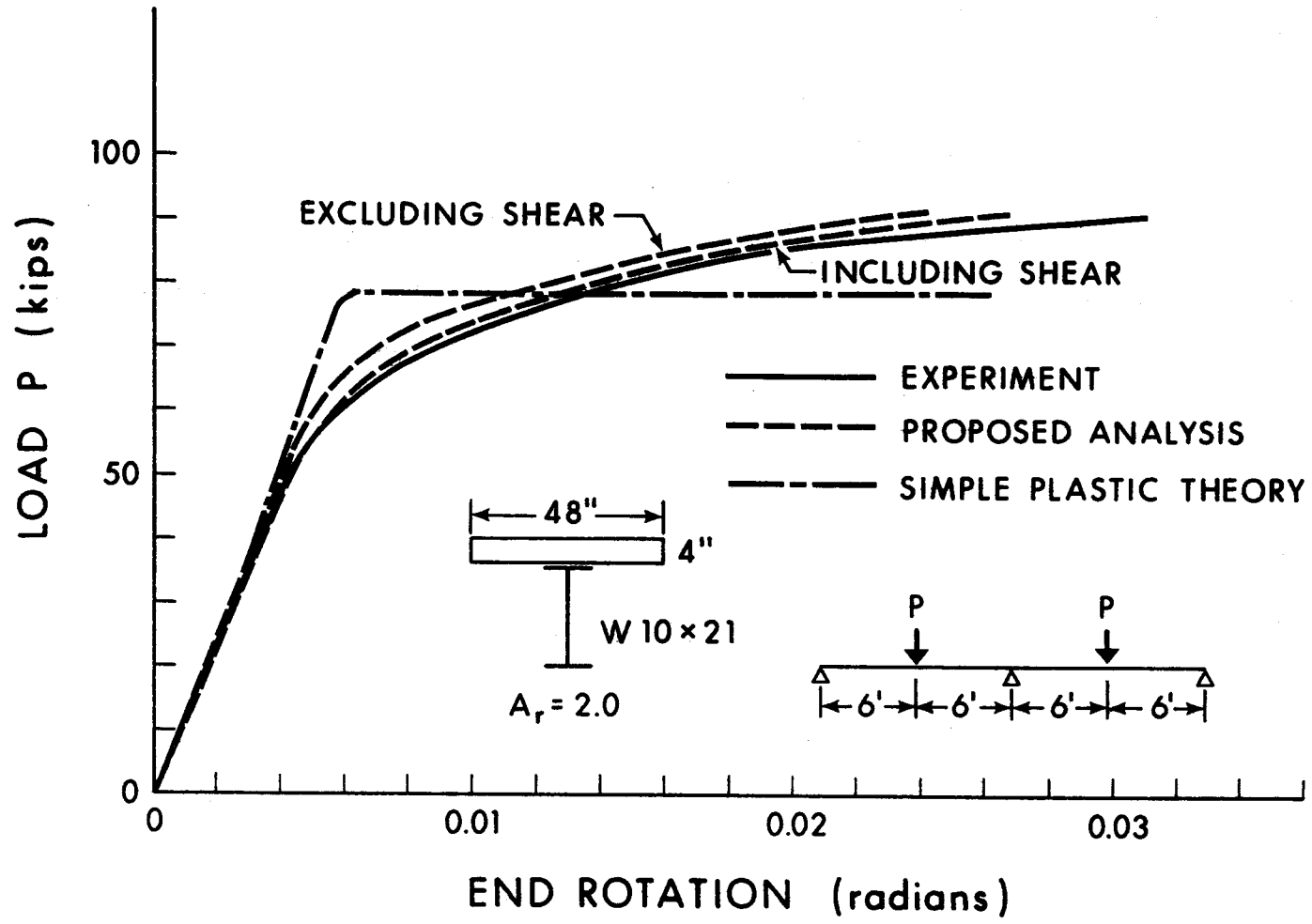

FIGURE 5.22 LOAD-ROTATION RELATIONSHIPS FOR BEAM CB3

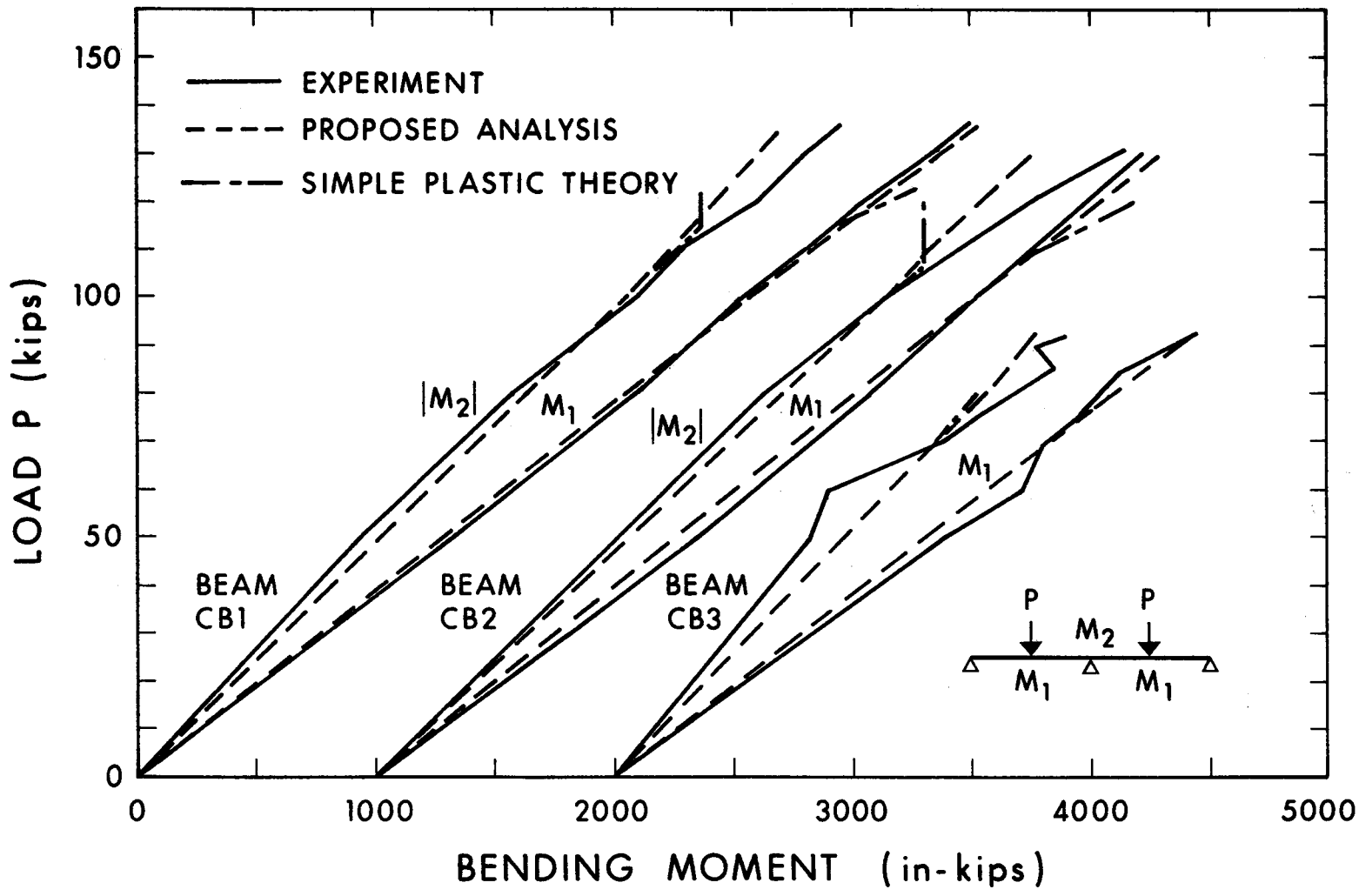

FIGURE 5.23 LOAD-MOMENT RELATIONSHIPS

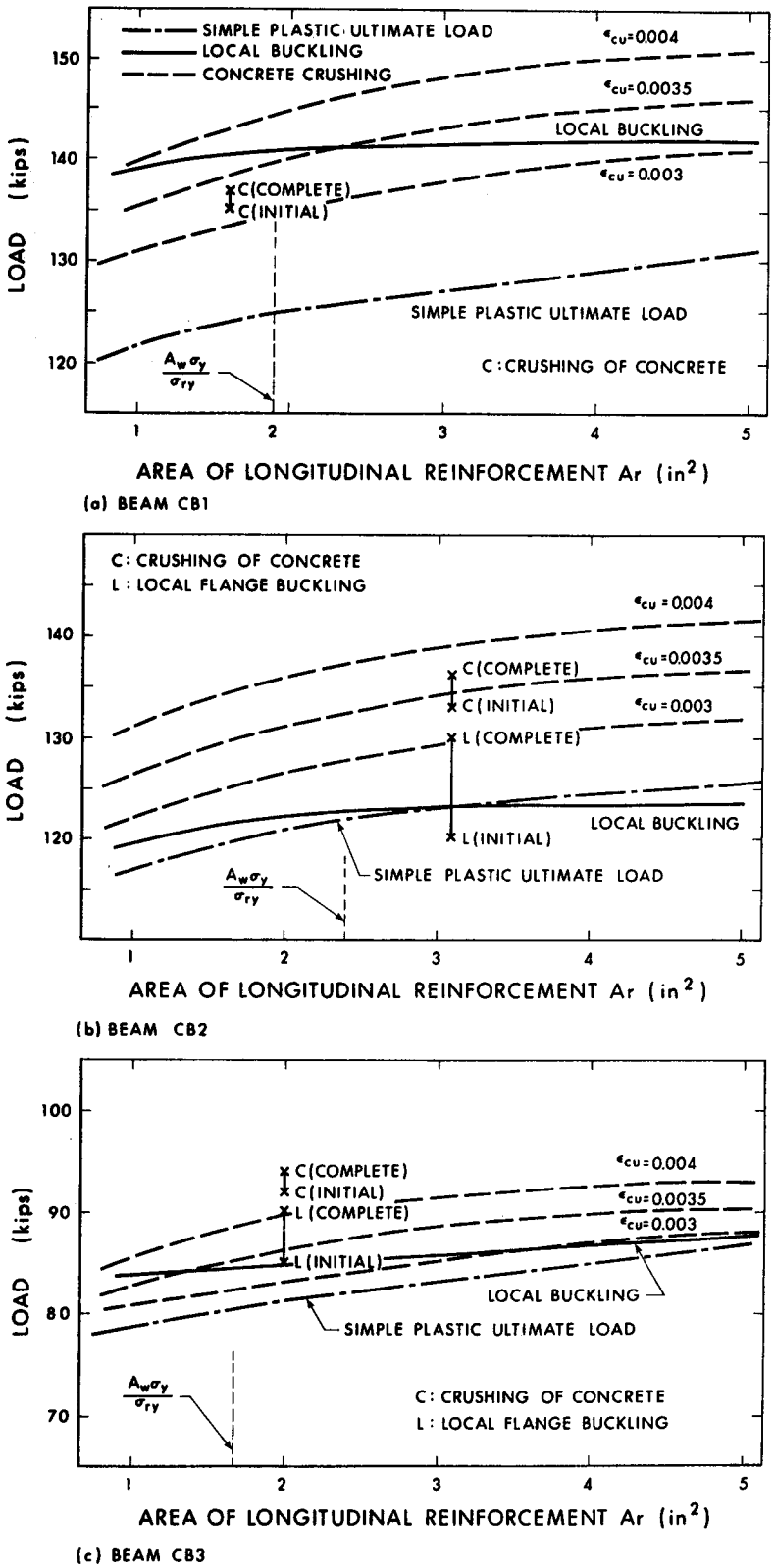

FIGURE 5.24 FAILURE LOADS AND FAILURE MODES FOR TEST BEAMS

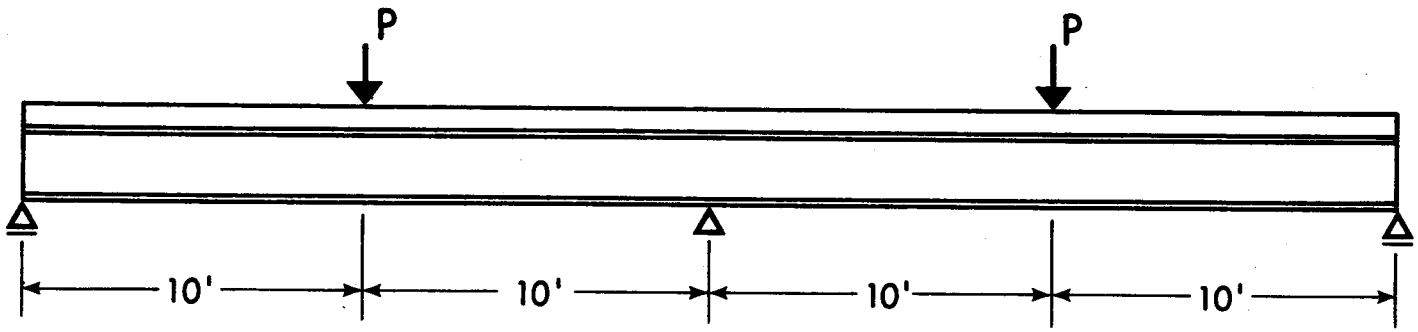

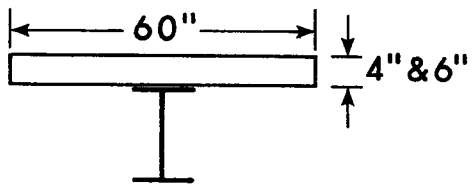

f'c = 3500 psi

PROPERTIES OF STEEL SECTION

YIELD STRESS = 44 Ksi

E/E_t = 35

b/t = 13.0 FOR W 10 × 25

= 16.3 FOR W 12 × 27

= 14.9 FOR W 14 × 34

= 16.3 FOR W 16 × 36

FIGURE 5.25 DETAILS OF BEAMS FOR BEHAVIORAL STUDY

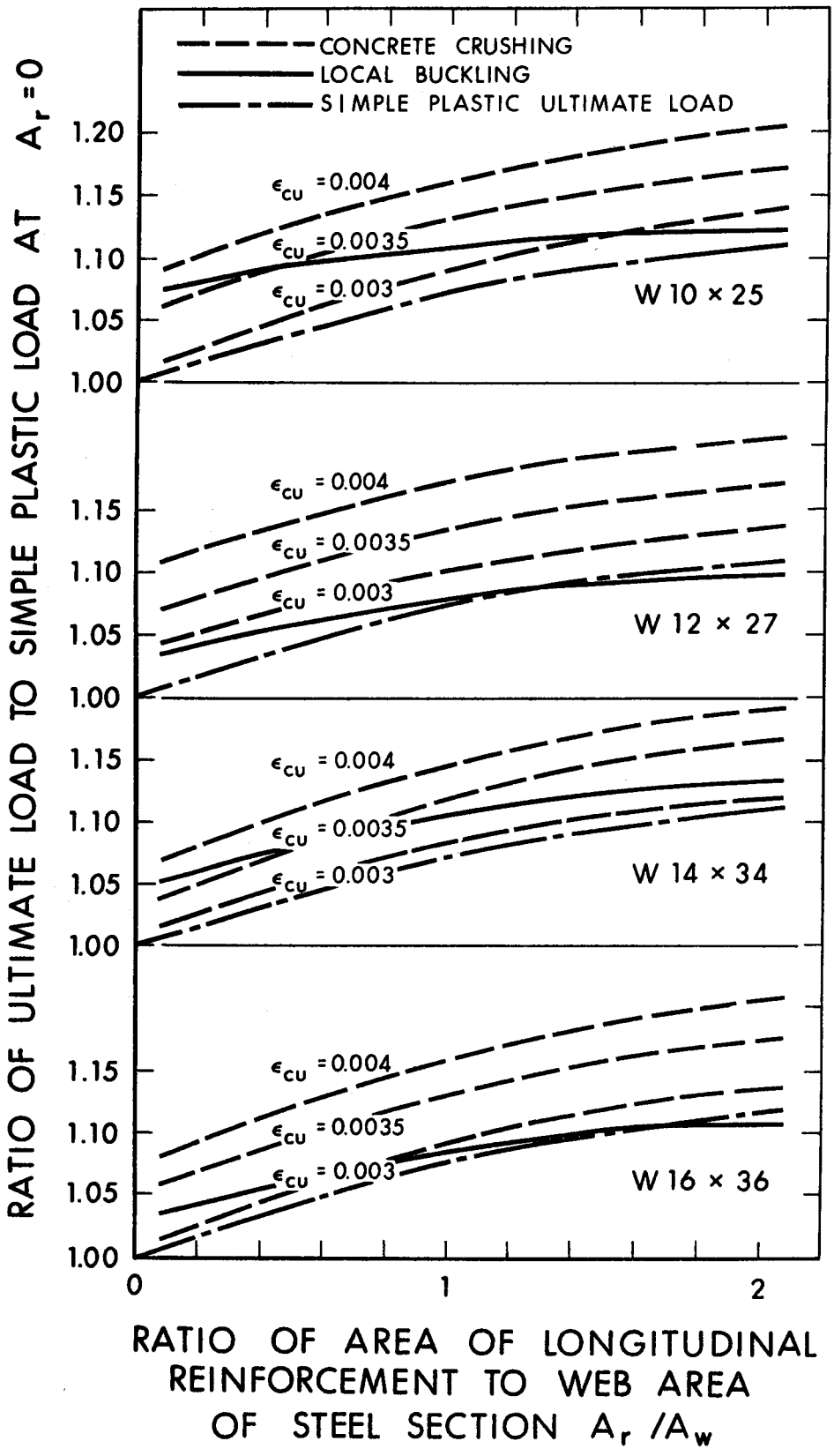

FIGURE 5.26 ULTIMATE LOADS FOR COMPOSITE BEAMS WITH 4" SLAB THICKNESS

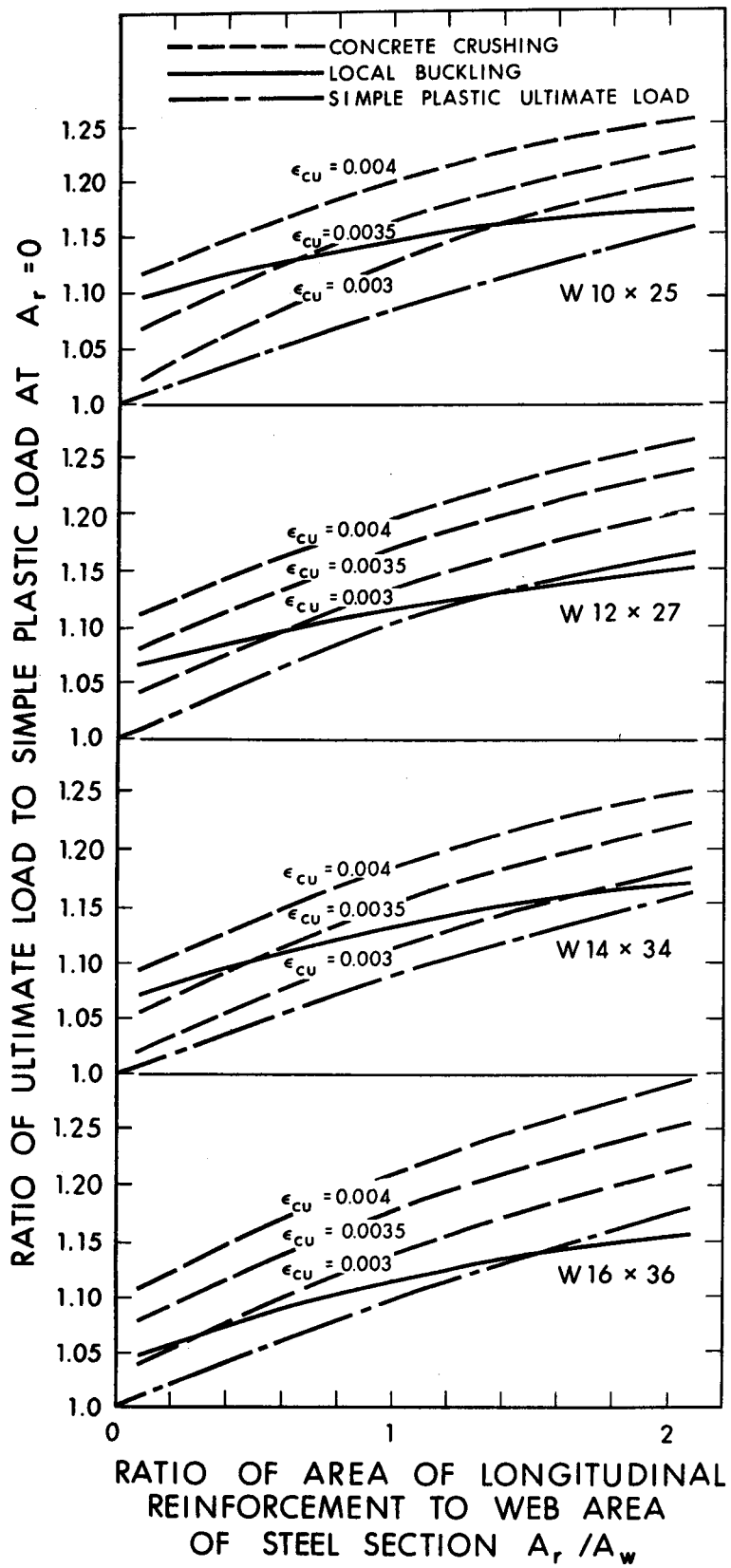

FIGURE 5.27 ULTIMATE LOADS FOR COMPOSITE BEAMS WITH 6" SLAB THICKNESS

CHAPTER VI

SUGGESTIONS FOR ULTIMATE STRENGTH DESIGN OF CONTINUOUS COMPOSITE BEAMS

6.1 Introduction

At present no design standards specifically cover ultimate strength design of continuous composite beams, although theoretical and experimental investigations provide substantial information on ultimate strength behavior of such members. British Standard CP 117 Part 1 includes provisions for ultimate strength design of simply-supported composite beams. However, additional requirements may be necessary for ultimate strength design of continuous beams. Such further requirements as discussed herein, are mainly based on the present investigation.

6.2 Present Specifications

In British Standard CP 117 Part 1, which specifies requirements for simply-supported beams, the specified load factor is 1.75 for both dead and live loads. The stress in the steel section at ultimate is the specified yield stress, whether in tension or compression. The concrete compression strength is 4/9 of the specified concrete cube strength. This fraction is derived from the assumption that the strength of the concrete in the slab is 2/3 of the cube strength and the pro-

vision of a higher factor against concrete crushing than the factor against yielding of the steel. This latter provision results in assuming compression strength as 2/3 of the slab strength. Furthermore the standard requires that in no case should elastic stress under working loads in the steel section exceed 0.9 times the specified yield stress and in the concrete exceed one third of the concrete strength. Deflections are calculated on the basis of a fully composite section, using a modular ratio of 15 for live loads and 30 for dead loads.

Reference might be made to ACI 318-71 for concrete ultimate strength design requirements in a positive moment region and CSA Standard S16-1969 for steel design requirements in a negative moment region. Provisions of ACI 318-71 for flexural members permit the use of an equivalent rectangular concrete stress distribution in which a concrete stress of 0.85 f'_c is assumed uniformly distributed over an equivalent depth of compression zone. Ultimate moment capacity is modified by introducing a capacity reduction factor equal to 0.9. CSA Standard S16-1969 requires a maximum flange width-thickness ratio for plastically designed steel sections. It also provides for the design of shear connectors based on ultimate strength considerations.

6.3 Moment Capacity

Test results[8][20][24] indicate that ultimate moment capacity in a positive moment region can be satisfactorily evaluated on the basis of an idealized stress distribution in which the steel stress is equal to the yield value and the stresses in the concrete slab are represented by an equivalent rectangular stress block with a value of stress

equal to 0.85 f'_c.

Test results[5][6][10] indicate that ultimate moment capacity in a negative moment region can be satisfactorily evaluated on the bases of an idealized stress distribution in which stresses in the steel section and in the longitudinal slab reinforcement are equal to their respective yield values. However, it is necessary to check for the possibility of premature local flange buckling which may have the effect of reducing the moment capacity.

6.4 Flange Width-Thickness Ratio

For plastic design CSA Standard S16-1969 requires a maximum flange width-thickness ratio equal to $54/\sqrt{\sigma_y}$ for compression flanges of plain steel beams. However, local flange buckling of composite beams is related to the area of longitudinal slab reinforcement as discussed in Section 5.8. Therefore it is suggested that the flange width-thickness ratio be a function of the longitudinal slab reinforcement area. For composite beams with an area of longitudinal slab reinforcement less than the web area of the steel section, a maximum flange width-thickness ratio equal to $54/\sqrt{\sigma_y}$ is suggested. If the area of longitudinal slab reinforcement is greater than the web area but less than twice that area, the flange width-thickness ratio should be reduced to $49/\sqrt{\sigma_y}$.

6.5 Shear Connectors in a Negative Moment Region

CSA Standard S16-1969 requires that shear connectors in a negative moment region resist a horizontal shear force equal to $A_r\sigma_{ry}$ which represents the force in the longitudinal slab reinforcement at

yield conditions. Based on results of pushout tests Van Dalen et al[13][14] proposed a design load per connector in a negative moment region equal to 80 percent of that in a positive moment region. However, results of beam tests conducted by Davison[5] and Lever[6] and results of the present beam tests do not indicate that a reduction in capacity is indicated. It is therefore suggested that the design of shear connectors in a negative moment region be based on the same connector strength as for a positive moment region, provided that the longitudinal slab reinforcement is adequately anchored in a positive moment region.

6.6 Deflection

At working loads, the deflection of composite beams may be based on elastic theory. The bending deformation at midspan may be expressed as

$$\delta_b = k_w \frac{q\ell^4}{384EI}$$

for a uniformly distributed load q and

$$\delta_b = k_c \frac{P\ell^3}{192EI}$$

for a concentrated load P at midspan. The coefficients k_w and k_c are functions of the ratio of stiffness in the negative moment region to that in the positive moment region as discussed in Appendix C. Values of these coefficients are given in Figure C.2(b). For a simply-supported

beam k_w and k_c are equal to 5 and 4, respectively, and for fixed end beams with equal stiffness in positive and negative moment regions k_w and k_c are each equal to 1.0.

Shear deflection of composite beams may be significant as discussed in Section 3.5. Since shear is primarily resisted by the web of the steel section only[67], the shear deflection may be expressed as

$$\delta_{sh} = \frac{q\ell^2}{8A_wG}$$

for a uniformly distributed load and

$$\delta_{sh} = \frac{P\ell}{4A_wG}$$

for a concentrated load at the midspan.

CHAPTER VII

SUMMARY AND CONCLUSIONS

7.1 Summary

Behavior of continuous composite beams has been investigated theoretically and experimentally. Analyses for local flange buckling and lateral buckling in a negative moment region are proposed and compared with experimental results. Deformations including the effects of shear and slip were studied in the elastic and inelastic region. Three two-span continuous composite beams were tested in order to provide additional information on deflections, moment redistribution and ultimate loads. The test beams varied in terms of steel section size and amount of longitudinal slab reinforcement in the negative moment region. Behavioral studies were conducted in order to obtain failure loads and modes of failure for continuous beams in which steel section size, concrete slab thickness and amount of longitudindal slab reinforcement were varied. Based on theoretical and experimental results, requirements are proposed for ultimate strength design of continuous beams.

7.2 Conclusions

The major conclusions resulting from the present investigation are:

1. The proposed analysis for local flange buckling in a negative

moment region gives good agreement with test results. The ratio of local flange buckling moment to simple plastic moment is decreased significantly with increase in the flange width-thickness ratio and is slightly affected by the amount of longitudinal slab reinforcement and the span length. Curvature at the local flange buckling moment is decreased significantly with increase in the amount of longitudinal slab reinforcement.

2. The proposed lateral buckling analysis based on thin-walled beam theory for composite beams in a negative moment region agrees with results of beam tests. The analysis indicates that the ratio of lateral buckling moment to simple plastic moment is decreased significantly with increase in span length and is slightly affected by the amount of longitudinal slab reinforcement and slightly affected by the size of coverplate on the compression flange.

3. The proposed analysis provides satisfactory predictions of ultimate load and failure modes, i.e., crushing of concrete in a positive moment region or local flange buckling in a negative moment region.

4. Failure modes are significantly affected by the amount of longitudinal slab reinforcement in the negative moment region.

5. The proposed analysis for deflections, which includes the effect of shear and slip, predicts satisfactorily the actual deflections obtained from the tests. The shear deformation was significant in the beams tested.

6. The proposed analysis for evaluation of moment-curvature relationships based on Newmark's integration is in good agreement with experimental values.

7. The effect of residual stress on the moment-curvature relationships in a negative moment region differs from that in a positive moment region.

8. The assumption that slip strain is constant throughout the shear span is a satisfactory approximation in the evaluation of the effect of slip on deflection.

9. A maximum compression flange width-thickness ratio equal to $54/\sqrt{\sigma_y}$ is required when the amount of longitudinal slab reinforcement is less than the web area of the steel section in order to prevent local flange buckling before a mechanism forms. This maximum ratio is reduced to $49/\sqrt{\sigma_y}$ for an amount of longitudinal slab reinforcement greater than the web area but less than twice the web area.

10. Moment redistribution in continuous beams is affected significantly by the inelastic stiffness in the positive and negative moment regions.

11. Shear connectors in a negative moment region are capable of developing the full yield value of the longitudinal reinforcement if sufficient development length of the longitudinal slab reinforcement is provided into the positive moment regions.

LIST OF REFERENCES

(1) Canadian Standard Association, "CSA Standard S16-1969--Steel Structures for Buildings", Ontario, 1969.

(2) American Institute of Steel Construction, "Specification for Design, Fabrication & Erection of Structural Steel for Buildings", New York, 1969.

(3) British Standard Institution,"C.P. 117: Part 1: 1965, British Standard Code of Practice, Composite Construction in Structural Steel and Concrete, Part 1: Simply-Supported Beams in Buildings",London, 1965.

(4) Piepgrass, E.B., "Behavior of Composite Beams in Negative Bending", Masters Thesis, Department of Civil Engineering, University of Alberta, June 1968.

(5) Davison, J.H., "Composite Beams in Negative Bending", Masters Thesis, Department of Civil Engineering, University of Alberta, May 1969.

(6) Lever, G.V., "Ultimate Strength of Composite Beams in Negative Bending", Masters Thesis, Department of Civil Engineering, University of Alberta, February 1970.

(7) Culver, C. Zarzeczny, P.J., and Driscoll, G.D. Jr., "Test of Composite Beams for Buildings, "Progress Report No. 2, Fritz Engineering Laboratory Report No. 279.10, January 1962.

(8) Barnard, P.R., "On the Collapse of Composite Beams", Ph.D.Thesis, University of Cambridge, September 1963.

(9) Barnard, P.R., and Johnson, R.P., "Plastic Behavior of Continuous Composite Beams," Proceedings, Institution of Civil Engineers, October 1965.

(10) Johnson, R.P., Van Dalen, K., and Kemp, A.R., "Ultimate Strength of Continuous Composite Beams", Proceedings, Conference on Structural Steelwork, British Constructional Steelwork Association, November 1967.

(11) Daniels, J.H., and Fisher, J.W., "Static Behavior of Continuous Composite Beams, "Fritz Engineering Laboratory Report No. 324.2, March 1967.

(12) Park, R., "The Ultimate Strength of Continuous Composite Beams", Civil Engineering Transactions, Australia, V.CE9, No. 2, October 1967.

(13) Van Dalen, K., "Composite Action at the Supports of Continuous Beams", Ph.D. Thesis, University of Cambridge, June 1967.

(14) Johnson, R.P., Greenwood, R. D., and Van Dalen, K., "Stud Shear Connectors in Hogging Moment Regions of Composite Beams", Structural Engineer, Vol.47, September 1969.

(15) Climenhaga, J.J., "Local Buckling in Composite Beams," Ph.D. Thesis, University of Cambridge, September 1970.

(16) Climenhaga, J.J., and Johnson, R.P., "Moment-Rotation Curves for Locally Buckling Beams", Journal of the Structural Division, ASCE, Vol. 98, No. ST6, June 1972.

(17) Kroll, G.D., "The Degree of Composite Action at Beam-to-Column Joists", Fritz Engineering Laboratory Report No. 338.4, Lehigh University, June 1968.

(18) Daniels, J.H., Kroll, G.D., and Fisher, J.W., "Behavior of Composite-Beam to Column Joists", Journal of the Structural Division, ASCE, Vol. 96, No. ST3, March 1970.

(19) duPlessis, D.P., and Daniels, J.H., "Experiments on Composite Beams under Positive End Moment", Fritz Engineering Laboratory Report No. 374.2, Lehigh University, June 1972.

(20) Ferrier, D., "Moment Curvature Relationship of Composite Steel and Concrete Beams", Master Thesis, Department of Civil Engineering, University of Alberta, November 1965.

(21) Climenhaga, J.J., and Johnson, R.P., "Local Buckling in Continuous Composite Beams", Structural Engineer, Vol. 50, No.9, September 1972.

(22) Whitney, C.S., "Plastic Theory in Reinforced Concrete Design", Transactions ASCE, Vol. 107, 1942.

(23) Slutter, R.G., "Composite Steel-Concrete Members", Structural Steel Design, Edited by L. Tall, Ronald Press Co., New York, 1964

(24) Slutter, R.G., and Driscoll, G.J. Jr., "Flexural Strength of Steel-Concrete Composite Beams", Journal of the Structural Division, ASCE, Vol. 91, No. ST2, April 1965.

(25) Canadian Institute of Steel Construction, "General Information on Structural Steel", Ontario, March 1970.

(26) Lay, M.G., and Smith, P.D., "Role of Strain Hardening in Plastic Design", Journal of the Structural Division, ASCE, Vol. 91, No. ST3, June 1965.

(27) Hognestad, E., "A Study of Combined Bending and Axial Load in Reinforced Concrete Members", University of Illinois Engineering Experiment Station Bulletin No. 399, June 1951.

(28) Smith, G.M., and Young, L.E., "Ultimate Flexural Analysis Based on Stress-Strain Curves of Cylinders", Journal of ACI, Vol. 53, December 1956.

(29) Desayi, P. and Krishnan, S., "Equation for the Stress-Strain Curve of Concrete", Journal of ACI, Vol. 61, March 1964.

(30) Chambaud, R., "Étude expérimentale de la flexion dans les piéces en béton armé", Annales de l'Institut Technique du Bâtiment et des Travaux Publics No. 61, Béton, Béton Armé No. 4, Paris, February 1949.

(31) Billet, D.F., and Appeleton, J.H., "Flexural Strength of Prestressed Concrete Beams", Journal of ACI, Vol. 51, June 1954.

(32) Roš, M., "Festigkeit und Verformung von auf Biegung beanspruchten Eisenbetonbalken", Eidg. Material-Prüfungsanstalt, Bericht No. 141, Zürich, October 1942.

(33) Brandtzaeg, A., "Die Bruchspannungen und die zulässigen Randspannungen in rechteckigen Eisenbetonbalken", Beton and Eisen, Vol. 35, No. 13, July 1936.

(34) Jensen, V.P., "Ultimate Strength of Reinforced Concrete Beams as Related to the Plasticity Ratio of Concrete", University of Illinois Engineering Experiment Station Bulletin No. 345, June 1943.

(35) Hognestad, E., Hansen, N.W., and McHenry, D., "Concrete Stress Distribution in Ultimate Strength Design", Journal of ACI, Vol. 52, December 1955.

(36) American Concrete Institute, "Building Code Requirements for Reinforced Concrete (ACI 318-71)", Michigan, 1971.

(37) American Concrete Institute, "Commentary on Building Code Requirements for Reinforced Concrete (ACI 318-71)", Michigan, 1971

(38) Holland, E.P., "Design for Flexure", Proceedings of the PCA-ACI Teleconference on ACI 318-71 Building Code Requirements, Portland Coment Association, 1972.

(39) Liebenberg, A.C., "A Stress-Strain Function for Concrete Subjected to Short-Term Loading", Magazine of Concrete Research, London, Vol. 14, No. 41, July 1962.

(40) Mainstone, R.J., and Menzies, J.B., "Shear Connectors in Steel-Concrete Composite Beams for Bridges", Concrete, September 1967.

(41) Yam, L.C.P., Chapman, J.C., "The Inelastic Behavior of Simply-Supported Composite Beams of Steel and Concrete", Proceedings of the Institution of Civil Engineers, Vol. 42, December 1968.

(42) Haaijer, G., "Plate Buckling in the Strain Hardening Range", Journal of the Engineering Mechanics Division, ASCE, Vol. 83, EM2, April 1957.

(43) Haaijer, G., and Thürlimann, B., "Inelastic Buckling in Steel", Transactions, ASCE, Vol. 125, 1960.

(44) Lay, M.G., "Flange Local Buckling in Wide-Flange Shapes", Journal of the Structural Division, ASCE, Vol. 91, No. ST6, December 1965.

(45) Donnel, L., "Plastic Flow as an Unstable Process", Journal of Applied Mechanics, Vol. 9, June 1942.

(46) Nádai, A., "Theory of Flow and Fracture in Solids", Vol. 1, McGraw-Hill Book Co. Inc., New York, N.Y., 1950.

(47) Lay, M.G., "Yielding of Uniformly Loaded Steel Members", Journal of the Structural Division, ASCE, Vol. 91, No. ST6, December 1965.

(48) Bijlaard, P., "Theory of Plastic Buckling of Plates", Journal of Applied Mechanics, Vol. 23, 1956.

(49) Vlasov, V.Z., "Thin-Walled Elastic Beams", 2nd Edition, Israel Program for Scientific Translations, Jerusalem, 1961.

(50) Oden, J.T., "Mechanics of Elastic Structures",McGraw-Hill Book Co., 1967.

(51) Timosenko, S., and Goodier, J.N., "Theory of Elasticity", McGraw-Hill Book Co., 1951.

(52) Bleich, F., "Buckling Strength of Metal Structures",McGraw-Hill Book Co., New York, 1952.

(53) Bulson, P.S., "Local Stability and Strength of Structural Sections", Thin-Walled Structures edited by Chilver, A.H., John Wiley and Sons, 1967.

(54) Rajasekaran, S., and Murray, D.W., "Finite Element Analysis of Thin-Walled Members of Open Section", Structural Engineering Report No. 34, University of Alberta, September 1971.

(55) Kaufmann, W., "Bemerkungen zur Stabilitat dunnwandiger Kreiszylindrischer Schalen oberhalb der Proportionalitats Grenze", Ingineur-Archiv, Vol. 6, 1947.

(56) Handelman, G.H., and Prager, W., "Plastic Buckling of Rectangular Plate with Edge Thrust", Technical Note 1530, 1948.

(57) Crandall, S.H., "Engineering Analysis, a Survey of Numerical Procedure", McGraw-Hill Book Company, Inc., New York 1956.

(58) Siess, C., Viest, I., and Newmark, N.M., "Study of Slab and Beam Highway Bridges", Part III, University of Illinois Engineering Experiment Station Bulletin, No. 396, 1950.

(59) Newmark, N.M., "Numerical Procedure for Computing Deflections, Moments and Buckling Loads", Transaction, ASCE, Vol. 108, 1943.

(60) Beedle, L.S., and Tall, L., "Basic Column Strength", Journal of the Structural Division, ASCE, Vol. 86, No. ST 7, July 1960.

(61) Tall, L., "Compression Members", Structural Steel Design, edited by Tall, Ronald Press Co., New York, 1964.

(62) Galambos, T.V., "Structural Members and Frames", Prentice-Hall Inc., 1968.

(63) Ketter, R.L., and Galambos, T.V., "Column Under Combined Bending and Thrust", Transactions, ASCE, Vol. 126(I), 1961.

(64) Lee, G.C., Fine, D.S., and Hastreiter, W.R., "Inelastic Torsional Buckling of H-Columns", Journal of the Structural Division, Vol. 93, 1967.

(65) Davies, C., "Tests on Half-Scale Steel-Concrete Composite Beams with Welded Stud Connectors", Structural Engineer, Vol. 47, No. 1, January 1969.

(66) Roderich, J.W., Hawkins, N.M., and Lim, L.C., "The Behavior of Composite Steel and Lightweight Concrete Beams", Civil Engineering Transactions, Australia Institute of Engineers, October 1967.

(67) Ostapenko, O., "Design of Braced Frames--Beams", Plastic Design of Multi-Story Frames, Fritz Engineering Laboratory Report No. 273.20, Lehigh University, 1965.

APPENDIX A

STABILITY EQUATIONS FOR THIN-WALLED BEAMS

A.1 Kinematics of Deformation

If displacements ξ and η in x and y directions, respectively, and angle of twist θ are applied to a thin-walled beam section at $A(a_x,a_y)$ as shown in Figure A.1, the displacements ξ_B and η_B of an arbitrary point $B(b_x,b_y)$ are

$$\xi_B = \xi - (b_y - a_y)\theta \qquad A.1(a)$$

$$\eta_B = \eta + (b_x - a_x)\theta \qquad A.1(b)$$

where the sign convention for θ is based on the right hand rule. The displacements v_s, w_s in the tangential and normal directions to the cross section at S are

$$v_s = \xi_s\cos\alpha + \eta_s\sin\alpha \qquad A.2(a)$$

$$w_s = -\xi_s\sin\alpha + \eta_s\cos\alpha \qquad A.2(b)$$

where ξ_s and η_s are displacement at S in the x and y directions, and α is the angle between the tangent at S and the Ox axis as shown in Figure A.1.

Substituting Equations A.1 with respect to S into Equations A.2, the displacements at S in the tangential and normal directions become

$$v_s = \xi\cos\alpha + \eta\sin\alpha + \theta r_t \qquad \text{A.3(a)}$$

$$w_s = -\xi \sin\alpha + \eta \cos\alpha + \theta r_n \qquad \text{A.3(b)}$$

where $r_t = (x - a_x) \sin\alpha - (y - a_y) \cos\alpha$

$$r_n = (x - a_x) \cos\alpha + (y - a_y) \sin\alpha$$

and are shown in Figure A.1.

Noting that the shear strain γ_{sz} is assumed to be zero for a thin-walled beam section in Figure A.2[49][50],

$$\gamma_{sz} = \frac{\partial u}{\partial s} + \frac{\partial v}{\partial z} = 0 \qquad \text{A.4}$$

the displacement u is obtained by integrating Equation A.4

$$u = \zeta - \int \frac{\partial v}{\partial z}\, ds \qquad \text{A.5}$$

where ζ is the initial displacement in z direction.

By differentiating v with respect to z in Equation A.3(a) and multiplying by ds, Equation A.5 may be expressed by

$$u = \zeta - \xi' x - \eta' y - \theta' \omega \qquad \text{A.6}$$

since $ds \cos\alpha = dx$

$$ds \sin\alpha = dy \qquad \text{A.7}$$

$$r_t \, ds = d\omega$$

The quantity ω is independent of x and y coordinates, and is called the warping function. The strain ε_z in the z direction is obtained by differentiating Equation A.6 with respect to z.

$$\varepsilon_z = \zeta' - \xi''x - \eta''y - \theta''\omega \qquad \text{A.8}$$

A.2 Normal Stress-Strain Relationship

From Hooke's law and ε_s equal to zero, the stress-strain relationships with respect to z and s directions may be given by

$$\varepsilon_z = \frac{1}{E}\left(\sigma_z - \nu\sigma_s \right)$$

$$\varepsilon_s = 0 = \frac{1}{E}\left(\sigma_s - \nu\sigma_z \right)$$

From these two equations, the relationship between the normal stress σ_z and normal strain ε_z may be obtained by

$$\sigma_z = \overline{E}\, \varepsilon_z$$

where $\overline{E} = \dfrac{E}{1 - \nu^2}$

$\bar{E}$ is defined as the modified elastic modulus. Since ν^2 is small, it may be neglected and the elastic modulus E used instead of $\bar{E}$. Then the normal stress becomes

$$\sigma_z = E\,(\zeta' - \xi''x - \eta''y - \theta''\omega) \qquad A.9$$

A.3 Equilibrium Equations for a Thin-Walled Beam

For a small element shown in Figure A.3 equilibrium in the longitudinal direction requires that

$$\frac{\partial \sigma_z}{\partial z} + \frac{\partial \tau_{sz}}{\partial s} = 0 \qquad A.10$$

Equilibrium of a strip of thin-walled beam between z and (z + dz) as shown in Figure A.4 may be expressed by the following equations

$$\Sigma Z = 0,\ \int_s \frac{\partial \sigma_z}{\partial z}\, tdzds + (T_L - T_R + q_z)\, dz = 0 \qquad A.11(a)$$

$$\Sigma X = 0,\ \int_s \frac{\partial \tau_{sz}}{\partial z}\, tdz\, \cos\alpha\, ds + q_x dz = 0 \qquad A.11(b)$$

$$\Sigma Y = 0,\ \int_s \frac{\partial \tau_{sz}}{\partial z}\, tdz\, \sin\alpha\, ds + q_y dz = 0 \qquad A.11(c)$$

$$\Sigma M_A = 0,\ \int_s \frac{\partial \tau_{sz}}{\partial z}\, tdz \left[(x - a_x)\sin\alpha - (y - a_y)\cos\alpha\right] ds$$

$$+ M'_{tt}\, dz + m_t dz = 0 \qquad A.11(d)$$

where M_{tt} is Saint Venant's torsional moment defined as

$$M_{tt} = GJ\theta' \qquad \text{A.12}$$

in which J is St. Venant's torsional constant.

Substituting Equations A.7 into Equations A.11 results in

$$\int_s \frac{\partial \sigma_z}{\partial \zeta} dA + T_R - T_L + q_z = 0 \qquad \text{A.13(a)}$$

$$\int_s \frac{\partial \tau_{sz}}{\partial z} tdx + q_x = 0 \qquad \text{A.13(b)}$$

$$\int_s \frac{\partial \tau_{sz}}{\partial z} tdy + q_y = 0 \qquad \text{A.13(c)}$$

$$\int_s \frac{\partial \tau_{sz}}{\partial z} td\omega + M'_{tt} + m_t = 0 \qquad \text{A.13(d)}$$

The first term in Equation A.13(d) contains the stress resultant due to the warping torsional moment. Differentiating equations in Equation A.13(b), (c) and (d) part by part and noting that shear flow τ_{sz} t at the boundary equals the external force, that is,

$$(\tau_{sz})_{s=s_L} t = T_L$$

$$(\tau_{sz})_{s=s_R} t = T_R$$

yields Equations A.14 as follows:

$$\int_s \frac{\partial \sigma_z}{\partial z} d A - T_R + T_L + q_z = 0 \qquad \text{A.14(a)}$$

$$- \int_s x \frac{\partial}{\partial z} \left[\frac{\partial \tau_{sz}}{\partial s} \right] ds + T_L' x_L - T_R' x_R + q_x = 0 \qquad \text{A.14(b)}$$

$$- \int_s y \frac{\partial}{\partial z} \left[\frac{\partial \tau_{sz}}{\partial s} \right] ds + T_L' y_L - T_R' y_R + q_y = 0 \qquad \text{A.14(c)}$$

$$- \int_s \omega \frac{\partial}{\partial z} \left[\frac{\partial \tau_{sz}}{\partial s} \right] ds + M_{tt}' + T_L' \omega_L - T_R' \omega_R + m_t = 0 \qquad \text{A.14(d)}$$

The functions $\partial \sigma_z / \partial z$ and $\partial \tau_{sz} / \partial s$ in Equations A.14 are obtained from Equations A.9 and A.10 as

$$\frac{\partial \sigma_z}{\partial z} = E \, (\zeta' - \xi'' x - \eta'' y - \theta'' \omega)' \qquad \text{A.15(a)}$$

$$\frac{\partial \tau_{sz}}{\partial s} = - \frac{\partial \sigma_z}{\partial z} = - E \, (\zeta' - \xi'' x - \eta'' y - \theta'' \omega)' \qquad \text{A.15(b)}$$

Substituting Equations A.15 in Equations A.14, the following equilibrium equations result:

$$E \, (A\zeta' - S_y \xi'' - S_x \eta'' - S_\omega \theta'')' = - q_z - T_L + T_R \qquad \text{A.16(a)}$$

$$E \, (-S_y \zeta' + I_y \xi'' + I_{xy} \eta'' + I_{x\omega} \theta'')'' = q_x + T_L' x_L - T_R' x_R \qquad \text{A.16(b)}$$

$$E\,(-S_x\zeta' + I_{xy}\xi'' + I_x\eta'' + I_{y\omega}\theta'')'' = q_y + T_L'y_L - T_Ry_R \qquad A.16(c)$$

$$E\,(-S_\omega\zeta' + I_{y\omega}\xi'' + I_{x\omega}\eta'' + I_\omega\theta'')'' - G(J\theta')' =$$

$$m_t + T_L'\omega_L - T_R'\omega_R \qquad A.16(d)$$

where

$$A = \int_A dA$$

$$S_x = \int_A ydA,\ S_y = \int_A xdA,\ S_\omega = \int_A \omega dA$$

$$I_{xy} = \int_A xydA,\ I_{x\omega} = \int_A x\omega dA,\ S_{\omega y} = \int_A \omega ydA \qquad A.17$$

$$I_x = \int_A y^2dA,\ I_y = \int_A x^2dA,\ I_\omega = \int_A \omega^2dA$$

Equations A.16 may be simplified by choosing a particular coordinate system, i.e., the principal coordinates. Some of the values in Equation A.17 become zero for principal coordinates and Equations A.17 may be expressed by

$$E\,(A\zeta')' = -q_z - T_L + T_R \qquad A.18(a)$$

$$E\,(I_x\xi'')'' = q_x + T_L'x_L - T_R'x_R \qquad A.18(b)$$

$$E\,(I_y\eta'')'' = q_y + T_L'y_L - T_R'y_R \qquad A.18(c)$$

$$E\,(I_\omega\theta'')'' - G\,(J\theta')' = M_t + T_L'\omega_L - T_R'\omega_R \qquad A.18(d)$$

By introducing Equation A.9 the stress resultants in the form of a normal force $N_z = \int_A \sigma_z dA$, bending moments $M_x = \int \sigma_z y dA$ and $M_y = \int \sigma_z x dA$, and a bimoment $B_\omega = \int \sigma_z \omega dA$ are defined as

$$N_z = EA\zeta \qquad A.19(a)$$

$$M_x = -EI_x\xi'' \qquad A.19(b)$$

$$M_y = -EI_y\eta'' \qquad A.19(c)$$

$$B_\omega = -EI_\omega\theta'' \qquad A.19(d)$$

The normal stress σ_z may be expressed in terms of stress resultants by substituting Equations A.18 into A.9 to give

$$\sigma_z = \frac{N_z}{A} + \frac{M_z}{I_y}x + \frac{M_x}{I_x}y + \frac{B_\omega}{I_\omega}\omega \qquad A.20$$

A.4 Stability Equations for a Thin-Walled Beam

In order to investigate torsional buckling of a thin-walled beam subjected to an axial force N_z and bending moments M_x and M_y, equilibrium after a small displacement must be stablished. The normal stress σ_z due to an axial force N_z and bending moments M_x and M_y is given by Equation A.20 as

$$\sigma_z = \frac{N_z}{A} + \frac{M_y}{I_y} x + \frac{M_x}{I_x} y \qquad \text{A.21}$$

Referring to Figure A.5, the components of the internal stress σ_z in x and y directions are

$$-\sigma_z \Delta A \frac{\partial \xi_s}{\partial z} + \left(\sigma_z + \frac{\partial \sigma_z}{\partial z} dz\right) \Delta A \left(\frac{\partial \xi_s}{\partial z} + \frac{\partial^2 \xi_s}{\partial z^2} dz\right)$$

and

$$-\sigma_z \Delta A \frac{\partial \eta_s}{\partial z} + \left(\sigma_z + \frac{\partial \sigma_z}{\partial z} d_z\right) \Delta A \left(\frac{\partial \eta_s}{\partial z} + \frac{\partial^2 \eta_s}{\partial z^2} dz\right)$$

respectively. Neglecting smaller quantities, the components can be expressed by $(\sigma_z \xi_s')' dz \Delta A$ and $(\sigma_z \eta_s')' dz \Delta A$, respectively. The total transverse forces per unit length q_x and q_y due to the components can be obtained as

$$q_x = \int_A (\sigma_z \xi_s')' \, dA \qquad A.22(a)$$

$$q_y = \int_A (\sigma_z \eta_s')' \, dA \qquad A.22(b)$$

The torque m_t produced by the internal force q_x and q_y is given by

$$m_t = \int_A \left\{ (\sigma_z \eta_s')' \, (x - a_x) - (\sigma_z \xi_s')' \, (y - a_y) \right\} dA \qquad A.23$$

Substituting Equations A.1 into Equations A.22 and A.23, and integrating across the cross section, results in

$$q_x = \left\{ N_z (\xi' + a_y \theta) \right\}' - (M_x \theta')' \qquad A.24(a)$$

$$q_y = \left\{ N_z (\eta' - a_x \theta') \right\}' + (M_y \theta')' \qquad A.24(b)$$

$$m_t = \left\{ N_z (-a_x \eta' + a_y \xi') \right\}' - (M_x \xi')' + (M_y \eta')' + (M_\rho \theta')' \qquad A.24(c)$$

where M_ρ is a new stress resultant defined by

$$M_\rho = \int_A \sigma_z \left\{ (x - a_x)^2 + (y - a_y)^2 \right\} \qquad A.25$$

Stability equations for thin-walled beams result from substituting

Equations A.24 into Equations A.18 as

$$E\,(I_x\xi'')'' = \left\{N_z(\xi' + a_y\theta)\right\}' - (M_x\theta')' + T_L'x_L - T_R'x_R \qquad A.26(a)$$

$$E\,(I_y\eta'')'' = \left\{N_z(\eta' - a_x\theta')\right\} + (M_y\theta')' + T_L'y_L - T_R'y_R \qquad A.26(b)$$

$$E\,(I_\omega\theta'')'' - G(J\theta')' = \left\{N_z(-a_x\eta' + a_y\xi')\right\}' - (M_x\xi')' +$$

$$(M_y\eta')' + (M_\rho\theta')' + T_L'\omega_L - T_R'\omega_R \qquad A.26(c)$$

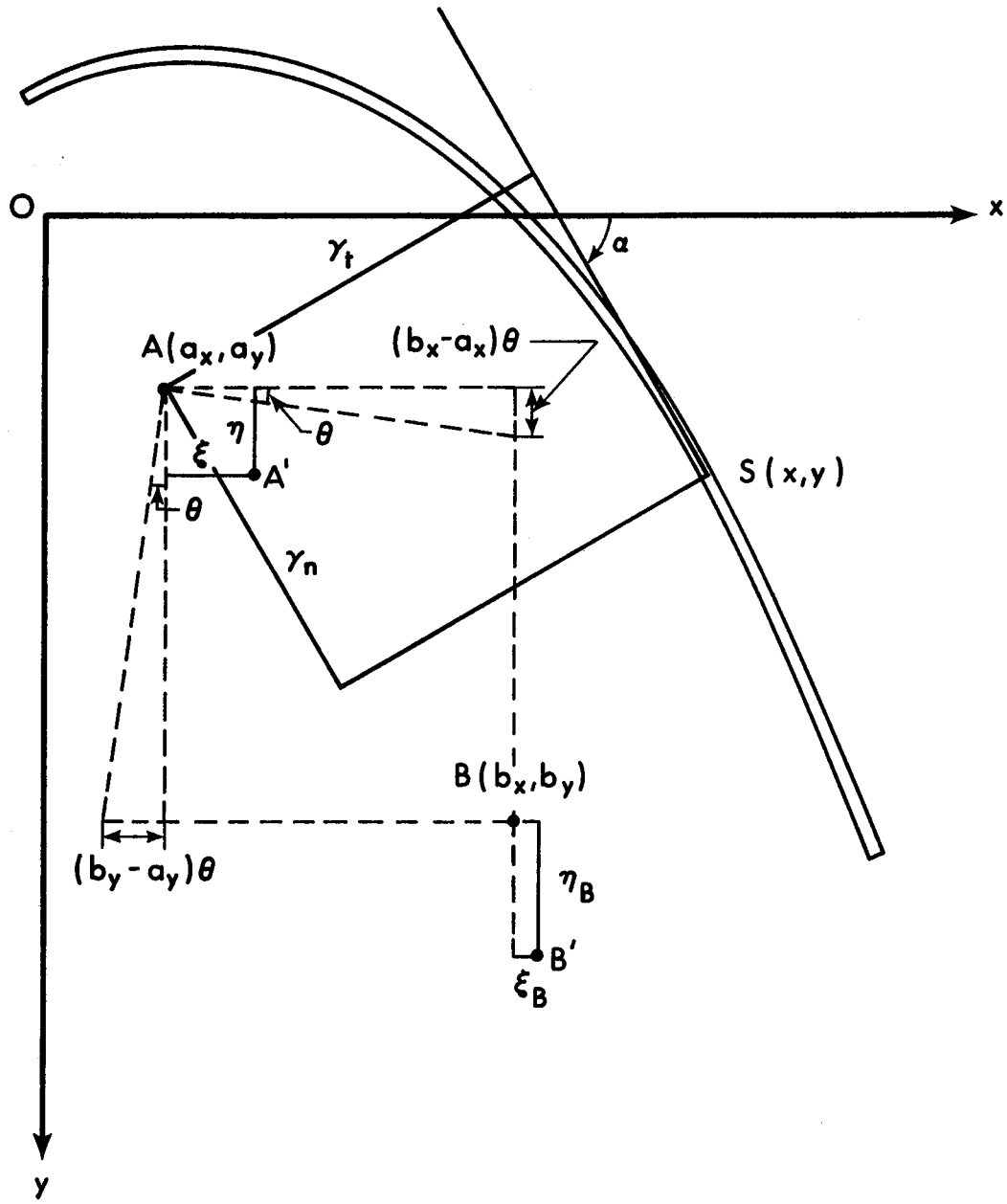

FIGURE A.1 DISPLACEMENTS FOR A THIN-WALLED BEAM

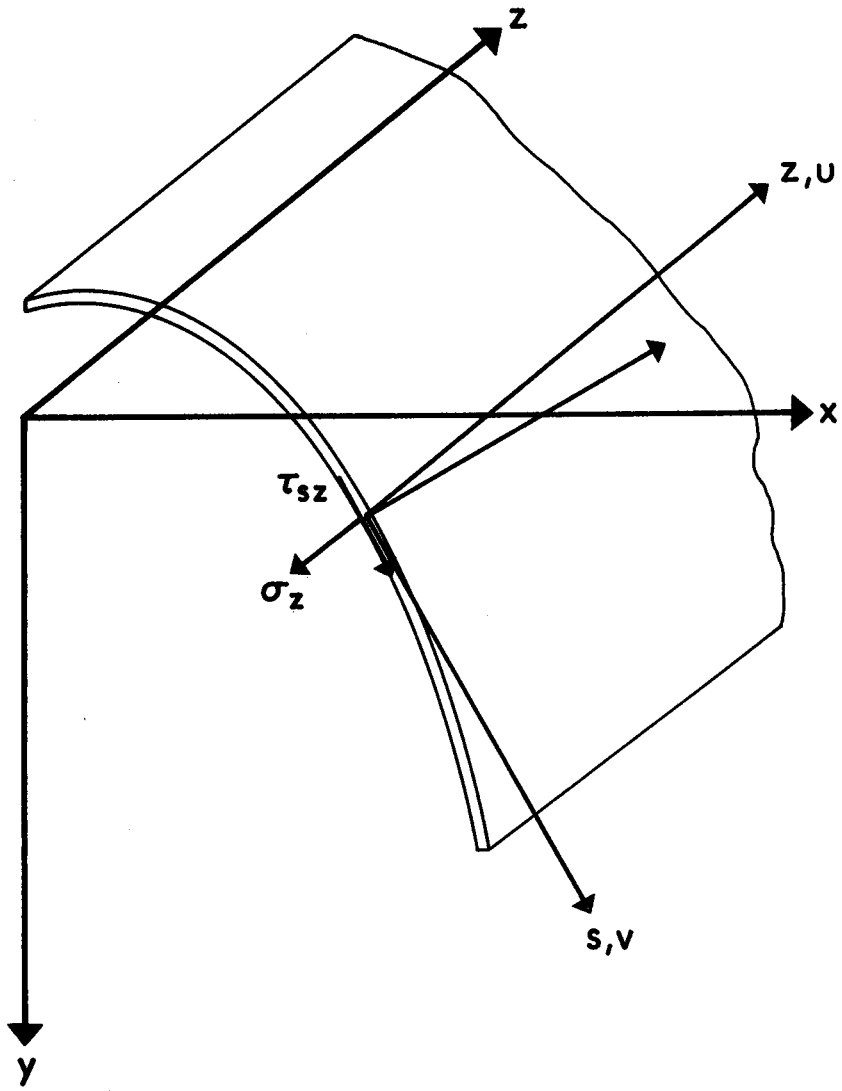

FIGURE A.2 CO-ORDINATE SYSTEM

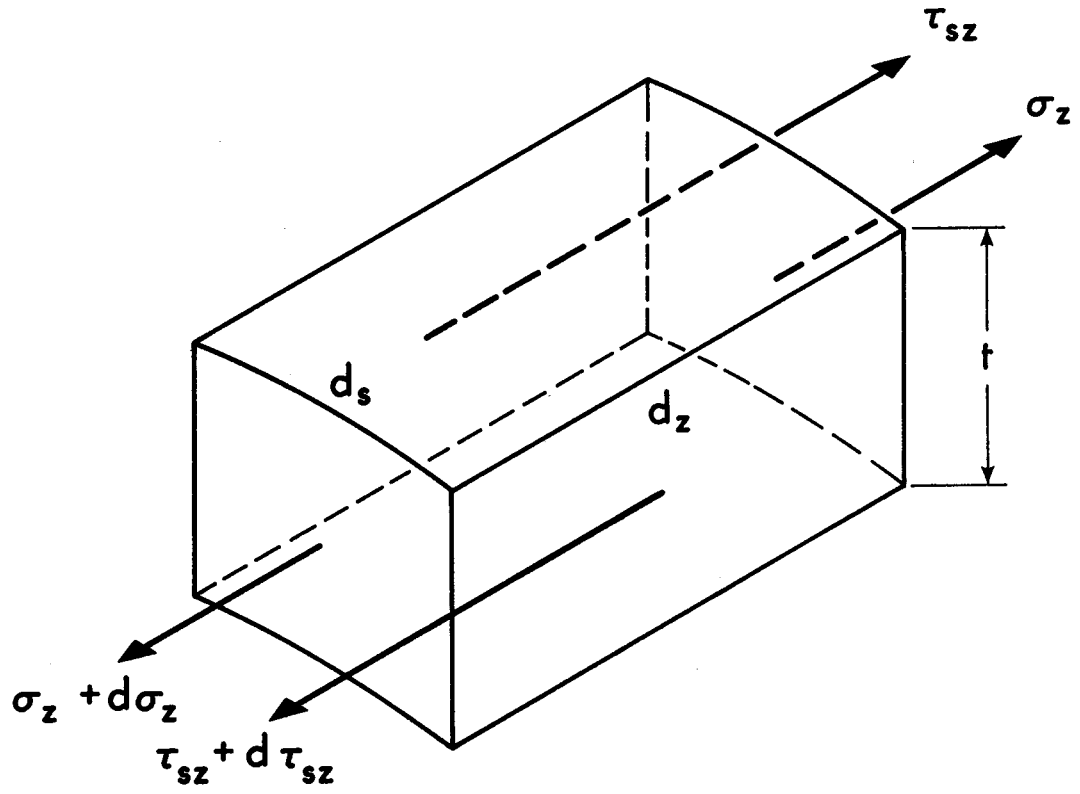

FIGURE A.3 STRESSES IN LONGITUDINAL DIRECTION

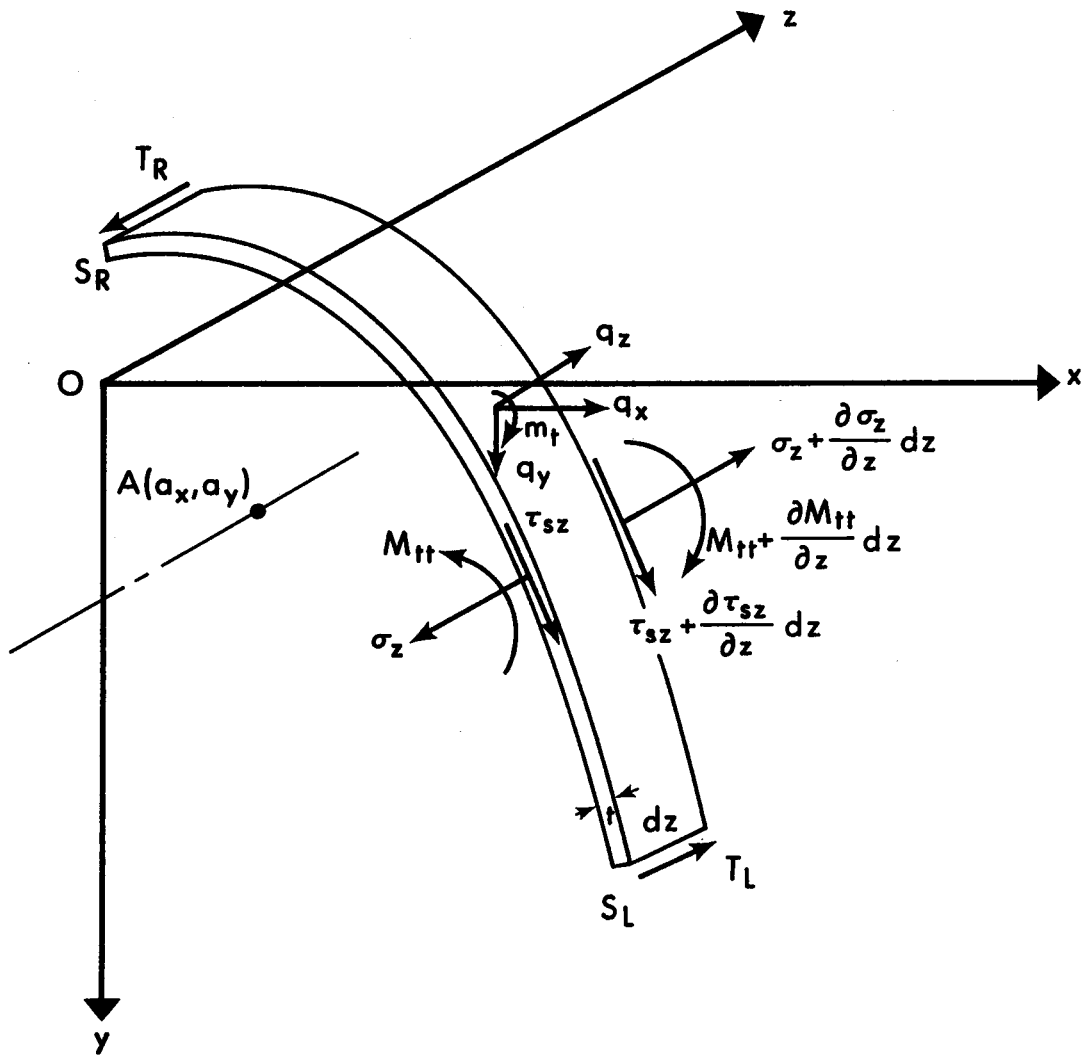

FIGURE A.4 STRESSES ON AN ELEMENT OF A THIN-WALLED BEAM

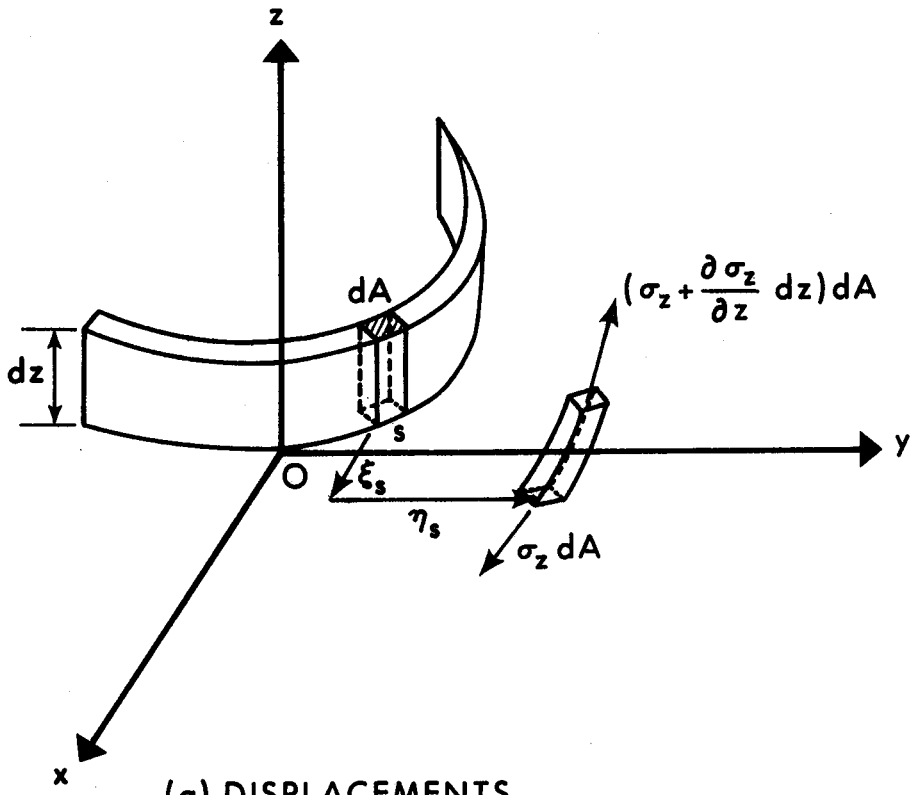

(a) DISPLACEMENTS

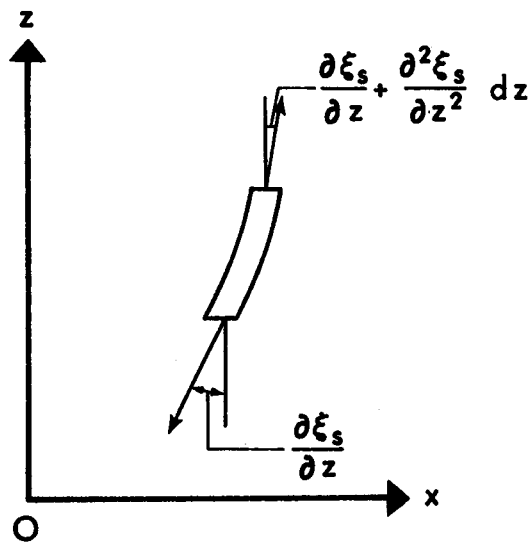

(b) PROJECTION ON xz PLANE

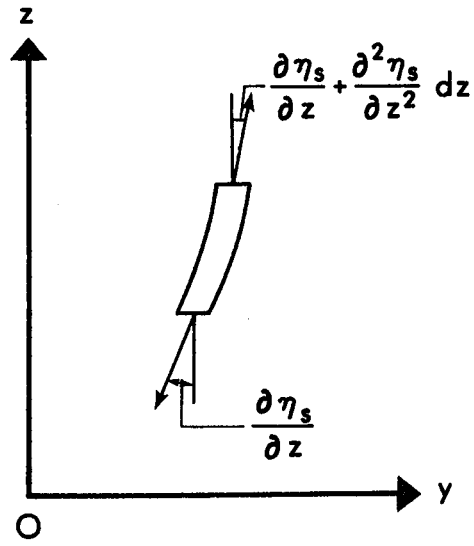

(c) PROJECTION ON yz PLANE

FIGURE A.5 DISPLACEMENT OF A STRIP

APPENDIX B

APPROXIMATE METHOD FOR DETERMINING THE EFFECT OF SLIP

The effect of slip on the stiffness of a composite beam may be calculated on the assumption that slip strain is constant along the shear span and is defined as the slip divided by the shear span. The stress-strain relationships for concrete and steel are assumed linearly elastic, the tensile strength of concrete is assumed to be zero and the force-slip relationship is assumed to be linear.

There are two specific cases to be considered in the evaluation of the stiffness as in the evaluation without slippage; namely, the neutral axis is in the concrete slab (Case I) and the neutral axis is in the steel section (Case II).

Case I: Neutral Axis in Concrete Slab

Based on conditions shown in Figure B.1(a), the equilibrium equation for the beam is

$$\int_A \sigma dA = \int_{A_c} \sigma dA + \int_{A_s} \sigma da$$

$$= -\phi E_c \frac{b_c}{2} y_d^2 + \phi EA_s \left(\frac{d}{2} + t_c - y_d - \varepsilon_d/\phi\right) = 0 \qquad B.1$$

where ε_d is slip strain and can be expressed as

$$\varepsilon_d = \Delta_s / L_s \qquad \text{B.2}$$

and L_s is the shear span. The relationship between concrete force C and slip Δ_s is expressed by

$$C = k_s \Delta_s \qquad \text{B.3}$$

The shear force on the shear connectors in the shear span is $\phi E_c b y_d^2/2$. Slip strain is then obtained from Equations B.2 and B.3 as

$$\varepsilon_d = \frac{\phi E_c b_c y_d^2}{2 k_s L_s} \qquad \text{B.4}$$

By introducing Equation B.4 into Equation B.1, the following equation related to y_d is obtained.

$$y_d^2 + 2py_d - p(d + 2t_c - k_s' y_d^2) = 0 \qquad \text{B.5}$$

where $$p = \frac{EA_s}{E_c b} = \frac{nA_s}{b}$$

and $$k_s' = \frac{E_c b_c}{2 b_s L} = \frac{E b_c}{2 n k_s L_s}$$

The solution of Equation B.5 gives the location of the neutral axis as

$$y_d = \frac{p}{1 + k_s' p} \left(\sqrt{1 + (d + 2t_c)(1 + k_s' p)/p} - 1\right) \qquad B.6$$

For a beam with complete interaction

$$y_d = p \left(\sqrt{1 + (d + 2t_c)/p} - 1\right)$$

The bending moment is defined by

$$M_x = \int_{A_c} \sigma y dA + \int_{A_s} \sigma y dA$$

$$= EI_{eq}\phi \qquad B.7$$

where I_{eq} is an equivalent moment of inertia for the section and is defined as

$$I_{eq} = I_s + A_s e_s^2 + I_c' \qquad B.8$$

in which I_s and I_c' are the moment of inertia of the steel section and concrete slab, respectively. I_c' is evaluated by $by_d^3/3$ and e_s is expressed by $d/2 + t_c - y_d - E_c b_c y_d^2/2k_s L_s$.

Case II: Neutral Axis in Steel Section

Based on Figure B.1(b) the equilibrium equation is

$$\int_A \sigma dA = \int_{A_c} \sigma dA + \int_{A_s} \sigma dA$$

$$= \frac{\phi E_c}{2} A_c(t_c + 2y_d) + \phi E A_s(d/2 - y_d - \varepsilon_d/\phi) = 0 \qquad B.9$$

Introducing the slip strain $\varepsilon_d = \varepsilon E_c(t_c + 2y_d)\, A_c/2L_s k_s$, the neutral axis location defined by y_d can be obtained as

$$y_d = \frac{t_c A_c/n - (d - k_s' t_c)A_s}{2\left\{\frac{A_c}{m} + (1 + k_s)A_s\right\}} \qquad B.10$$

For a beam with complete interaction

$$y_d = \frac{t_c A_c/M - dA_s}{2(A_c/M + A_s)} \qquad B.11$$

The bending moment M_x is expressed as

$$M_x = \int \sigma y dA$$

$$= EI_{eq}\phi \qquad B.12$$

where I_{eq} is an equivalent moment of inertia expressed by

$$I_{eq} = I_s + A_s e_s^2 + I_c + A_c e_c^2 \qquad B.13$$

where

$$e_s = d/2 - y_d - \frac{E_c(t_c + 2y_d)A_c}{2L_s k_s}$$

$$e_c = t_c/2 - y_d$$

In the evaluation of the beam stiffness by the above procedure, the value of the constant k_s is required. This value may be obtained from a force-slip relationship obtained from push-out tests.

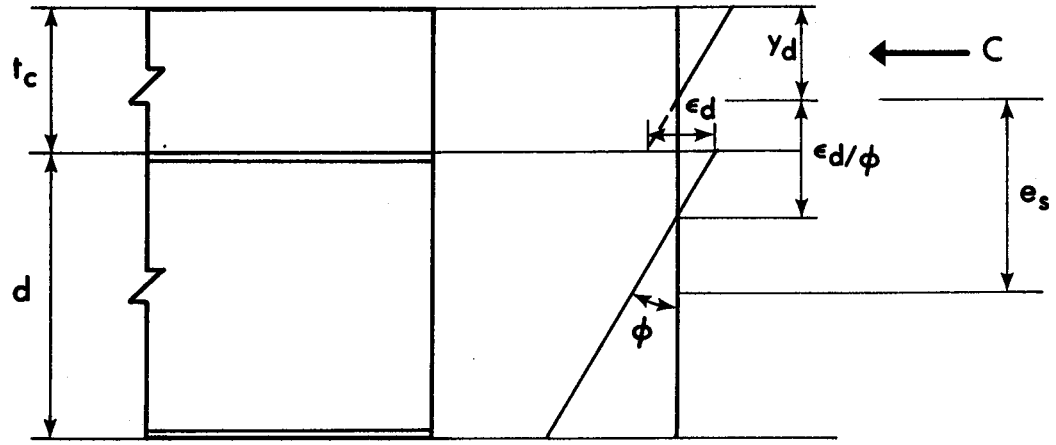

(a) NEUTRAL AXIS IN SLAB

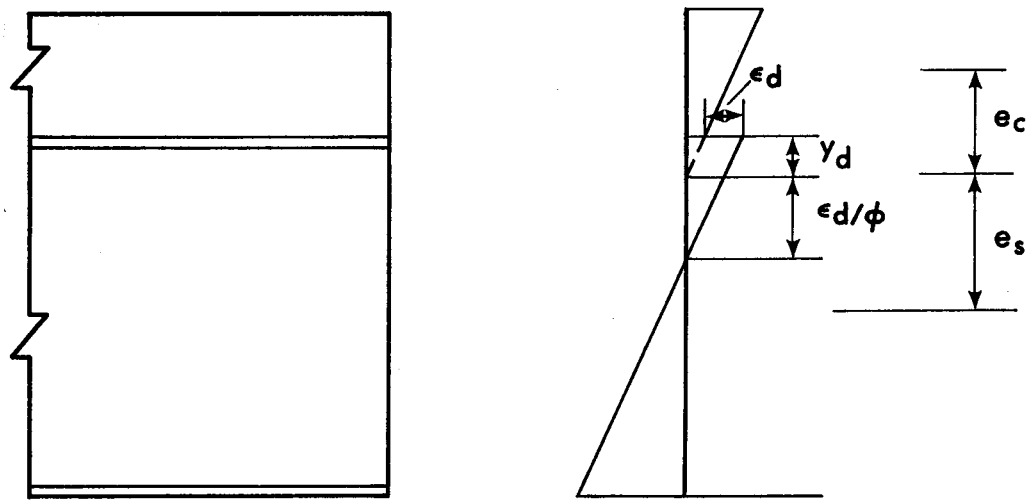

(b) NEUTRAL AXIS IN STEEL SECTION

FIGURE B.1 EFFECT OF SLIP ON STRESS DISTRIBUTION

APPENDIX C

APPLICATION OF SLOPE-DEFLECTION METHOD TO COMPOSITE BEAMS

C.1 Deflection at Ultimate Moment for Simple Plastic Theory

For a segment between sections at which plastic hinges are located elastic continuity exists up to the load at which the last hinge forms. Therefore slope-deflection equations may be used to determine deflections. The slope-deflection equation is given for a beam with constant rigidity by

$$\theta_{AB} = \theta'_{AB} + \frac{\Delta}{\ell} + \frac{\ell}{3EL}\left(M_{AB} - \frac{M_{BA}}{2}\right) \qquad C.1$$

where the sign convention is defined in Figure C.1(a).

Since stiffness is not constant for a composite beam subjected to positive and negative moments, equation C.1 can not be directly employed. However, the case may be handled by means of equations similar to Equation C.1.

$$\theta_{AB} = \theta'_{AB} + \frac{\Delta}{\ell} + \frac{\ell}{EI_p}(k_{11}M_{AB} + k_{12}M_{BA}) \qquad C.2(a)$$

$$\theta_{BA} = \theta'_{BA} + \frac{\Delta}{\ell} + \frac{\ell}{EI_p}(k_{21}M_{AB} + k_{22}M_{BA}) \qquad C.2(b)$$

where EI_p is the rigidity of a positive moment region. The quantities

θ'_{AB} and θ'_{BA} are rotations at ends A and B, as shown in Figure C.1(b), due to similar loading of a simply supported beam. The constants k_{11}, k_{12}, k_{21} and k_{22}, which are related to the flexibility co-efficients, are defined by

$$k_{11} = \frac{1}{3}\left\{1 - \rho'(1 - \beta^3)\right\}$$

$$k_{12} = k_{21} = -\frac{1}{6}\left\{1 - \rho'(3\alpha^2 - 2\alpha^3)\right\}$$

$$k_{22} = \frac{1}{3}(1 - \rho'\alpha^3)$$

and $$\rho' = 1 - \frac{1}{\rho}$$

where α and β are illustrated in Figure C.1(c) and ρ is the ratio of stiffness in a negative moment region to that in a positive moment region. The co-efficients k_{11}, k_{12} and k_{22} are tabulated in Table C.1 to C.3.

For constant stiffness the rotations θ'_{AB} and θ'_{BA} for a uniformly distributed load are given as

$$\theta'_{AB} = -\theta'_{BA} = \frac{q\ell^3}{24EI} \qquad \text{C.3}$$

For composite beams with different stiffness in positive and negative moment regions, these rotations become

$$\theta'_{AB} = s_1 \frac{q\ell^3}{24EI_p} \qquad \text{C.4(a)}$$

$$\theta'_{BA} = -s_2 \frac{q\ell^3}{24EI_p} \qquad C.4(b)$$

where $s_1 = 1 - \rho'\alpha^2(6 - 8\alpha + 3\alpha^2)$

$$s_2 = 1 - \rho'\alpha^3(4 - 3\alpha)$$

Co-efficients S_1 and S_2 are tabulated for values of α and ρ in Tables C.4 and C.5. The deflection at ultimate moment can be evaluated from Equations C.2, since the moments are equal to the plastic moment values.

C.2 Slope-Deflection Equations for Composite Beams

The equations in Section C.1 are applicable between plastic hinges, therefore they are based on one positive and one negative moment region as shown in Figure C.1. However an interior span consists of one positive and two negative moment regions as shown in Figure C.2. For such cases the flexibility co-efficients k_{11} ~ k_{22} are given by

$$k_{11} = \frac{1}{3}\left\{1 - \rho'_1(1 - \beta_1^3) - \rho'_2\alpha_2^3\right\}$$

$$k_{12} = k_{21} = -\frac{1}{6}\left\{1 - \rho'_1\,(3\alpha_1^2 - 2\alpha_1^3) - \rho'_2\,(3\alpha_2^2 - 2\alpha_2^3)\right\}$$

$$k_{22} = \frac{1}{3}\left\{1 - \rho'_1\alpha_1^3 - \rho'_2\,(1 - \beta_2^3)\right\}$$

$$\rho_1' = 1 - \frac{1}{\rho_1}$$

and $$\rho_2' = 1 - \frac{1}{\rho_2}$$

where the co-efficients α_1, α_2, β_1, β_2, ρ_1 and ρ_2 are shown in Figure C.2.

The values of S_1 and S_2 in Equations C.4 are given by

$$S_1 = 1 - \rho_1'\alpha_1^2 (6 - 8\alpha_1 + 3\alpha_1^2) - \rho_2'\alpha_2^3 (4 - 3\alpha_2)$$

$$S_2 = 1 - \rho_1'\alpha_1^3 (4 - 3\alpha_1) - \rho_2'\alpha_2^2 (6 - 8\alpha_2 + 3\alpha_2^2)$$

Solving Equations C.2, the end moments M_{AB} and M_{BA} may be expressed by

$$M_{AB} = \frac{EI_p}{\ell} \left(a_{11}\theta_A + a_{12}\theta_B - C_1 \frac{\Delta}{\ell} \right) + M_{AF}^1 \qquad C.5(a)$$

$$M_{BA} = \frac{EI_p}{\ell} \left(a_{21}\theta_A + a_{22}\theta_B - C_2 \frac{\Delta}{\ell} \right) + M_{BF}^1 \qquad C.6(b)$$

where $$\begin{bmatrix} a_{11} & a_{12} \\ a_{21} & a_{22} \end{bmatrix} = \begin{bmatrix} k_{11} & k_{12} \\ k_{21} & k_{22} \end{bmatrix}^{-1}$$

$$C_1 = a_{11} + a_{12}$$

$$c_2 = a_{21} + a_{22}$$

and M'_{AF} and M'_{BF} are fixed-end moments at A and B, and are expressed by

$$M'_{AF} = b_1 M_{AF}$$

$$M'_{BA} = b_2 M_{BF}$$

where M_{AF} and M_{BF} are the fixed end moments for a beam with constant stiffness. The values of b_1 and b_2 for a uniformly distributed load are given by

$$b_1 = a_{11} s_1 - a_{12} s_2$$

$$b_2 = a_{21} s_1 - a_{22} s_2$$

The midspan deflection for a uniformly loaded beam with span ℓ and fixed ends may be expressed by

$$\Delta_c = k_w \frac{q\ell^4}{384EI_p} \qquad \text{C.6}$$

where

$$k_w = \frac{12}{C_1 + C_2}\left(1 - \frac{c_1 S_2}{12} + \frac{c_2 S_2}{12}\right)$$

For a concentrated load at midspan, the midspan deflection becomes

$$\Delta_c = k_c \frac{P\ell^3}{192EI_p}$$

where $$k_c = \frac{12}{c_1 + c_2}$$

The values of k_w and k_c are shown in Figure C.3(a). For a uniform load the bending moment M_{fe} at the ends is given by

$$M_{fe} = -m_w \frac{q\ell^2}{12}$$

where $$m_w = \frac{b_1}{3} + \frac{c_1 k_w}{9}$$

and for concentrated load P at the midspan as

$$M_{fe} = -m_c \frac{PL}{8}$$

where $$m_c = \frac{c_1}{6}$$

The values of m_w and m_c are shown in Figure C.3(b) as a function of the ratio of stiffness in a negative and positive moment region. The moment at midspan is obtained from the equilibrium equation for a statically determinate beam, if the bending moment at the ends is known.

TABLE C.1 VALUES OF CO-EFFICIENT k_{11} IN EQUATION C.2

ρ \ α	0.15	0.20	0.25	0.30	0.35	0.40	0.45	0.50	0.55
0.20	0.8478	0.9840	1.1042	1.2093	1.3005	1.3787	1.4448	1.5000	1.5452
0.25	0.7192	0.8213	0.9115	0.9903	1.0587	1.1173	1.1670	1.2083	1.2422
0.30	0.6335	0.7129	0.7830	0.8443	0.8975	0.9431	0.9817	1.0139	1.0402
0.35	0.5722	0.6354	0.6912	0.7400	0.7824	0.8187	0.8494	0.8750	0.8960
0.40	0.5263	0.5773	0.6224	0.6618	0.6960	0.7253	0.7501	0.7708	0.7878
0.45	0.4905	0.5321	0.5689	0.6010	0.6289	0.6527	0.6730	0.6898	0.7036
0.50	0.4620	0.4960	0.5260	0.5523	0.5751	0.5947	0.6112	0.6250	0.6363
0.55	0.4386	0.4664	0.4910	0.5125	0.5312	0.5472	0.5607	0.5720	0.5812
0.60	0.4191	0.4418	0.4618	0.4793	0.4945	0.5076	0.5186	0.5278	0.5353
0.65	0.4026	0.4209	0.4371	0.4513	0.4635	0.4741	0.4830	0.4904	0.4965
0.70	0.3885	0.4030	0.4159	0.4272	0.4370	0.4453	0.4524	0.4583	0.4632
0.75	0.3762	0.3876	0.3976	0.4063	0.4139	0.4204	0.4260	0.4306	0.4343
0.80	0.3655	0.3740	0.3815	0.3881	0.3938	0.3987	0.4028	0.4063	0.4091
0.85	0.3560	0.3620	0.3673	0.3720	0.3760	0.3795	0.3824	0.3848	0.3868
0.90	0.3476	0.3514	0.3547	0.3577	0.3602	0.3624	0.3642	0.3657	0.3670
0.95	0.3401	0.3419	0.3435	0.3449	0.3461	0.3471	0.3480	0.3487	0.3493
1.00	0.3333	0.3333	0.3333	0.3333	0.3333	0.3333	0.3333	0.3333	0.3333

	0.60	0.65	0.70	0.75	0.80	0.85	0.90	0.95	1.00
0.20	1.5813	1.6095	1.6307	1.6458	1.6560	1.6622	1.6653	1.6665	1.6667
0.25	1.2693	1.2905	1.3063	1.3177	1.3253	1.3300	1.3323	1.3332	1.3333
0.30	1.0613	1.0778	1.0901	1.0990	1.1049	1.1085	1.1103	1.1110	1.1111
0.35	0.9128	0.9258	0.9357	0.9427	0.9474	0.9503	0.9518	0.9523	0.9524
0.40	0.8013	0.8119	0.8198	0.8255	0.8293	0.8316	0.8328	0.8333	0.8333
0.45	0.7147	0.7233	0.7297	0.7344	0.7375	0.7394	0.7403	0.7407	0.7407
0.50	0.6453	0.6524	0.6577	0.6615	0.6640	0.6655	0.6663	0.6666	0.6667
0.55	0.5886	0.5944	0.5987	0.6018	0.6039	0.6051	0.6058	0.6060	0.6061
0.60	0.5413	0.5460	0.5496	0.5521	0.5538	0.5548	0.5553	0.5555	0.5556
0.65	0.5013	0.5051	0.5080	0.5100	0.5114	0.5122	0.5126	0.5128	0.5128
0.70	0.4670	0.4701	0.4723	0.4740	0.4750	0.4757	0.4760	0.4762	0.4762
0.75	0.4373	0.4397	0.4414	0.4427	0.4436	0.4441	0.4443	0.4444	0.4444
0.80	0.4113	0.4131	0.4144	0.4154	0.4160	0.4164	0.4166	0.4167	0.4167
0.85	0.3884	0.3896	0.3906	0.3912	0.3917	0.3920	0.3921	0.3921	0.3922
0.90	0.3680	0.3688	0.3694	0.3698	0.3701	0.3702	0.3703	0.3704	0.3704
0.95	0.3498	0.3501	0.3504	0.3506	0.3507	0.3508	0.3509	0.3509	0.3509
1.00	0.3333	0.3333	0.3333	0.3333	0.3333	0.3333	0.3333	0.3333	0.3333

TABLE C.2 VALUES OF CO-EFFICIENTS $-k_{12}$ AND $-k_{21}$ IN EQUATION C.2

ρ \ α	0.15	0.20	0.25	0.30	0.35	0.40	0.45	0.50	0.55
0.20	0.2072	0.2360	0.2708	0.3107	0.3545	0.4013	0.4502	0.5000	0.5498
0.25	0.1970	0.2187	0.2448	0.2747	0.3075	0.3427	0.3793	0.4167	0.4540
0.30	0.1903	0.2071	0.2274	0.2507	0.2762	0.3036	0.3320	0.3611	0.3902
0.35	0.1855	0.1989	0.2150	0.2335	0.2539	0.2756	0.2983	0.3214	0.3446
0.40	0.1819	0.1927	0.2057	0.2207	0.2371	0.2547	0.2730	0.2917	0.3104
0.45	0.1790	0.1879	0.1985	0.2107	0.2241	0.2384	0.2533	0.2685	0.2837
0.50	0.1768	0.1840	0.1927	0.2027	0.2136	0.2253	0.2375	0.2500	0.2625
0.55	0.1750	0.1808	0.1880	0.1961	0.2051	0.2147	0.2247	0.2348	0.2450
0.60	0.1734	0.1782	0.1840	0.1907	0.1980	0.2058	0.2139	0.2222	0.2305
0.65	0.1721	0.1760	0.1807	0.1861	0.1920	0.1983	0.2048	0.2115	0.2182
0.70	0.1710	0.1741	0.1778	0.1821	0.1868	0.1918	0.1970	0.2024	0.2077
0.75	0.1700	0.1724	0.1753	0.1787	0.1823	0.1862	0.1903	0.1944	0.1986
0.80	0.1692	0.1710	0.1732	0.1757	0.1784	0.1813	0.1844	0.1875	0.1906
0.85	0.1685	0.1697	0.1713	0.1730	0.1750	0.1770	0.1792	0.1814	0.1836
0.90	0.1678	0.1686	0.1696	0.1707	0.1719	0.1732	0.1745	0.1759	0.1773
0.95	0.1672	0.1676	0.1680	0.1686	0.1691	0.1698	0.1704	0.1711	0.1717
1.00	0.1667	0.1667	0.1667	0.1667	0.1667	0.1667	0.1667	0.1667	0.1667

	0.60	0.65	0.70	0.75	0.80	0.85	0.90	0.95	1.00
0.20	0.5987	0.6455	0.6893	0.7292	0.7640	0.7928	0.8147	0.8285	0.8333
0.25	0.4907	0.5258	0.5587	0.5885	0.6147	0.6363	0.6527	0.6630	0.6667
0.30	0.4187	0.4460	0.4716	0.4948	0.5151	0.5319	0.5447	0.5527	0.5556
0.35	0.3672	0.3890	0.4093	0.4278	0.4440	0.4574	0.4675	0.4739	0.4762
0.40	0.3287	0.3462	0.3627	0.3776	0.3907	0.4015	0.4097	0.4149	0.4167
0.45	0.2987	0.3130	0.3264	0.3385	0.3492	0.3580	0.3647	0.3689	0.3704
0.50	0.2747	0.2864	0.2973	0.3073	0.3160	0.3232	0.3287	0.3321	0.3333
0.55	0.2550	0.2646	0.2736	0.2817	0.2888	0.2947	0.2992	0.3020	0.3030
0.60	0.2387	0.2465	0.2538	0.2604	0.2662	0.2710	0.2747	0.2770	0.2778
0.65	0.2248	0.2311	0.2370	0.2424	0.2471	0.2510	0.2539	0.2558	0.2564
0.70	0.2130	0.2180	0.2227	0.2269	0.2307	0.2338	0.2361	0.2376	0.2381
0.75	0.2027	0.2066	0.2102	0.2135	0.2164	0.2188	0.2207	0.2218	0.2222
0.80	0.1937	0.1966	0.1993	0.2018	0.2040	0.2058	0.2072	0.2080	0.2083
0.85	0.1857	0.1878	0.1897	0.1915	0.1930	0.1943	0.1953	0.1959	0.1961
0.90	0.1787	0.1800	0.1812	0.1823	0.1833	0.1841	0.1847	0.1851	0.1852
0.95	0.1724	0.1730	0.1735	0.1741	0.1745	0.1749	0.1752	0.1754	0.1754
1.00	0.1667	0.1667	0.1667	0.1667	0.1667	0.1667	0.1667	0.1667	0.1667

TABLE C.3 VALUES OF CO-EFFICIENT k_{22} IN EQUATION C.2

ρ \ α	0.15	0.20	0.25	0.30	0.35	0.40	0.45	0.50	0.55
0.20	0.3378	0.3440	0.3542	0.3693	0.3905	0.4187	0.4548	0.5000	0.5552
0.25	0.3367	0.3413	0.3490	0.3603	0.3762	0.3973	0.4245	0.4583	0.4997
0.30	0.3360	0.3396	0.3455	0.3543	0.3667	0.3831	0.4042	0.4306	0.4627
0.35	0.3354	0.3383	0.3430	0.3500	0.3599	0.3730	0.3897	0.4107	0.4363
0.40	0.3350	0.3373	0.3411	0.3468	0.3548	0.3653	0.3789	0.3958	0.4165
0.45	0.3347	0.3366	0.3397	0.3443	0.3508	0.3594	0.3705	0.3843	0.4011
0.50	0.3345	0.3360	0.3385	0.3423	0.3476	0.3547	0.3637	0.3750	0.3888
0.55	0.3343	0.3355	0.3376	0.3407	0.3450	0.3508	0.3582	0.3674	0.3787
0.60	0.3341	0.3351	0.3368	0.3393	0.3429	0.3476	0.3536	0.3611	0.3703
0.65	0.3339	0.3348	0.3361	0.3382	0.3410	0.3448	0.3497	0.3558	0.3632
0.70	0.3338	0.3345	0.3356	0.3372	0.3395	0.3425	0.3464	0.3512	0.3571
0.75	0.3337	0.3342	0.3351	0.3363	0.3381	0.3404	0.3435	0.3472	0.3518
0.80	0.3336	0.3340	0.3346	0.3356	0.3369	0.3387	0.3409	0.3438	0.3472
0.85	0.3335	0.3338	0.3343	0.3349	0.3359	0.3371	0.3387	0.3407	0.3431
0.90	0.3335	0.3336	0.3339	0.3343	0.3349	0.3357	0.3367	0.3380	0.3395
0.95	0.3334	0.3335	0.3336	0.3338	0.3341	0.3345	0.3349	0.3355	0.3363
1.00	0.3333	0.3333	0.3333	0.3333	0.3333	0.3333	0.3333	0.3333	0.3333

	0.60	0.65	0.70	0.75	0.80	0.85	0.90	0.95	1.00
0.20	0.6213	0.6995	0.7907	0.8958	1.0160	1.1522	1.3053	1.4765	1.6667
0.25	0.5493	0.6080	0.6763	0.7552	0.8453	0.9475	1.0623	1.1907	1.3333
0.30	0.5013	0.5469	0.6001	0.6615	0.7316	0.8110	0.9003	1.0002	1.1111
0.35	0.4670	0.5033	0.5457	0.5945	0.6503	0.7135	0.7846	0.8641	0.9524
0.40	0.4413	0.4706	0.5048	0.5443	0.5893	0.6404	0.6978	0.7620	0.8333
0.45	0.4213	0.4452	0.4731	0.5052	0.5419	0.5835	0.6303	0.6826	0.7407
0.50	0.4053	0.4249	0.4477	0.4740	0.5040	0.5380	0.5763	0.6191	0.6667
0.55	0.3922	0.4082	0.4269	0.4484	0.4730	0.5008	0.5322	0.5672	0.6061
0.60	0.3813	0.3944	0.4096	0.4271	0.4471	0.4698	0.4953	0.5239	0.5556
0.65	0.3721	0.3826	0.3949	0.4091	0.4252	0.4436	0.4642	0.4872	0.5128
0.70	0.3642	0.3726	0.3823	0.3936	0.4065	0.4211	0.4375	0.4558	0.4762
0.75	0.3573	0.3638	0.3714	0.3802	0.3902	0.4016	0.4143	0.4286	0.4444
0.80	0.3513	0.3562	0.3619	0.3685	0.3760	0.3845	0.3941	0.4048	0.4167
0.85	0.3460	0.3495	0.3535	0.3581	0.3635	0.3695	0.3762	0.3838	0.3922
0.90	0.3413	0.3435	0.3460	0.3490	0.3523	0.3561	0.3603	0.3651	0.3704
0.95	0.3371	0.3382	0.3394	0.3407	0.3423	0.3441	0.3461	0.3484	0.3509
1.00	0.3333	0.3333	0.3333	0.3333	0.3333	0.3333	0.3333	0.3333	0.3333

TABLE C.4 VALUES OF CO-EFFICIENT s_1 IN EQUATION C.4

ρ \ α	0.15	0.20	0.25	0.30	0.35	0.40	0.45	0.50	0.55
0.20	1.0479	1.1088	1.2031	1.3348	1.5059	1.7168	1.9659	2.2500	2.5639
0.25	1.0359	1.0816	1.1523	1.2511	1.3794	1.5376	1.7244	1.9375	2.1729
0.30	1.0280	1.0635	1.1185	1.1953	1.2951	1.4181	1.5635	1.7292	1.9123
0.35	1.0223	1.0505	1.0943	1.1554	1.2349	1.3328	1.4485	1.5804	1.7261
0.40	1.0180	1.0408	1.0762	1.1255	1.1897	1.2688	1.3622	1.4687	1.5865
0.45	1.0146	1.0332	1.0621	1.1023	1.1546	1.2190	1.2951	1.3819	1.4779
0.50	1.0120	1.0272	1.0508	1.0837	1.1265	1.1792	1.2415	1.3125	1.3910
0.55	1.0098	1.0223	1.0415	1.0685	1.1035	1.1466	1.1976	1.2557	1.3199
0.60	1.0080	1.0181	1.0339	1.0558	1.0843	1.1195	1.1610	1.2083	1.2607
0.65	1.0065	1.0146	1.0273	1.0451	1.0681	1.0965	1.1300	1.1683	1.2105
0.70	1.0051	1.0117	1.0218	1.0359	1.0542	1.0768	1.1035	1.1339	1.1676
0.75	1.0040	1.0091	1.0169	1.0279	1.0422	1.0597	1.0805	1.1042	1.1303
0.80	1.0030	1.0068	1.0127	1.0209	1.0316	1.0448	1.0604	1.0781	1.0977
0.85	1.0021	1.0048	1.0090	1.0148	1.0223	1.0316	1.0426	1.0551	1.0690
0.90	1.0013	1.0030	1.0056	1.0093	1.0141	1.0199	1.0268	1.0347	1.0434
0.95	1.0006	1.0014	1.0027	1.0044	1.0067	1.0094	1.0127	1.0164	1.0206
1.00	1.0000	1.0000	1.0000	1.0000	1.0000	1.0000	1.0000	1.0000	1.0000

	0.60	0.65	0.70	0.75	0.80	0.85	0.90	0.95	1.00
0.20	2.9008	3.2519	3.6068	3.9531	4.2768	4.5619	4.7908	4.9439	5.0000
0.25	2.4256	2.6889	2.9551	3.2148	3.4576	3.6714	3.8431	3.9579	4.0000
0.30	2.1088	2.3136	2.5206	2.7227	2.9115	3.0778	3.2113	3.3006	3.3333
0.35	1.8825	2.0455	2.2103	2.3711	2.5214	2.6538	2.7600	2.8311	2.8571
0.40	1.7128	1.8445	1.9775	2.1074	2.2288	2.3357	2.4216	2.4790	2.5000
0.45	1.5808	1.6881	1.7965	1.9023	2.0012	2.0884	2.1583	2.2051	2.2222
0.50	1.4752	1.5630	1.6517	1.7383	1.8192	1.8905	1.9477	1.9860	2.0000
0.55	1.3888	1.4606	1.5332	1.6040	1.6703	1.7286	1.7754	1.8067	1.8182
0.60	1.3168	1.3753	1.4345	1.4922	1.5461	1.5937	1.6318	1.6573	1.6667
0.65	1.2559	1.3031	1.3509	1.3975	1.4411	1.4795	1.5103	1.5309	1.5385
0.70	1.2037	1.2413	1.2793	1.3164	1.3511	1.3816	1.4062	1.4226	1.4286
0.75	1.1584	1.1877	1.2172	1.2461	1.2731	1.2968	1.3159	1.3287	1.3333
0.80	1.1188	1.1407	1.1629	1.1846	1.2048	1.2226	1.2369	1.2465	1.2500
0.85	1.0839	1.0993	1.1150	1.1303	1.1446	1.1571	1.1672	1.1740	1.1765
0.90	1.0528	1.0626	1.0724	1.0820	1.0910	1.0989	1.1053	1.1096	1.1111
0.95	1.0250	1.0296	1.0343	1.0389	1.0431	1.0469	1.0499	1.0519	1.0526
1.00	1.0000	1.0000	1.0000	1.0000	1.0000	1.0000	1.0000	1.0000	1.0000

TABLE C.5 VALUES OF CO-EFFICIENT s_2 IN EQUATION C.4

ρ \ α	0.15	0.20	0.25	0.30	0.35	0.40	0.45	0.50	0.55
0.20	1.4381	1.7232	2.0469	2.3932	2.7481	3.0992	3.4361	3.7500	4.0341
0.25	1.3286	1.5424	1.7852	2.0440	2.3111	2.5744	2.8271	3.0625	3.2756
0.30	1.2555	1.4219	1.6107	1.8127	2.0197	2.2245	2.4210	2.6042	2.7699
0.35	1.2034	1.3358	1.4860	1.6468	1.8116	1.9746	2.1310	2.2768	2.4087
0.40	1.1643	1.2712	1.3926	1.5224	1.6555	1.7872	1.9135	2.0313	2.1378
0.45	1.1339	1.2210	1.3199	1.4257	1.5341	1.6414	1.7444	1.8403	1.9271
0.50	1.1095	1.1808	1.2617	1.3483	1.4370	1.5248	1.6090	1.6875	1.7585
0.55	1.0896	1.1479	1.2141	1.2850	1.3576	1.4294	1.4983	1.5625	1.6206
0.60	1.0730	1.1205	1.1745	1.2322	1.2913	1.3499	1.4060	1.4583	1.5057
0.65	1.0590	1.0974	1.1409	1.1875	1.2353	1.2826	1.3279	1.3702	1.4084
0.70	1.0469	1.0775	1.1122	1.1493	1.1873	1.2249	1.2610	1.2946	1.3251
0.75	1.0365	1.0603	1.0872	1.1161	1.1457	1.1749	1.2030	1.2292	1.2528
0.80	1.0274	1.0452	1.0654	1.0871	1.1093	1.1312	1.1523	1.1719	1.1896
0.85	1.0193	1.0319	1.0462	1.0615	1.0771	1.0926	1.1075	1.1213	1.1339
0.90	1.0122	1.0201	1.0291	1.0387	1.0486	1.0583	1.0677	1.0764	1.0843
0.95	1.0058	1.0095	1.0138	1.0183	1.0230	1.0276	1.0321	1.0362	1.0399
1.00	1.0000	1.0000	1.0000	1.0000	1.0000	1.0000	1.0000	1.0000	1.0000

	0.60	0.65	0.70	0.75	0.80	0.85	0.90	0.95	1.00
0.20	4.2832	4.4941	4.6652	4.7969	4.8912	4.9521	4.9852	4.9981	5.0000
0.25	3.4624	3.6206	3.7489	3.8477	3.9184	3.9641	3.9889	3.9986	4.0000
0.30	2.9152	3.0382	3.1380	3.2148	3.2699	3.3054	3.3247	3.3322	3.3333
0.35	2.5243	2.6222	2.7017	2.7628	2.8066	2.8349	2.8503	2.8562	2.8571
0.40	2.2312	2.3103	2.3745	2.4238	2.4592	2.4820	2.4945	2.4993	2.5000
0.45	2.0032	2.0676	2.1199	2.1602	2.1890	2.2076	2.2177	2.2216	2.2222
0.50	1.8208	1.8735	1.9163	1.9492	1.9728	1.9880	1.9963	1.9995	2.0000
0.55	1.6716	1.7147	1.7497	1.7766	1.7959	1.8084	1.8152	1.8178	1.8182
0.60	1.5472	1.5823	1.6109	1.6328	1.6485	1.6587	1.6642	1.6663	1.6667
0.65	1.4420	1.4704	1.4934	1.5111	1.5238	1.5320	1.5365	1.5382	1.5385
0.70	1.3518	1.3744	1.3927	1.4068	1.4169	1.4234	1.4270	1.4284	1.4286
0.75	1.2736	1.2912	1.3054	1.3164	1.3243	1.3293	1.3321	1.3332	1.3333
0.80	1.2052	1.2184	1.2291	1.2373	1.2432	1.2470	1.2491	1.2499	1.2500
0.85	1.1448	1.1542	1.1617	1.1675	1.1717	1.1744	1.1758	1.1764	1.1765
0.90	1.0912	1.0971	1.1018	1.1055	1.1081	1.1098	1.1107	1.1111	1.1111
0.95	1.0432	1.0460	1.0482	1.0500	1.0512	1.0520	1.0524	1.0526	1.0526
1.00	1.0000	1.0000	1.0000	1.0000	1.0000	1.0000	1.0000	1.0000	1.0000

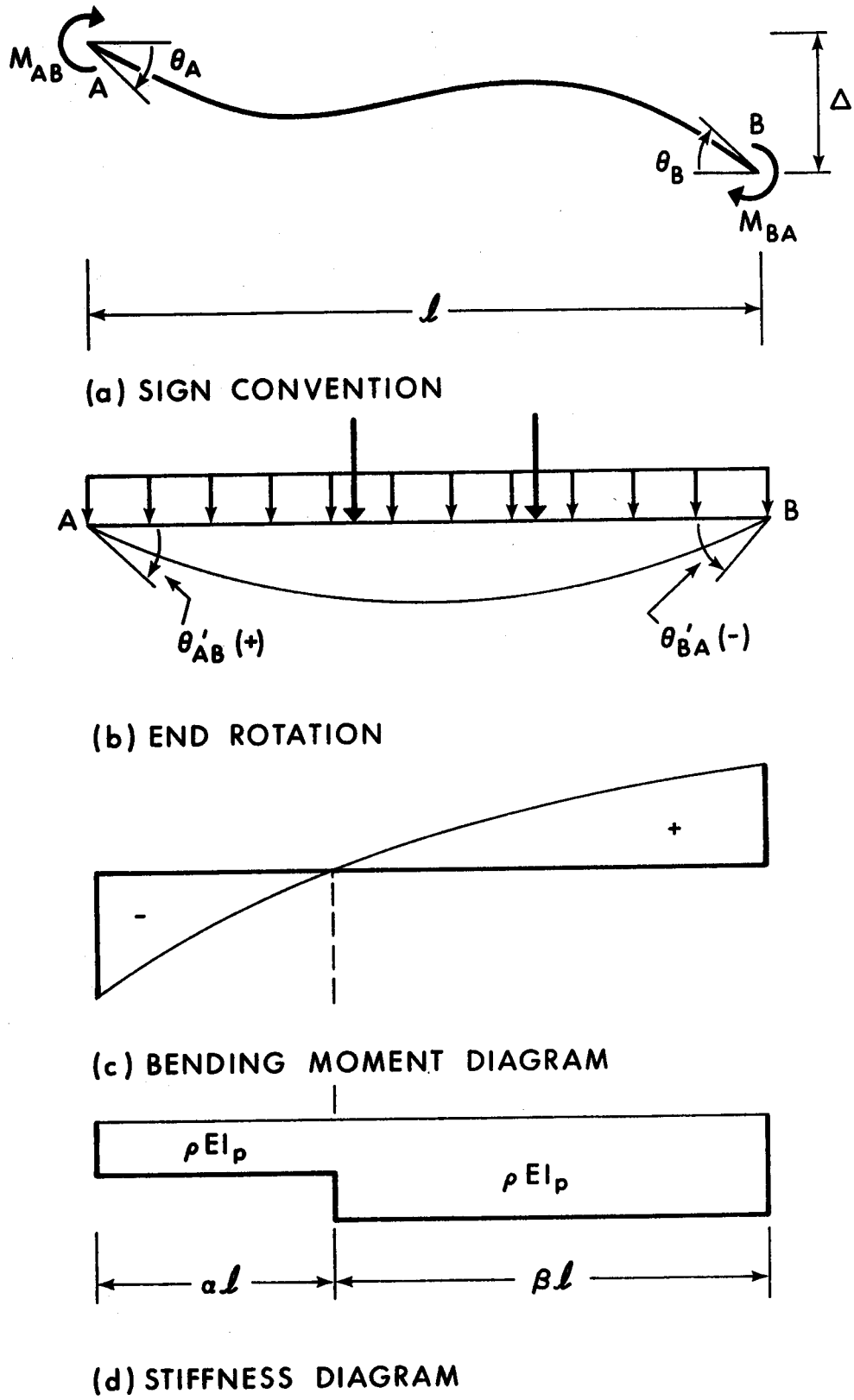

FIGURE C.1 BASIS FOR SLOPE DEFLECTION EQUATIONS BETWEEN PLASTIC HINGES

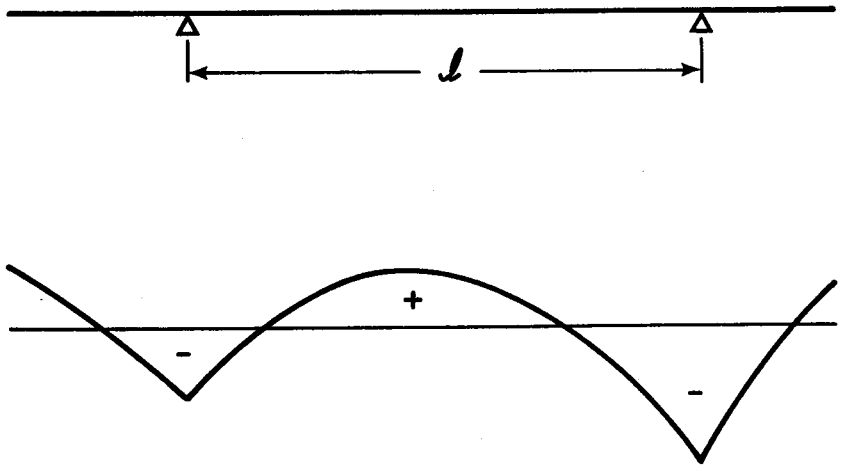

(a) MOMENT DIAGRAM

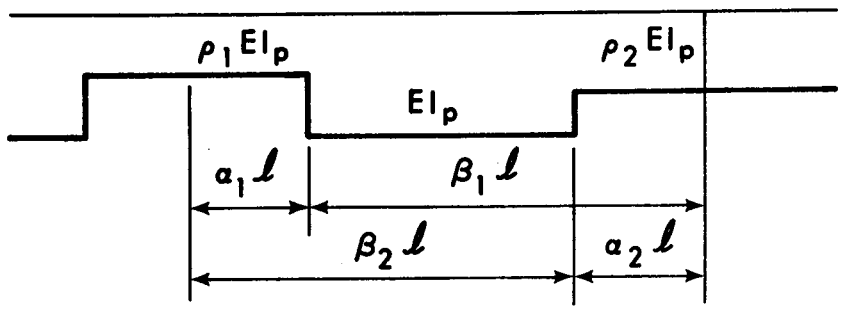

(b) STIFFNESS DIAGRAM

FIGURE C.2 BASIS FOR SLOPE DEFLECTION EQUATIONS BETWEEN SUPPORTS

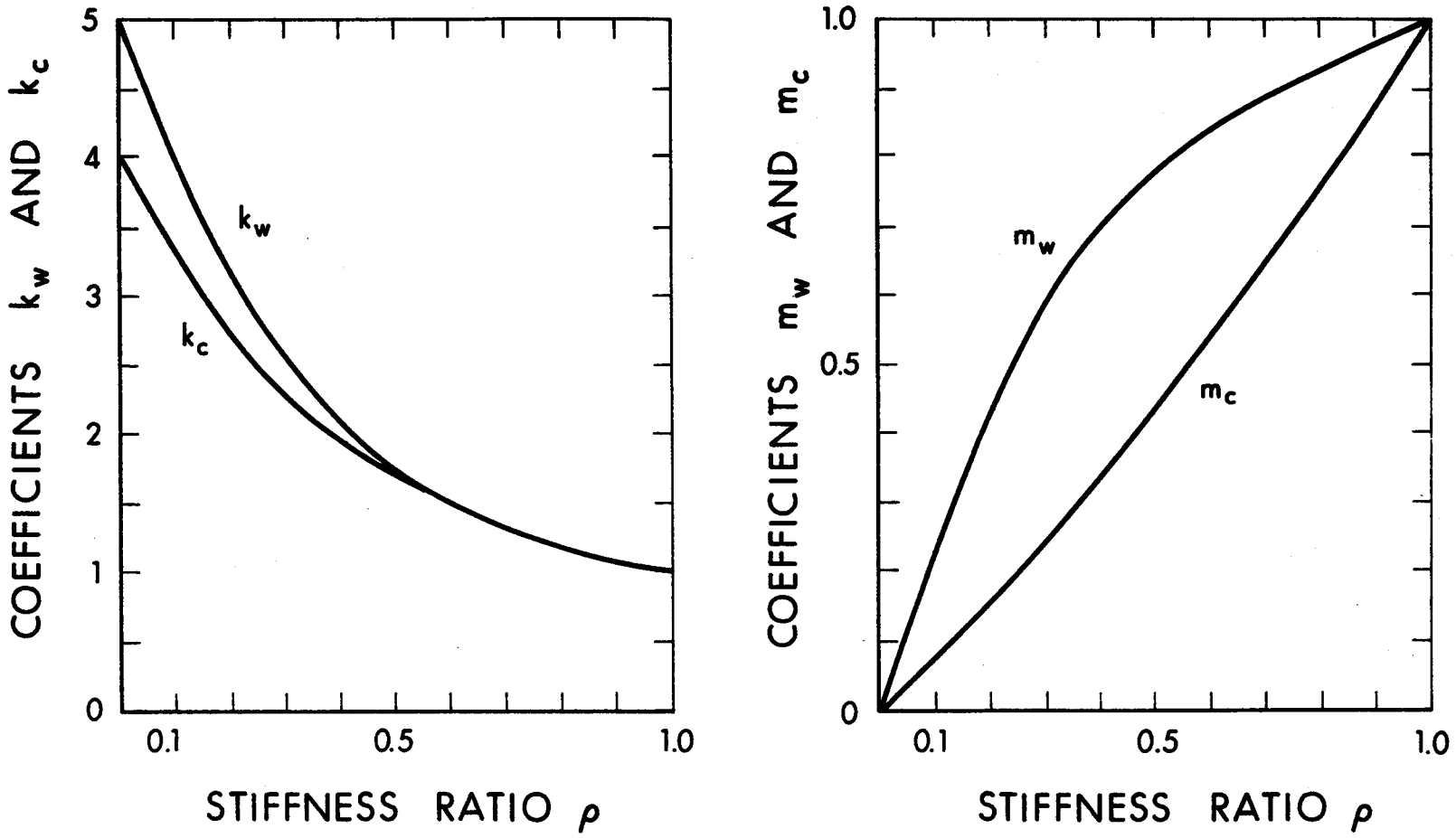

FIGURE C.3 CO-EFFICIENTS k_w, k_c, m_w and m_c FOR DEFLECTION ANALYSIS

APPENDIX D

COMPUTER PROGRAM

D.1 Introduction

The following steps are required in the computations for deformations and local flange buckling for a given load:

1. Compute moment-curvature relationships in positive and negative moment regions. Moment-curvature relationships in positive moment regions include the effect of slip.
2. Compute bending moments and bending deflection by employing the finite difference method. Rotation and shear are computed from deflection and moment values respectively. Shear deformation is computed by the virtual work method. In the inelastic region the bending deformation is obtained by an iterative procedure described in Section 3.9.
3. Check local flange buckling in the negative moment region.
4. Compute the maximum concrete strain in the positive moment regions

The computer program was written in Fortran IV and computations were carried out on the IBM 360/67 computer at the University of Alberta Computing Center. The flow chart in Figure D.1 outlines the sequence of the computations required for the analysis of the continuous beams. The program consists of 24 subroutines and 3 functions.

D.2 Description of Subroutines and Functions

READA — reads and writes the beam dimensions

DEBU — computes and writes elastic properties and consists of subroutines NUE, MISB, MISC, SCF and QX2.

MC — computes the moment-curvature relationships in positive and in negative moment regions. The outline of MC is given in Figure D.2.

READB — reads and writes the beam length, number of spans, locations of intermediate supports, loads and load locations.

DERM — computes bending moment, shear, deflection and rotation including effects of shear and slip. The outline of the computations is shown in Figure D.2.

LOCAL — computes local flange buckling values. If the first eigenvalue is greater than 1.0, buckling may occur. LOCAL consists of subroutines YAMA, SHUKI, TOKYO and PORT. SHUKI and TOKYO compute eigen values and were developed by M. Suko. YAMA is the memory for the moment-curvature relationship and location of neutral axis. PORT computes inelastic tangent modulus and inelastic shear modulus.

MX — computes maximum slab strain in each span.

NAPB — computes moment for given curvature or curvature for given moment. The outline of NAPB is illustrated in Figure D.3.

FORCE — computes normal force and moment for a rectangular element for a given material (i.e., steel or concrete), neutral axis location and curvature. FORCE includes the functions STRES and FOC which are the stress-strain relationships for steel and concrete, respectively.

SLIP	computes slip deformation of shear connectors.
REACT	computes redundant forces. REACT includes FDM and SMA.
MMI	computes additional external moment for inelastic regions.
DS	computes shear deformation and includes SHERG
SHERG	computes shear energy in a segment.
SMA	solves equations by Gauss elimination.
CPRINT	writes computational results of forces and deformations.
FDM	computes deflection, rotation, shear and moments by means of the finite difference method.

D.3 Input Data

Input data required for this analysis is listed in the following, and input format is illustrated in Figure D.4. Explanation of the symbols for input data are listed as below.

B	Flange width for steel section
T	Flange thickness for steel section
D	Beam depth for steel section
W	Web thickness
SIGY	Yield stress for steel section
H	Ratio of elastic modulus to strain hardening modulus for steel beam
RSN	Ratio of the strain at strain hardening to yield strain
SIGU	Ultimate strength for steel section
K1	Number of segments of flange in thickness direction
K2	Number of segments of web in depth direction
KF	Number of segments of flange in width direction
RA	Area of longitudinal slab reinforcement in negative-moment

YRA	Yield stress for longitudinal reinforcement
DRS	Distance from centroid of longitudinal reinforcement to top of steel section
HR	H for reinforcement
RSNR	RSN for reinforcement
RK	Interaction factor of the strain in longitudinal reinforcement
BC	Concrete slab width
BT	Slab thickness
FC	Concrete strength
EN	Ratio of elastic modulus for steel to that for concrete
KT	Number of segments of slab in thickness direction
AL	Beam length
N	Number of segments in length direction
NM	Number of intermediate supports
NR(I)	Location of intermediate support
NL	Number of load stages
K(I)	Location of concentrated load
A(I)	Concentrated load
B(I)	Uniformly distributed load

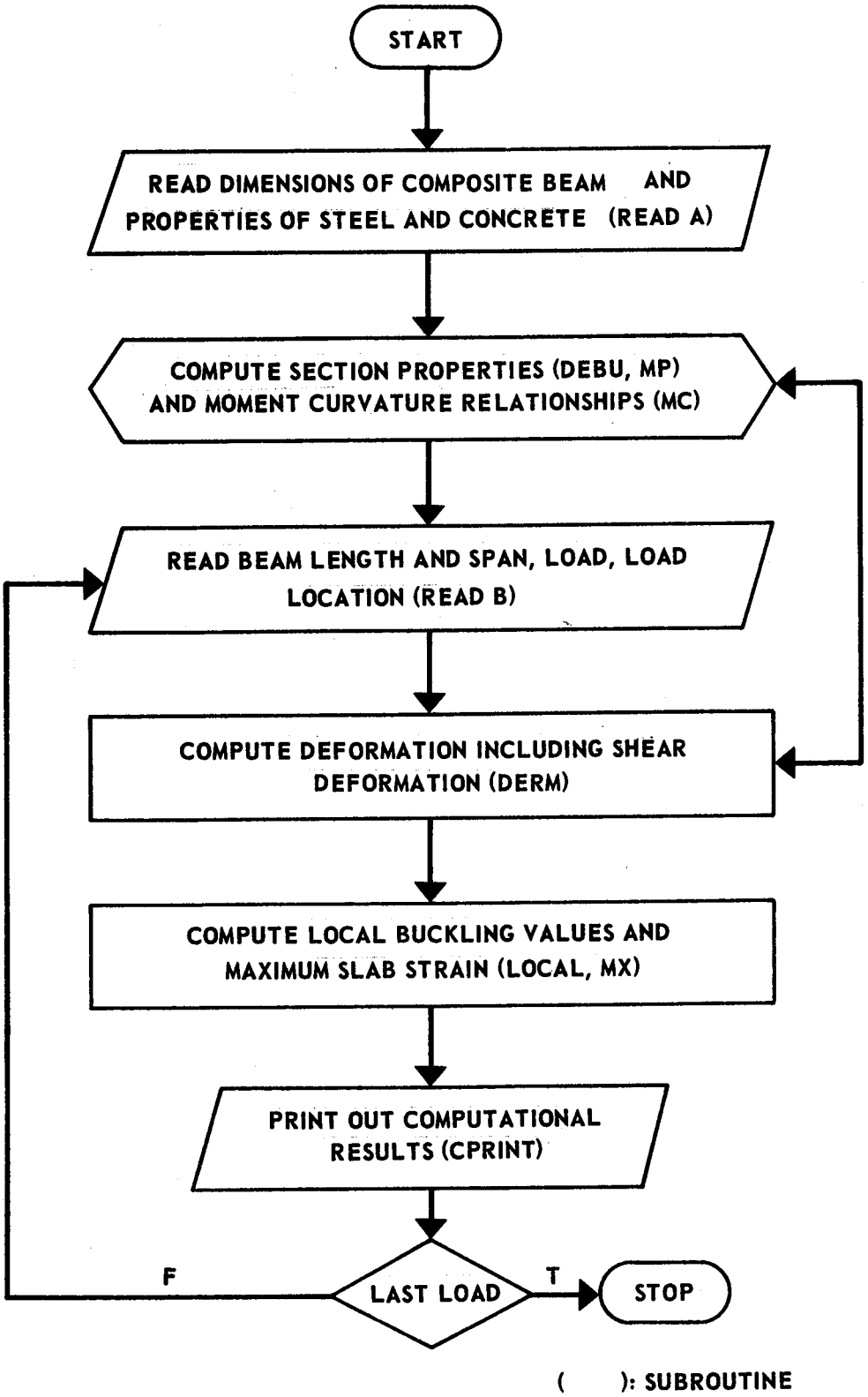

FIGURE D.1 MAIN PROGRAM OUTLINE

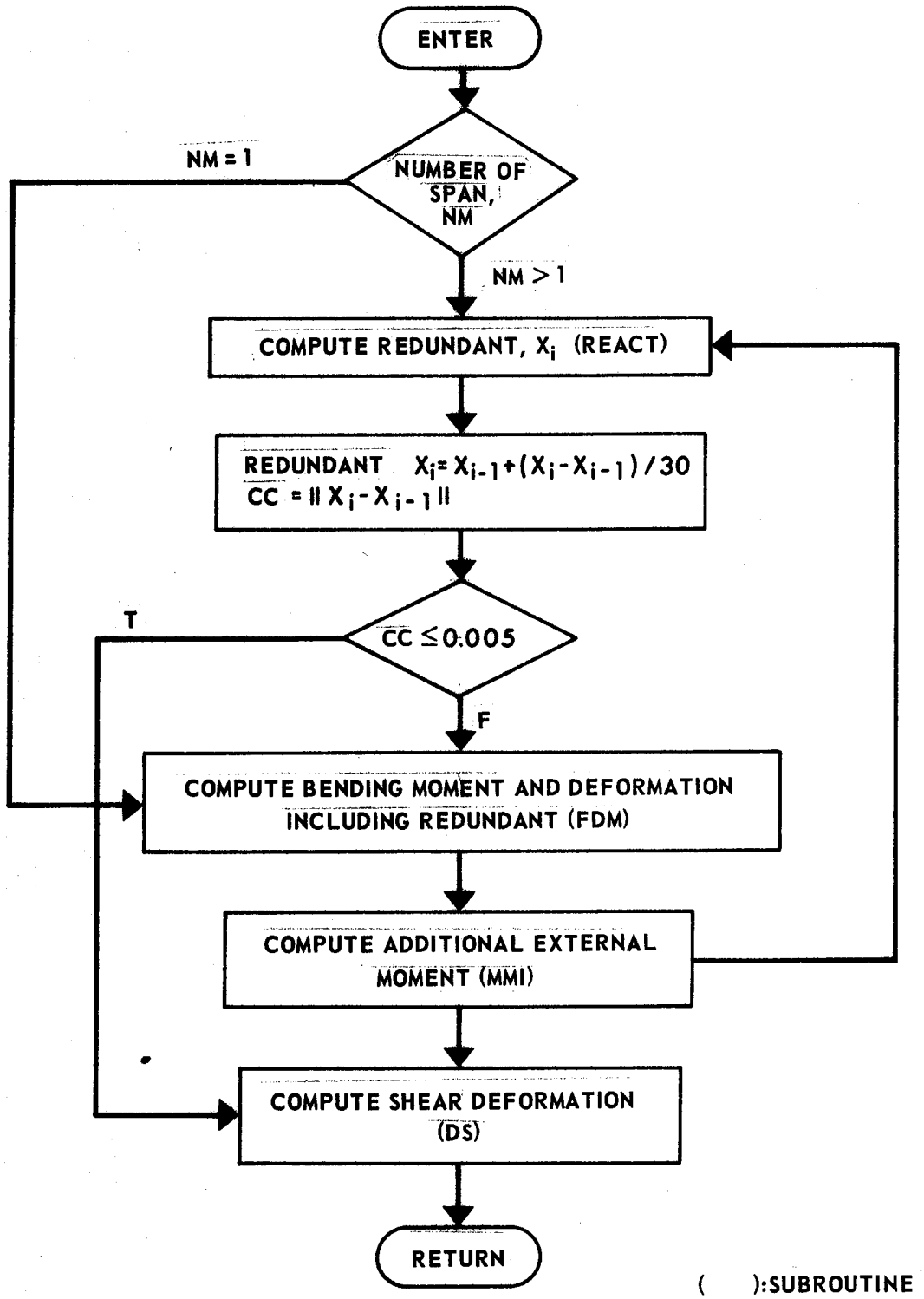

FIGURE D.2 OUTLINE OF DEFORMATION PROGRAM (DERM)

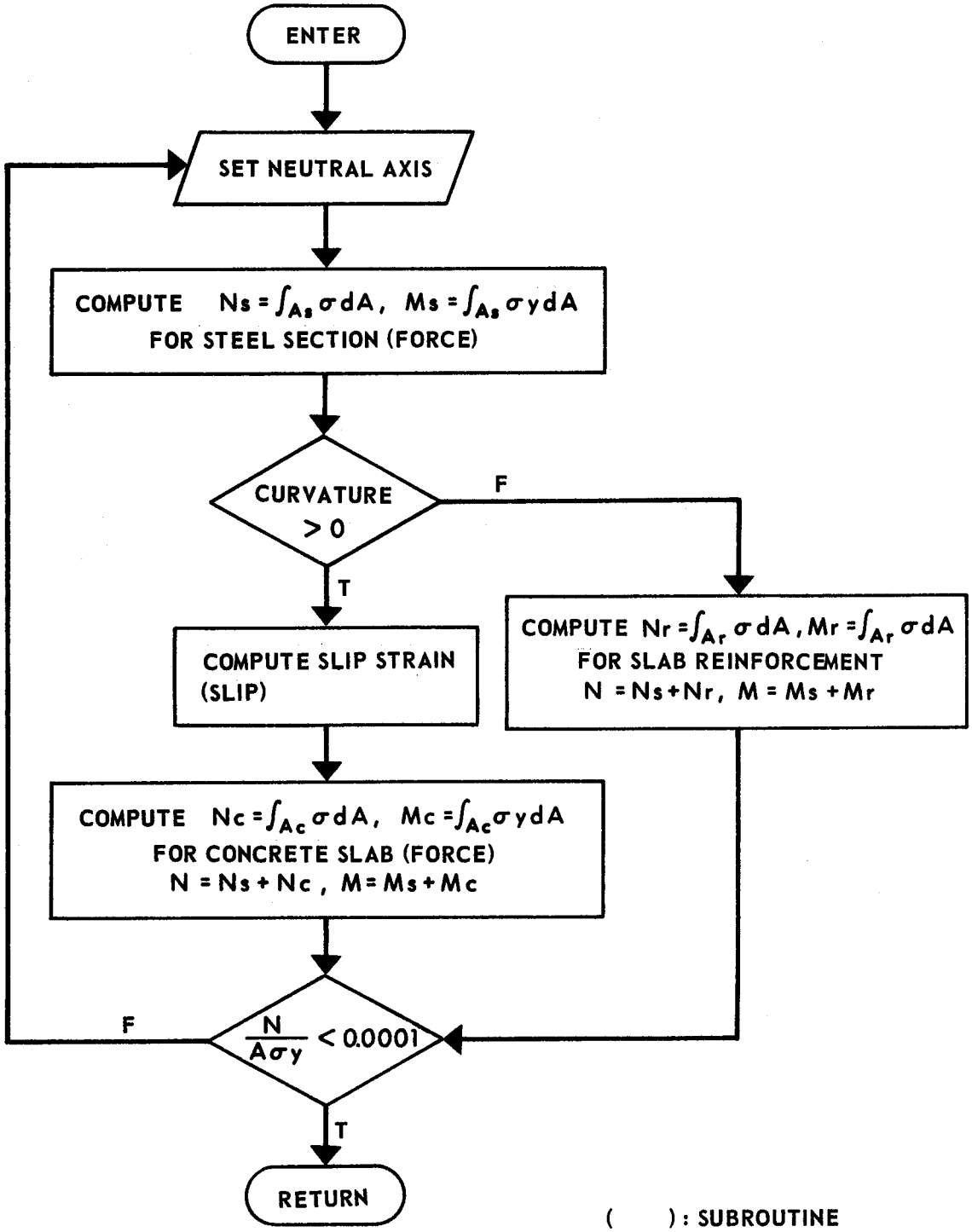

FIGURE D.3 OUTLINE OF PROGRAM FOR MOMENT-CURVATURE RELATIONSHIPS (NAPB) IN (MC)

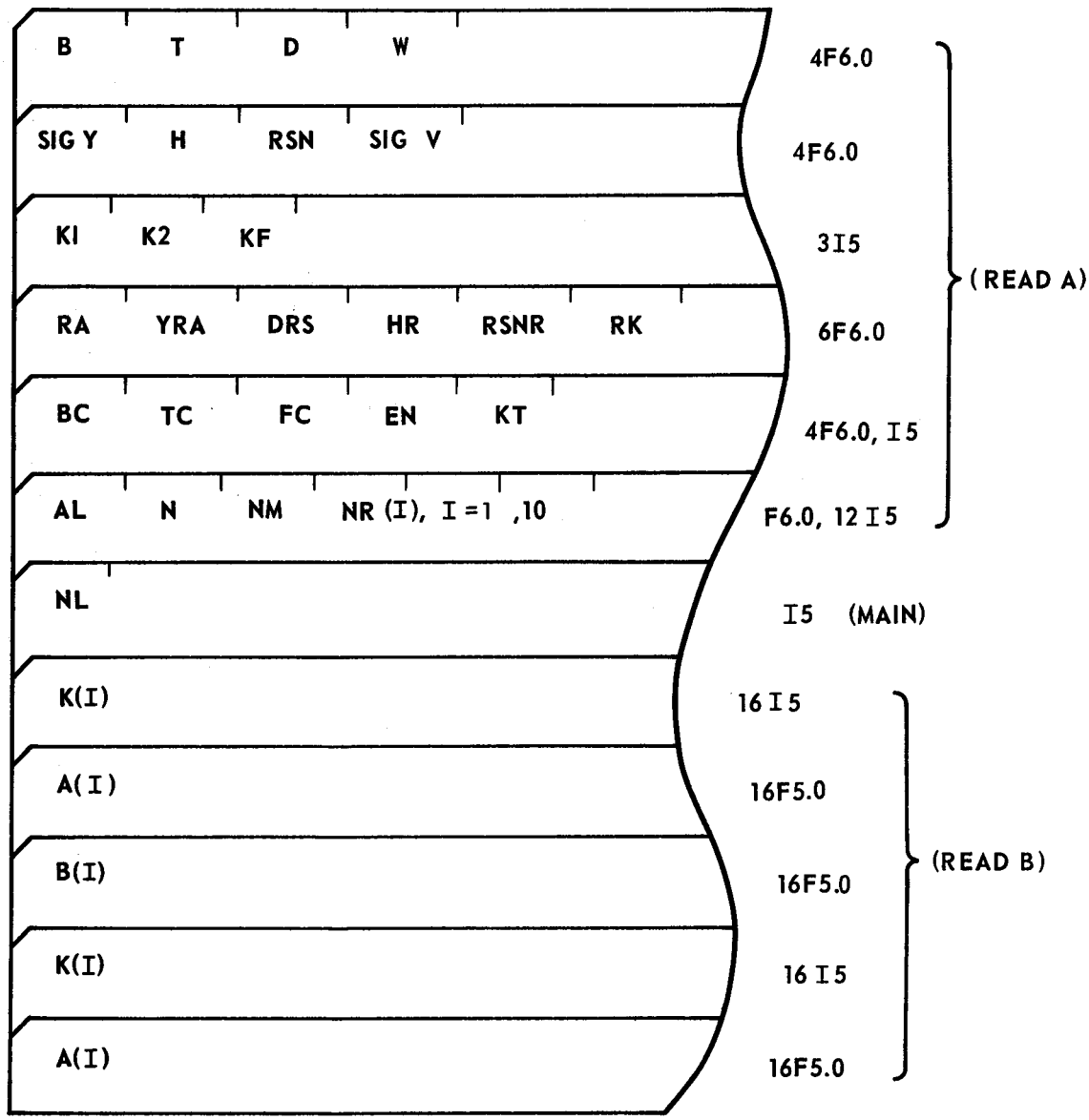

FIGURE D.4 INPUT DATA

```
      IMPLICIT REAL*8(A-H,O-Z)
      COMMON/TEA2/SIGY,YS,AH,RSN,RES,FYP,EPM,SIGU
      COMMON/BL1/N,N1,AL,NM,NR(10)
      COMMON/BL2/CIP,CIN,AKP,AKN,ATP,ATN,BYP,BYN
      COMMON/BL3/AS,SI,X,CI,AK,BY,EQI,AT
      COMMON/BL5/SP(5),SCR(6,50,4),PRO(4,100)
      COMMON/COS1/CU(6,61)
      COMMON/BL4/XX(4,100),YY(3,100)
      DIMENSION BM(100),R(100),SR(100),DEF(100),SD(100)
      DIMENSION  Q(100),SH(100),P(100),BL(10)
      ELM=3.0*10.0**4
    9 CALL READA
      DO 10 I=1,100
      DO 11 J=1,4
   11 XX(J,I)=0.0
      DO 12 J=1,3
   12 YY(J,I)=0.0
   10 CONTINUE
      WRITE(6,5)
      WRITE(6,4)
      CALL DEBU(1)
      CALL MP(1,BMU)
      CIP=EQI*ELM
      AKP=AK
      ATP=AT
      BYP=BY
      WRITE(6,5)
      WRITE(6,3)
      CALL DEBU(-1)
      CALL MP(-1,BMU)
      CIN=CI*ELM
      AKN=AK
      ATN=AT
      BYN=BY
      CALL MC
      READ(5,2)NL
      NNL=0
    1 CALL READB(P,Q)
      CALL DERM(Q,P,BM,SH,R,DEF,SR,SD)
      CALL CPRINT(SH,BM,R,DEF,SR,SD)
      DO 6 I=1,50
      DO 6 J=1,3
      JJ=J+3
      IF(J.EQ.1.OR.J.EQ.2)CU(JJ,I)=-SCR(6,I,J)
      IF(J.EQ.3)CU(JJ,I)=SCR(6,I,J)
    6 CONTINUE
      CU1=CU(4,1)*SIGY/(CU(5,1)*CU(6,1)*ELM)
      IF(NM.EQ.0)GO TO 14
      CALL NLE(BM,BL)
      DO 13 I=1,NM
      BS=BM(NR(I))
       BSS=DABS(BS)
      IF(BSS.LT.(CU1*1.05))GO TO 13
      PS=BSS/BL(I)
      CALL LOCAL(20,BL(I),CU1,PS,EIG1)
      CALL MX(BM,PRO)
   13 CONTINUE
   14 NNL=NNL+1
```

```
      IF(NNL.LT.NL)GO TO 1
      GO TO 9
    2 FORMAT(10I5)
    3 FORMAT(/5X,'$$$$ NEGATIVE MOMENT REGION $$$$')
    4 FORMAT(/5X,'$$$$ POSITIVE MOMENT REGION $$$$')
    5 FORMAT(/20X,'$$$$$$$$$$$$$$$$')
   99 FORMAT(/5X,8E14.5)
      STOP
      END




      SUBROUTINE CPRINT(SH,BM,R,DEF,SR,SD)
      IMPLICIT REAL*8(A-H,O-Z)
      COMMON/BL1/N,N1,AL,NM,NR(10)
      DIMENSION BM(100),R(100),SR(100),DEF(100),SD(100),SH(100)
      WRITE(6,2)
      DO 1 I=1,N1
    1 WRITE(6,3)I,SH(I),BM(I),R(I),DEF(I),SR(I),SD(I)
    2 FORMAT(//5X,'**** BENDING MOMENT AND DEFORMATION ****',
     1/7X,'I',10X,'SHEAR',10X,'BM',13X,'R',13X,'DEF',13X,'SR',13X,'SD')
    3 FORMAT(5X,I3,2X,6E15.6)
      RETURN
      END




       SUBROUTINE MX(BM,PRO)
      IMPLICIT REAL*8(A-H,O-Z)
      COMMON/BL1/N,N1,AL,NM,NR(10)
      COMMON/TEA4/BC,TC,FC,KT
      DIMENSION BM(100),PRO (4,100)
      NM1=NM+1
      WRITE(6,11)
      DO 1 I=1,NM1
      BE=0.0
      J2=1
      J3=N1
      IF(I.NE.1)J2=NR(I-1)
      IF(I.NE.NM1)J3=NR(I)
      DO 2 J=J2,J3
      IF(BM(J).GT.BE)MB=J
      IF(BM(J).GT.BE)BE=BM(J)
    2 CONTINUE
      SNM=PRO(2,MB)*(TC+PRO(3,MB)-PRO(4,MB))
      WRITE(6,10)I,SNM,MB
    1 CONTINUE
      RETURN
   11 FORMAT(/5X,'****** MAXIMUM STRAIN ON CONCRETE SLAB ******')
   10  FORMAT(/5X,'****',I2,'TH SPAN IS',F7.5,'AT THE LOCATION',I3)
      END
```

```
      SUBROUTINE NLE(BM,BL)
      IMPLICITREAL*8(A-H,O-Z)
      COMMON/BL1/N,N1,AL,NM,NR(10)
      DIMENSION BL(10),BM(100)
      H=AL/DFLOAT(N)
      DO 1 I=1,NM
      J=0
    4 NK=NR(I)-J-1
      IF(NK.LE.0)GO TO 3
      IF(BM(NK))2,2,3
    2 J=J+1
      BL(I)=DFLOAT(J)*H
      GO TO 4
    3 JJ=0
   14 NL=NR(I)+JJ+1
      IF(NL.GE.N1)GO TO 6
      IF(BM(NL))5,5,6
    5 JJ=JJ+1
      GO TO 14
    6 IF(JJ.GT.J)BL(I)=DFLOAT(JJ)*H
    1 CONTINUE
      RETURN
   98 FORMAT(/5X,6I5)
      END
```

```
      SUBROUTINE READB(P,Q)
      IMPLICIT REAL*8(A-H,O-Z)
      COMMON/BL1/N,N1,AL,NM,NR(10)
      DIMENSION P(100),K(16),A(16),B(10),Q(100)
      NM1=NM+1
      READ(5,1)(K(I),I=1,16)
      READ(5,2)(A(I),I=1,16)
      READ(5,2)(B(I),I=1,10)
      WRITE(6,5)
      DO 3 I=1,16
      IF(A(I).EQ.0.0)GO TO 3
      WRITE(6,4)K(I),A(I)
    3 CONTINUE
      WRITE(6,11)
      DO 10 I=1,NM1
   10 WRITE(6,12)I,B(I)
      DO 7 I=1,N1
    7 P(I)=0.0
      DO 6 I=1,16
    6 P(K(I))=A(I)
      DO 8 I=1,NM1
      JJ=1
      JJJ=N1
      IF(I.NE.1)JJ=NR(I-1)
      IF(I.NE.NM1)JJJ=NR(I)
      DO 8 J=JJ,JJJ
      Q(J)=B(I)
```

```
 8 CONTINUE
   DO 9 I=1,NM
 9 Q(NR(I))=Q(NR(I))/2.0
   Q(1)=Q(1)/2.0
   Q(N1)=Q(N1)/2.0
   RETURN
 1 FORMAT(16I5)
 2 FORMAT(16F5.0)
 5 FORMAT(1H1,5X,'**** LOAD POINTS ****',/)
 4 FORMAT(5X,'LOAD POINT AT',I3,3X,F6.2,'KIPS.')
11 FORMAT(/5X,'**** DISTRIBUTED LOADS ****')
12 FORMAT(/5X,'****',I3,'TH SPAN',F8.2,'KIPS/INCH ****')
   END



   SUBROUTINE MP(K,BMU)
   IMPLICIT REAL*8(A-H,O-Z)
   COMMON/TEA1/B,T,D,W,K1,K2,KF
   COMMON/TEA2/SIGY,YS,H,RSN,RES,FYP,EPM,SIGU
   COMMON/TEA3/RA,YRA,HR,RSNR,FYPR,DRS,RK
   COMMON/TEA4/BC,TC,FC,KT
   DW=D*W
   DM=DW*1.1
   BT=B*T
   BH1=D/2.0+T
   BA=DW+2.0*BT
   BTC=BC*TC
   IF(K ) 1,2,3
 1 RAA=RA*YRA/SIGY
   Y4=D/2.0+RAA/W/2.0
   IF(Y4.GT.D) GO TO 4
   ZB=B*T*(T+D)+W*(Y4**2/2.0+(D-Y4)**2/2.0)*1.1+(D-Y4+T+DRS)*RAA
   BMU=ZB*SIGY
   WRITE(6,10)BMU
   RETURN
 4 X=(BA-RAA)/2.0/B
   XX=T-X
   Z=(XX+D+T/2.0)*BT+(XX+D/2.0)*DM+(XX**2+X**2)*B/2.0+RAA*(DRS+X)
   BMU=Z*SIGY
   WRITE(6,10)BMU
   RETURN
 2 A3=B*T*(D+T)/2.
   A4=W*D**2/4.
   BMU=(A3*2.+A4)*SIGY
   WRITE(6,10)BMU
   RETURN
 3 Y2=+BA*SIGY/(BC*0.85*FC)
   BMU=BA*SIGY*(BH1+TC-Y2/2.0)
   IF(Y2.LT.TC) WRITE(6,10)BMU
   IF(Y2.LT.TC) RETURN
   RRS=(BA*SIGY-0.85*FC*BTC)/2.0
   IF(RRS.GT.B*T) GO TO 20
   Y2=RRS/B
   BMU=SIGY*(B*T*(D+T+T/2.0-Y2)+D*W*1.1*(D/2.0+T-Y2) +
  1B*(Y2**2/2.0+(T-Y2)**2/2.0))+0.85*FC*BTC*(TC/2.0+Y2)
   WRITE(6,10)BMU
```

```
      RETURN
   20 Y2=(RRS-B*T)/W
      BMU=SIGY*(B*T*(D+T)+W*1.1*(Y2**2/2.0+(D-Y2)**2/2.0))
     1+0.85*FC*BTC*(TC/2.0+T+Y2)
      WRITE(6,10)BMU
      RETURN
  100 FORMAT(10X,E15.7)
   10 FORMAT(5X,'**** IDEALIZED PLASTIC MOMENT IS',F9.1,' KIP-IN****')
      END




      SUBROUTINE DS(SH,PRO,SD)
      IMPLICIT REAL*8(A-H,O-Z)
      COMMON/BL1/N,N1,AL,NM,NR(10)
      COMMON/BL2/CIP,CIN,AKP,AKN,ATP,ATN,BYP,BYN
      DIMENSION  BM(100),SH(100),SD(100),S(10),SG(100),EM(100)
      DIMENSION PRO(4,100)
      NM1=NM+1
      AH=AL/DFLOAT(N)
      DO 1 I=2,N
      FY=PRO(2,I)
      YP=PRO(3,I)
      YD=PRO(4,I)
      IF(FY.LT.0.0)K=-1
      IF(FY.GT.0.0)K=1
      IF(FY.EQ.0.0)K=0
      IF(FY.LT.0.0)CI=CIN
      IF(FY.GE.0.0)CI=CIP
      IF(SH(I).NE.0.0)BS=DABS((FY*CI-PRO(1,I))/SH(I) )
      IF(SH(I).NE.0.0)FYM=FY*AH/BS
      IF(SH(I).EQ.0.0)FYM=0.0
      CALL SHERG(K,0.0,0.0,0.0,FYM,YP,YD,AH,SG(I))
      IF(SH(I).NE.0.0)SG(I)=SG(I)/SH(I)
      DI=DFLOAT(I)
    1 CONTINUE
      SG(1)=SG(2)
      SG(N1)=SG(N)
      DO 18 I=1,N1
   18 SD(I)=0.0
      DO 19 I=1,NM1
      JJ=2
      JJJ=N
      IF(I.NE.1)JJ=NR(I-1)+1
      IF(I.NE.NM1)JJJ=NR(I)-1
      DO 19 J=JJ,JJJ
      A=DFLOAT(JJJ-J)/DFLOAT(JJJ-JJ)
      DO 20 K=JJ,J
   20 SD(J)=SD(J)+SG(K)*A
       DO 21 K=J,JJJ
   21 SD(J)=SD(J)+SG(K)*(A-1.0)
   19 CONTINUE
      RETURN
   98 FORMAT(5X,5I5)
   99 FORMAT(5X,8E15.5)
      END
```

```
      SUBROUTINE LOCAL(N,AL,BMC,PY,EIG1)
        IMPLICIT REAL*8(A-H,O-Z)
      COMMON/TEA1/B,T,D,W,K1,K2,KF
      COMMON/TEA2/SIGY,YS,AH,RSN,RES,FYP,EPM,SIGU
      DIMENSION H1(20),H2(20),H3(20),H4(20),H5(20),WA(20,20),WAA(20,20)
      ELM=3.0*10.**4
      EIW=ELM*B**3*T**3/144.0
      AFAC=(B**2+T**2)/12.0
      G=ELM/2.6
      GJD=G*B*T**3/3.0
      NO=N-1
      NT=N-2
      N1=N+1
      ITE=1
      AMC=PY*AL
      BL=AL*(1.0-BMC/AMC)
      IF(BL.LE.0.0)RETURN
      H=BL/DFLOAT(N1)
      H10=H**(-2)
      H20=H10**2
    9 DO 1 I=1,N
      DIM=DFLOAT(I)/DFLOAT(N)
      H1(I)=BMC+(AMC-BMC)*DIM
      HM=H1(I)
      CALL YAMA(HM,AF,Y1)
      O1=-AF*Y1
      O2=STRES(O1,SIGY,FYP,AH,SIGU)
      CALL PORT(O1,ER,GR)
      H2(I)=EIW*ER*H20
      H3(I)=GJD*GR*H10
      H4(I)=B*T*O2*AFAC*H10
      H5(I)=ELM*W**3/3.0/Y1
    1 CONTINUE
      DO 2 I=1,N
      DO 2 J=1,N
      WA(I,J)=0.0
      WAA(I,J)=0.0
    2 CONTINUE
      DO 3 I=1,N
      I1=I-1
      I2=I+1
      IF(I.EQ.1)GO TO 4
      IF(I.EQ.N)GO TO 5
      Z1=H2(I1)+4.0*H2(I)+H2(I2)
      Z2=H3(I1)/2.0+H3(I)+H3(I2)/2.0
      Z3=-(H4(I1)/2.0+H4(I)+H4(I2)/2.0)
      GO TO 6
    4 Z1=6.0*H2(1)+H2(2)+0.5*H3(1)
      Z2=1.5*H3(1)+H3(2)/2.0
      Z3=-(H4(1)+H4(2))/2.0
      GO TO 6
    5 Z1=+H2(NO)+6.0*H2(N)+0.5*H3(N)
      Z2=H3(NO)/2.0+1.5*H3(N)
      Z3=-2.0*H4(N)
    6 WA(I,I)=Z1+Z2+H5(I)*.666667
```

```
      WAA(I,I)=Z3
    3 CONTINUE
      DO 7 I=1,NO
      I2=I+1
      Z1=-2.0*(H2(I)+H2(I2))-(H3(I)+H3(I2))/2.0
      Z2=(H4(I)+H4(I2))/2.0
      WA(I2,I)=Z1+H5(I)*.1666667
      WA(I,I2)=WA(I2,I)
      WAA(I2,I)=Z2
      WAA(I,I2)=Z2
    7 CONTINUE
      DO 8 I=1,NT
      I2=I+1
      I3=I+2
      WA(I3,I)=H2(I2)
      WA(I,I3)=WA(I3,I)
    8 CONTINUE
      CALL SHUKI(WAA,WA,N,EIG1,4)
      RETURN
  101 FORMAT(/5X,5I5)
  100 FORMAT(/5X,5E15.5)
      END
```

```
      SUBROUTINE YAMA(AM,AF,Y1)
      IMPLICIT REAL*8(A-H,O-Z)
      COMMON/COS1/CU(6,61)
      MT=-1
      IF(MT.EQ.1)MRI=1
      IF(MT.EQ.1)MO=2
      IF(MT.EQ.1)MK=3
      IF(MT.EQ.-1)MRI=4
      IF(MT.EQ.-1)MO=5
      IF(MT.EQ.-1)MK=6
      HAM=CU(MRI,1)
      IF(DABS(AM).LE.DABS(HAM))GO TO 1
      MW=1
    2 MW=MW+1
      H1=CU(MRI,MW)
      IF(DABS(AM).GT.DABS(H1))GO TO 2
      MW1=MW-1
      H2=AM-CU(MRI,MW1)
      H3=H1-CU(MRI,MW1)
      H4=CU(MO,MW)-CU(MO,MW1)
      AF=CU(MO,MW)+H2*H4/H3
      Y1=CU(MK,MW)+H2*(CU(MK,MW)-CU(MK,MW1))/H3
      RETURN
    1 AF=CU(MO,1)*AM/HAM
      Y1=CU(MK,1)
      RETURN
      END
```

```
 40 DO 50 I=1,NA
    YY(I)=0.0
    DO 60 J=1,NA
    YY(I)=YY(I)+H(I,J)*Y(J)
 60 CONTINUE
    IF(I .EQ. 1) A=YY(I)
 50 CONTINUE
    IF(DABS(A) .GT. 10.0E-15) GO TO 56
    DO 55 I=1,NA
    Y(I)=Y(I)+DFLOAT(I)
 55 CONTINUE
    GO TO 40
 56 DO 70 I=1,NA
    Y(I)=YY(I)/A
 70 CONTINUE
    S=A/B
    B=A
    IF(S .GT. 1.00001) GO TO 40
    IF(S .LT. 0.99999) GO TO 40
    IF(KK .EQ. KA) GO TO 75
    AA=A
    DO 71 I=1,NA
    Z(I)=Y(I)
 71 CONTINUE
    GO TO 10
 75 IF(A .GE. AA) GO TO 80
    A=AA
    DO 76 I=1,NA
    Y(I)=Z(I)
 76 CONTINUE
 80 IF(KK .EQ. 2) GO TO 200
200 A1=A
    GO TO 220
210 A=D(1,1)/C(1,1)
220 WRITE(6,230) A
230 FORMAT(/1X,'THE FIRST EIGEN VALUE IS',E12.4)
    RM1=A
    IF(N .EQ. 1) RETURN
    WRITE(6,240) (Y(I),I=1,N)
240 FORMAT( 3X,'CORRESPONDING MODE **'/(3X,8E14.4))
    RETURN
    END
    SUBROUTINE TOKYO (NO,A)
    IMPLICIT REAL*8(A-H,O-Z)
    DIMENSION AC(20),AB(20),A(20,20)
    NO1=NO-1
    A(1,1)=1.0/A(1,1)
    IF(NO .EQ. 1) RETURN
    DO 80 N=1, NO1
    DO 50 I=1,N
    AB(I)=0.0
    AC(I)=0.0
    DO 50 J=1,N
    AB(I)=AB(I)+A(I,J)*A(J,N+1)
    AC(I)=AC(I)+A(N+1,J)*A(J,I)
 50 CONTINUE
    ACB=0.0
    DO 60 I=1,N
    ACB=ACB+AC(I)*A(I,N+1)
 60 CONTINUE
```

```
      SUBROUTINE LOCAL(N,AL,BMC,PY,EIG1)
        IMPLICIT REAL*8(A-H,O-Z)
      COMMON/TEA1/B,T,D,W,K1,K2,KF
      COMMON/TEA2/SIGY,YS,AH,RSN,RES,FYP,EPM,SIGU
      DIMENSION H1(20),H2(20),H3(20),H4(20),H5(20),WA(20,20),WAA(20,20)
      ELM=3.0*10.**4
      EIW=ELM*B**3*T**3/144.0
      AFAC=(B**2+T**2)/12.0
      G=ELM/2.6
      GJD=G*B*T**3/3.0
      NO=N-1
      NT=N-2
      N1=N+1
      ITE=1
      AMC=PY*AL
      BL=AL*(1.0-BMC/AMC)
      IF(BL.LE.0.0)RETURN
      H=BL/DFLOAT(N1)
      H10=H**(-2)
      H20=H10**2
    9 DO 1 I=1,N
      DIM=DFLOAT(I)/DFLOAT(N)
      H1(I)=BMC+(AMC-BMC)*DIM
      HM=H1(I)
      CALL YAMA(HM,AF,Y1)
      O1=-AF*Y1
      O2=STRES(O1,SIGY,FYP,AH,SIGU)
      CALL PORT(O1,ER,GR)
      H2(I)=EIW*ER*H20
      H3(I)=GJD*GR*H10
      H4(I)=B*T*O2*AFAC*H10
      H5(I)=ELM*W**3/3.0/Y1
    1 CONTINUE
      DO 2 I=1,N
      DO 2 J=1,N
      WA(I,J)=0.0
      WAA(I,J)=0.0
    2 CONTINUE
      DO 3 I=1,N
      I1=I-1
      I2=I+1
      IF(I.EQ.1)GO TO 4
      IF(I.EQ.N)GO TO 5
      Z1=H2(I1)+4.0*H2(I)+H2(I2)
      Z2=H3(I1)/2.0+H3(I)+H3(I2)/2.0
      Z3=-(H4(I1)/2.0+H4(I)+H4(I2)/2.0)
      GO TO 6
    4 Z1=6.0*H2(1)+H2(2)+0.5*H3(1)
      Z2=1.5*H3(1)+H3(2)/2.0
      Z3=-(H4(1)+H4(2))/2.0
      GO TO 6
    5 Z1=+H2(NO)+6.0*H2(N)+0.5*H3(N)
      Z2=H3(NO)/2.0+1.5*H3(N)
      Z3=-2.0*H4(N)
    6 WA(I,I)=Z1+Z2+H5(I)*.666667
```

```
 40 DO 50 I=1,NA
    YY(I)=0.0
    DO 60 J=1,NA
    YY(I)=YY(I)+H(I,J)*Y(J)
 60 CONTINUE
    IF(I .EQ. 1) A=YY(I)
 50 CONTINUE
    IF(DABS(A) .GT. 10.0E-15) GO TO 56
    DO 55 I=1,NA
    Y(I)=Y(I)+DFLOAT(I)
 55 CONTINUE
    GO TO 40
 56 DO 70 I=1,NA
    Y(I)=YY(I)/A
 70 CONTINUE
    S=A/B
    B=A
    IF(S .GT. 1.00001) GO TO 40
    IF(S .LT. 0.99999) GO TO 40
    IF(KK .EQ. KA) GO TO 75
    AA=A
    DO 71 I=1,NA
    Z(I)=Y(I)
 71 CONTINUE
    GO TO 10
 75 IF(A .GE. AA) GO TO 80
    A=AA
    DO 76 I=1,NA
    Y(I)=Z(I)
 76 CONTINUE
 80 IF(KK .EQ. 2) GO TO 200
200 A1=A
    GO TO 220
210 A=D(1,1)/C(1,1)
220 WRITE(6,230) A
230 FORMAT(/1X,'THE FIRST EIGEN VALUE IS',E12.4)
    RM1=A
    IF(N .EQ. 1) RETURN
    WRITE(6,240) (Y(I),I=1,N)
240 FORMAT( 3X,'CORRESPONDING MODE **'/(3X,8E14.4))
    RETURN
    END
    SUBROUTINE TOKYO (NO,A)
    IMPLICIT REAL*8(A-H,O-Z)
    DIMENSION AC(20),AB(20),A(20,20)
    NO1=NO-1
    A(1,1)=1.0/A(1,1)
    IF(NO .EQ. 1) RETURN
    DO 80 N=1, NO1
    DO 50 I=1,N
    AB(I)=0.0
    AC(I)=0.0
    DO 50 J=1,N
    AB(I)=AB(I)+A(I,J)*A(J,N+1)
    AC(I)=AC(I)+A(N+1,J)*A(J,I)
 50 CONTINUE
    ACB=0.0
    DO 60 I=1,N
    ACB=ACB+AC(I)*A(I,N+1)
 60 CONTINUE
```